DOCTOR OF PHILOSOPHY

Effects of turbulence on suspended sediment concentrations in a tidal flow.

Campbell, Andrew Robert

Award date:
1996

Awarding institution:
Bangor University

Title : Effects of turbulence on suspended sediment concentrations in a tidal flow.

A thesis submitted in accordance with the requirements of the University of Wales for the degree of Doctor of Philosophy.

by Andrew Robert Campbell.

University of Wales, Bangor

School of Ocean Sciences

Menai Bridge

Anglesey

LL59 5EY

United Kingdom

March 1996.

Page Numbering as Bound

ABSTRACT

Vertical profiles of turbulent dissipation rate, current velocity, density and suspended particulate matter (SPM) concentrations have been made at three contrasting sites in the Irish Sea using a combination of moored and profiling instrumentation. Measurements were made over two tidal cycles at two well mixed and one thermally stratified site.

The observations indicate that at all sites there is a strong correlation between SPM concentrations and levels of turbulent dissipation rate, both of which are closely related to the tidal flow. The principal variations in SPM concentration are due to resuspension and settling of bed material and advection of horizontal concentration gradients. Turbulent dissipation rate depends closely on local vertical shear in the horizontal velocity. The vast majority of energy is dissipated in the high shear region near the bed with higher dissipation rates measured at the more energetic sites.

An M_4 harmonic analysis reveals the nature of the sediment resuspension/settling and turbulent dissipation rate signals. Where confidence in the analysis is significant, the phase of both signals increases with height. In mixed waters, the dissipation rate M_4 phase increases steadily up to the surface whereas the SPM phase increases more rapidly in the near bed region. In the interior of the water column, both phases increase at approximately the same rate.

Density stratification has a strong effect on the vertical distribution of fine suspended sediments and the dissipation of turbulent kinetic energy. The M_4 variation in both SPM and dissipation rate is confined below 40m and the phase of both M_4 signals increases rapidly with height so that lags relative to the bed variation are significantly larger at this site. Semi-diurnal variation in the height of the pycnocline is a further control on the distribution of sediment in the near bed region.

A 1-d, level 2.0 turbulence closure model has been used to hindcast the observations. The model is successful in simulating the mean flow, density and turbulent dissipation rate at both mixed sites. SPM concentration predictions are broadly in line with observations although simulation of the phase relationship between dissipation rate and SPM is only partially successful, probably because the model over-simplifies the nature of the sediment population. At the stratified site, limitations in the model's ability to accurately simulate the density field mean that the SPM results deviate from the observations.

ACKNOWLEDGEMENTS

My principal thanks go to my supervisors : Professor John Simpson and Dr. Sarah Jones for their guidance, especially during the writing of this thesis when I believe I benefitted the most from their help and advice. Thanks are also due to the other members of my supervisory committee, Dr. Alan Davies and Dr. John Howarth.

Central to this study is a large dataset that was collected during two cruises in 1993. I am indebted to the captain and crew of both the RRS Challenger (cruise 102) and RV Prince Madog. I am also grateful for the excellent work of the technical department at Bangor and to Dr. Bill Crawford (IOS, Sidney, B.C.) and Chris Mackay (Sy-Tech research) who provided the FLY probe hardware and expertise and participated in the turbulence measurements. Many thanks also to the other students and research staff who participated in the field work.

The turbulence closure model forcing and improvements were provided by Joseph Cheok who was always enthusiastic and willing to help, often without request. Tom Rippeth visited Canada to process the FLY turbulent dissipation rate data, many thanks for the numbers and the postcards.

During my time at Bangor I have enlisted the help of many of my fellow inmates in room 204 and would like to thank them for their advice and more importantly for providing an excellent (if not entirely productive) working environment. Thanks are also due to NERC for the studentship.

For their continuous support and encouragement my warmest thanks go to my parents, Morven and Ailsa and especially to Noreen.

To my parents,

with love

TABLE OF CONTENTS

LIST OF FIGURES

LIST OF TABLES

CHAPTER ONE

Introduction

1.1 Background and Motivation for the Study.

In recent times, there has been an increased focus on the oceanography of the dynamically active and energetic shelf sea regime. This is due in part to an increased awareness of the practical and economic importance of the continental shelf seas and the need to improve our understanding of the processes that affect them.

Shelf seas are now extensively used as both a source of food and as a convenient site for the disposal of waste products. Over the last 30 years hydrocarbon exploration and extraction has also become extremely important. An entire nation's prosperity can depend on its natural resources and the competitiveness of its industry and so economics plays an important role in determining how the shelf seas are treated both as a source of minerals and food and as a dumping ground. Unfortunately, the effects of such activities on the marine environment are rarely the first consideration.

Given the vast surface area and volume of the world ocean, it is not difficult to appreciate how initially, assumptions were made that the effects of human activity would be negligible. However, the detrimental impact of excessive fishing and the disposal of unwanted by-products is now all too obvious. Entire marine populations have been eradicated as fishing equipment and techniques have improved and unsustainable, short-term fishing policies have been adopted. For example, in 1977 there was a total ban on herring fishing which eventually allowed stocks to return to acceptable levels but also resulted in overfishing of other species such as mackerel and cod.

Since the 19th century dumping in the shelf seas has been on the increase. Both the Irish and North Seas are heavily polluted with waste from industrial processes (*e.g.* heavy metals, low level radioactive materials), farming (pesticides, fertilisers) and

the human population (raw and treated sewage). Waste input via outfalls, rivers and both intentional and accidental dumping results in poor water quality in many sea areas, and can have serious consequences on the ecology of the area. Even the apparently innocent discharge of warm water from power stations can have a significant local effect as the warmer water stimulates biological activity.

Incidents such as the *Torrey Canyon* and *Sea Empress* oil spills, the disposal of the *Brent Spar* oil storage facility, the dramatic decline in the common seal population and increased levels of toxins in fish caught for human consumption have raised public awareness and focused attention on the requirement for a greater understanding of the impact of human activities on the shelf seas. With the world population (most of whom live relatively close to the sea) forecast to double by 2050 and pressure on the shelf sea system continuously increasing, the need to improve our understanding of the dynamics of coastal waters and the continental shelf seas is paramount.

In addition to the practical motivation outlined above, research into the behaviour and response of the world's seas and oceans is driven by the great scientific challenge that they present. Oceans dominate the surface of the globe and have an effect on almost every living being. They interact with the land masses, the atmosphere and each other, constantly moving and shaping the environment in which we live.

The world ocean and, in particular the energetic continental shelf region is host to numerous physical, biological and chemical processes which combine and interact to form the complex marine system that scientists endeavour to predict and understand. The regular rise and fall of the tide is probably the most familiar characteristic of the sea to most. Tidal motions are important but do not solely account for the behaviour of the sea. Buoyancy input, for example via solar heating and river runoff leads to the formation of density driven flows, stratification, frontal systems and their associated circulation. Winds generate currents and waves which can enhance the effect of the currents on the seabed. Turbulence created at the bed suspends and transports sediments and mixes heat, salt and nutrients throughout the

water column. The combination of all of these and other physical processes coupled with biological activity, chemical interactions and the seasonal cycle make the shelf seas a vibrant and dynamic system which provokes much scientific interest. Taken together, the inherent scientific interest of the shelf seas and the increasingly urgent practical requirement to manage them provides us with powerful motivation to identify and study the quantities and processes associated with the shelf sea system.

1.2 The Shelf Sea Regime.

Whereas tidal currents in the deep ocean are usually only of the order of a few cms^{-1}, currents on the continental shelf where depths are generally less than 200m can exceed $1ms^{-1}$. The proximity of land masses and the effects of bottom topography result in a large dynamic range in tidal currents over the continental shelf. Because velocities are high, tidal currents on the shelf are very energetic. While some of this energy is expended in mixing waters of differing densities, the proximity of the sea bed means that its frictional influence can extend all the way to the surface and up to 90% of the total energy contained in the flow is dissipated as heat.

A second important influence on the shelf sea is the buoyancy input that they receive. High levels of freshwater are input directly via precipitation or at the lateral boundaries via run off. This input of lighter water can result in significant density driven flow, the establishment of permanent and/or periodic haline stratification and an associated frontal regime. Surface heating during the summer months can also result in the development of thermal stratification as the tidal currents which dominate the flow field may not be sufficiently strong to maintain a fully homogeneous water column as is the case in the Western Irish Sea where a strong thermocline develops. This competition between the stratifying influence of solar heating and the tidal stirring mechanism leading to stratification in certain areas and a frontal system separating mixed from stratified water masses has been widely studied (Simpson (1971), Simpson and Hunter (1974), Durazo-Arvizu (1993)).

Most large-scale fluid flows in nature are turbulent and the currents in both the deep ocean and on the continental shelf are no exception. Turbulent flows are highly irregular, very diffusive and dissipative so that they require a constant energy input such as that from the shear in the mean (tidal) flow in order to be maintained. The non-linear and high frequency behaviour of turbulent flows means that their study is complicated. The majority of experiments have concentrated on atmospheric and laboratory flows and most approaches have been mathematical in nature although recent advances in instrument technology have allowed more accurate monitoring of turbulence in the sea.

One of the distinctive characteristics of turbulent flows is their high diffusivity. They display a rapid rate of mass transfer and diffusion of momentum and scalars thus facilitating exchange throughout the water column. Turbulent diffusion dominates over molecular diffusion and is responsible for almost all vertical exchange of heat, salt, nutrients and sediments in the ocean. High levels of vertical exchange are characteristic of, and strongly influence, shelf seas.

The shelf seas with their high tidal currents, high levels of nutrients and frequent complete vertical mixing are biologically very active and an extremely productive medium for flora and fauna. In the spring, when the water starts to warm up and the duration and intensity of the incoming solar radiation increases, phytoplankton growth in the surface layers is stimulated and aided by the onset of stratification which ensures an abundant supply of light by confining phytoplankton to the surface layer. High phytoplankton concentrations result in increased levels of grazing by secondary producers so that overall levels of organic material in the water column increase. After the spring bloom, when all of the nutrients in the surface waters have been exhausted, the organic material dies and decays as it sinks to the bed where it is re-mineralised and nutrients are released.

The dumping into the sea of raw and treated sewage as well as agricultural waste provides high quantities of nutrients. The enhanced levels of nutrients can interfere

with the natural cycle of production and re-cycling and, combined with large quantities of sunlight, this excess nutrient-rich material may lead to a 'nuisance bloom'. In some cases the excess plant and animal matter resulting from enhanced biological activity is washed up onto the beach where it rots. Most of the biological matter remains in the water column so that when it dies it sinks to the bed. Decaying material uses up the dissolved oxygen in the water often to the point where the oxygen in the bottom waters is exhausted, leading to hypoxia so that the water can no longer sustain any aerobic activity. Phytoplankton blooms, in particular those caused by flagellate phytoplankton can have dramatic effects. If concentrations are sufficiently high then they can prevent marine life from breathing resulting in significant fish kills. Such blooms can also be toxic to both marine organisms and humans.

1.3 The Importance and Role of Particulates.

The weak tidal currents and the remoteness of the world's oceans from the continents mean that the ocean floor is covered with a layer of slowly accumulating fine sediments. In contrast to this, the large dynamic range of the tides and the proximity to sources of terrestrial sediments such as cliffs and rivers results in the floor of the continental shelf seas consisting of a wide range of sediment size fractions. Areas of mud, silt, sand and gravel are all common across the North-West European Shelf.

Muddy deposits tend to accumulate where the tidal currents are weak whereas areas of coarse silt and sand build up in more energetic locations. Generally, the sea bed consists of unconsolidated sediments which are continuously reworked and resuspended by the flow. Resuspension of the coarser silts and sands usually only occurs in very energetic zones, for example, near beaches where the effects of wave activity can also be felt at the bed. Much of the work to date has concentrated on the transport of sand, which is via the process of bedload. The lighter sediment fractions, with which this study is concerned are especially subject to resuspension and

advection by the tidal flow. The importance of fine sediments in many shelf sea processes is recognised but not well understood.

Resuspension and vertical mixing of particulate matter by turbulence derived from the energy of the mean flow determines the vertical distribution and transport of this material. Particulate matter plays an essential role in the determination of water quality in the shelf seas as it strongly influences biological and chemical processes both in and on the sea bed and throughout the water column. For example, high concentrations of particulates in the surface waters may block and scatter the incoming radiation, inhibiting plankton growth (Tett *et al.* (1993)) which can have serious consequences for species higher up the food chain. Conversely, sinking detrital matter may remove particulates from the water column, depositing them on the bed.

Particles in suspension have a larger surface area exposed to the water than when they are on the bed so that the potential for physical and chemical exchange between the two media is greater. As more particles are resuspended off the bed they may interact with each other, flocculating and aggregating before settling to the bed once more or being broken up again by the shear in the mean flow.

Pollutants adhere to and react with particulates in suspension and on the bed so that sediments are important vectors for the dispersion of a wide range of waste products. For many contaminants, transport in particulate form constitutes an important fraction (up to 70%) of the total transport (Eisma and Irion (1988)). Modern industrial processes discharge large and diverse quantities of toxic and poisonous materials often without prior knowledge of how they will disperse or react with the surroundings. Heavy metals such as mercury are commonly used in the chemicals industry. Their extraction from the waste material is expensive and so they are not removed and are discharged into the sea where, in many cases, they are absorbed on to the sediment to be introduced into the seabed via deposition and consolidation and then perhaps reintroduced back into the water column and transported to a

different area through the processes of resuspension and advection. Such contaminants may also be incorporated into the food chain as demonstrated by increased levels of mercury in fish.

The single most important factor that has hindered greater advances in the study of suspended particulate matter (SPM) is that a multidisciplinary approach is required. Physical, chemical, and biological effects all need to be taken into consideration. The nature of the sediment population is determined by many factors including the local geology and topography, the dynamical conditions and biological activity which itself may be the most important factor in determining the role of the seabed as a source and sink for particulates (McCave (1984)).

Central to increased understanding of the processes affecting levels of SPM are accurate measurement techniques. Early attempts to monitor SPM concentrations involved taking water samples for subsequent analysis, an extremely time consuming and labour intensive processes. However, advances in instrumentation technology allow us to monitor SPM concentrations *in situ* for long periods with increasing accuracy using instruments such as the beam transmissometer.

1.4 The Current State of Play.

So far in this chapter the importance of the role played by sediments and in particular the suspended fraction in the determination of water quality has been discussed. The sediment population is an important component, strongly influencing and being affected by many of the physical, chemical and biological processes found on the continental shelf. The relative importance of these processes will change both temporally and spatially. To date, their interaction with the sediment population has been subject to individual study but the necessity of a multi-disciplinary approach is becoming apparent.

Tidal forcing, known to be the primary driving force for currents on the continental shelf is well understood. We have a good understanding and predictive capability of tidal flow and recognise that it provides the energy necessary for the initiation and maintenance of turbulence. The important properties of turbulent flow, in particular the enhanced levels of vertical mixing have been recognised. Coupled with relatively shallow waters this means that heat, salt, nutrients and sediments can all be mixed throughout much of the water column, an important aspect of biological and chemical cycling.

Unfortunately, the small scales and high frequency fluctuations associated with turbulent flow mean that accurate observation, often a necessary precursor to increased understanding, is very difficult. Many questions exist relating to the generation, transport (via advective and/or diffusive processes) and subsequent decay of turbulence. As a consequence of this we have a poor appreciation of the interaction between the turbulent flow field and SPM population. Research has shown that SPM concentrations are often related to variations in the tidal signal (Weeks (1989)). However, erosion and the subsequent vertical transport of fine sediments in the water column is due almost exclusively to turbulence and it is unclear how levels of suspended sediment respond to the turbulent flow field. Turbulent activity, along with biological and chemical processes also affects the nature of the particle population itself, the monitoring of which is a major challenge being undertaken by scientists.

Instrumentation advances mean that we can now accurately monitor both SPM concentrations and the mean flow field throughout the entire water column for an appreciable period and certainly over the period of a tidal cycle. It is also possible to monitor certain aspects of the turbulent flow field over similar temporal and spatial scales. This means that the mean flow, turbulent flow and SPM concentration fields can all be observed simultaneously. This capability forms the basis of this study, the aims of which are presented below.

1.5 Aims of the Project.

This study aims to elucidate the response of the suspended particulate matter (SPM) population to changes in the mean and turbulent flow fields. The project is designed around an extensive observational program which uses advanced instrumentation for the study of suspended sediments and turbulent flow. The aim of the observations was to determine the mean and turbulent flow fields and the SPM concentration throughout the entire water column over two tidal cycles. This was accomplished at both mixed and thermally stratified sites ensuring spatial and temporal coverage of these parameters unavailable until now.

This thesis aims to present and interpret the results of my observations in order to reveal the principal processes which determine how concentrations of SPM react to variations in the nature of the flow and to the structure of the water column. Analysis techniques applied to the datasets isolate and quantify the important features and signals present in the results, permitting further insights into the nature of the interaction.

In order to test the process interpretation, a 1-d numerical model is used to hindcast the observations. The basic hydrodynamic model has been in use for some time (Simpson and Sharples (1991), Sharples (1992)). It incorporates all of the relevant physical processes and utilises a turbulence closure scheme for parameterisation of vertical exchange of momentum, heat and salt. A separate study (Cheok (1996)) uses this model to hindcast the mean and turbulent flow field observations. Earlier observations of suspended sediment concentrations and tidal current measurements led to the development of a sediment dynamics module for inclusion within this model (Jones *et al.* (1996a,b)). The applicability of the scheme is investigated by comparing simulated and observed data. This process is also useful in that the model may be used as a diagnostic tool with which to study the relative importance of the existing model inputs and perhaps to suggest additional processes that require consideration and parameterisation within the model framework.

1.6 Thesis Structure.

The remainder of this thesis is organised as follows.

Chapter Two — The properties of turbulent flows are discussed. The mathematical approach used in the study of such flows is applied to the continuity and energy equations and turbulence spectra are introduced. Finally, the range of instrumentation available for monitoring turbulence is discussed with a view to the dissipation rate measurements made during my observational program.

Chapter Three — The origin and composition of the shelf sea sediment population is discussed. Also considered are the fundamental physical processes that determine the vertical profiles of SPM concentration and simple vertical processes models used in the prediction of concentration profiles are presented. The chapter concludes with an introduction to the range of instrumentation used to measure SPM concentrations.

Chapter Four — The experiment sites are described in terms of what is currently known about the tidal regime, seasonal stratification and the nature of the sediment population. The instrumentation used and the mooring configurations for each experiment are described and the cruises are recounted.

Chapter Five — A large range of instrumentation was used throughout the experimental program. In this chapter the principles and modes of operation of these instruments are described. Also presented are the techniques employed for processing the data available for analysis.

Chapter Six

This chapter starts with a discussion of the data available for analysis. The water column structure measurements made at each site are then considered and this is followed by a discussion of the mean flow results. The sediment concentration measurements made during each survey are then discussed and assimilated. The final section considers the turbulent flow (velocity microstructure) measurements.

Chapter Seven

In this chapter the harmonic analysis results are discussed. The datasets present a unique opportunity to study the interaction of turbulent dissipation rate, SPM concentration and mean current. In particular, the phase relationships between the various signals are explored via detailed analysis of the temporal variability of the parameters under investigation at a specific height above the bed and of the depth variability of SPM concentration and turbulent dissipation rate.

Chapter Eight

In this chapter an existing turbulence closure model that satisfactorily reproduces the mean flow conditions and has been developed to simulate SPM concentrations is introduced and used to hindcast the data obtained during the observational program. This model provides an insight into the physical processes responsible for distribution of SPM. Several important conclusions are made considering present understanding of the production/diffusion/dissipation of turbulent kinetic energy and resuspension and settling of fine-grained marine sediments.

Chapter Nine

The significance of the results presented is discussed. Some possibilities for future work in the area of fine sediments and turbulence are presented and general conclusions regarding the results and success of the work undertaken are outlined.

CHAPTER TWO

The Physics of Turbulent Flow in the Shelf Seas

2.1 The Nature of Turbulence.

Many attempts have been made to describe the nature of turbulent motion. One of the simplest and most straight-forward descriptions is simply that a flow is turbulent when it is *"in a state of continuous instability"* (Tritton (1977)). Turbulence is the most common, arguably one of the most important and certainly the most complicated kind of fluid motion. Such flow is not easy to define precisely but it does however, exhibit certain characteristics.

• Irregularity	Turbulent flows are highly non-linear and completely random.
• Diffusivity	A rapid rate of mass transfer and diffusion of momentum and heat is typical of turbulent flows.
• Fluctuating Vorticity	High levels of 3-d fluctuating vorticity are exhibited by turbulent flows. 3-d fluctuations are necessary for vortex stretching to occur, the process through which energy is transferred to molecular scales where it is dissipated as heat.
• Dissipative	Because turbulent flows are dissipative, they require a continuous supply of energy to be maintained.
• High Reynolds Number	Turbulent flows only occur at large values of the Reynolds number.

Recognising these characteristics it is now possible to give a more accurate

description of turbulence as *"a 3-d time dependent motion in which vortex stretching causes velocity fluctuations to spread to all wavelengths between a minimum determined by viscous forces and a maximum determined by the boundary conditions of the flow. It is the usual state of fluid motion except at low Reynolds numbers."* (Bradshaw (1971)).

The consequence of the properties outlined above is that turbulent flows do not lend themselves readily to strict analytical study and a deterministic description is generally not possible. For example, important features of the flow such as large eddy motions can arise from apparently insignificant initial perturbations. Instead, when the level of predictability is as low as it is for turbulent flow, it becomes necessary to adopt a statistical approach *i.e.* to treat variables as stochastic or random quantities. Generally this means that equations are formulated in terms of average quantities. This statistical description of turbulence and the equations used to describe turbulent motion and its related properties (such as turbulent intensity and kinetic energy) are the subject of sections 2.3 and 2.4. Also introduced is the spectral approach to the description of turbulent energy and dissipation, necessary because of the large range of spatial and temporal scales involved. Observational techniques used in the study of turbulent flows are the subject of the final section of this chapter. However, we firstly take a brief look at the structure and principal features of turbulent flow in the context of the shelf sea environment.

2.2 Turbulence and the Water Column.

As far as SPM is concerned, the most important part of the water column is the bottom boundary layer, this being both a major source and sink for particles. The thickness δ of the bottom boundary layer (BBL) is often defined as that part of the water column where the flow velocity rises from zero at the bed to 99% of its free-stream value. δ can be tens of meters thick and so, in shelf seas can extend through the entire water column or coincide with the height of the pycnocline.

Currents over the bed in shelf seas tend to be dominated by tidal flow as opposed to wind-driven or wave-induced oscillatory currents. Although these tidal currents can actually be quite weak compared to those due to wave action, they nearly always result in turbulent flow over the bed.

The classical measure of the turbulent state of a flow is given by the dimensionless Reynolds number (Re) where

$$\mathbf{Re} = \frac{\mathbf{u\,h}}{\boldsymbol{\nu}} \qquad (2.01)$$

ν is the kinematic viscosity (m^2s^{-1}) and u (ms^{-1}) and h (m) are characteristic speed and length scales respectively. Thus, the Reynolds number can be thought of as the ratio of the inertial forces, which represent the resistance of the fluid mass to accelerations, to the viscous forces which resist deformation of the fluid. Experiments have shown that, for 2-d free surface flow, if the Reynolds number is less than 890 then the flow is laminar whereas if Re is greater than 5000 it is fully turbulent. Taking typical values for the kinematic viscosity ($10^{-6}m^2s^{-1}$), the tidal current ($0.2ms^{-1}$) and the water depth (100m), then the Reynolds number is much greater than 5000 and the flow is fully turbulent. Therefore, for the purpose of this study the BBL structure for laminar flow need not be considered.

The BBL as introduced above is often subdivided into three separate layers : the bed layer, the logarithmic layer and the outer layer. If the water is sufficiently deep then there will also exist a free-stream layer above the BBL. The turbulent energy and shear stress generally decrease with height from a maximum value at the bed.

The bed layer is of the order of a few cms thick in the sea and the flow structure adopts one of two forms, depending on the bed roughness. If the bed is sufficiently smooth and lacking in 'roughness elements' then the flow dynamics in the bed layer tend to be dominated by viscosity and the flow is known as 'smooth' turbulent flow. Very close to the bed (within 1cm) turbulent fluctuations in the vertical are inhibited,

resulting in the development of the viscous sublayer (VSL). As the bed roughness elements increase in size so that they protrude through the top of the VSL then the classification of the flow alters from smooth through transitional to rough turbulent flow. In rough turbulent flow the thickness of the bed layer coincides with the height at which the local topographic variations die out.

Between the bed layer and the outer layer in which the flow approaches the free-stream value is the logarithmic layer which is of the order of a few meters thick in the sea. Within this layer (often called the constant stress layer (CSL)) the velocity profile follows the von Kármán-Prandtl relation

$$\frac{u}{u_*} = \frac{1}{\kappa} \ln \frac{z}{z_0} \qquad (2.02)$$

where u=velocity at height z

u_*=friction velocity=$(\tau_b/\rho)^{1/2}$ where τ_b is the bottom stress

κ=von Kármán constant ($\approx$0.41)

z_0 is known as the roughness length scale and is dependent on the bedform.

2.3 The Statistical Description of Turbulence.

It is apparent from earlier discussion that turbulent flow is a very complicated phenomenon. In the study of such flow it is therefore necessary to make assumptions regarding the nature of the turbulence under investigation. Before proceeding with a mathematical description of turbulence in the next section we will first introduce and define some of the concepts commonly used to aid us in the study of turbulent flows.

- Homogeneity — Homogeneity implies that the flow under consideration and its statistical properties are unchanged by a spatial translation.

- Isotropy

This is a common assumption made about the directional symmetry of the average properties of the turbulent motion so that homogeneous, isotropic turbulence depends on neither the position nor the direction of the axes of reference. However, the assumption of homogeneity is a necessary prerequisite to that of isotropy, for certain directions would be preferred by a lack of homogeneity (Batchelor (1953)).

- Stationarity

Stationarity is concerned with the time domain so that the statistics of a stationary flow can be considered to be unchanging in time. On the other hand, the statistics of a non-stationary flow exhibit a time dependence. A comparison of stationary and non-stationary flows is shown in figure 2.01.

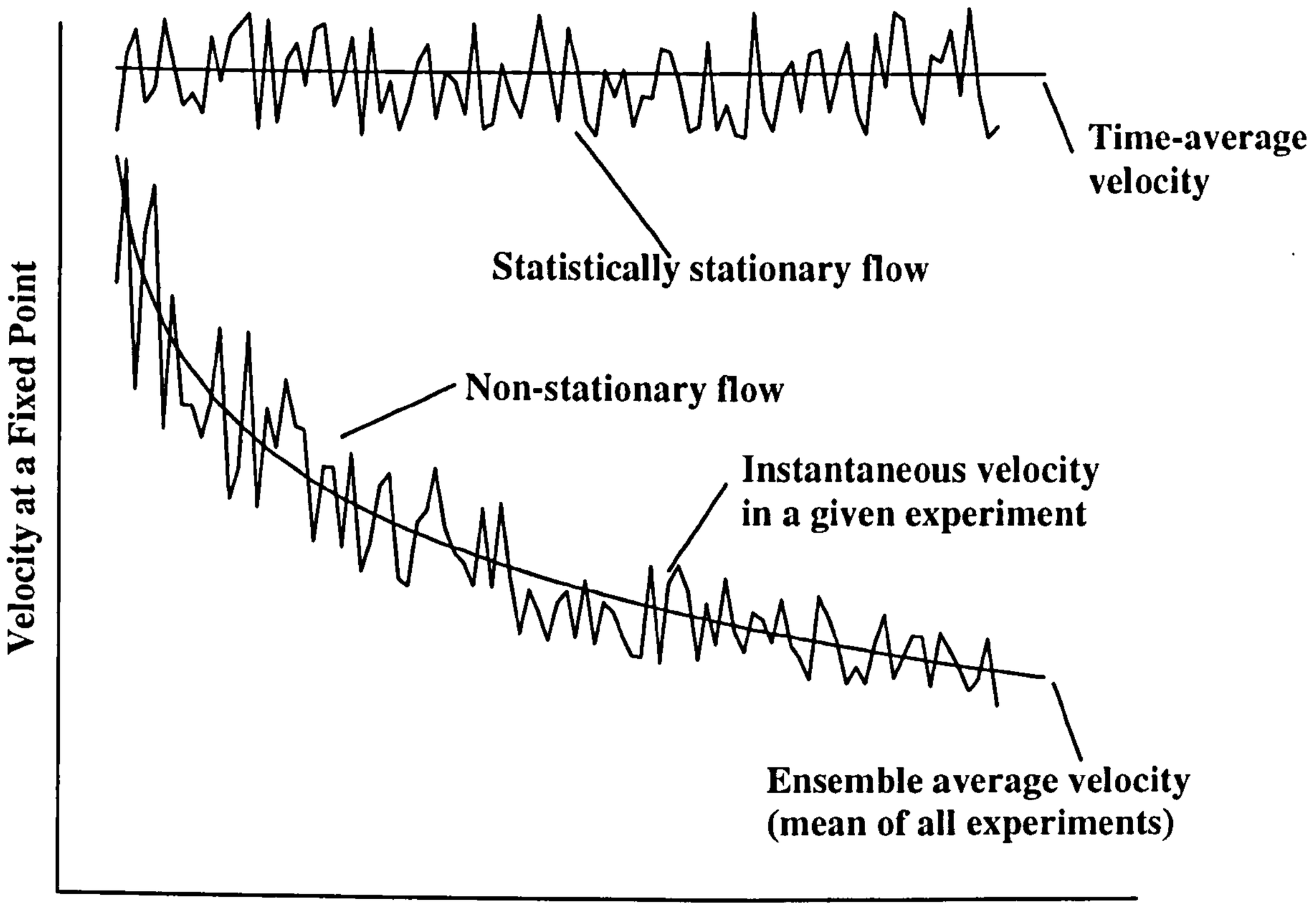

Figure 2.01 : Schematic comparison of statistically stationary and non-stationary turbulent flows.

Because of the high frequency fluctuations characteristic of a turbulent flow parameter (consider here a speed, denoted u(t)), it is necessary to formulate equations for such flows in terms of average quantities. If the flow in question is statistically stationary then the time-average is used, denoted $\overline{u}$. For more realistic, non-stationary flows a different average known as the ensemble average or expected value is used. This is not independent of time and is denoted $\overline{u}(t)$.

Some flows can be both homogeneous and stationary if small enough time and space scales are considered. Conversely, real flows are always inhomogeneous and non-stationary if large enough time and space scales are considered. Such is the poor understanding that we have of the nature of turbulent flows, it often becomes necessary to assume homogeneity and/or stationarity when studying them.

Three further statistical quantities commonly used are the variance (Var), the root mean square (rms) and the standard deviation (Sd), defined below.

$$u_{Var} = \overline{(u - \overline{u})^2} \quad , \quad u_{rms} = \left(\overline{u^2}\right)^{\frac{1}{2}} \quad , \quad u_{Sd} = \overline{[(u - \overline{u})^2]}^{\frac{1}{2}} \tag{2.03}$$

The starting point for the statistical description of turbulent flow is the division of the velocity field into mean and fluctuating components *i.e.*

$$\begin{aligned} u &= U + u' \\ v &= V + v' \\ w &= W + w' \end{aligned} \tag{2.04}$$

U,V and W represent the mean, non-fluctuating components in the x,y and z directions respectively. The high frequency turbulent components are represented by u′,v′ and w′. The time-averages of these components are zero by definition and so they do not contribute to any advective transport.

In order to be concise, suffix notation is commonly employed so that the velocity field is represented by

$$\underline{U} + \underline{u}' = U_i + u'_i \qquad (2.05)$$

where the underbar represents a vector quantity and i can take the value 1,2 or 3 (representative of the 3 Cartesian coordinate directions). The concepts and definitions introduced here in equations (2.03) to (2.05) form the basis for analysis of turbulent motions in terms of their statistical properties. We now proceed to apply this notation for the turbulent velocity field to the equations for fluid flow.

2.4 Turbulence Equations and Spectra.

In this section, equations representing the basic physical laws of fluid flow such as the conservation of mass and the application of Newton's second law of motion are applied to turbulent flows using the statistical approach described previously. Also presented are quantities particular to turbulent flows such as the turbulent kinetic energy and the intensity of a turbulent flow field. The spectral approach often adopted by scientists to describe the nature of the turbulent energy and dissipation fields is also described.

Both the continuity and the Navier-Stokes equations represent physical laws (the conservation of mass and Newton's second law of motion respectively) which will always apply to every fluid particle at any particular moment in time. Employing the above notation for the turbulent velocity field, the continuity equation is given by

$$\underline{\nabla}(U_i + u_i') = 0 \qquad \text{where} \qquad \underline{\nabla} = \left(\frac{\partial}{\partial x}, \frac{\partial}{\partial y}, \frac{\partial}{\partial z} \right) = \frac{\partial}{\partial x_i} \qquad (2.06)$$

In vector notation, the Navier-Stokes equation is given by

$$\frac{\partial \underline{u}}{\partial t} + \underline{u} \cdot \underline{\nabla} \underline{u} = -\frac{1}{\rho} \underline{\nabla} p + \nu \underline{\nabla}^2 \underline{u} + \frac{1}{\rho} \underline{F} \tag{2.07}$$

where $\nu = \mu/\rho$ is the kinematic viscosity and $\underline{F}$ represents the contribution of body forces (assumed to be zero here). Applying (2.07) to the turbulent velocity field gives

$$\frac{\partial (U_i + u_i')}{\partial t} + (U_j + u_j') \frac{\partial (U_i + u_i')}{\partial x_j} = -\frac{1}{\rho} \frac{\partial (P + p')}{\partial x_i} + \nu \frac{\partial^2 (U_i + u_i')}{\partial x_j^2} \tag{2.08}$$

Averaging (2.08), focusing on steady flow so that time derivatives drop out and with the use of the continuity equation (2.06), (2.08) may be written as

$$U_j \frac{\partial U_i}{\partial x_j} = -\frac{1}{\rho} \frac{\partial P}{\partial x_i} + \nu \frac{\partial^2 U_i}{\partial x_j^2} - \frac{\partial}{\partial x_j} \overline{(u_i' u_j')} \tag{2.09}$$

Equation (2.09) differs from that for laminar flow (2.07) by the addition of the final term. This term represents the actions of the turbulent velocity fluctuations on the mean flow. It is often large when compared with the viscous term and the final two terms in (2.09) can be written as

$$\frac{1}{\rho} \frac{\partial}{\partial x_j} \left(\mu \frac{\partial U_i}{\partial x_j} - \rho \overline{(u_i' u_j')} \right) \tag{2.10}$$

This demonstrates that the velocity fluctuations produce a stress on the mean flow. A gradient of this produces a net force on the fluid particle in the same way as a gradient of the viscous stress. The quantity involving the product of velocity fluctuations which arises from the correlation of the velocity fluctuation at the same point, is called a Reynolds stress.

So, if the turbulent notation for the velocities is substituted into the Navier-Stokes equation of incompressible motion then the result is that the usual viscous stresses

are augmented by the Reynolds stresses. They are proportional to the mean values of the squares and products of the eddy velocities and represent the turbulent flux of momentum. In any one direction there are 3 such turbulent stresses, one that acts normally (a pressure) and two that act tangentially. Thus, in total there are nine components of turbulent stress:

$$\begin{aligned} \textbf{x-direction} \quad &: \quad \rho\overline{(u_1')^2}, \rho\overline{(u_1'u_2')}, \rho\overline{(u_1'u_3')} \\ \textbf{y-direction} \quad &: \quad \rho\overline{(u_2')^2}, \rho\overline{(u_2'u_1')}, \rho\overline{(u_2'u_3')} \\ \textbf{z-direction} \quad &: \quad \rho\overline{(u_3')^2}, \rho\overline{(u_3'u_1')}, \rho\overline{(u_3'u_2')} \end{aligned} \tag{2.11}$$

Equation (2.11) represents the turbulent fluxes of momentum in the x,y and z-directions respectively. However, u_1',u_2' and u_3' are very small and fluctuate rapidly so that any accurate measurement is very difficult. Also, because of the small time scales involved, modelling would require a very short time step so that impractical amounts of computer time are required. To overcome these difficulties it has become conventional to draw an analogy between the Reynolds frictional stresses and the internal stresses in a fluid which can be described via classical fluid dynamics. It is assumed that the relatively large scale turbulent motion behaves in a similar way to molecular viscosity so that

$$\rho\overline{u_1'u_3'} = -\rho N_z \frac{\partial U_1}{\partial x_3} \tag{2.12}$$

with similar expressions for the other stress components. N_z is known as the eddy, or turbulent viscosity. Just as viscous stresses are augmented by the Reynolds stresses then molecular viscosity is augmented by the eddy viscosity. However, unlike the molecular viscosity, N_z is a property of the flow and not of the fluid.

The above argument considers only the turbulent transport of momentum and introduces the eddy viscosity which has become the most common approach in parameterising momentum transport. However, as mentioned earlier, one of the

outstanding characteristics of turbulent motion is not only its ability to transport momentum but also scalar quantities such as heat, salt and particulate matter. The rates of transfer and mixing are several orders of magnitude greater than the rates due to molecular diffusion alone (Tennekes and Lumley (1972)). An alternative way in which to view the effectiveness of turbulent flow as a mixing process is to interpret the Reynolds number of a flow as the inverse ratio of a turbulent time scale to a molecular time scale that would exist in the absence of turbulence.

Representing the quantity of a scalar s within a control volume of dimensions $\delta x,\delta y,\delta z$ in the same manner as the turbulent velocity *i.e.*

$$\mathbf{s = S + s'} \tag{2.13}$$

then the rate of change of s within the control volume can be expressed as

$$\frac{\partial \mathbf{s}}{\partial \mathbf{t}} = -\mathbf{U_i}\frac{\partial \mathbf{S}}{\partial \mathbf{x_i}} - \frac{\partial \mathbf{G_i}}{\partial \mathbf{x_i}} + \mathbf{\Sigma} \tag{2.14}$$

where the first term on the right hand side represents the advective flux, the second the turbulent flux and Σ represents any source or sink for s within the control volume. The vector G_i represents the correlation between the turbulent components and as such determines the turbulent flux of the scalar s. It is given by

$$\mathbf{G_i = \overline{u'_i s'}} \tag{2.15}$$

The three components of G_i are known as the Reynolds fluxes. As mentioned previously, the quantities u',v',w' and s' are extremely difficult to measure and so, in a fashion analogous to the eddy viscosity concept, the eddy diffusivity, or eddy diffusion coefficient K_i (i=1,3) is frequently introduced so that

$$G_i = -K_i \frac{\partial S}{\partial x_i} \tag{2.16}$$

i.e. the flux is proportional to the concentration gradient. Just as the eddy viscosity is a convenient way of parameterising turbulent transport of momentum so the eddy diffusivity is used for the transport of scalar quantities such as heat, salinity and sediment by turbulence and so its units are m^2s^{-1}. If K can be considered constant then the diffusion is known as Fickian diffusion. In the case of turbulent mixing which is being considered here, the mixing of the scalar will be dominated by the turbulent flow itself and so it is common to assume that the eddy diffusivity is the same for all scalars, unlike its molecular counterpart.

The eddy diffusivity assumption introduced here is again a reflection of our limited understanding of the nature of turbulent flow. By using an effective diffusivity, turbulence is frequently treated as a property of the fluid and not of the flow. This approach is potentially dangerous but is the only way in which to make the mathematics of the problem tractable.

U_i describes the mean motion of the fluid whereas u'_i describes the turbulent velocity fluctuations about the mean. The amplitude of the turbulent velocity field is defined as

$$\overline{(q^2)}^{\frac{1}{2}} = (\overline{u'^2_1} + \overline{u'^2_2} + \overline{u'^2_3})^{\frac{1}{2}} \tag{2.17}$$

This quantity is directly related to the kinetic energy density associated with the velocity fluctuations (TKE)

$$TKE = \frac{1}{2}\rho\,\overline{q^2} \tag{2.18}$$

Further understanding of the interaction between the mean flow and the turbulent flow can be gained from an examination of the TKE budget. For steady flow in

homogeneous water, this is given by (Tritton (1977)).

$$\frac{1}{2}U_j\frac{\partial(\overline{u'^2_i})}{\partial x_j} = -\overline{u'_i u'_j}\frac{\partial U_i}{\partial x_j} - \frac{1}{\rho}\frac{\partial}{\partial x_i}(\overline{p' u'_i}) - \frac{1}{2}\frac{\partial}{\partial x_j}(\overline{u'^2_i u'_j}) + \nu\overline{u'_i\frac{\partial^2 u'_i}{\partial x_j^2}} \qquad (2.19)$$

Equation (2.19) amounts to a statement of energy conservation for the turbulent velocity fluctuations and the terms can be interpreted as follows.

1) Transfer of TKE by the mean flow (advection).

2) The production of TKE by shear in the mean flow.

3) Transport of TKE by turbulent pressure gradients.

4) Another transport mechanism for TKE, this time by turbulent convection. These turbulent transfer terms represent the transport of TKE from low to high wavenumbers where it is eventually dissipated as heat.

5) Transformation of TKE to heat plus an additional small amount of energy diffusion by the working of viscous stress fluctuations.

The transfer of TKE, originally derived from the shear in the mean flow down to molecular scales where it is dissipated as heat has come to be known as the energy cascade and was first introduced by Kolmogoroff (Kolmogoroff (1941)).

The cascade concept is based on a representation of turbulent energy in terms of a spectrum or spectral energy density function which expresses the distribution of TKE with wavenumber or frequency. A number of different forms of the spectrum are possible so here we shall briefly discuss those forms which are most useful to us in the present study.

$E(\underline{k})$ is known as the 3-d energy density spectrum and it is found by taking the Fourier Transform of the autocorrelation function $R(\underline{x})$.

$$E(\underline{k}) = \frac{1}{(2\pi)^{1/3}} \int_{-\infty}^{\infty} e^{i\underline{k}\underline{x}} R(\underline{x})\, d\underline{x} \qquad (2.20)$$

where $\underline{k}$ is the 3-d wavenumber and $d\underline{x}$ is a volume element in 3-d space (=dxdydz). $R(\underline{x})$ is the spatial correlation function. A non-zero value means that two quantities are not independent of each other.

In order to calculate R(x) and thus E(k), an instantaneous measurement of u(x) as a function of position is required. This is extremely difficult. It is easier to measure a time series u(t) and to invoke G.I.Taylor's *frozen field* hypothesis. Essentially, it is assumed that the speed of the measurement platform is sufficiently fast so that the turbulence field can be assumed to be "frozen" and that it does not change during the measurement. This means that, although recording a time series, it is possible to convert to a spatial series *i.e.* the turbulent fluctuations at a point are described by the advection of a frozen field past that point *i.e.*

$$\frac{\partial u}{\partial z} = \frac{1}{w} \frac{\partial u}{\partial t} \qquad (2.21)$$

where w is the speed at which the measurement platform is moving through the turbulent field in the z-direction.

At low wavenumbers *i.e.* large wavelengths, where the scale of the turbulent motion can be as large as the physical dimensions constraining the mean flow, much of the turbulent kinetic energy is to be found. In this region of the spectrum the structure of the turbulence is determined by the mean flow itself and hence the turbulence is strongly anisotropic. However, as the scale of the motion decreases the turbulent velocity field can be considered to be homogeneous and isotropic since it becomes decoupled from the mean flow. This is important since any results obtained in this lower energy regime can be considered as typical of turbulence in itself, rather than turbulence derived from a particular flow. This assumption is a descriptive form of

the Kolmogoroff hypothesis (Kolmogoroff (1941)).

When contemplating measurement of the turbulent velocity field the quantity most often used is the 1-d energy spectrum function $\phi(k)$ (where k is now the 1-d wavenumber). This is because its 3-d counterpart cannot be measured. However, if isotropy is assumed then $\phi(k)$ can be expressed in terms of the turbulent velocity fluctuation (Monin and Yaglom (1975)).

$$\int_0^\infty \phi(k)\,dk = u'^2_1 \tag{2.22}$$

When the scale of the motion becomes sufficiently small for inter-molecular forces to become important the TKE is dissipated as heat (so that the majority of energy dissipation occurs at high wavenumbers). The spectrum of the dissipation $D(\underline{k})$ is given by (Tennekes and Lumley (1972)).

$$D(\underline{k}) = 2\nu \underline{k}^2 E(\underline{k}) \tag{2.23}$$

We can calculate ϵ, the dissipation rate per unit volume (W/m^3) by integrating $D(\underline{k})$ over the complete range of wavenumbers. Unfortunately, it is impossible to measure the 3-d dissipation spectrum directly. However, via the assumption of isotropy it is possible to relate ϵ to the 1-d dissipation spectrum ($k^2\phi(k)$) so that (Monin and Yaglom (1975))

$$\epsilon = 7.5\,\mu \int_0^\infty k_3^2 \phi_{11}(k_3)\,dk_3 \tag{2.24}$$

where μ is the dynamic viscosity of sea water, k is the 1-d (z) wavenumber and $\phi(k)$ is the 1-d (x) spectrum function as introduced earlier. It is possible to measure the 1-d dissipation spectrum since its interal over k is equivalent to the variance of the horizontal velocity shear signal *i.e.*

$$\epsilon = 7.5\,\mu\overline{\left(\frac{\partial u}{\partial z}\right)^2} \qquad (2.25)$$

This result means that, by monitoring the horizontal velocity shear, it is possible to calculate the turbulent dissipation rate per unit volume. This is the approach adopted for the results presented later in this thesis.

In order to more easily visualise where most of the TKE lies and where it is dissipated within the wavenumber spectrum, figure 2.02 shows typical 1-d dissipation and energy spectra.

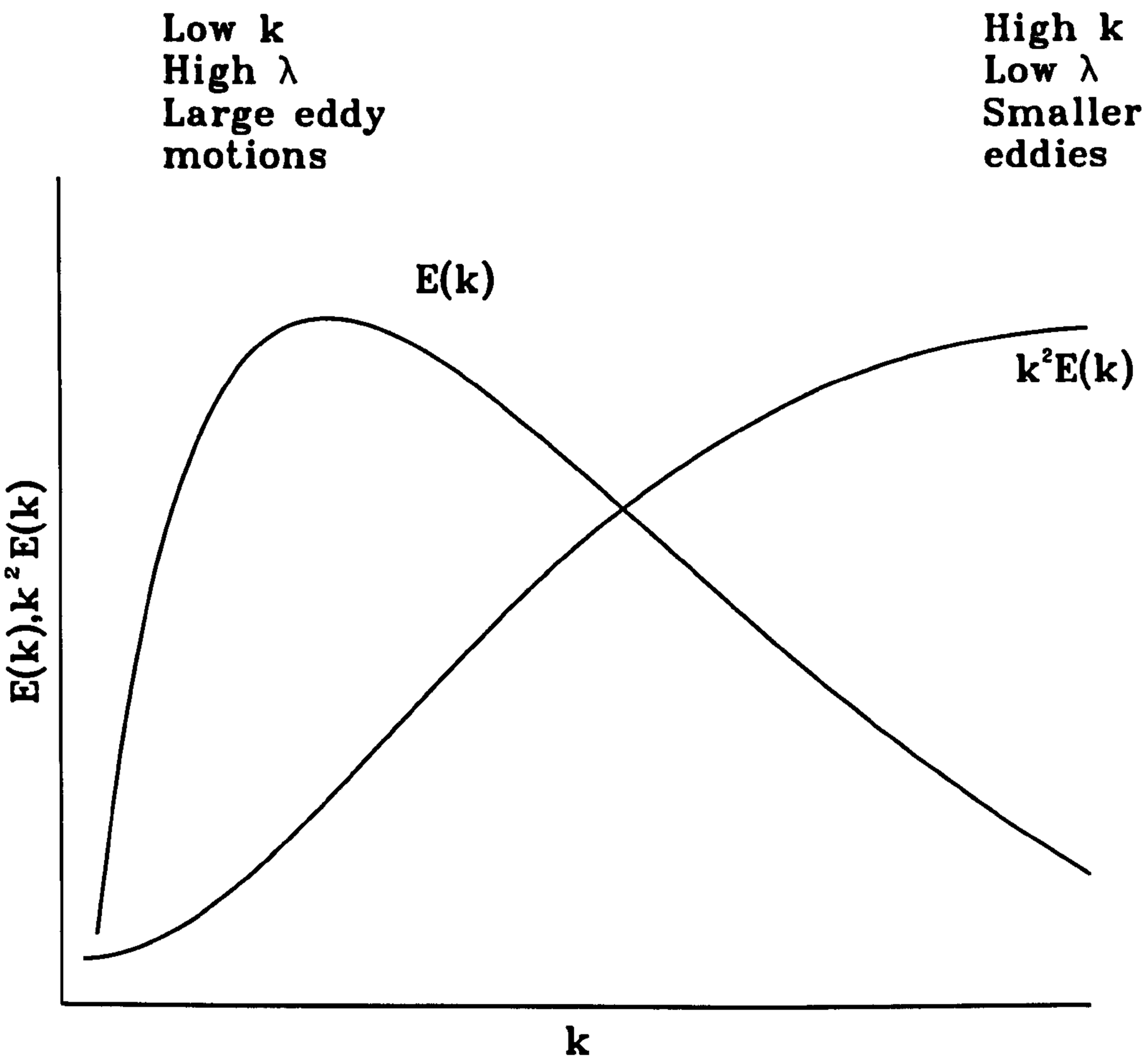

Figure 2.02 : Typical energy and dissipation spectra.

Figure 2.02 shows that the majority of the TKE is dissipated at high wavenumbers (low wavelengths) and that most of the energy is indeed contained within the large scale eddy motions. The small dissipative eddies are generated from the larger ones. At first, the energy fed into the turbulent field (from shear in the mean flow) goes primarily to the large eddies from which smaller and smaller ones are generated. This is achieved via the process of vortex stretching. The turbulent velocity field interacts with itself so that eddy motions, in response to an accelerating flow in one direction, contract in another direction in order to conserve mass. The result of this is a transfer of energy to ever smaller scales, known as the energy cascade.

For wavenumbers large compared with those at which energy production occurs $E(\underline{k})$ depends only on the wavenumber, dissipation rate and the viscosity so that

$$\mathbf{E = E(k,\epsilon,\nu)} \tag{2.26}$$

If the energy cascade is sufficiently long (*i.e.* it extends through several decades of k) then the energy production (at low k) and dissipation (at high k) regions are separated by an intermediate range where the action of viscosity is not felt. Dimensional analysis can then be used to arrive at the conclusion that

$$\mathbf{E(\underline{k}) = A\,\epsilon^{\frac{2}{3}}\underline{k}^{-\frac{5}{3}}} \tag{2.27}$$

where A is the Kolmogoroff constant, approximately equal to 1.5 for all turbulent flows (Kundu (1990)).

Equation (2.27) is the spectrum for the inertial subrange and is usually called the Kolmogoroff $k^{-5/3}$ law. This region of the spectrum is so-called because the only transfer of energy from small to large wavenumbers is by inertial forces. In the inertial subrange, $E(\underline{k})$ is dependent only on $\underline{k}$ and ϵ and not ν which is the case at larger wavenumbers where the energy is dissipated. A schematic energy spectrum is shown in figure 2.03.

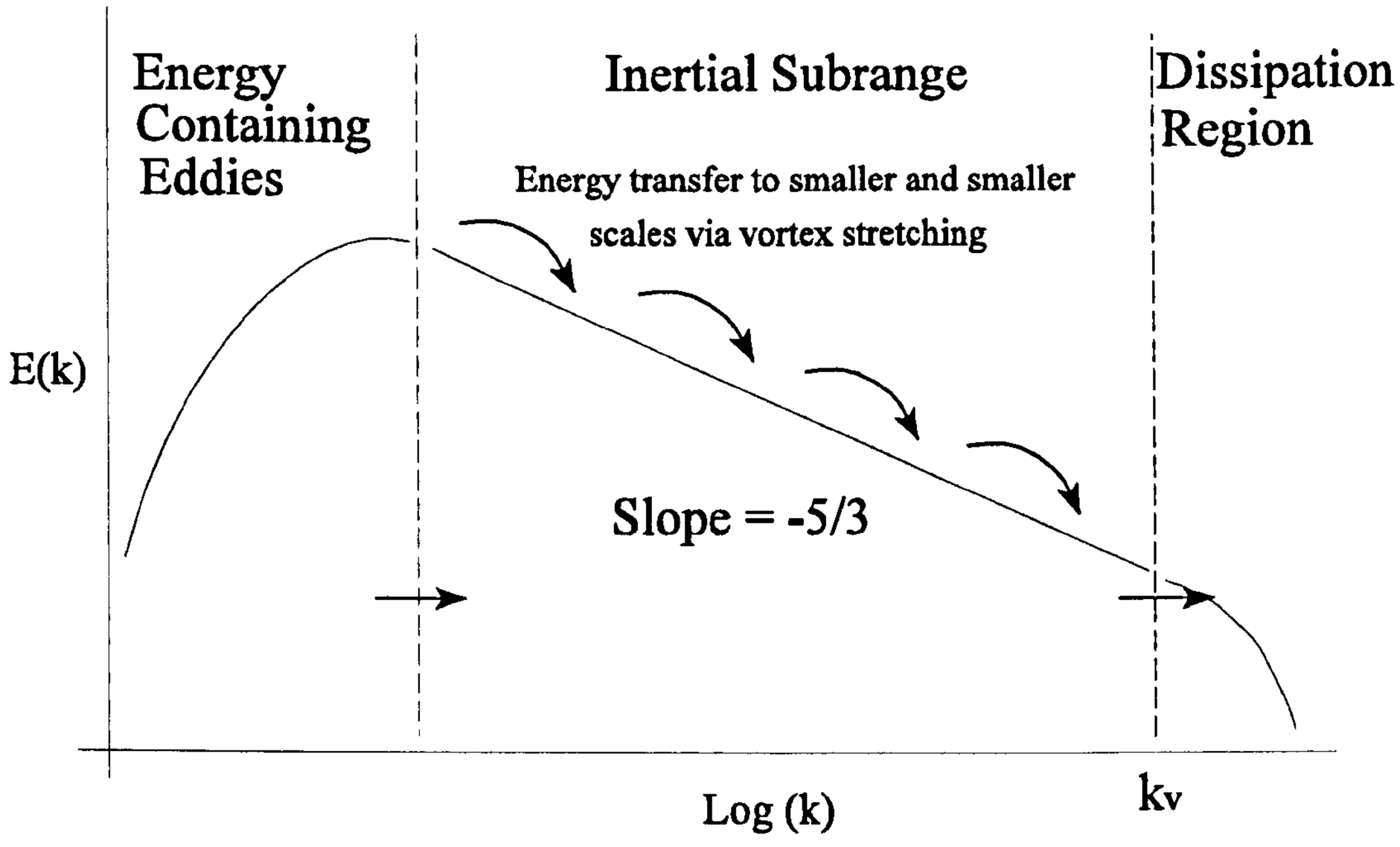

Figure 2.03 : Schematic energy spectrum.

The length scale (η) and turbulent velocity (v) at which dissipation becomes important (*i.e.* at k_v) are known as the Kolmogoroff microscales and are given by

$$\eta = \left(\frac{\nu^3}{\epsilon} \right)^{\frac{1}{4}} , \quad v = (\nu \epsilon)^{\frac{1}{4}} \tag{2.28}$$

The Reynolds number at these microscales is equal to unity. If the viscosity of the fluid is decreased then the length scale η is increased and k_v increases so that the 'roll-off' into the dissipation region moves to a higher wavenumber.

2.5 Turbulence Measurements.

Measurement of turbulent flows in the ocean are generally difficult because of the

high frequency and small scales of the turbulent velocity field. Turbulent fluctuations in velocity occur over a wide range of spatial and temporal scales and must be distinguished from the mean flow upon which they are superimposed. Thus, to measure turbulent velocity fluctuations, the velocity sensitive element must have small size, high sensitivity and good high-frequency response (Grant *et al.* (1961)). Added complications include the fact that turbulence is a three-dimensional phenomenon and it displays a high degree of intermittency both in time and space. All of the above criteria cannot usually be met by a single instrument so that a trade off has to be made. In the past the only viable observations were those made at a single height close to the bed. Such velocity measurements are commonly made using any of three different instruments.

One of the most obvious approaches to measuring current velocity is via flow induced rotation of either a single impellor or a three to four cup vane. However, only the very smallest devices are suitable for turbulence observations as they usually have a diameter of 1cm or larger. Such devices are frequently used in regions of high energy, usually in estuaries or on beaches where wave motion may also be under study (Soulsby *et al.* (1984)). The principal disadvantage of such instruments is that they are confined to a single height above the bed as they are mounted on a frame which usually restricts their use to within the bottom boundary layer. In order to measure the velocity they have to integrate over a finite period of time so that the higher frequency turbulent fluctuations cannot be measured. Also, they are capable of measuring only a single component of the flow and, as they rely on mechanical motion, they are vulnerable to damage, especially in the high energy environment of the bottom boundary layer. Their main advantage is that they are relatively cheap instruments.

A more common instrument is the electromagnetic flowmeter which has been in use since the 1950s. A magnetic field is produced and the water flowing through the field, acting as a moving conductor has an emf induced in it. The potential differences between diametrically opposed electrodes are measured giving output

proportional to the water velocity so that more than one component of the flow can be measured by a single instrument. Bowden and Fairbairn (1956) measured two components of flow at 50cm and 175cm above the bed allowing calculation of the Reynolds stress. The electromagnetic instrument has an advantage over the propeller current meters of having no moving parts thus making it more robust and able to withstand the often high stresses placed upon it. It also has a superior frequency response. However, these instruments are often rather large in the context of turbulent motion and so are unable to measure the smallest scales of motion. Again, they are confined to a single height and tend to be used exclusively near the bed, mounted on frames which can themselves affect the flow under investigation as can the current meter itself which can induce flow separation. Unless mounted as an array, only two-dimensional measurement is possible.

Based on measurements of atmospheric turbulence, the hot-film flowmeter has been successfully developed for measurements of oceanic turbulence. It is based on the principle of heat loss from a heated wire or film to the surroundings. Such an instrument has a superior size and frequency response compared with propellers or electromagnetic meters. The flowmeter can be towed behind a ship at the desired depth and measures the downstream component of turbulence. Grant *et al.* (1961) measured turbulence spectra in a tidal channel by towing such an instrument behind a ship at a depth of 50 feet. They were able to measure turbulence in both the inertial and dissipation subranges. The principal drawbacks to using such an instrument are its fragility (of the wire or film elements), uncontrolled variation in heat loss due to progressive build up of foreign particles and probe vibration which can restrict the frequency range of operation.

In addition to impellors, electromagnetic and hot film devices, recent developments have allowed laser velocimetry and ultrasonic techniques to be applied to turbulent flows. However, both techniques are still in their infancy and are currently very expensive.

A recent and proven technique for the measurement of turbulence is to use a sensitive shear probe to measure the vertical shear in the water column (Simpson (1972), Osborn and Crawford (1980), Dewey *et al.* (1987)). This needs to be achieved on a scale of centimetres (Osborn and Crawford (1980)) using a free fall probe since any coupling to a ship or other measurement platform would render shear measurements useless. Such a probe can be extremely small and recent advances in piezoelectric and ceramic materials science coupled with improved electronics and signal processing techniques means that very high resolution data can be obtained. By allowing the probe to free fall through the water column the cross-wise component of turbulence through the entire water column can be profiled. Given the high intermittency displayed by turbulent flow a high temporal and spatial resolution is required if any overall appreciation of the nature of the flow field is to be obtained. It is this approach that has been most successful in recent years (Dewey and Crawford (1988), Crawford and Dewey (1988), Crawford (1992)) and such an instrument has been used for the purpose of this study.

CHAPTER THREE

Shelf Sea Sediment Dynamics

3.1 Introduction.

The vertical distribution of suspended sediment (also termed seston or suspended particulate matter-SPM) in shelf seas depends on many factors such as the nature of the sediment source, the tidal regime, meteorological conditions and the season. As a result, SPM concentrations fluctuate at many different frequencies. Long term transport occurs over many years and tidal resuspension usually every six hours whereas turbulent signals have a much shorter period so that concentrations vary over time scales ranging from years to seconds. Present day understanding of the effects that the above factors have on SPM concentrations is largely empirical, especially for cohesive sediments which dominate in the marine environment. The relevant processes determining concentrations of SPM can be divided into four categories : erosion (resuspension), deposition and consolidation, transport and the nature of the sediment population itself.

What follows in this chapter is a review of present day understanding of the above processes as well as the current status of SPM concentration measurement techniques. Recent advances in computing power have made mathematical modelling of the effects of these processes on SPM levels more accessible. In the final section of this chapter some of these models and their limitations are discussed.

3.2 The Origin and Composition of Shelf Sea SPM.

The SPM population found in shelf sea waters is usually composed of several individual populations from a number of diverse sources. The particles also vary widely in composition, size and shape. In general, inorganic particles in suspension range from clays which tend to be flat and platelike to fine sands which are more

rounded *i.e.* from <1μm up to 63μm diameter for the sand fraction. Sources of inorganic particles include coastal erosion, river runoff and erosion of terrigenous sea bed sediments so that the concentration of such particles tends to decrease with increasing distance from land. Levels of organic particles on the other hand tend to depend more upon the seasonal cycle. Such particles include phytoplankton, zooplankton, bacteria, yeasts and fungi and can be both living or detrital matter. Another significant contribution to the total suspended matter load is from anthropogenic sources. This population is derived from discharges of sewage and industrial wastes and so has become more important in recent times as the burden placed upon the world ocean by a developing and expanding global population has increased.

In addition to the SPM populations described, flocculation results in new sediment fractions as the particles adhere to each other, altering the nature of the SPM population. Physical, biological and chemical interactions are all common sources of flocculation. These new larger particles ('flocs') may then settle to the bed or may be broken up into their original constituent parts.

In attempting to increase our understanding of SPM dynamics, it becomes apparent that the nature of the sediment population and the interactions within it are a major source of difficulty. Both the ocean floor and the sea water itself are very productive media for marine flora and fauna so that biological influences are many and play an important role in the production, supply or modification of SPM. Thus, not only is it necessary to understand the physical aspects of the situation but to consider biological, geological and chemical effects also.

3.3 Sediment Deposition.

This is parameterised by the settling velocity, denoted w_s and is determined by a combination of factors. A particle will move under the influence of gravity if its

density is different to that of the surrounding fluid. The settling velocity is then the terminal velocity attained by the particle, which occurs when the gravitational force balances the drag force. The terminal velocity will depend upon the density difference between the particle and the water, the viscosity (and thus temperature) of the water and the particle size and volume. Considering only viscous forces, Stokes (using the Navier-Stokes equation) derived an expression for the drag force on a spherical particle falling through a viscous fluid at terminal velocity ($F=3\pi\mu D w_s$), leading to (by balancing F against the immersed weight)

$$w_s = \frac{\rho_s - \rho}{\rho} \frac{g D^2}{18 \nu} = \frac{(\rho_s - \rho) g D^2}{18 \mu} \qquad (3.01)$$

where ρ_s is the sediment density and μ is the molecular viscosity of water. Experiments have shown that Stokes' Law is only successful for spherical particles with diameters smaller than ≈0.1mm. This is because only viscous forces were considered when equation (3.01) was formulated so that it is only applicable in the viscous regime. The law ultimately fails because it does not take into account boundary layer separation which occurs at high Reynolds numbers, when the drag force experienced by the particle is proportional to the square of the velocity rather than to the first power as in the Stokes' relationship.

Two further factors affecting the settling velocity of a particle are its shape and the total particle concentration. Stokes' Law assumes spherical particles which is rarely the case. Large flat particles have lower settling velocities than long thin particles due to larger drag. Shape effects are often combined into empirical relations via the use of a shape factor such as the Corey shape factor (Corey (1949)), the Janke shape factor (Janke (1966)) and the Wadell sphericity which is based on the ratio of the surface area of a sphere with the same weight as the particle to the actual surface area of the particle. If the concentration of particles is sufficiently high (≈10kgm^{-3} (McCave (1984)) then particles will interact through differential setting and hindered settling may result so that at sufficiently high concentrations, the settling velocity is

also a function of concentration.

Equation (3.01) considers static fluid only. In reality the fluid is usually exerting additional forces upon the particles and the vertical structure of the water column will also affect particle motion. Turbulence, produced at the bed by the current flowing over it plays a major role in determining the vertical distribution of SPM, especially if the particles are small. In order to obtain the net vertical particle flux it is necessary to superimpose the settling flux for a static fluid on the turbulent velocity field which will transport sediment both up and down the water column.

A further complication to be considered is that due to flocculation (also termed aggregation). The settling velocity distribution of a sediment population will alter as its size distribution alters. Particles can flocculate in two ways. The first method is by adhering together because one or both of the particles is covered in a biogenic film. This is known as bioflocculation and is the dominant process when considering particle interactions on the bed. The second method takes place between clay particles. These tend to be platelike and less than 2μm in diameter and, generally they carry a negative charge. This attracts the positive ions in the seawater, reducing the electrostatic (repulsive) force between particles so that the molecular (attractive) Van der Waals force dominates, resulting in flocculation. These inter-molecular forces act only over very short distances and so processes such as Brownian motion, fluid shear and differential settling are required to bring the clay particles close enough together for flocculation to take place. The bonding between particles resulting from interaction via the rather low energy processes of Brownian motion and differential settling tend to be weak and flocs are easily broken up by turbulence whereas aggregation as a result of fluid shear produces stronger flocs. However, fluid shear is also an effective process for breaking up aggregates.

3.4 Sediment Erosion and Resuspension Rates.

Four different types of erosion have been identified (Mehta (1991)). These are surface erosion, where particles or aggregates are removed as a result of the weakening of the bonds between particles and the sediment surface, mass erosion where large parts of the bed are torn away, bed fluidisation where the mud changes from being particle supported to a fluid supported slurry and the entrainment of fluidised mud. All but the first of these mechanisms operate only in high energy (shallow) environments and hence only surface erosion need be considered here.

In the study of erosion there are two quantities of interest: the threshold for erosion *i.e.* the minimum stress that must be applied to move the sediment off the bed and the erosion rate (or rate at which sediment is removed from the bed) after the erosion threshold has been exceeded. The erosion threshold has been extensively researched and a good formulation exists for the prediction of the erosion threshold for non-cohesive sediment consisting of spherical grains larger than approximately 1mm. The erosion rate is much less well known although several relationships have been proposed linking erosion rates to the properties of the overlying flow.

The quantity most commonly used to describe the potential that a certain flow has for the erosion of sediment is the bed shear stress τ_b, with the value for the onset of erosion given by τ_c and known as the critical bed shear stress. For the more dominant cohesive sediments there are two critical stresses. The first and largest of these is the stress required to erode a particle from the bed. The second is the value of the bed shear stress that allows deposition of a particle already in suspension. For a non-cohesive sediment these two quantities are considered to be the same.

Fundamentally, the bed shear stress is given by one of the Reynolds stresses. However, as they are almost impossible to measure accurately, the bed shear stress for a particular flow is commonly determined by assuming that the velocity profile can be described by the von Kármán-Prandtl velocity profile given by equation

(2.02), so that for a plot of u against ln(z) for velocity measurements made within the log layer, a line of slope (u_*/κ) and intercept $-(u_*/\kappa)\ln(z_0)$ results, allowing calculation of u_*. This can then be used to calculate τ_b using the equation

$$\tau_b = \rho |u_*|^2 \tag{3.02}$$

Another common method for predicting the bed shear stress is through a quadratic friction law

$$\tau_b = \rho C_D u^2 \tag{3.03}$$

where u is an available *i.e.* measured or predicted velocity (averaged over turbulent variations) and C_D is the dimensionless drag coefficient dependent on the roughness of the bed. For sediment studies, velocity measurements are usually made at a height of 1m.

The erosion of non-cohesive sediments is, empirically at least, fairly well known. The most significant result in this area was obtained by Shields in 1936 whose entrainment function is well-known:

$$\Theta = \frac{\tau_b}{(\rho_s - \rho) g D} \tag{3.04}$$

When Θ represents the threshold condition for entrainment it is known as the Shield's criterion, Θ_r. The Shields diagram is a plot of this quantity versus the grain Reynolds number of the flow. Such a diagram, based on the work of others as well as Shields is shown in figure 3.01. Other workers have extended this empirical result to a greater range of Reynolds numbers.

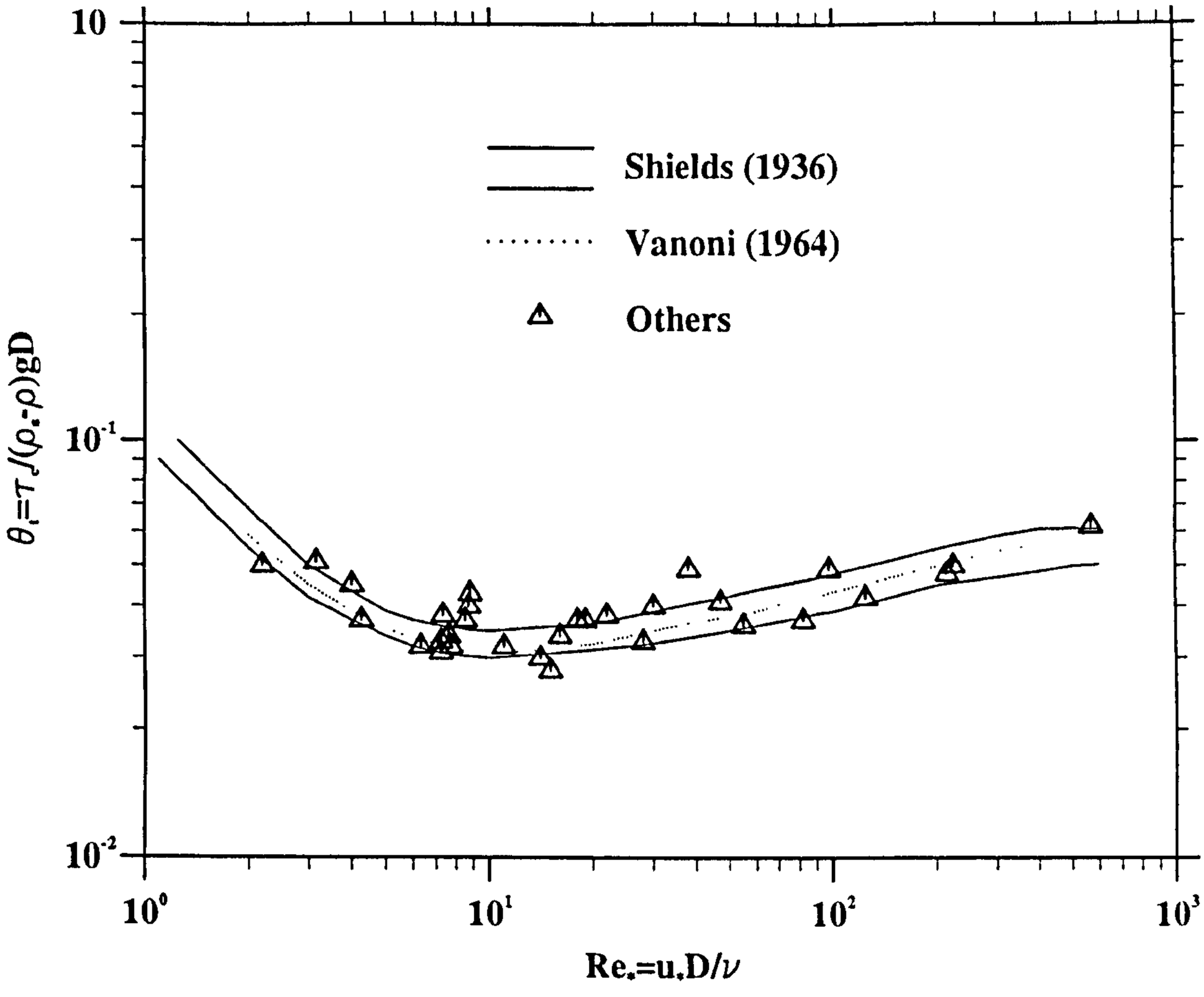

Figure 3.01 : The original Shields threshold curve of the grain Reynolds number Re_* versus the Shields threshold criterion θ_t along with some results from later investigators (Miller *et al.* (1977)).

Many different sediment threshold relationships exist but none are general and all are limited to certain water and grain densities. It is generally accepted that the Shields curve is adequate for calculating the entrainment velocity for sediments that are cohesionless, well sorted and situated on flat, planar beds (Sternberg (1971), Drake and Cacchione (1986)). It is impossible to predict the critical erosion threshold solely from particle size unless the sediment is non-cohesive (McCave (1984)). Measurements to establish a threshold criterion for cohesive sediments have been much less successful than those for non-cohesive sediment populations and there still exists much ambiguity as to the nature of the threshold. Some authors (Lavelle and Mofjeld (1987)) question the very existence of a threshold given that as long as a flow

is turbulent, there will exist bursts capable of lifting sediment from the bed, even if the mean flow does not possess enough energy. Several authors find no minimum bed shear stress for observable transport. However, the Shields formulation is the most widely used and the term threshold is usually taken to imply motion of the bed and not of single particles.

When erosion of the bed has commenced then the particles are being transported by the flow. Sediment transport can be sub-divided into two main categories : bedload and suspended load. By far the most efficient of these is suspended load transport which occurs when the vertical component of the turbulent velocity is sufficient to overcome the effects of gravity. After the particle has been resuspended it is carried along at the speed of the flow.

Transport as bedload can be divided into a further three categories namely sliding, rolling and saltation when the particles move in a series of short hops and jumps along the bed at a fraction of the flow speed (Bridge and Dominic (1984), Francis (1973)). This is the most common bedload transport mechanism. Grains transported as bedload are thus supported by both fluid and solid transmitted stresses. The fluid transmitted stresses are due to turbulence and they become more important as pure suspended load transport is approached. Generally, grains of sand size and larger tend to be transported as bedload and the suspended load tends to consist of the fine silts and clays with which this study is concerned.

After erosion of the bed has started then the quantity of interest becomes the erosion rate, defined as the mass of sediment eroded per unit bed area per unit time as a function of the bed shear stress in steady turbulent flows (Mehta (1991)). As bed shear stress increases then so does the quantity of sediment in suspension unless there is no more resuspendable sediment on the bed at which point the levels of SPM become source-limited. The erosion rate will only increase with increasing bed shear stress if the erodibility of the bed remains constant or falls so that the history of formation of the bed plays an important role in its erodibility.

Generally, the equation used to describe the erosion rate depends upon whether or not an erosion threshold is being used. While some authors have used a power law, the majority of workers employ a threshold condition and use a linear equation (McCave (1984), Teisson (1991)). If the critical shear stress has been exceeded by the bed shear stress then erosion is occuring at a rate given by

$$E = \alpha \left(\frac{\tau_b}{\tau_c} - 1 \right) \tag{3.05}$$

where α is the erosion rate constant. Lavelle *et al.* (1984) did not consider a threshold shear stress and their equation takes the form of a power law:

$$E = \alpha \, | \tau_b |^n \tag{3.06}$$

A wide range of values for the constants α and n have been reported, indicating a site dependence of erosion rate which is to be expected since E is a function of bed composition and history. It is clear that there are many parameters determining the erodibility of a sediment structure. These include the composition of the sediment population so that factors that need to be considered include the particle size distribution, the level of organic matter and the population mineralogy (Mehta (1991)). Also important is the composition of both the pore and eroding fluids. Properties such as cation concentration, pH, salinity and temperature all affect the erosion characteristics of the bed.

Biological effects can be the most important single factor affecting bed erodibility (McCave (1984)) as they can both bind together or destabilize sediment populations. Organisms can also affect the entrainment of sediment by influencing the properties of the boundary layer flow and the nature of the bed. Jumars and Nowell (1984) identify four mechanisms by which biological activity can influence the erodibility of the bed. Benthic organisms can influence the fluid momentum impinging on the bed since mounds, pits and tracks can cause local enhancement of the fluid velocity

field. Also, they can affect the particle exposure to the flow, the adhesion between particles as they often excrete mucous films and/or rework the sediment and the particle momentum since filter feeding organisms remove fine sediment and return it to the bed in the form of larger faecal pellets.

Only qualitative results have emerged on the effect of biological activity on bed stability. Since most biological activities involve the production of mucous films, this is likely to be the most important effect of biological activity on bed erodibility (Dyer (1986)).

3.5 SPM Measurements.

Only in recent years has instrumentation technology advanced sufficiently to allow reliable, high frequency measurement of SPM concentrations to be made. Originally, the only available method for measuring sediment concentration was to collect and filter samples, a time consuming process. This resulted in extremely limited spatial and temporal coverage. *In situ* SPM concentration measurements are now almost exclusively made using either acoustic or optical systems. This section will present a short review of the more commonly used instruments.

The use of an optical system to determine SPM concentrations relies on a measurement of the extinction or backscatter experienced by a collimated beam of light. One such instrument is the transmissometer (Bartz *et al.* (1978)) which is used as part of this study and described in chapter five. With careful calibration, transmissometers are capable of measuring SPM concentrations as low as a fraction of a milligram per litre. Technological advances also mean they are capable of high frequency operation, storage of large quantities of data and high accuracy. They are equally well suited to deployment at a single depth on a mooring or as a profiling instrument mounted on a CTD frame. The principal disadvantage of the transmissometer is that it is only capable of monitoring SPM concentrations at a

single height above the bed unless used in profiling mode which necessitates the presence of a ship. They are also prone to fouling by biological matter which can grow on the instrument housing and interfere with the light path. This problem is especially acute during summer. Transmissometers are, however reliable and relatively cheap instruments. Another optical approach is that adopted by the optical backscatter sensor (OBS) which measures the backscattered signal as opposed to the transmitted fraction. OBS's have poorer resolution than transmissometers and tend to only be used in regions of high turbidity. A major disadvantage of both these instruments is that they provide no information regarding the sediment size distribution.

In recent years acoustic methods for monitoring SPM concentrations have been developed. They rely on the backscattered acoustic signal as a measure of the turbidity. They have an advantage over the optical systems described above in that they are capable of taking measurements from several heights above the bed, where they are usually deployed. Also, by using several acoustic frequencies, acoustic backscatter (ABS) devices can theoretically measure the size of the sediment in suspension. The ABS device was developed for measuring sediment concentrations in the bottom few meters of the water column. They can now provide provide good temporal (≈0.1s) and spatial (≈1cm) resolution and with further development are potentially very powerful (Thorne *et al.* (1991)). However, conversion from acoustic backscatter into SPM concentrations is not trivial and the best approach at present would seem to be the use of several sensors in conjunction.

Another acoustic approach has been to use Acoustic Doppler Current Profiler (ADCP) data. In addition to its primary function of monitoring the current speed, the ADCP also measures the strength of the acoustic backscatter from which SPM concentrations may be inferred. This technique is recent but has shown significant potential (Jones *et al.* (1994)).

The role of remote sensing in the determination of oceanographic parameters has

increased in recent years as technology has advanced and the excellent spatial coverage afforded by satellite systems has been recognised. Indeed, remote sensing techniques provide the only viable means for routine monitoring of large water bodies (Prangsma and Roozekrans (1989)).

Information regarding SPM concentrations can be obtained via measurement of subsurface reflectance. The most popular systems for such measurements are AVHRR (Advanced Very High Resolution Radiometer) and CZCS (Coastal Zone Colour Scanner) and to a lesser extent the Landsat MSS and French SPOT systems as they have poorer temporal coverage (Landsat passes over only once every 16 days). AVHRR is mounted on the NOAA TIROS-N platforms and has two visible channels providing daily coverage. Algorithms have been developed to calculate the total suspended matter (TSM) from atmospherically corrected water column reflectance (Prangsma and Roozekrans (1989), Spitzer *et al.* (1990)). However, these algorithms change with both location and season and tend to be as diverse as the environments they attempt to describe (Topliss *et al.* (1990)). Additionally, each radiometer is different and requires its own calibration.

In all cases where remotely sensed data is used to infer TPM concentrations, extensive *in situ* measurements over a large range of concentrations are required in order to accurately calibrate the radiometer. Despite disadvantages such those already outlined and others including the persistent problem of cloud cover, the lack of any depth information and the relatively low frequency sampling rate, such an approach has proved useful for monitoring long term changes in TPM concentrations over a wide area (Weeks and Simpson (1991), Boudjelas (1994)). The variation in the spectral characteristics of the upwelled visible light from different sediment populations provides information concerning the sediment properties as well as concentrations. Topliss (1986) used both Landsat and *in situ* data to determine the nature of the suspended sediment population and Stumpf (1988) was able to distinguish between suspended sediments from different rivers entering Chesapeake Bay using Landsat, AVHRR and *in situ* data.

3.6. Sediment Dynamics Modelling.

Previously, the majority of sediment modelling studies have concerned themselves with the prediction of a total sediment transport rate as researchers have concentrated on long term processes. However, the interest here is in the resuspension and depositional processes in a tidal current and so such models are of limited interest. Hence, a vertical process model is more applicable for this study.

Balancing the upward turbulent diffusive flux of sediment with the downward settling flux we have for the rate of change of sediment concentration in a horizontally uniform flow

$$\frac{\partial c}{\partial t} = w_s \frac{\partial c}{\partial z} + \frac{\partial}{\partial z}\left(K_z \frac{\partial c}{\partial z} \right) \tag{3.07}$$

where w_s is the sediment settling velocity, c is the concentration and K_z is a vertical diffusion coefficient for sediment. If we assume steady state conditions, constant K_z and no net deposition or erosion of sediment then the solution to (3.07) is given by

$$c = A\, e^{-\frac{w_s}{K_z} z} \tag{3.08}$$

where A is a constant. To calculate A a bottom boundary condition is required. This will usually take the form of a reference concentration or a pick-up function.

If employing the reference concentration approach, the bottom boundary condition (BBC) takes the form of a sediment concentration (c_{ref}) at a known height above the bed (z_{ref}). Frequently, this height is taken to be twice the diameter of the grains on the bed or z_o, the bed roughness. c_{ref} is usually calculated from the bed shear stress. Several formulations for c_{ref} exist such as

$$c_{ref} = \frac{c_b \gamma S}{1 + \gamma S} \quad , \quad c_{ref} = \alpha\, c_b S^{\frac{1}{2}} \tag{3.09}$$

These formulas are due to Smith (1977) and Shi *et al.* (1985) respectively. S is the normalised bed shear stress, c_b is a bed concentration and γ and α are site specific numerical constants.

The reference concentration approach is best suited to the study of concentration profiles when the flow is steady. If the flow is time varying then there exists a phase lag between events taking place at the bed and those at a height z_{ref} above the bed *e.g.* there may exist considerable near bed sediment concentrations at times of zero bed shear stress, due to sediment arriving from above. If this is the case then the most appropriate approach is to parameterise the sediment entrainment rate at the bed using bed properties such as bed shear stress. This is achieved via a pick-up function. Many such functions have been proposed and they are usually derived from tank experiments.

Both the reference concentration and pick-up function BBCs provide the same answer for steady flows. If this is the case then equation (3.07) reduces to

$$K_z \frac{\partial c}{\partial z} = -w_s c \tag{3.10}$$

Assuming that the velocity profile is logarithmic (a linear shear stress distribution) and that K_z is equal to the diffusion coefficient for momentum *i.e.*

$$K_z = \kappa u_* z\left(1 - \frac{z}{h}\right) \tag{3.11}$$

where h is the total water depth, then employing the reference concentration approach, integration of (3.10) leads to the well known Rouse (1937) equation.

$$\frac{c}{c_{ref}} = \left[\frac{h-z}{z}\frac{z_{ref}}{h-z_{ref}}\right]^{\frac{w_s}{\kappa u_*}} \tag{3.12}$$

The exponent $w_s/\kappa u_*$ is known as the Rouse number (B). It is proportional to the

ratio of the settling velocity to the friction velocity. Three different concentration profiles are shown in figure 3.02.

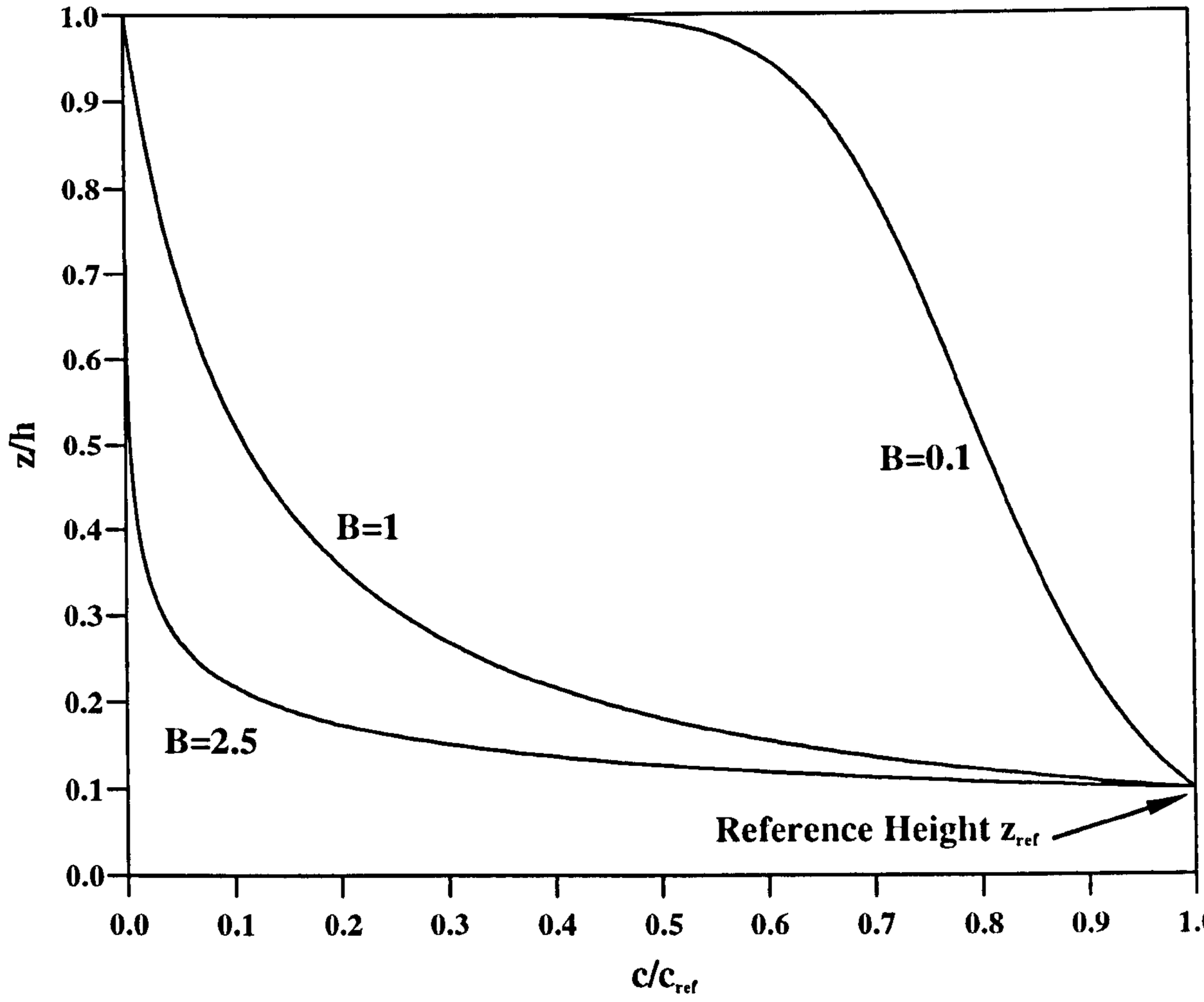

Figure 3.02 : Relative concentration profiles calculated from equation (3.12) for varying values of the Rouse number, B.

Figure 3.02 shows that for large grains in a relatively slow flow (large w_s/u_*) then, as expected the upper layers are clear whereas as the grains get smaller and the flow faster (decreasing w_s/u_*) concentrations further from the bed are larger.

The Rouse formulation matches well with flume measurements, when the exponent is used as a fitting parameter (Dyer (1986)). However, for fine sediments it fails near the bed since, unless concentrations are very low hindered settling occurs close to the bed. Such particle-particle interactions are not accounted for in the Rouse formulation. When calculating concentration profiles using the Rouse formulation,

Kineke and Sternberg (1989) recommend that the settling velocity be determined from *in situ* measurements. It is also necessary to determine the friction velocity and the reference concentration c_{ref}. This is extremely difficult in the field, especially for the reference concentration and such studies are really only applicable to flume experiments. Smith (1977) concluded that the specification of c_{ref} was one of the weakest points in sediment transport prediction.

In deriving the Rouse profile several assumptions were made, most noticeably the form of the K_z profile and the steady nature of the flow. The majority of studies to date have concentrated solely on the bottom boundary layer and any sediment populations have consisted of non-cohesive sands. This thesis is concerned with fine marine sediments and the entire water column. It is therefore unlikely that the Rouse approach will succeed as the addition of an outer and perhaps also a free-stream layer as well as a vertical density gradient will affect the K_z profile. Shelf sea flows are rarely steady and so it is desirable to solve equation (3.07) for $K_z(z,t)$. An analytical approach to this is possible but it involves complex calculations *e.g.* Davies (1986). A more popular method, given advances in computing power is to use a numerical scheme to obtain c(z,t) profiles.

A more straight-forward approach was adopted by Weeks (1989) after a series of SPM concentration and current measurements in the Irish Sea. The SPM signal was found to be consistently tidally dominated and may be understood in terms of SPM variations due to erosion and displacement. A characteristic sediment signal was observed with strong variation at both semi- and quarter-diurnal frequencies. This has come to be known as the 'twin-peaks' signal and is typical of sites where currents are strong enough to resuspend the bed material which then settles out again at slack water. Essentially, there are 3 processes in operation which, when combined, result in an SPM concentration record of this type. These processes are outlined below.

1) Resuspension of the bed material.

This will occur whenever the magnitude of the current exceeds a critical level,

providing that there is sediment on the bed available for resuspension. It is the insensitivity of the resuspended bed material to the direction of the current that means this manifests itself in the SPM signal as a quarter rather than semi-diurnal variation. If the currents on the flood and ebb are different then different amounts of material may be resuspended on each phase of the tide. Often, the availability of erodible sediment leads to a limitation of the resuspended SPM concentration. In this case the SPM signal is known as 'source-limited'. Additionally, the springs-neaps and seasonal cycles will also affect the quantity and characteristics of sediment eroded.

2) Advection of a horizontal background sediment concentration gradient.

This will occur at the semi-diurnal frequency. Such a gradient may exist because of spatial variation in the sea bed composition, resulting in a non-local source of SPM. These sediments tend to remain in suspension for periods longer than a tidal cycle so that they are never able to settle to the bed. The population is likely to consist of fine silt particles and clays as the coarser silts and sands have too great a settling velocity and rapidly settle to the bed. These are the sediments likely to be resuspended by the current as described above.

3) Net advection due to a non-zero tidal excursion.

Asymmetry between the tidal phases does not lead only to different quantities of resuspended sediment. It often also means a non-zero tidal excursion *i.e.* a net transport of water over the tidal cycle, so that there will also be a net transport of the background sediment concentration gradient. This can result in an overall increase or decrease in the observed sediment concentration.

A schematic of these processes is shown in figure 3.03. Figure 3.03(a) represents the background sediment concentration gradient with a non-zero tidal excursion, (b) shows the resuspended sediment signal with larger quantities eroded on the stronger flood phase and (c) depicts the combined effects of (a) and (b).

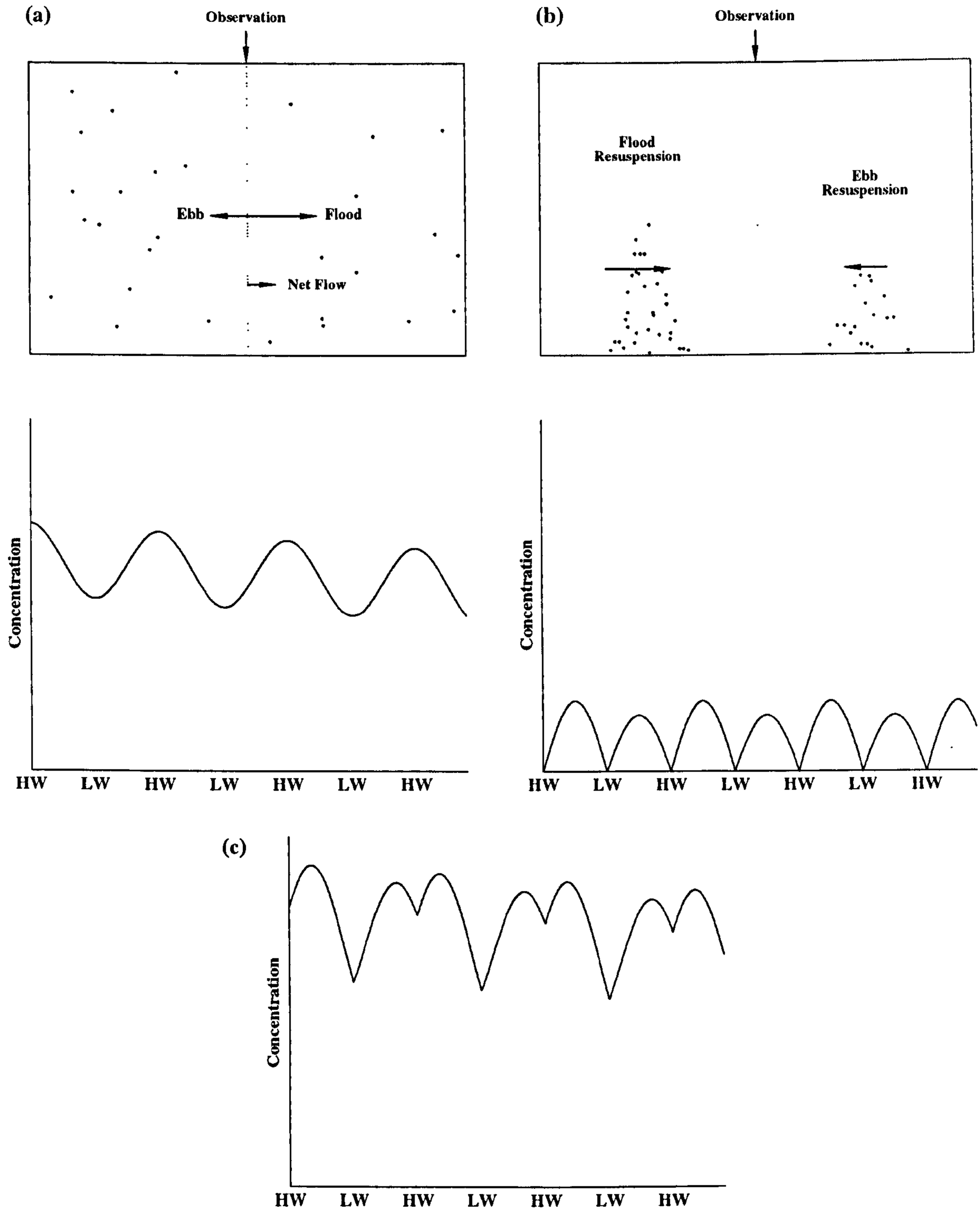

Figure 3.03 : Twin-peaks schematic.

(a) Advected background component.

(b) Resuspended component.

(c) Total sediment signal.

This approach is a successful one in terms of appreciating the fundamental processes taking place. However, in order to improve understanding of the vertical processes occurring it is desirable to be able to model the hydrodynamics and water column structure and to use this in a coupled physics/SPM model. In recent years turbulence closure (TC) models based on the schemes of Mellor and Yamada (1974) have been used to model shelf sea flows and structure (*e.g.* Simpson and Sharples (1991)). One such model has been developed to include a sediments module to allow prediction of SPM concentration profiles (Jones *et al.* (1996a,b)) and it is this formulation that is used to hindcast the data presented in the thesis. This model and the simulation results are fully discussed in chapter eight.

CHAPTER FOUR

The Observational Program

4.1 Introduction to the Study Area : The Irish Sea.

4.1.1 Location and Description.

Forming part of the north-west European shelf, the Irish Sea is the body of water separating Ireland from the British mainland. As such it is semi-enclosed, open at its northern and southern extremities. It extends northwards from 52°N where it meets the Celtic Sea via St.George's Channel to approximately 55°N where it connects with the Atlantic Ocean through the narrower and relatively deep North Channel. This gives the Irish Sea an overall length of about 300km. There is great variation in its width from only 20km across the North Channel to over 190km between NW England and Ireland and 75km across the southern extremity of St. George's Channel.

Major cities bordering the Irish Sea include Dublin, Belfast and Liverpool and there are many rivers that discharge a sizeable quantity of freshwater into the basin. The Irish Sea thus receives freshwater run-off from a large area of land. The total catchment area is approximately 43000km^2 whereas the sea area is 47000km^2. The Irish Sea also has many important and heavily used fishing grounds and shipping lanes. At a latitude of 54.5°N, midway between Ireland and Britain is the Isle of Man. To the south-east of the island, between the coasts of North Wales and NW England is situated Liverpool Bay.

Depths throughout the Irish Sea are generally less than 100m. However, there is great variation in depth from the British mainland in the east to Ireland in the west. A channel deeper than 80m runs northwards from west of the Isle of Man to the North Channel whereas depths further east and in Liverpool Bay are less than 50m. In St. George's Channel between Wales and Ireland depths approach 100m. The general location and bathymetry of the Irish Sea is shown in figure 4.01.

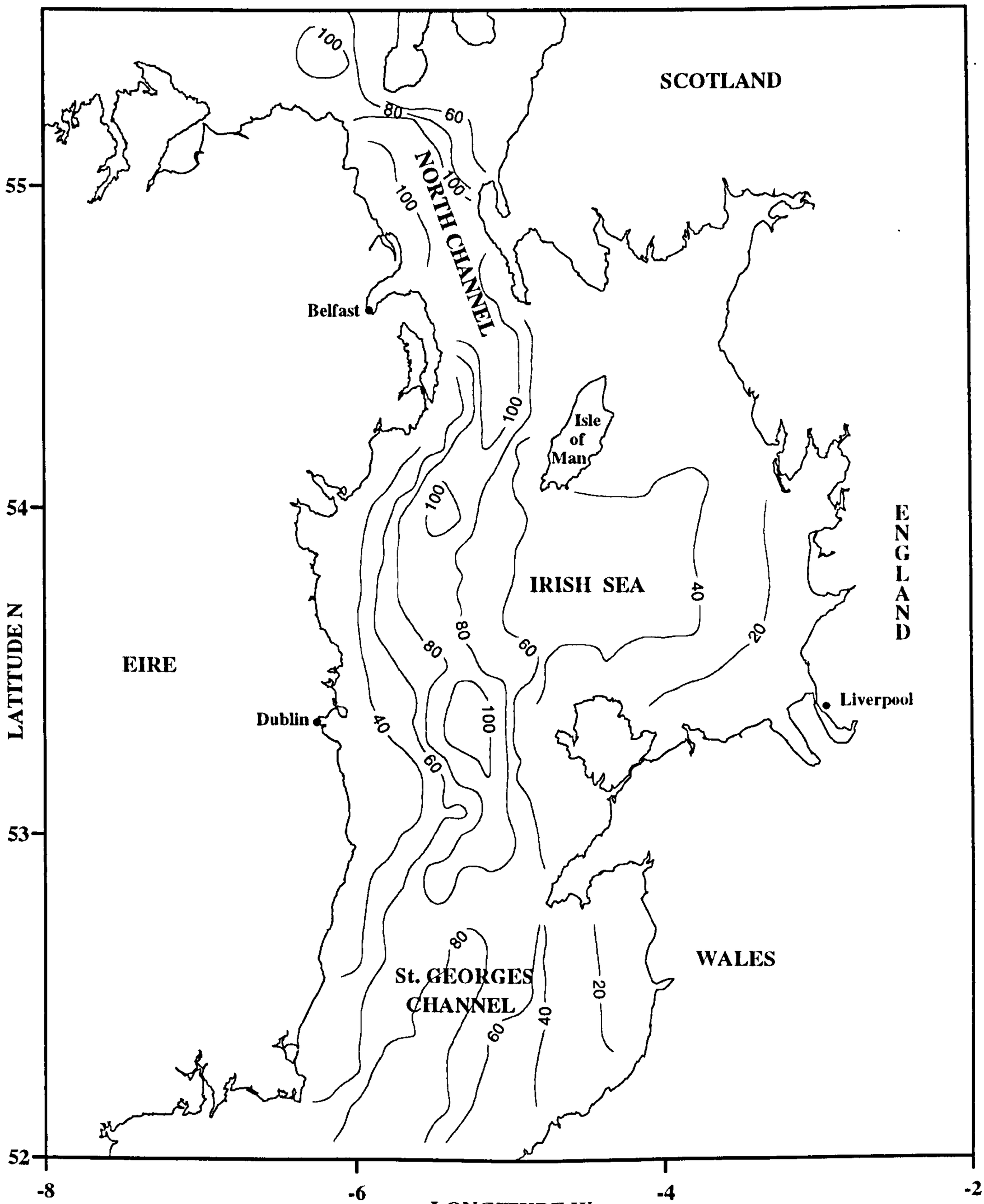

Figure 4.01 : Location and bathymetry of the Irish Sea. Depth contours are given in meters.

4.1.2 Currents and Circulation.

Water movements in the Irish Sea are dominated by the regular tidal flow. There is great variation in the amplitude of the tidal signal with currents ranging from moderate to strong (typically $0.3ms^{-1}$ to $1.2ms^{-1}$). The variations are predominantly semi-diurnal in nature and there is a significant springs-neaps signal. A cotidal chart of the largest (M_2) constituent computed using a three dimensional numerical model (Davies and Jones (1992)) is shown in figure 4.02. The S_2 amplitudes are typically one third to one half of the M_2 values.

Figure 4.02 : Cotidal chart of the M_2 constituent for the Irish and Celtic Seas computed using a three dimensional numerical model (from Davies and Jones (1992)).

Figure 4.02 shows the existence of a degenerate amphidrome on the west side of St. George's Channel with amplification of the amplitude in the eastern half of the Irish Sea. The distribution of the major and minor axes of the M_2 current ellipses at the surface were also computed by Davies and Jones (1992) and are shown in figure 4.03.

Figure 4.03 : Surface distribution of the major and minor axes of the M_2 current ellipses in the Irish and Celtic Seas (from Davies and Jones (1992)).

The M_2 ellipses in the Irish Sea are seen to be generally rectilinear with flow principally north-south in St. George's Channel and east-west in Liverpool Bay. The flow to the north of the Isle of Man remains in an east-west orientation. In the North

Channel the flow is also rectilinear but in an along channel (NW-SE) direction.

While tidal currents dominate the flow field in the Irish Sea there is also an observed residual flow. This flow could be due to wind effects, density gradients or the inflow of Atlantic water. In general, there is a residual flow northwards through the Irish Sea of the order of a few cms^{-1}. The relative importance of the three effects mentioned above will vary both temporally (for example, wind driven flows are likely to be larger in winter than summer) and spatially (density-driven flows can become significant near estuaries).

4.1.3 Seasonal Stratification.

Although strong tidal currents ensure complete vertical mixing throughout most of the Irish Sea and St. George's Channel, there is an area to the south-west of the Isle of Man where currents are sufficiently weak to allow thermal stratification to develop in the summer months. This is because there is insufficient energy available from the tidal flow to break down the stratification that results from daily surface heating. The Western Irish Sea front marks the transition between this stratified region and the mixed water column in the more energetic eastern Irish Sea so that at the front the mixing and stratifying influences balance.

Stratification in the western Irish Sea was first reported by Matthews (1913). There were few studies made until the 1970s when Simpson (1971) observed bottom-surface temperature differences of more than 5°C. In the region of the front itself strong horizontal gradients were observed with temperature changes of 2°C over a distance of less than 2km.

A cross-frontal temperature distribution measured during the July 1993 cruise described in §4.3 is shown in figure 4.04.

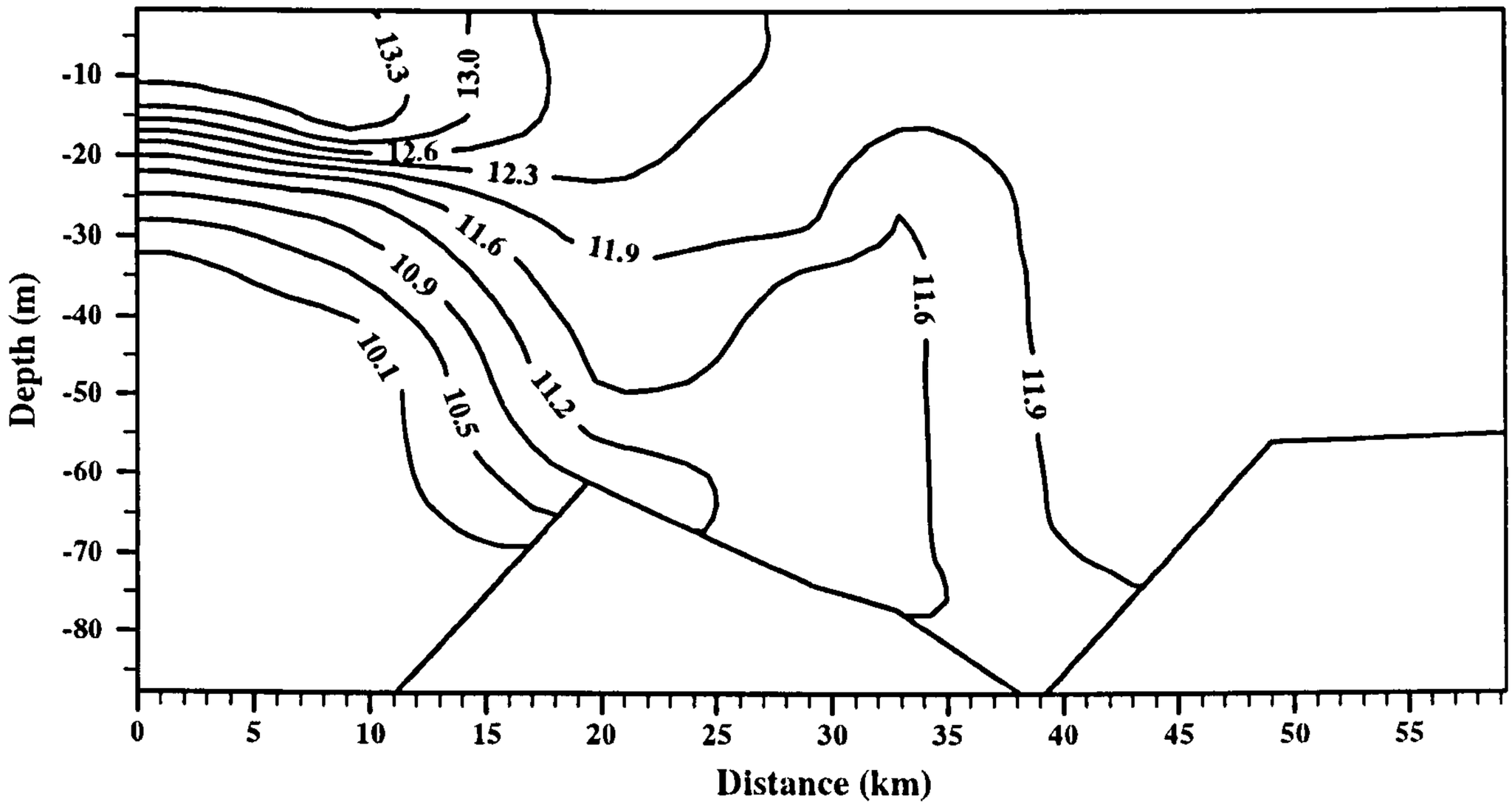

Figure 4.04 : Cross-frontal temperature distribution from the western Irish Sea, July 1993.

Once well established, the position of the Western Irish Sea front does not vary greatly (Simpson and Hunter (1974)). The average position of such a tidal front can be inferred via the now well known h/u^3 criterion. Simpson and Hunter (1974) adopt a potential energy approach to describe the degree of stratification at a particular position, where a stratified water column has a lower potential energy than a completely mixed one. Assuming that the buoyancy input (in this case surface heating) is uniformly distributed and that the majority of the mixing is due to shear stress in the near bed region from the tidal current, then the rate of change of the potential energy of the water column is given by

$$\frac{dV}{dt} = \frac{4\epsilon k \rho u^3}{3\pi} - \frac{\alpha g Q h}{2c} \qquad (4.01)$$

The first term on the right hand side of equation (4.01) is that due to tidal stirring and the second represents the stratifying influence of surface heating where

k is a bottom friction coefficient,

u is the amplitude of the tidal current,

ϵ is the mixing efficiency of the tidal energy,

g is the acceleration due to gravity,

Q is the rate of heat input to the surface,

h is the water depth and

c is the specific heat of sea water.

At the position of the front the two terms on the right hand side of equation (4.01) balance so that if k, ϵ, g, Q, ρ and c can be considered constant then this position will coincide with a critical value of h/u^3. Figure 4.05 shows the approximate position of the Western Irish Sea front.

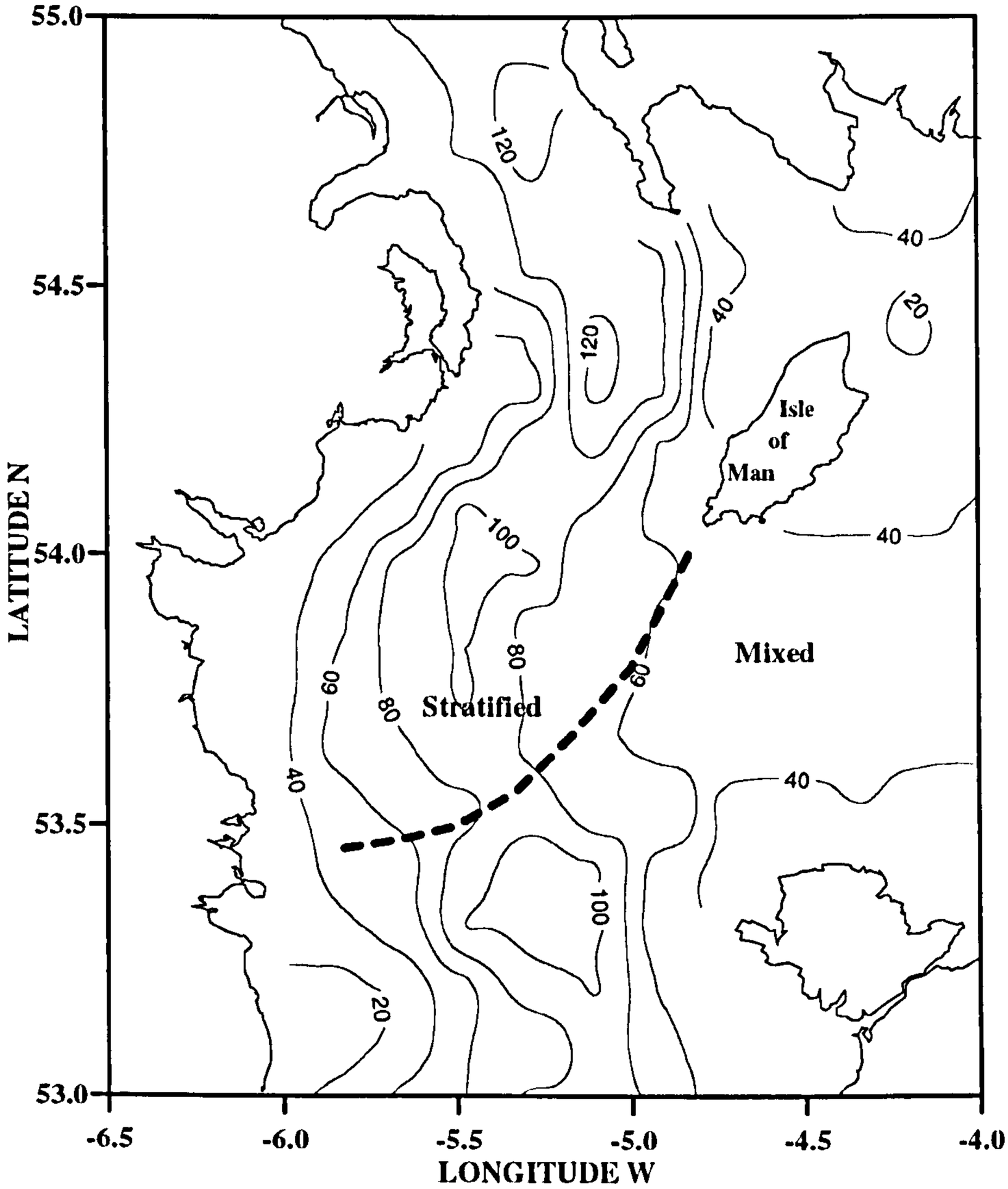

Figure 4.05 : Approximate position of the Western Irish Sea front.

4.1.4 Sea Bed Sediments.

Just as there is a wide range in the strength of the tidal current and depth across the Irish Sea and St.George's Channel, there is also wide range of sediment sizes across the sea-floor from gravel to muds. The surficial distribution of sediment on the bed of the study area is shown in figure 4.06.

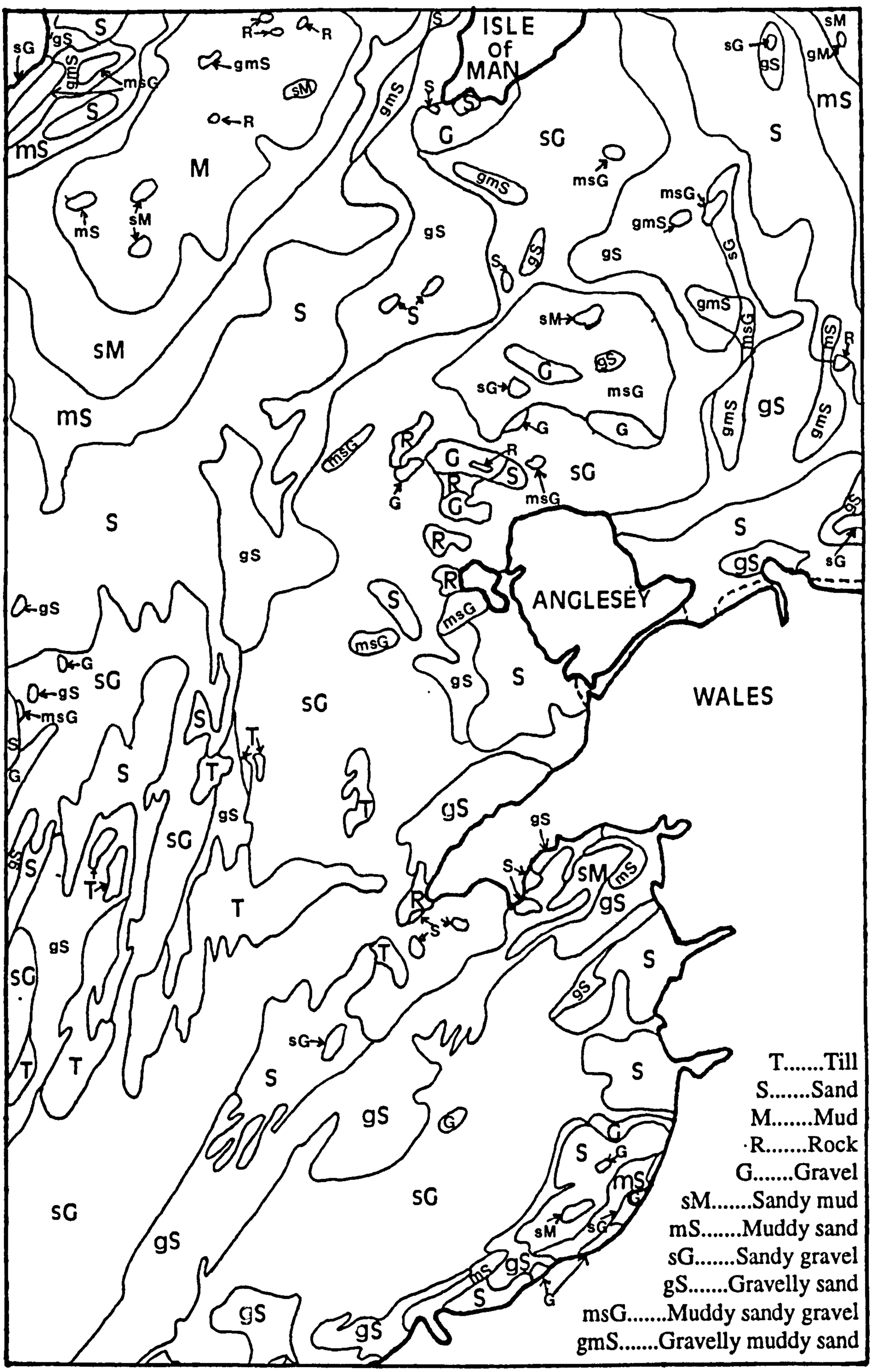

Figure 4.06 : Surficial sediments on the bed of the Irish and Celtic Seas.

The sea-floor sediments in the Irish Sea were deposited during the Quaternary period and are mainly unconsolidated. Large areas of mud exist, especially in the western Irish Sea, deposition of which commenced in the Holocene, about 10 000 years ago (Belderson (1964)).

Figure 4.06 shows additional areas of mud off the Cumbrian coast and the west coast of Anglesey. Comparison of figures 4.06 and 4.02 shows that areas characterised by mud or muddy deposits are generally associated with the weakest tidal currents to be found in the Irish Sea. Unsurprisingly, the strongest currents coincide with the heaviest, gravelly sediments.

Between areas of mud and gravel there are significant deposits of sand, especially north of 53°N. Since sand grains are relatively large and do not remain in suspension for an appreciable time, most sand transport is via the bedload mechanism. Kenyon and Stride (1970) showed that there is a net transport of sand in a northerly and north-easterly direction, coinciding with the net flow of water in the Irish Sea.

4.2 The March 1993 Experiment (CH102).

The RRS Challenger was made available by her owners, the Natural Environment Research Council for this cruise. The principal aim of the study was to monitor mean and turbulent flow conditions in conjunction with levels of suspended particulate matter. The intention was to measure the appropriate variables for a full 25 hours in a well mixed regime in an area to the south of the Isle of Man. For this purpose a large range of instrumentation was used including moored current meters and transmissometers, ship based profilers and settling velocity tubes.

A pair of U-shaped moorings were deployed at positions IS1 (54m depth) and IS2 (62m) as shown in figure 4.07. Additional positions are also indicated and will be

introduced later in this and the next section.

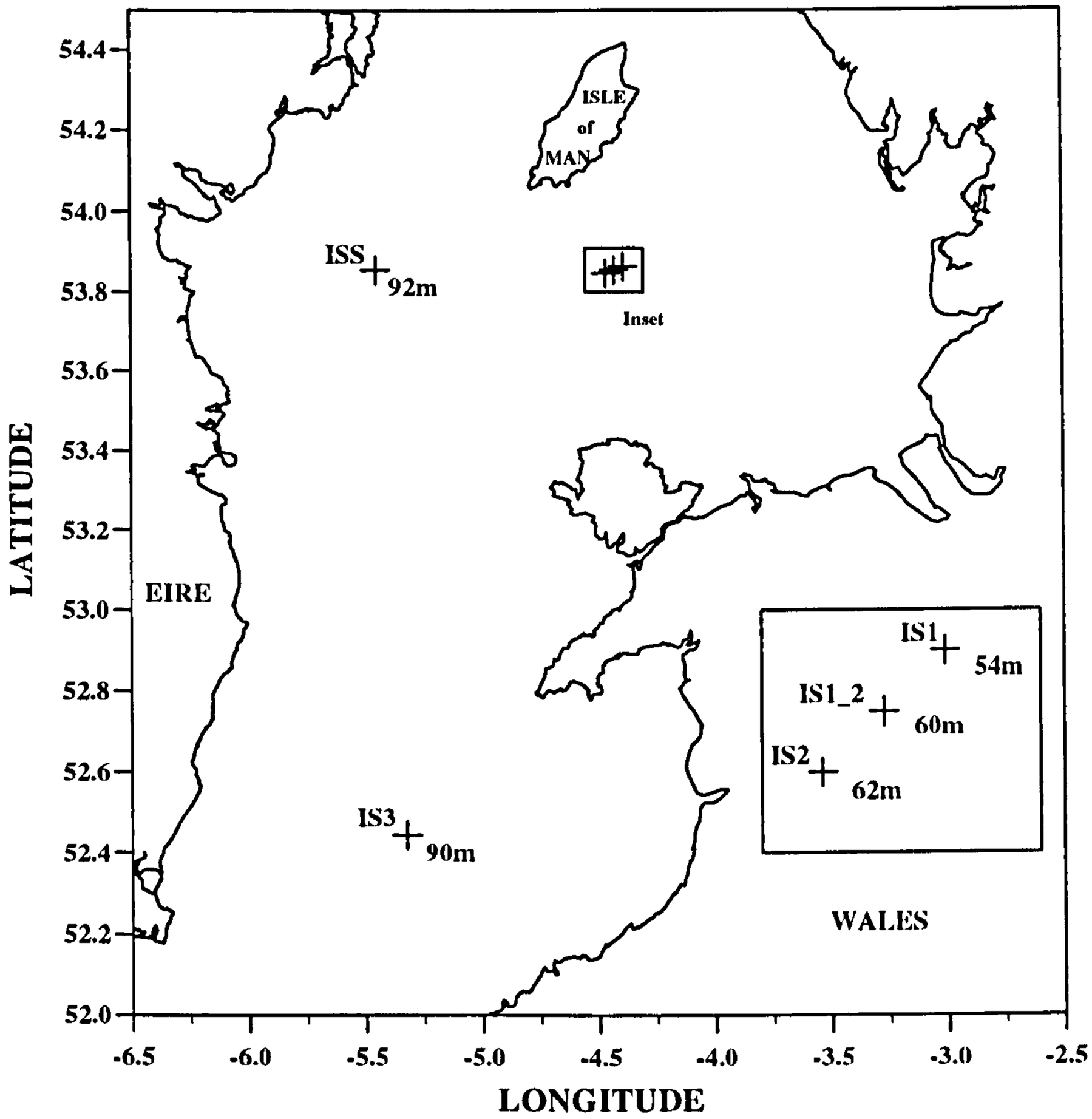

Figure 4.07 : Positions of moorings and survey sites.

The distance between IS1 and IS2 was approximately 12km, and they were aligned in the direction of the largely rectilinear currents. According to figure 4.06, the bed material at both sites was sandy gravel. The U-shaped moorings deployed at IS1 and IS2 consisted of two legs positioned 150m apart and connected by a groundline. One leg extended from the bed to a surface toroid marker and the other to a subsurface buoy, keeping the instrument string taut. The mooring deployed at IS1, with its associated instrumentation is shown in figure 4.08.

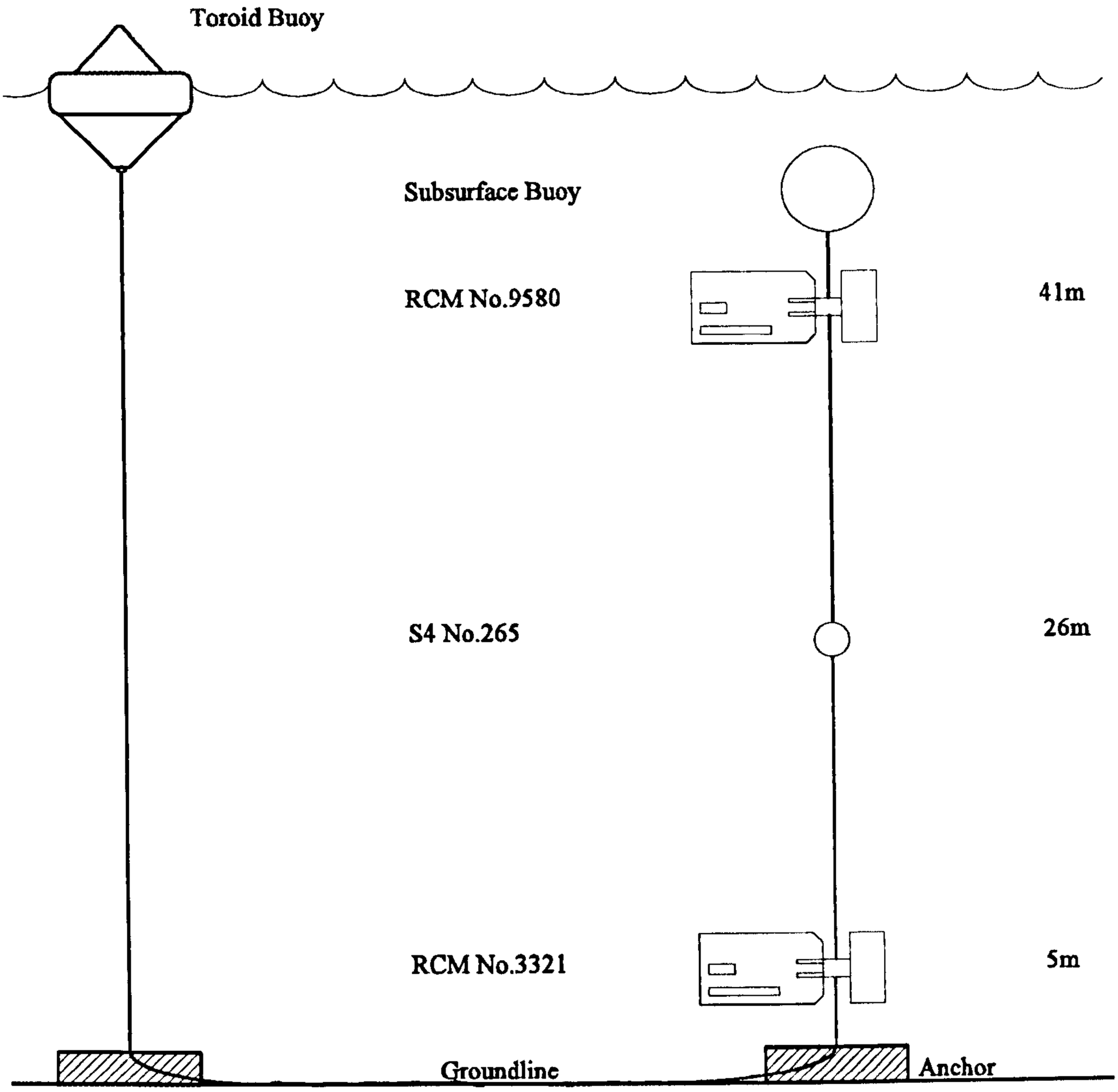

Figure 4.08 : Mooring IS1 configuration and instrumentation.

As can be seen from figure 4.08, mooring IS1 was instrumented with a pair of Aanderaa current meters (RCMs) recording current speed and direction, temperature and salinity. They are rotor and vane instruments that align themselves into the flow recording every minute and thus monitoring the mean flow. Also deployed in the middle of the water column was an InterOcean S4 current meter. In burst sampling mode, S4s are capable of high frequency current measurements due to the fact that they do not use a rotor but rather they monitor electromagnetic field distortion caused by the current. However, their deployment (on IS2 also) was largely unsuccessful and the data will not be presented in this thesis. The mooring deployed

at the second site IS2 was more heavily instrumented and is shown in figure 4.09.

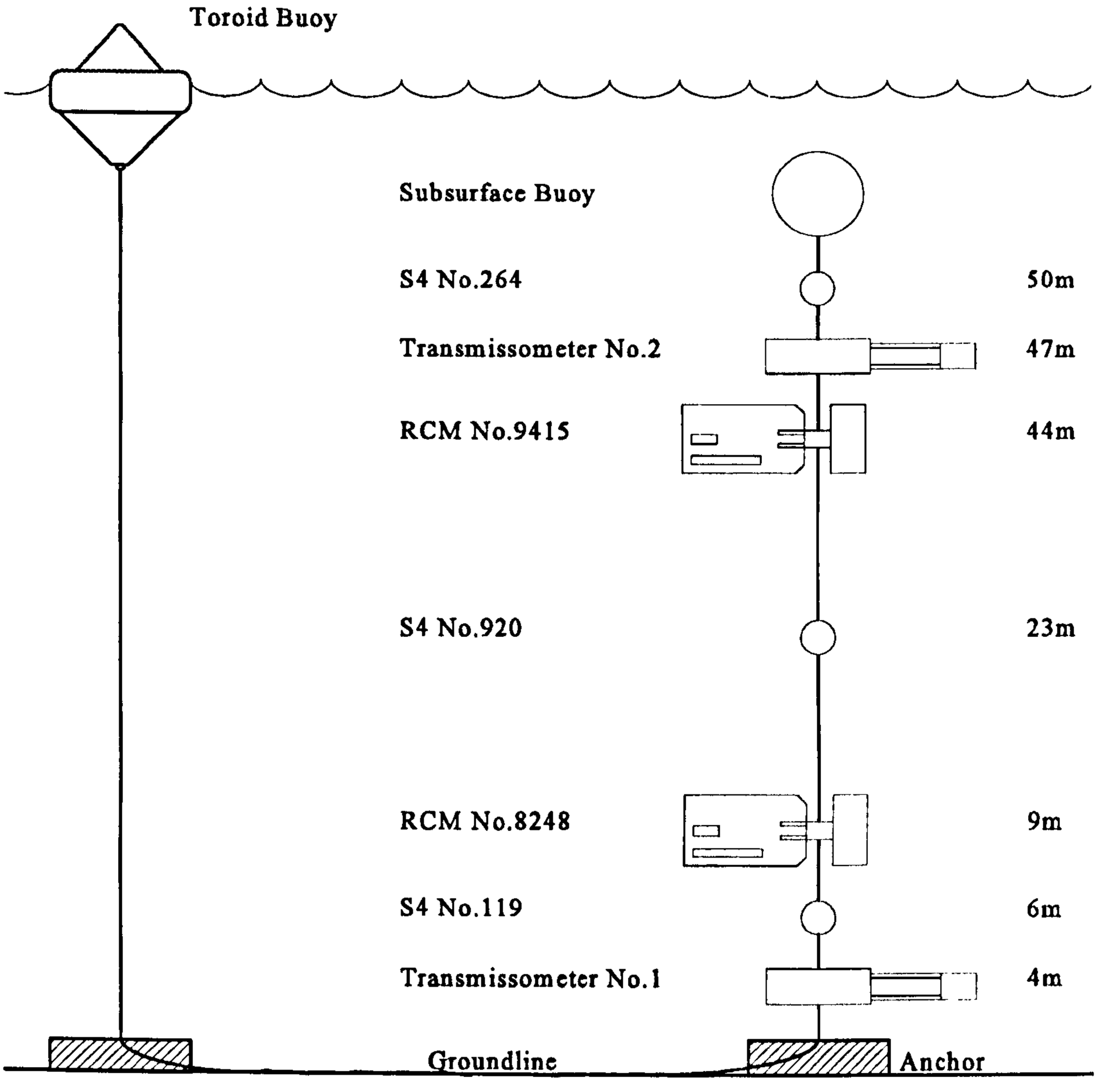

Figure 4.09 : Mooring IS2 configuration and instrumentation.

In addition to two Aanderaa current meters and three Interocean S4 current meters, two transmissometers were deployed on IS2. These instruments, developed at the University of Wales, Bangor, were used to monitor the levels of suspended particulate matter by measuring the attenuation suffered by a light beam as it passes through the water. They take spot readings of attenuation every minute and store the data internally, on a solid state memory card. The instruments on IS2 were

positioned in groups with an RCM, S4 and transmissometer in the near bed region and another set in the surface waters. This was so that the different datasets could be easily compared.

After the deployment of moorings IS1 and IS2, RRS Challenger took up station midway between them (at IS1_2) and a 26 hour CTD survey was conducted in association with measurements of turbulent dissipation. The CTD profiler was equipped with the usual sensors as well as a Sea-Tech transmissometer for measuring suspended sediment concentration profiles. Also used were reversing thermometers and several water bottles for calibration of the temperature and conductivity sensors respectively. Further water samples were also taken so that gravimetric analysis could be done for calibration of the transmissometer. A settling velocity tube was deployed in midwater at the beginning of the survey.

A further means of monitoring the currents was provided by the ship-mounted Acoustic Doppler Current Profiler (ADCP) which recorded velocity profiles every 10 minutes from 6m above the bed to 6m below the ship. For this site, the vertical resolution was 2m.

The CTD duty cycle was one hour. Depending on the state of the tide, CTD casts took about 15 minutes. The remaining time was then used to measure the turbulent dissipation rate. This was done using a probe known as the Fast, Light Yo-Yo (FLY) turbulence profiler. The probe is allowed to free fall from the stern of the ship to the bed at which point it is hauled back up to the surface. It measures the vertical velocity shear via a piezoelectric probe, data being sent to an on board PC in real time for later analysis. The depth of water dictated how many profiles could be made between CTD casts. For survey site IS1_2, 10 profiles were completed every hour. Upon completion of the IS1_2 survey, moorings IS1 and IS2 were recovered and an *in situ* post deployment calibration was done.

The successful conclusion of the experiment described above meant that there was

sufficient shiptime for a second survey to be conducted. After the recovery of moorings IS1 and IS2, it was decided to undertake a further 24 hour CTD/FLY survey at a site chosen in St.George's Channel. This site was named IS3 and is shown in figure 4.07. The water at IS3 is deeper (90m) than at IS1 or IS2, the tidal currents are weaker and the bed is once again sandy gravel. Even though mooring equipment was not available the mean flow could still be monitored using the 150kHz ship-mounted ADCP.

The IS3 survey was also a success and a full 25 hours of CTD and turbulent dissipation rate data was gathered. Additionally, further samples were taken for calibration purposes and three settling velocity tubes were deployed at a height of 70m above the bed throughout the survey so that the spectrum of particle sizes could be studied. The CTD duty cycle was again one hour. The deeper water meant that the number of turbulent dissipation rate profiles taken between CTD casts was reduced to 6. The deeper water also meant that vertical resolution from the ADCP was reduced to 4m.

4.3 The July 1993 Experiment (PM93).

The vessel used for this week long cruise was the R.V. Prince Madog, owned by the University of Wales. Once again, the intention was to monitor the mean and turbulent flow conditions in conjunction with SPM concentrations over a 25 hour period. Except for settling velocity tubes which were unavailable and the ship-mounted ADCP which was inoperational, identical instrumentation to that used on cruise CH102 was used. Experiments at both a mixed and a thermally stratified site were planned. Unfortunately, only one of the experiments was completed, that at the stratified site, denoted ISS and shown in figure 4.07. The water depth is 90m and the bed consists principally of mud as is usually the case with areas in the Irish Sea where currents are relatively weak.

A single U-shaped mooring of similar design to that deployed at IS2 during cruise CH102 was used at ISS. Once again Aanderaa current meters were used to monitor the mean flow with transmissometers for the SPM measurements. The instruments were positioned as a near bed group and a surface group, designed to be above the thermocline. The configuration of the mooring is shown in figure 4.10.

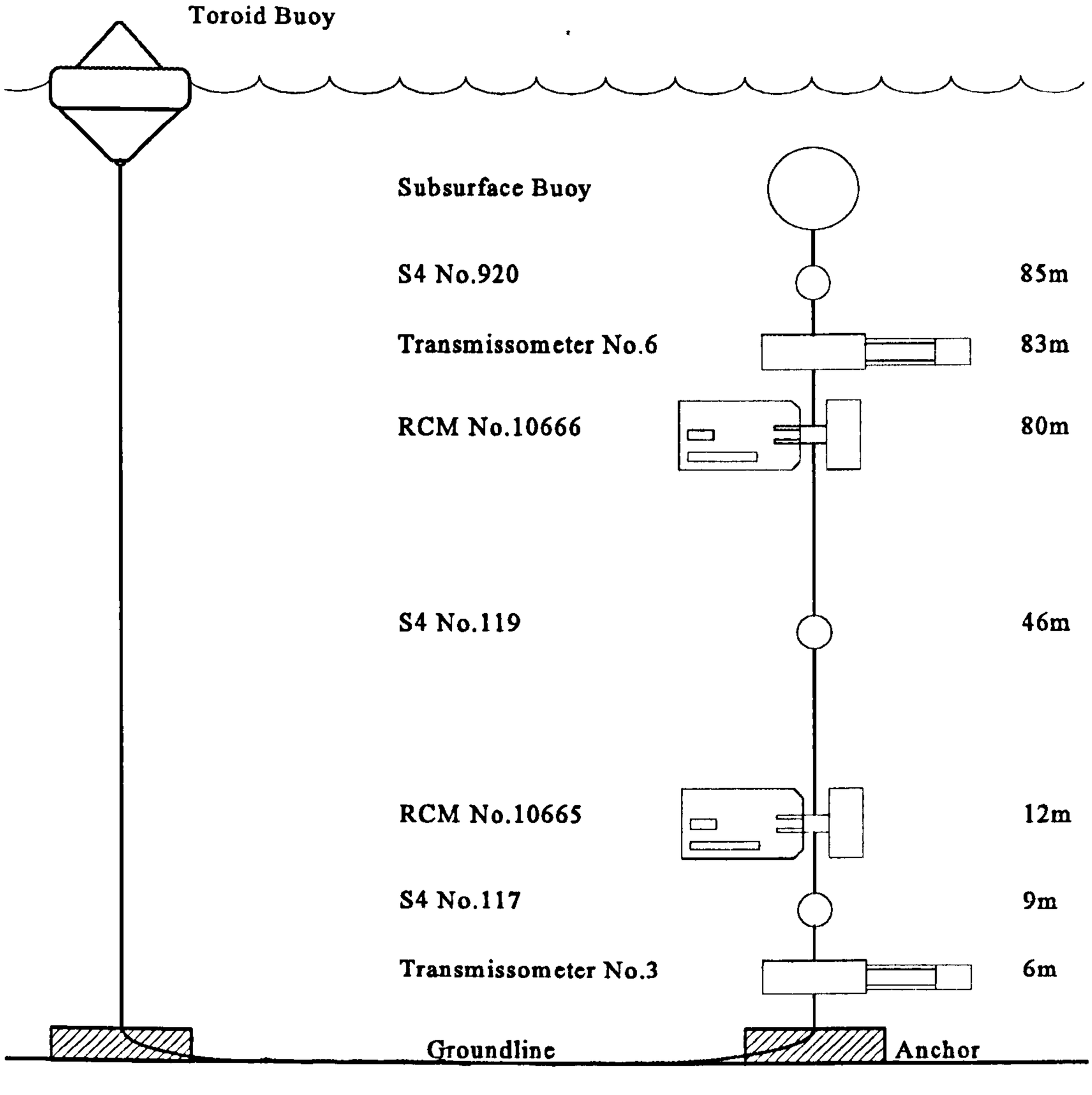

Figure 4.10 : Mooring ISS configuration and instrumentation.

After the deployment of mooring ISS a 25 hour CTD/FLY survey was undertaken nearby. Once again, CTD casts were made every hour allowing, in 90m of water, 6

FLY profiles to be measured between CTD profiles. Reversing thermometer measurements and samples were taken for calibration of the CTD sensors and transmissometer. Upon recovery of mooring ISS an *in situ* post deployment was completed.

Due to complications whilst recovering the mooring it was necessary to return to port for a day which proved to be sufficient delay so that the experiment at the mixed site could not proceed. However, several CTD profiles were completed across the Western Irish Sea front and 6 hours CTD/FLY measurements were made at the mixed site. The results of the cross-frontal section were presented earlier (figure 4.04) and the limited dataset available from the mixed site will not be presented in this thesis.

4.4 Summary.

Two cruises were successfully undertaken in March (CH102) and July (PM93) 1993. Mean and turbulent flow conditions were measured in conjunction with SPM concentrations at three contrasting sites in the Irish Sea and St.George's Channel over two tidal cycles. The sites visited during the cruises are summarised in table 4.01.

Table 4.01 : Experiments conducted during cruises CH102 and PM93.

Site	Cruise	Depth	Bed	Position
IS1 (M)	CH102	54m	sandy gravel	53° 51.78' , 004° 23.30'
IS2 (M)	CH102	62m	sandy gravel	53° 50.67' , 004° 27.65'
IS1_2 (S)	CH102	60m	sandy gravel	53° 51.23' , 004° 25.48'
IS3 (S)	CH102	90m	sandy gravel	52° 26.70' , 005° 19.45'
ISS (M&S)	PM93	90m	mud	53° 51.25' , 005° 27.13'

M - Mooring deployment, S - CTD/FLY survey.

CHAPTER FIVE

Instrumentation and Data Analysis

5.1 Introduction.

In the previous chapter, the cruise program was described and the wide range of instrumentation used in the study was introduced. The purpose of this chapter is to give a detailed description of the instrumentation used and the analysis techniques employed to convert the raw datasets into engineering units. In section 5.2 the turbulence profiling system is described in some detail. There then follows information on the CTD unit and the Acoustic Doppler Current Profiler before the final sections which describe the moored instrumentation, namely the beam transmissometer and the Aanderaa current meter.

5.2 The Turbulence Profiling System.

5.2.1 The Fast, Light, Yo-Yo (FLY) Turbulence Profiler.

Turbulent dissipation rate (ϵ) was measured using a free-falling FLY probe developed by Dewey *et al.* (1987). The instrument measures velocity shear, pressure, temperature and salinity from the surface to within 15cm of the ocean bottom. It is allowed to free-fall from the stern of the vessel until it hits the bed at which point it is hoisted to the surface ready for re-use. This means that rapid sampling of the water column is possible, depending on the water depth and instrument fall speed, which is controlled by flotation attached to the instrument. The profiler is shown in figure 5.01.

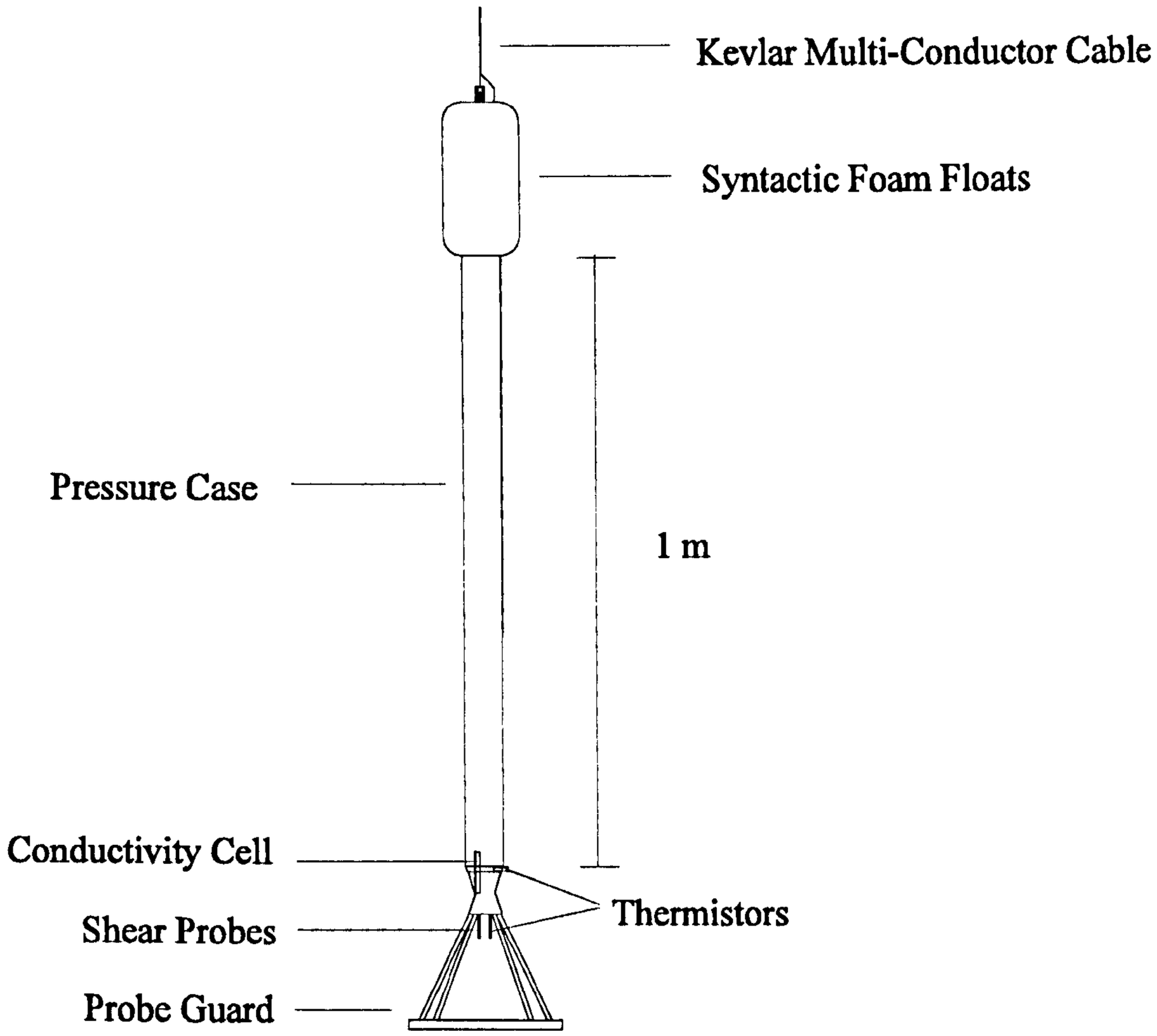

Figure 5.01 : The FLY microstructure profiler.

The probe guard on the lower end on the profiler protects the delicate sensors on impact with the bed. Sensors carried on the instrument include two airfoil shear probes, slow and fast response thermistors, a conductivity cell, two tilt gauges and a pressure gauge. The two shear probes and the fast response thermistor are located at the bottom of the profiler. Just above them is the second thermistor and the conductivity cell. The two tilt gauges are located inside the pressure case along with the signal amplifiers, analogue to digital electronics and the power supply. The pressure sensor is located at the top of the instrument. Also attached to the top of the pressure case are syntactic floats which are used to control the fall velocity of the

profiler and to ensure that it remains vertical during descent. Kevlar multi-conductor cable permits real time output of the sensor readings and also allows the operator to determine when the profiler has reached the bed. The FLY can then be winched to the surface ready for the next profile. Sensor specifications are shown in table 5.01.

Table 5.01 : Sensor specifications for the FLY microstructure profiler (from Dewey *et al.* (1987)).

Sensor	Range	Accuracy	Response Time
Conductivity	20 to 60 mmho/cm	±0.05 mmho/cm	0.34s
Fast thermistor	1.5°C to 13°C	±0.004°C	0.018s
Slow thermistor	1.8°C to 17°C	±0.006°C	0.3s
Pressure	0 to 250m	±0.5m	
Tilt	0 to 45°	±0.5°	
Shear Probe	0 to $4s^{-1}$	±5%	1 to 2cm

The shear sensors are piezoelectric probes which output a voltage proportional to the stress they experience. This stress is directly proportional to the product of the horizontal and vertical velocities and so, if the vertical velocity is constant, the voltage output by the piezoelectric sensor will be representative of the horizontal velocity. This voltage is recorded 274 times each second so that for a typical fall speed of $80cms^{-1}$, shear measurements are made every 3mm. The remaining sensors sample at a rate of 34 times per second.

5.2.2 FLY Data Processing.

As the FLY profiler descends through the water column it transmits data to the on-board computer in real time for analysis. Firstly, the microstructure shear is obtained from the differentiated shear probe signal. Employing Taylor's frozen field hypothesis (§2.1.4):

$$\frac{\partial u}{\partial z} = \frac{1}{w}\frac{\partial u}{\partial t} = \frac{V_0}{G2\sqrt{2}Sw^2} \qquad (5.01)$$

where G is the differentiator gain, S is the shear probe sensitivity, V_0 is the output voltage and w is the fall speed. The fall speed is calculated from the pressure record which is fit to a least squares cubic. The differentiated equation can then be used to obtain w.

The water column is then subdivided into vertical sections or bins. Bin length is determined by a number of factors. The longer the bin length, the more low frequency information is available. However, this must be balanced against the need for stationarity of the mean flow and homogeneity of turbulence in the bin. This is not a serious problem in the main part of the water column and bin lengths corresponding to 512 data points are used. This involves a time series of length 2s and a vertical fall of 1.6m for a typical fall speed of 80cms^{-1}.

Shorter bin lengths are required in areas of high shear such as the near bed region in order to reduce the effects of non-stationarity. The sections nearest the bed contain 64 data points . These shorter sections improve vertical resolution and reduce the non-stationarity problem. However, confidence in the individual ϵ values is reduced. Dewey and Crawford (1988) estimate that in these high shear areas an overestimate in dissipation may result, even when shorter bin lengths are used.

The bins are overlapped and the sectioning of the water column is shown in figure 5.02. Although overlapping reduces the number of independent observations, it is one of the most efficient methods of sectioning. The bottom 15cm of the water column is unavailable for measurement because of the presence of the probe guard.

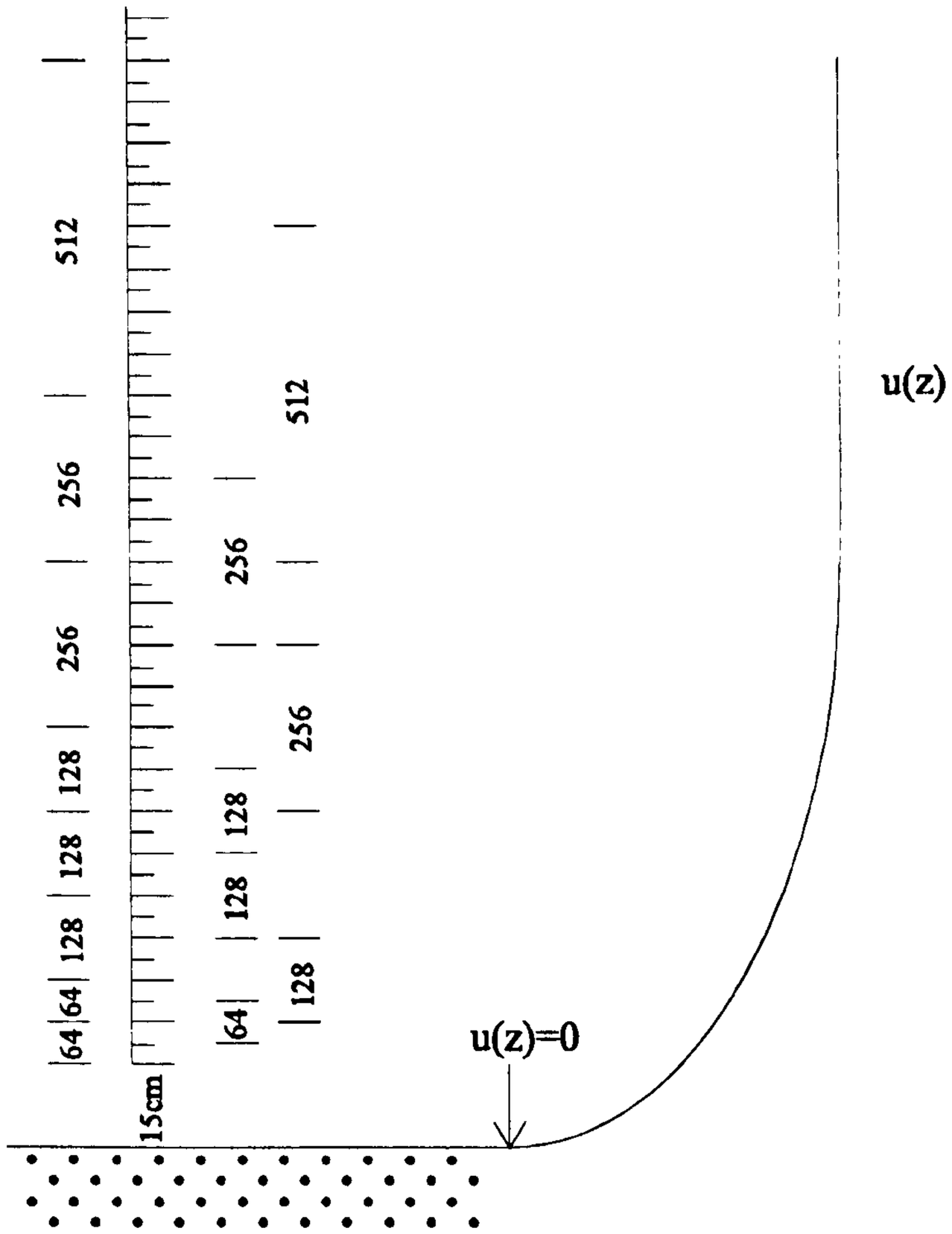

Figure 5.02 : Sectioning of the water column/FLY data bin lengths.

In order to reduce the leakage of low frequency energy to dissipation scales, the mean and linear trend in the data is removed. The shear data for each of the bins are then cosine-tapered. The cosine-taper takes the form of a multiplying factor between 0 and 1. It forces the shear signal to be zero at the bin extremities. This ensures that the signal is cyclic for the Fast Fourier Transform operation. The FFT is then performed on the shear signal for each bin to calculate the power spectrum of $\partial u/\partial z$ which is the 1-d dissipation spectrum $k_3^2\phi_{11}(k_3)$. From the assumption of isotropy the dissipation rate per unit volume is calculated from the variance of the shear time series (Monin and Yaglom (1975), Osborn (1974)).

$$\epsilon = 7.5\,\mu \int_0^{\infty} k_3^2 \phi_{11}(k_3)\, dk_3 = 7.5\,\mu \overline{\left(\frac{\partial u}{\partial z}\right)^2} \qquad (5.02)$$

where the symbols are as defined in §2.4.

The variance is estimated from the power spectrum of the shear signal. Spectral techniques are used so that noise in the signal can be isolated and so that the spatial response of the shear probe and high and low frequency attenuation in the electronics can be compensated for.

The response of the airfoil shear probes will deteriorate at high frequencies *i.e.* low wavenumbers, due to their physical dimensions. The velocity shear is linearly dependent on the probe sensitivity which is reduced at high frequency (Ninnis (1984)). Ninnis (1984) derived a transfer function to account for this high-frequency fall off. The function is shown in figure 5.03 and is given by:

$$T = 1.0 - 0.164\,a - 4.537\,a^2 + 5.503\,a^3 - 1.804\,a^4 \qquad (5.03)$$

where $a=(1.7\lambda)^{-1}$ and λ is the wavelength in cm.

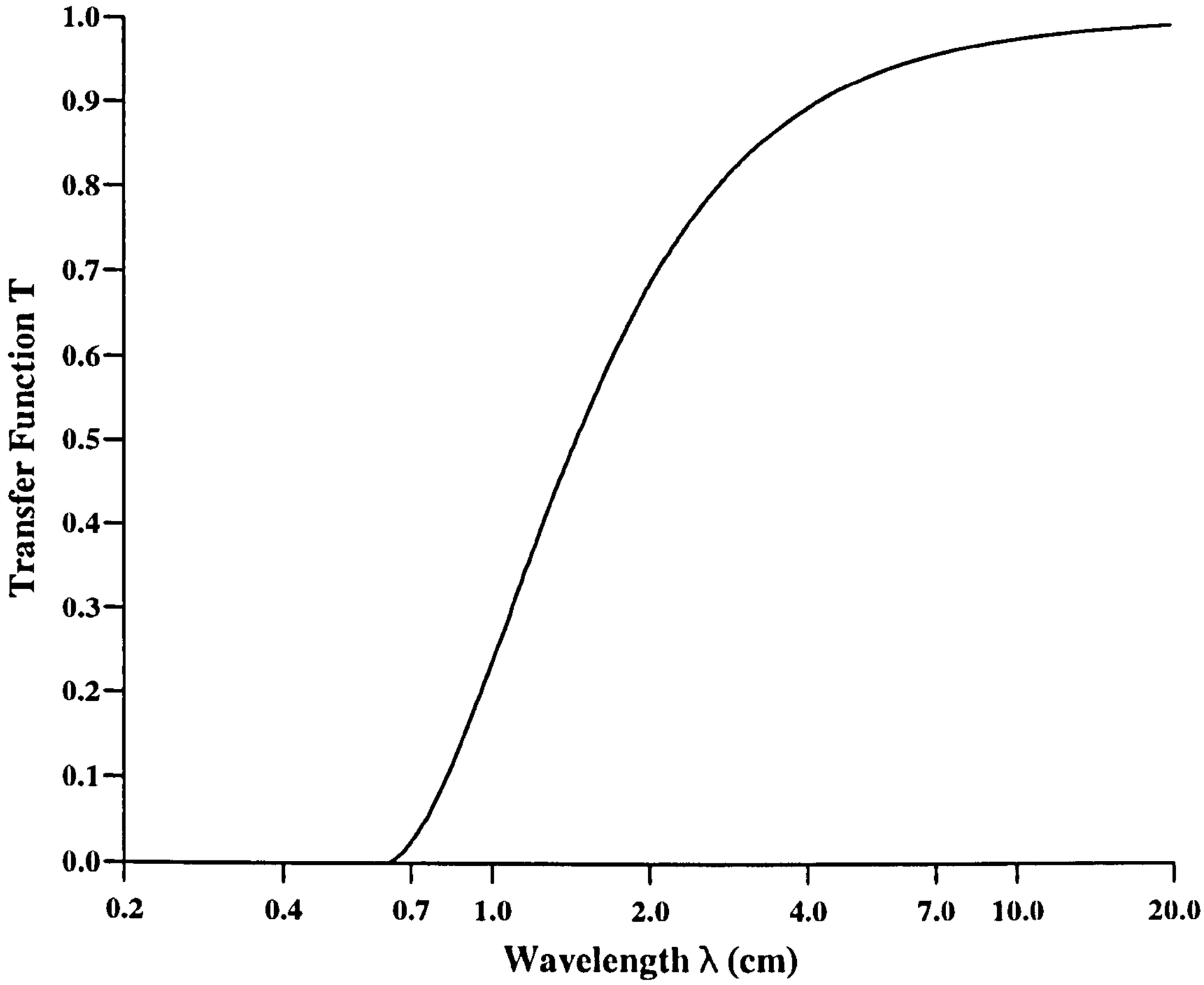

Figure 5.03 : Transfer function used to compensate for high frequency roll-off in shear probe performance (Ninnis (1984)).

Because of the reduction in probe performance at high frequencies (low wavelengths), it is necessary to impose an upper limit on the frequency range. This is normally chosen as the point where the probe sensitivity has decreased by $\sqrt{2}$, corresponding to a wavelength of 1.45cm or a frequency of 55Hz at a fall speed of $80cms^{-1}$. At this point the transfer function (T) is a half and the power spectrum is boosted by a factor of 2 ($Power \propto Signal^2$). However, in low dissipation cases most of the energy is contained in the lower frequency range. It is thus advantageous to choose lower values of the high frequency cut-off point, the aim being to minimise noise contamination. The cut-off chosen is dependent on the dissipation levels observed. Four different frequency values are used. They are summarised in table 5.02.

Table 5.02 : High frequency cut-off limits with wavenumber (k) and wavelength (λ) based on a fall velocity of 80cms^{-1}.

Dissipation Range (Wm^{-3})	f (Hz)	k (m^{-1})	λ (m)
$\epsilon>3x10^{-4}$	55	433	0.0145
$3x10^{-5}<\epsilon<3x10^{-4}$	40	314	0.0200
$1x10^{-5}<\epsilon<3x10^{-5}$	30	236	0.0266
$\epsilon<1x10^{-5}$	20	157	0.0400

By imposing an upper frequency limit, a fraction of the energy present in the complete signal is thus unaccounted for. This is compensated for via the Kolmogoroff hypothesis *i.e.* it is assumed that the measured spectrum will assume a certain spectral form. The spectrum to which the data is fitted is that due to Nasmyth (1970). This allows the measured signal to be boosted to account for the energy lying outside the spectral range of the observations. The boost factor is calculated taking into account spectral limits, fall speed and the water temperature. The signal is also boosted to account for high frequency amplifier roll-off.

At low frequencies there is some leakage of energy from the mean flow due to non-stationarity within a depth bin. In order to avoid including this noise in the dissipation spectrum as well as low frequency resonant wobbles of the instrument the low frequency cut-off is set to 2Hz.

Figure 5.04 shows predictions of how much of the dissipation spectrum is directly observed using the spectral cut-offs specified above. It shows that for the majority of the observed dissipations ($1x10^{-6}$ to $1x10^{-2}$ Wm^{-3}) over 80% of the dissipation spectrum is observed, and so the uncertainty introduced by assuming the spectral shape of Nasmyth (1970) is small. This uncertainty is increased for higher dissipations as more of the dissipation occurs at frequencies greater than the cut-off and it becomes necessary to boost the spectrum by over 50%. Gargett *et al.* (1984)

suggest that the spectrum may become distorted so that isotropy breaks down very near the bed. The largest uncertainty in the measurements is therefore for the highest values of dissipation measured near the bed.

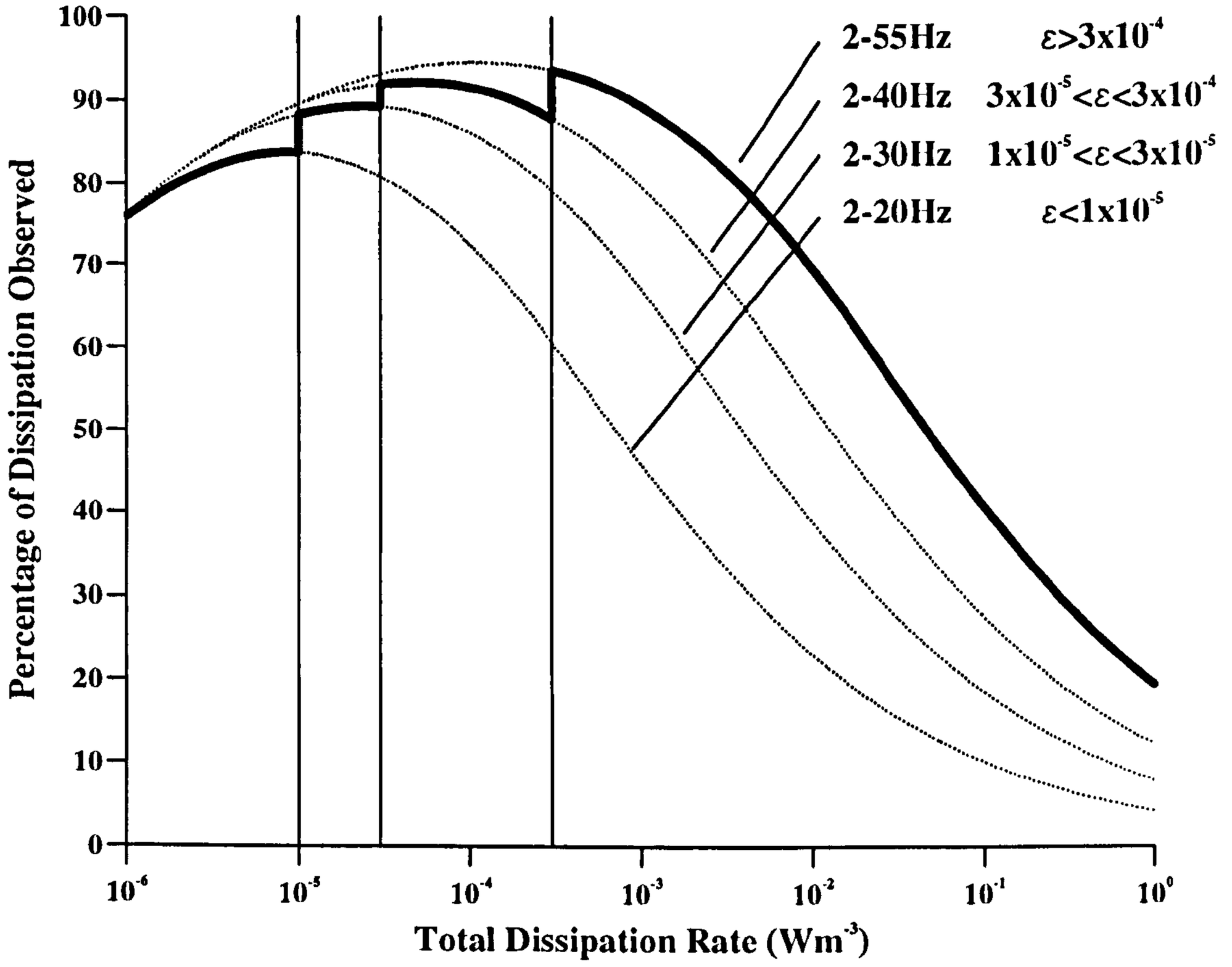

Figure 5.04 : Estimates of the percentage of total dissipation measured for particular spectral cut-offs, assuming the spectral shape of Nasmyth (1970).

5.2.3 Noise Levels in the FLY System.

Noise is present in any measurement system. The amount of noise present will determine the lowest dissipation levels measurable. For this system low levels of noise, equivalent to a dissipation rate of $\approx 3.0 \times 10^{-7}$ Wm^{-3} are present (Dewey *et al.* (1987)). There are two principal sources of noise : electronic noise and instrument vibration.

Electronic noise may be present as low level noise both throughout the spectrum and

as spectral peaks. However, these peaks tend to be at high frequencies and as such, do not contribute to the dissipation rate in regions of weak turbulence.

Mechanical instrument vibrations present themselves as peaks throughout the lower end (<20Hz) of the spectrum. There are two sources, namely structural resonance of the probe guard-profiler system and vibrations caused by the shedding of eddies from leading edges of the profiler. The profiler is designed to minimise and spread such noise through the spectrum.

Very low frequency noise contamination of the dissipation spectrum is avoided by the 2Hz low frequency cut-off already described.

The lowest dissipations result from calculations where the spectral limits are chosen to be 2 and 20Hz. This frequency range represents eddies ranging from 4 to 40cm in diameter. When dissipation levels are very low, the majority of the turbulent kinetic energy lies at frequencies less than 10Hz. To examine the noise contribution at these low dissipation levels, consider the ratio of dissipation at frequencies 2-10Hz (assumed to be real dissipation) and 2-20Hz which contains the part of the spectrum most contaminated by noise (10-20Hz). This comparison is shown in figure 5.05. Also shown is the theoretical result from the Nasmyth (1970) spectrum which contains no noise contribution.

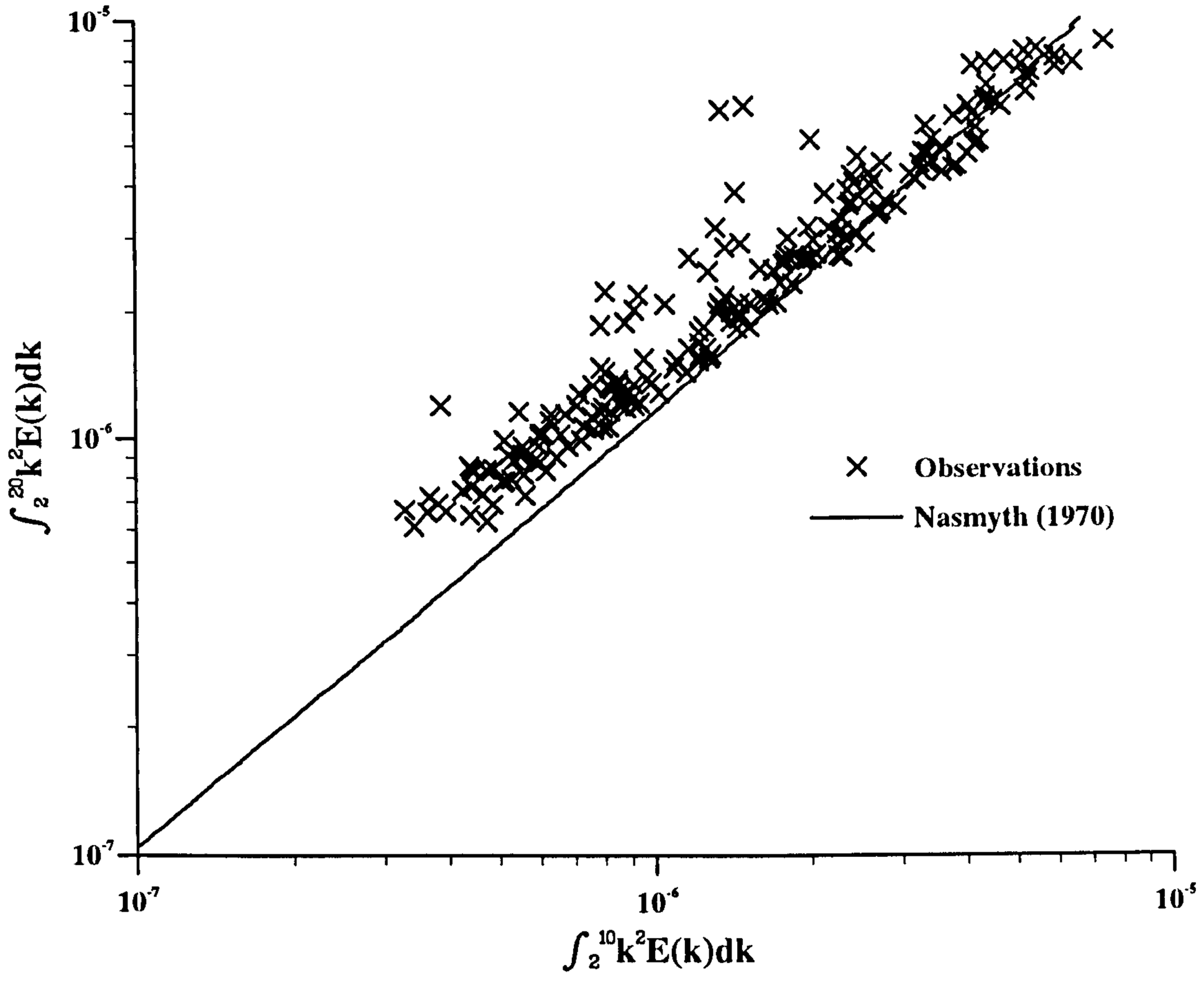

Figure 5.05 : Noise contamination at low dissipations.

It can be seen that noise contamination is small at dissipation levels as low as $1x10^{-6}$ Wm^{-3} since the observations start to deviate from the noiseless Nasmyth (1970) result at dissipations below this value.

5.2.4 Errors and Uncertainties in ϵ.

There will always be a random error with a single estimate of ϵ. This is why between 6 and 10 profiles of dissipation are measured and averaged each time the dissipation rate is measured. For this approach to be valid it has to be assumed that the flow is stationary for the duration of these 6 to 10 drops which is valid for this study, where the mean flow is a semi-diurnal tidal flow.

The uncertainties associated with sensor calibrations and with using equation (5.01) to calculate the microstructure shear are significant and are detailed below, as given

by Dewey and Crawford (1988). The fall speed w changes very slowly with depth and is calculated at each depth from the differentiated fourth order fit to the pressure record. The maximum error in w is 5% which results in a 10% error in the microstructure shear and a 20% error in the variance from which ϵ is calculated. The differentiator gain is known to approximately 2% and the shear probe sensitivity to approximately 7%. The dynamic viscosity is calculated from the formula of Miyake and Koizumi (1988) and is known to within 5%. All of the above, when added together give a total uncertainty in ϵ of approximately 43%. However, this is a conservative estimate since all the errors have been added linearly. A more realistic estimate is obtained by adding the square root of the individual uncertainties which results in a total uncertainty in ϵ of approximately 20%.

Part of the uncertainty in the shear probe sensitivity is due to the fact that S is dependent on water temperature. In general S increases with temperature. Historical calibrations were used for each shear probe (several probes were used throughout the course of the experiments) to adjust the probe sensitivities to their appropriate values, given the observed water temperature. Typical sensitivity-temperature data shows the sensitivity increasing approximately linearly with temperature.

The shear probe sensitivity is also dependent on the angle of attack of the probe *i.e.* the angle from the vertical at which the probe is falling through the water. Provided that this angle is less than 5° then the deviation in S is only a few percent (Dewey *et al.* (1987)). Tilt data from several probe drops during the survey at IS1_2 shows an average tilt of about 3°-4°. Variations from the mean are to be found at the surface but this is unimportant since dissipation measurements made within 10m of the surface are ignored due to the turbulence generated by the ship wake. For all of the turbulence data used, the tilts were observed to exceed a 1.5° shift from the mean value in 3% of the bins analysed and 3° in 0.5% of the depth bins. It can therefore be assumed that the variation in angle of attack is not sufficient to lead to a deterioration in the 7% error figure.

5.3 The CTD Profiling System.

5.3.1 The CTD.

The profiling CTD used was a Neil Brown MkIIIb unit equipped with auxiliary sensors and mounted on an aluminium frame along with a Sea-Tech transmissometer and a rosette sampler. Data is transmitted in real time to a micro-computer on both the down and upcasts via a single conductor armoured cable.

Pressure is measured using a high performance strain gauge bridge transducer. The temperature sensor is a platinum resistance sensor coupled with a fast response thermistor. Conductivity is measured using a four-electrode conductivity cell. Sensor specifications are shown in table 5.03.

Table 5.03 : Sensor specifications for the Neil Brown MkIIIb CTD unit.

Sensor	Range	Accuracy	Resolution	Response Time (ms)
Pressure (dBar)	0 to 320	±0.5	0.005	
Temperature (°C)	-3 to 32	±0.005	0.0005	200
Conductivity (mmho/cm)	1 to 65	±0.001	0.003	30

5.3.2 CTD Sensor Calibration.

The CTD temperature reading is calibrated using results from SIS RTM4002 reversing thermometers. These instruments have an accuracy of ±0.001 °C and were mounted on the side of one of the GO-FLO water bottles on the rosette sampler. They reverse and record the *in situ* temperature when the bottle is fired. It was therefore necessary to ensure that the entire CTD unit was in homogeneous water when firing the bottles.

Upon completion of a cruise the reversing thermometer temperatures were averaged (3 in the case of the March cruise and 2 for the July study) and T_{AVG} was plotted against the corresponding CTD values (T_{CTD}). After the removal of any obviously spurious data points a regression analysis was performed. This provided an equation which could be used to correct the CTD temperatures

$$T_{AVG} = A\,T_{CTD} + B \qquad (5.04)$$

To check for any drift in instrument performance throughout a cruise period, the difference between the T_{CTD} and the T_{AVG} was plotted against time. The results showed no obvious drift for any of the cruises.

Salinity was calibrated by comparing the CTD salinity (S_{CTD}) with the salinity of a bottle sample (S_{BOT}) which was determined using a Guildline AutoSal (Guildline Instruments (1985)). Regression analyses were then performed in an identical fashion to before, providing coefficients for the equation

$$S_{BOT} = C\,S_{CTD} + D \qquad (5.05)$$

Again, there was no significant drift in instrument performance over the period of any of the cruises.

The coefficients obtained for both the temperature and salinity calibrations are shown in table 5.04 along with the R^2 values obtained from the regressions.

Table 5.04 : CTD temperature and salinity calibrations.

Cruise	A	B	C	D	R^2_T(%)	R^2_S (%)	$NOBS_{T,S}$
March 1993	1.001	-0.008	0.997	0.185	100.0	99.9	52,67
July 1993	1.013	-0.137	0.999	0.096	99.9	86.9	28,24

To calibrate the pressure sensor, pressure recorded with the instrument sitting on deck was noted and subtracted from pressure recorded during profiling. For the March 1993 cruise there was no correction whilst for the July 1993 cruise the reading from the pressure sensor in air was 0.9m and so this was the correction applied. It did not drift during the cruise.

Calibration of the Sea-Tech transmissometer is described in section 5.5.2.

5.3.3 CTD Data Processing.

Salinity was calculated from conductivity and temperature by the Practical Salinity Scale 1978 (Unesco (1981)) and densities from the international equation of state 1980 (Unesco (1981)). For all the data in this study the effect of pressure on these calculations is negligible. The data was pressure averaged (to account for the motions of the ship during profiling) into bins of length 0.2m.

5.4 Acoustic Doppler Current Profile (ADCP) Measurements.

Acoustic Doppler Current Profilers (ADCPs) emit an acoustic signal and detect the backscattered signal from particles moving with the water column (whose frequency has been shifted by the Doppler effect).

There are essentially two classes of ADCP : (i) ship-mounted where the instrument protrudes through the hull of the ship and the acoustic signal is transmitted down towards the bed and (ii) bottom-mounted where the instrument is fixed on a frame designed to sit on the seabed and the signal is transmitted up towards the surface. Both instruments use an array of transducers to emit and receive the acoustic pulses, commonly known as 'pings'. Typically, pings are transmitted at an angle of 30° to the vertical.

The water velocity relative to the instrument platform is calculated by examining the

Doppler shift of the acoustic pulse returned from 'depth bins' set by range gating. Horizontal and vertical velocities can then be calculated from the along-beam velocities although vertical velocities tend to be smaller than instrument noise levels. Depth bins can be as small as 1m giving good vertical resolution which is the principal advantage that the ADCP has over a moored array of current meters. On cruise CH102, the R.R.S. Challenger's ship-mounted ADCP was used to monitor the currents at IS1_2 and IS3.

5.4.1 The R.R.S. Challenger's Ship-Mounted ADCP.

The instrument on board the R.R.S. Challenger is a Rowe and Dinas (RDI) instrument. The operating frequency is 153.6kHz. It uses an array of four transducers to emit and detect the acoustic signal. Because the instrument is ship-mounted the water velocity is measured relative to the hull of the ship which may itself be moving. Thus, a separate acoustic pulse is used to determine the velocity of the ship so that it can be subtracted from the recorded water velocity. This is known as bottom-tracking and can only be used in water less than 200m in depth which is the case in the present study where the depth is less than 100m. The ADCP was used at both tidal cycle stations to monitor the mean flow and the essential instrument settings for each survey are shown in table 5.05.

Table 5.05 : ADCP set-up for March 1993 (CH102) cruise.

Site	IS1_2	IS3
Sampling Interval	10 mins	5 mins
Bin Size	2m	4m
First Bin Depth	6m	7m

5.4.2 Errors and Uncertainties Pertaining to ADCP Operation.

The ADCP was used only in bottom-tracking mode and, in this case absolute water velocities have a relatively small error of approximately $1cms^{-1}$, after processing and averaging (Joyce (1989)). Several errors arise when calculating absolute velocities.

Some are inherent to the instrument and some depend on the movement of the ship. One source of error is the short-term error, inherent to individual velocity profiles. Lwiza *et al.* (1991) give the expression for the short-term random error as

$$\sigma_v = \frac{1.5\sqrt{2}\,c^2}{16\,\pi\,F\,D\,\tan\gamma\,\sqrt{N}} \qquad (5.06)$$

where c is the speed of sound in ms^{-1}, F is the transmitting frequency in Hz, D is the vertical bin length in m, γ is the inclination angle of the transducer with the vertical (30°) and N is the number of pings transmitted during an averaging ensemble.

For the IS1_2 and IS3 survey stations values of σ_v are calculated to be $2.2cms^{-1}$ and $1.6cms^{-1}$ respectively.

Further errors arise from the pitch and roll of the ship and transducer misalignment, an error incurred when the instrument is fitted. Except under extremely rough conditions, the errors introduced by pitch and roll are insignificant (Lwiza (1990)). One method for investigating the system misalignment was suggested by Joyce (1989) and Pollard and Read (1989). The method involves comparison of the ship velocity calculated from the ADCP with velocities estimated from navigation data. The correcting procedure is in the form of a rotation and scaling of the ADCP velocities as

$$\begin{aligned} u_s &= -A\,(u_d\cos\phi + v_d\sin\phi) \\ v_s &= -A\,(-u_d\sin\phi + v_d\cos\phi) \end{aligned} \qquad (5.07)$$

where u_s and v_s are the ship velocities calculated from the navigation data (such as GPS), u_d and v_d are the ADCP derived ship velocities, A is the scaling factor required to correct the ADCP velocities and ϕ is the clockwise misalignment angle by which the transducers are rotated on installation. Thus, from (5.07)

$$A = \left(\frac{u_s^2 + v_s^2}{u_d^2 + v_d^2} \right)^{\frac{1}{2}} \quad , \quad \tan\phi = \left(\frac{u_d v_s - v_d u_s}{v_d v_s + u_d u_s} \right) \tag{5.08}$$

The majority of the time that the ADCP was in use the ship was holding station and so no ship speeds were recorded. However results from two previous studies gave values for A of 0.999±0.009 and 1.02±0.01 and ϕ values of 2.0°±1.0° and -1.5°±0.5° (Durazo-Arvizu (1993), Souza (1994)).

5.5 Suspended Particulate Matter (SPM) Measurements.

5.5.1 The Transmissometer.

When a collimated beam of light propagates through a medium, it will suffer a loss in intensity. This loss, also termed extinction or attenuation, is wavelength dependent and is due to two processes: absorption and scattering. The attenuation in intensity (ΔI) experienced by a light beam as it propagates along a path length Δr is given by

$$\frac{\Delta I}{I} = -(A+S)\Delta r \tag{5.09}$$

where I is the radiant flux, A represents losses due to absorption (by the water and any solute) and S represents losses due to scattering processes. Integrating with respect to path length from 0 to r gives

$$\ln\left(\frac{I}{I_0} \right) = -(A+S)r \tag{5.10}$$

So that the attenuation coefficient α is given by

$$\alpha = (A+S) = -\frac{1}{r}\ln\left(\frac{I}{I_0}\right) \qquad (5.11)$$

where I is now the measured radiant flux and I_0 is the incident radiant flux.

Thus, by measuring I and I_0 the transmissometer is capable of calculating an attenuation coefficient which will be proportional to the amount of absorption and scattering by the water column. However, it has to be assumed that the spectrum of sediment sizes remains unchanged throughout the measurement period and herein lies one of the weakpoints of such an attenuation measurement.

The transmissometer used to monitor the levels of suspended particulate matter (SPM) was designed and built at the University of Wales, Bangor (UWB). A schematic diagram is shown in figure 5.06. These instruments have been in use for several years and have proved to be reliable.

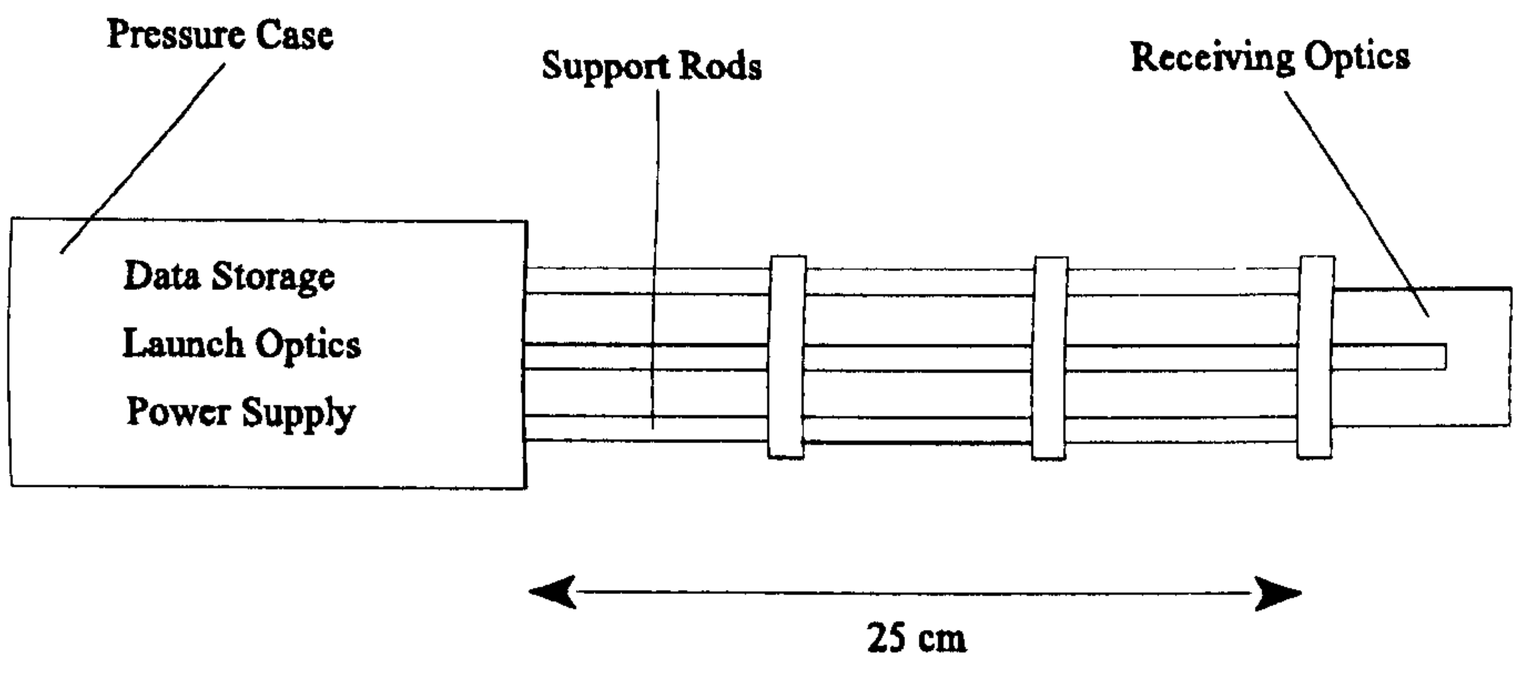

Figure 5.06 : Schematic diagram of the UWB transmissometer.

The optics of the transmissometer are similar to those of the Sea-Tech instrument used on the CTD frame (Bartz *et al.* (1978)). It emits a collimated beam of light at 665nm ± 11nm from a light emitting diode (LED). This wavelength is chosen in

order to minimise the effect of light absorbance by gelbstoff (Jerlov (1976)). It is necessary that the light beam is collimated so that any losses experienced are due only to absorption and scattering by the water and its components. The attenuated light is then detected by the photocell and instantaneous (compensated for ambient light) values are logged on a solid state memory card at one minute intervals. The memory card is capable of storing 3 months worth of data.

5.5.2 Transmissometer Calibration.

The calibration procedure is in two stages. Firstly, gravimetric analysis is used to calibrate the CTD transmissometer. Throughout both cruises, GO-FLO bottle samples were collected during CTD casts. Known volumes of water were filtered through pre-weighed GF/F glass microfibre filters which were then dried and re-weighed, allowing gravimetric determination of the total SPM concentration. The beam attenuation measured by the CTD transmissometer was then calibrated against the SPM concentration. Finally, the moored transmissometers were calibrated against the CTD instrument in a similar fashion to the way in which the RCMs were calibrated *i.e.* the moored instruments were suspended below the CTD and the entire assembly was placed in homogeneous water for several sampling intervals (see section 4.5). The calibrations for the CTD (Sea-Tech) transmissometer for the March 1993 and July 1993 cruises are shown in figure 5.07.

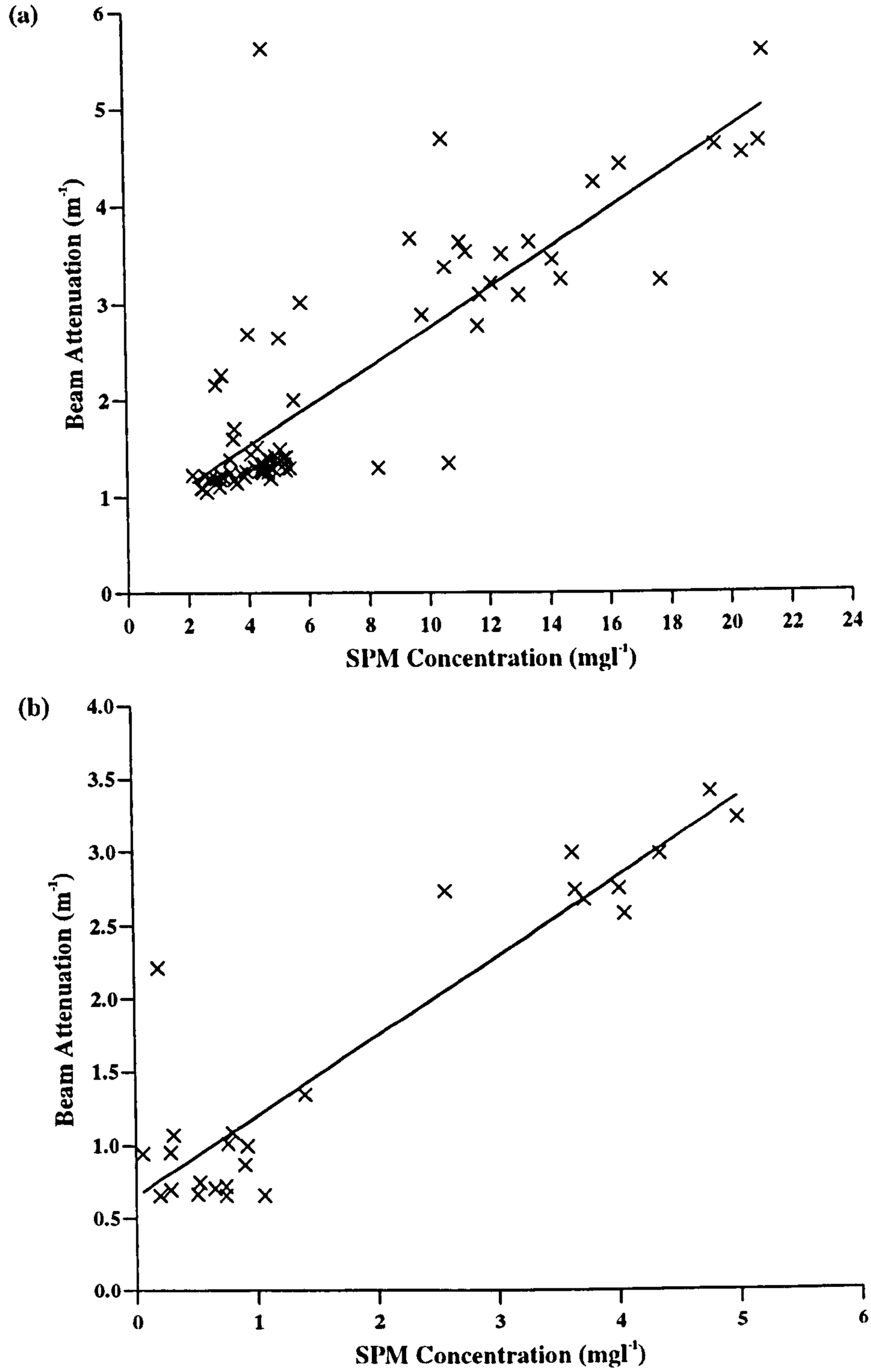

Figure 5.07 : Transmissometer calibrations.

a) March 1993.

b) July 1993.

The results of the regression analyses are summarised in table 5.06.

Table 5.06 : CTD transmissometer regression coefficients.

Cruise	RK_{CON}	RK_{INT}	R^2	NOBS
March 1993	0.202	0.714	68.3%	74
July 1993	0.542	0.653	84.6%	26

The regression coefficients obtained are highly significant despite the considerable scatter observed. The scatter is due to the gravimetric technique used and localised or temporal variations in the particle population characteristics such as size, shape and refractive index variations.

5.5.3 Moored Transmissometer Data Processing.

Voltages are logged onto the solid state memory every minute. The data is downloaded from the instrument onto a PC and the memory card cleared so that it can be re-used. The recorded voltages are first converted into transmittance values (Trans) using

$$\mathbf{Trans} = 100\left(\frac{V - V_0}{V_{100} - V_0}\right) \qquad (5.12)$$

Before and after deployment of the instrument a dark voltage (V_0) is measured. The instrument is out of the water and several readings are averaged with the LED covered. The V_{100} values are obtained from the intercalibration between the moored (UWB) transmissometers and the CTD (Sea-Tech) instrument. This is usually performed after the moored instrument has been recovered. If pre- and post-deployment V_o and V_{100} values are available and there is any drift over the deployment period then a linear interpolation is used to find the intermediate values, otherwise the single value available is used for the entire deployment. This is justifiable since the moored transmissometers were only deployed for a single day.

The beam attenuation is then calculated using the equation

$$\mathbf{BA\ (m^{-1}) = -\frac{1}{r}\ln\left(\frac{Trans}{100}\right) = -4.0\ln\left(\frac{Trans}{100}\right)} \qquad (5.13)$$

Finally, using the calibration constants obtained earlier for the CTD instrument, the SPM concentration can be calculated using

$$\mathbf{SPM\ \ Conc\ \ (gl^{-1}) = \frac{(BA - RK_{INT})}{RK_{CON}}} \qquad (5.14)$$

5.6 Current Measurements from Moored Instruments.

5.6.1 The Aanderaa Recording Current Meter (RCM 7/8).

The RCMs used are self-recording current meters which are capable of monitoring vector-averaged speed, direction and temperature. Conductivity and water pressure sensors can also be fitted. The instrument records data internally in a removable and re-usable solid state Data Storage Unit (DSU). The measuring cycle is accurately monitored by a built-in quartz clock.

Temperature is measured using a thermistor which extends into the water and conductivity is measured by an electrodeless induction type conductivity cell. The current meter aligns itself in the current and the orientation of the instrument is measured by an internal compass. A rotor at the top of the instrument is used to measure current speed. Rotor revolutions are magnetically transferred to an electronic counter which counts every half revolution. A vector-averaging method is used for recording the speed and direction of the current.

The current meter consists of two main parts, a vane assembly including tail fins and balance weights to ensure the meter orientates itself with the flow and a pressure case housing all of the electronics and data storage equipment. The two are attached to

a spindle through which the mooring wire runs. The entire instrument is gimballed allowing it to deviate up to 27° in any direction.

5.6.2 RCM Calibration.

Different procedures were adopted for calibration of the conductivity and temperature sensors.

Conductivity cell.

The conductivity measured by the RCM (C_{RCM}) is related to the true conductivity as given by the calibrated CTD value (C_{CTD}) through the use of a form factor, denoted *ff*. These discrepancies arise because of small, but significant changes in the geometry of the conductivity cell. Thus,

$$\mathbf{C_{CTD} = ff \times C_{RCM}} \qquad (5.15)$$

So, all conductivity measurements are calibrated by multiplying the measured conductivity value by the mean value of the form factor for each current meter.

Temperature sensor.

In this case calibration is achieved by using the mean difference, denoted ΔT, between the RCM temperature and the calibrated CTD temperature. This mean difference was then added/subtracted from the RCM temperature.

The principal errors in the temperature and conductivity readings produced by the RCM are due to the resolution of the instrument and uncertainty in ΔT and *ff*. The combination of these errors gives a final error of ±0.05 °C in temperature and ±0.07 psu in salinity. The calibrations used for each current meter are summarised in table 5.07.

Table 5.07 : Current meter calibrations.

Mooring	Position	Height Above Bed (m)	Current Meter No.	*ff*	ΔT	Comments
IS1	53°51.78'N	41	9580		+0.0364	no conductivity data
	04°23.30'W	5	3321	1.0004	+0.0625	
IS2	53°50.66'N	44	9415	1.0027	+0.1328	
	04°27.64'W	9	8248	1.0004	+0.1493	
ISS	53°51.48'N	80	10666	1.0148	-0.0493	
	05°27.09'W	12	10665	1.0163	-0.1519	

Speed and direction.

Facilities were not available for calibration of these sensors, although the compasses had previously been calibrated by the manufacturers and Research Vessel Services, Barry, South Wales. The manufacturer quotes the accuracy to which the speed can be measured as either ±1 cms^{-1} or ±2% of the measured speed, whichever is the greater. The error in the direction from the RCM compass is given as ±5° (Aanderaa (1992)).

5.6.3 RCM Data Processing.

After recovery and an *in situ* post deployment calibration the current meters were cleaned and the DSU was removed from inside the pressure casing. The data was then downloaded to a PC before being transferred to a mainframe computer for processing. The conversion from raw data to engineering units was achieved using formulae supplied by the manufacturer. The above calibrations and magnetic corrections were then applied to give time series of temperature, salinity, north-south and east-west velocity components. There is no pressure data since none of the instruments was fitted with a pressure sensor.

CHAPTER SIX

Mean Flow, SPM and Turbulent Flow Results

6.1 Introduction.

In this chapter, the various datasets obtained from the experiments conducted during the cruises described in chapter four are presented. Water column structure (CTD), mean flow (RCM and ADCP), SPM concentration (transmissometer and settling velocity tube) and turbulent dissipation rate (FLY) results are presented for each of the three sites investigated during the course of the experimental program. Some general comments are made concerning data reliability and quality and evident trends in the data are discussed.

As described in chapter four, two cruises were conducted in 1993 : one from the Natural Environment Research Council vessel R.R.S. Challenger (cruise CH102) in March and another in July from R.V. Prince Madog (cruise PM93). Cruise CH102 concentrated on two sites where the water column was vertically homogeneous. The first experiment was conducted south of the Isle of Man at IS1_2 where a pair of moorings were deployed (IS1 and IS2). A CTD/FLY survey was conducted midway between IS1 and IS2 (at IS1_2) over two tidal cycles. A second 24hr CTD/FLY survey was undertaken at IS3 in St. George's Channel. For both these experiments the data return was good. The only failures were two of the InterOcean S4 current meters deployed on mooring IS2 and the conductivity cell of RCM 9580 which was deployed on mooring IS1. A summary of the data avaliable for analysis is shown in table 6.01.

Table 6.01 : Data return from cruise CH102.

SITE -depth	INSTRUMENT -height	DATA RETURN
IS1 (54m)	RCM 9580 (41m)	Temp, Spd & Dir
	S4 265 (26m)	Spd, Dir, Instrument Tilt & Heading
	RCM 3321 (5m)	Temp, Sal, Spd & Dir
IS2 (62m)	S4 265 (50m)	Spd, Dir, Instrument Tilt & Heading
	Tr 2 (47m)	SPM Concentration
	RCM 9415 (44m)	Temp, Sal, Spd & Dir
	S4 920 (23m)	No Data
	RCM 8248 (9m)	Temp, Sal, Spd & Dir
	S4 119 (6m)	No Data
	Tr 1 (4m)	SPM Concentration
IS1_2 (60m)	CTD (2m-60m)	Temp, Sal & SPM Conc. Profiles
	FLY (0m-50m)	Turbulent Dissipation Rate Profiles
	SVT (30m)	Sediment Size Distribution (1 sample)
	ADCP (9m-53m)	U & V Current Profiles
IS3 (90m)	CTD (2m-90m)	Temp, Sal & SPM Conc. Profiles
	FLY (0m-75m)	Turbulent Dissipation Rate Profiles
	SVT (70m)	Sediment Size Distribution (3 samples)
	ADCP (7m-75m)	U & V Current Profiles

Key : RCM = Aanderaa Recording Current Meter.

S4 = InterOcean S4 Current Meter.

Tr = UWB Recording Transmissometer.

FLY = Turbulent Dissipation Rate Profiler.

SVT = Settling Velocity Tube.

Meterological data is available in the form of wind speed (measured at Ronaldsway on the Isle of Man) and incident radiation (from Aughton, near Liverpool) and is shown in figure 6.01. The two experimental periods were from Julian days 84.4 to 85.6 (for moorings IS1 and IS2 and survey site IS1_2) and 87.4 to 88.6 (for survey site IS3).

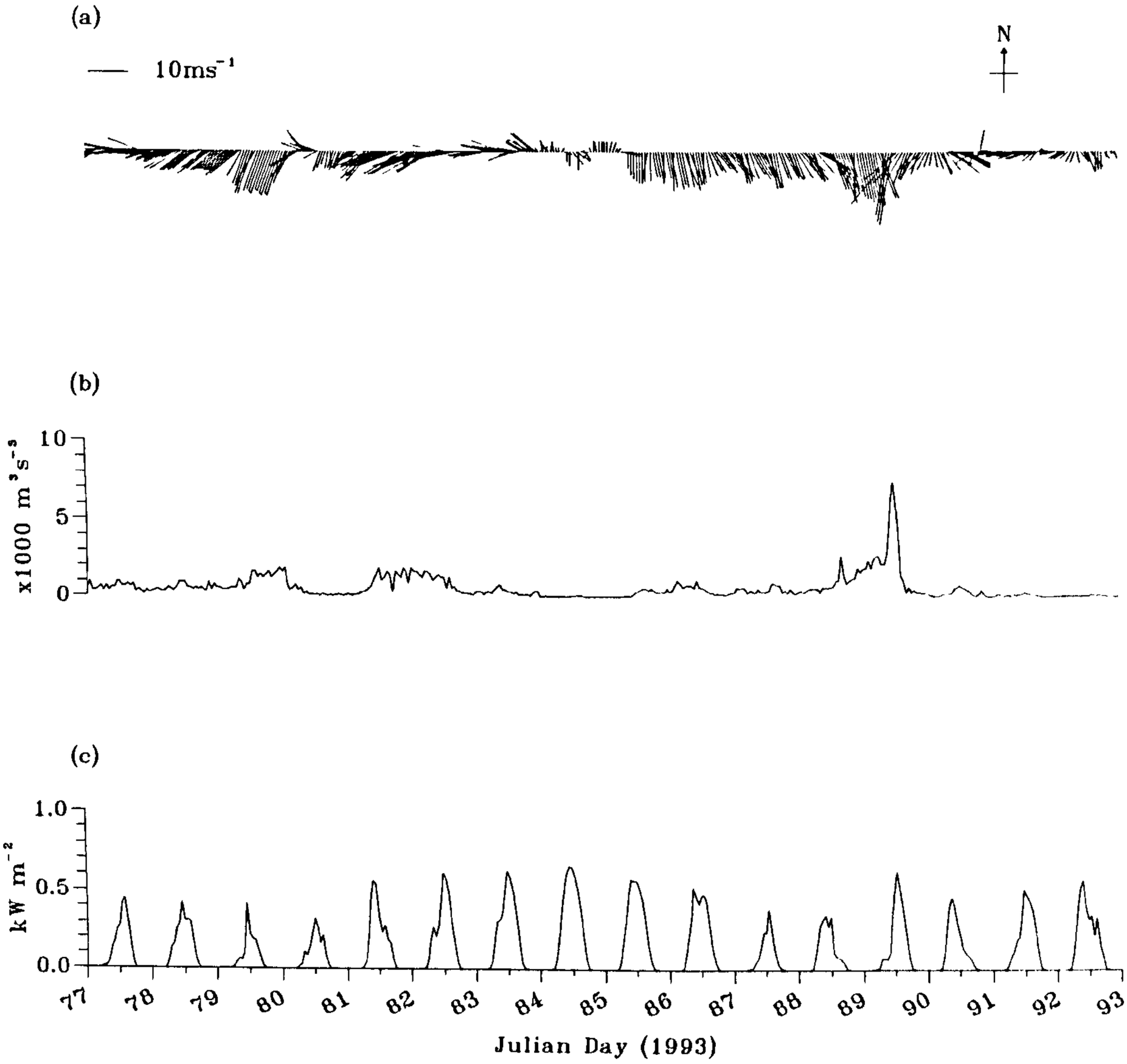

Figure 6.01 : Meterological data for Julian days 77 → 93, 1993.

a) Surface wind vector.

b) Wind speed cubed.

c) Incident radiation.

In July 1993, cruise PM93 returned to waters south of the Isle of Man in order to carry out a study similar to that made in March but in thermally stratified as well as mixed waters. A single mooring, instrumented with Aanderaa RCM and InterOcean S4 current meters and transmissometers was to be deployed for two tidal cycles at both mixed and stratified sites. A CTD/FLY survey was also to be undertaken alongside each of the moorings. However, only one of the experiments was completed, that at the thermally stratified site (ISS). This was due to a mishap on recovery of this mooring and subsequent bad weather preventing its redeployment at the mixed site (ISM). The data return from the moored instruments and the survey at ISS is summarised below in table 6.02.

Table 6.02 : Data return from cruise PM93.

SITE -depth	INSTRUMENT -height	DATA RETURN
ISS (90m)	S4 920 (85m)	No Data
	Tr 6 (83m)	SPM Concentration
	RCM 10666 (80m)	Temp, Sal, Spd & Dir
	S4 119 (46m)	No Data
	RCM 10665 (12m)	Temp, Sal, Spd & Dir
	S4 117 (9m)	No Data
	Tr 3 (6m)	SPM Concentration
	CTD (2m-90m)	Temp, Sal & SPM Conc. Profiles
	FLY (0m-80m)	Turbulent Dissipation Rate Profiles

There is no settling velocity tube or ADCP data as neither instrument was available for this cruise. The major failure was that of the InterOcean S4 current meters, none of which produced any useful data.

Meterological data is available from the same stations as before (Ronaldsway and Aughton) and is shown in figure 6.02. The deployment period of mooring ISS was from Julian day 187.2 to 188.6. Winds are seen to be light and incident radiation is

typical for July at this latitude.

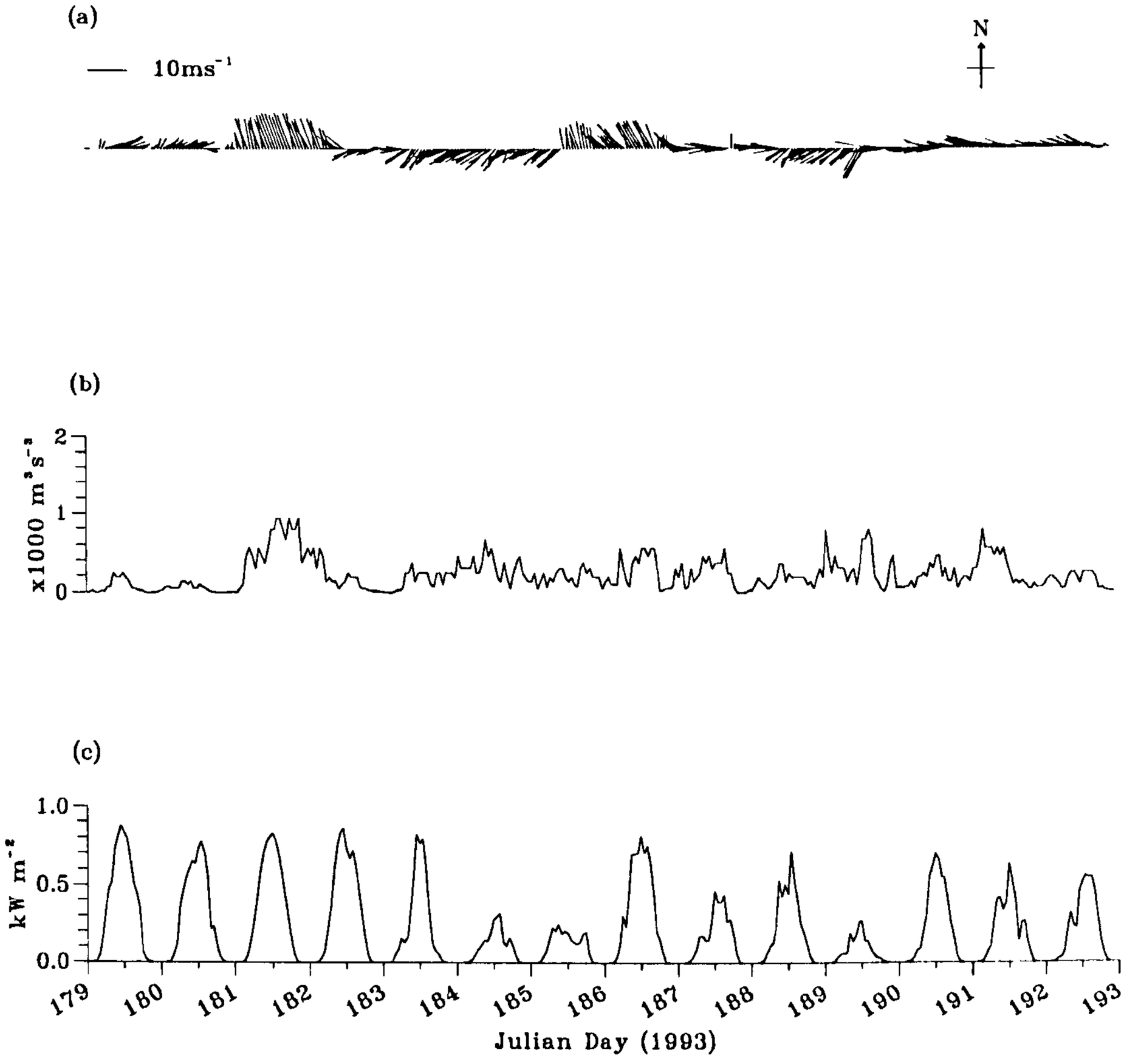

Figure 6.02 : Meterological data for Julian days 179 → 193, 1993.

a) Surface wind vector.

b) Wind speed cubed.

c) Incident radiation.

In the next section (6.2) the CTD water column structure measurements made at each of IS1_2, IS3 and ISS are presented and discussed. A combination of both moored (RCM) and profiling (ADCP) current meters were used to monitor the mean flow

conditions during the experiments. These results are the subject of §6.3. Sections 6.4 and 6.5 then discuss the SPM results (from the transmissometry and settling velocity tube studies) and turbulent dissipation rate measurements obtained using the FLY profiler. The final section of this chapter consists of a brief summary.

6.2 CTD Survey Results.

6.2.1 IS1_2 CTD Time Series Results.

Cruise CH102 was scheduled for March 1993 so that the water column at IS1_2 would be vertically homogeneous. During the CTD survey, 22 vertical profiles of temperature, salinity and SPM concentration were completed *i.e.* approximately one every hour. The calibrated data from the downcasts has been interpolated and is presented in the form of a contour plot, created using the UNIMAP graphics package. Contour plots of the temperature (°C), salinity (psu) and σ_t (kgm^{-3}) results are shown in figure 6.03. The vertical arrows indicate the timing of the CTD casts.

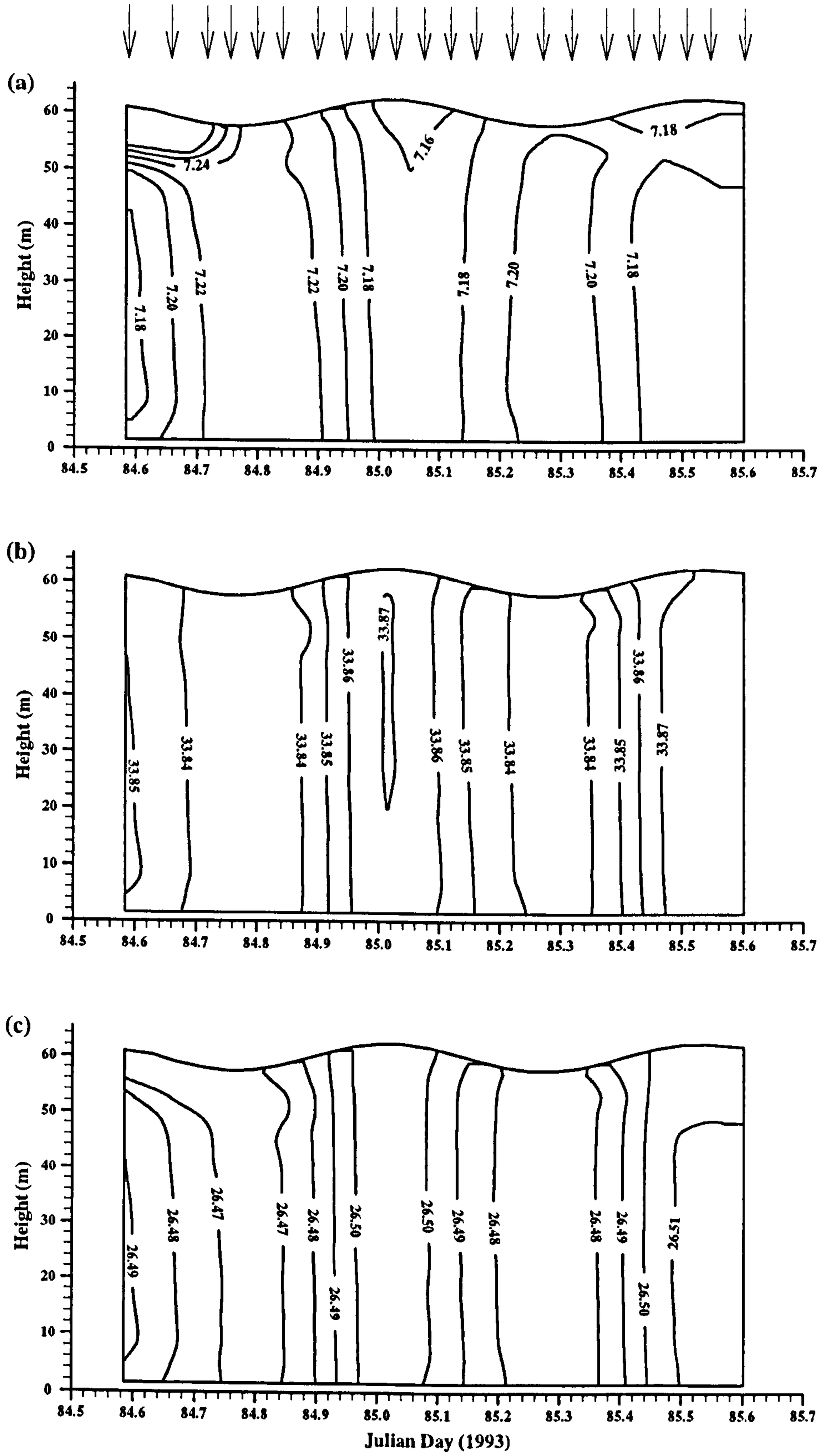

Figure 6.03 : IS1_2 CTD survey results : (a) temperature, (b) salinity and (c) σ_t.

Figure 6.03(a) shows evidence of diurnal (surface) heating, especially on Julian day 84, during which the strongest incident radiation was measured (0.65kWm^{-2}). Aside from this buoyancy input, the water column remained vertically mixed, with variations in temperature due primarily to advection of weak, horizontal temperature gradients. Between slack water events, the tidal excursion is approximately 8km, and the temperature changes by approximately 0.04°C. Thus, apart from the heating event, the temperature field for the duration of the survey can be given by T = 7.2°C ± 0.02°C.

The variation in salinity over the tidal cycle is 0.04 psu and is again, primarily due to the advection of horizontal gradients so that S = 33.85psu ± 0.02psu. The effect of diurnal heating at the start of the experiment can be seen in the σ_t contour plot (figure 6.03 (c)). However, for the purpose of this study, the water column can be considered vertically mixed for the duration of the survey since σ_t = 26.49kgm^{-3} ± 0.02kgm^{-3}.

Temperature, salinity and σ_t variations at a single height are available from the auxiliary sensors on Aanderra current meters, two of which were deployed on each mooring. This data is given in appendix A. The minor variations in temperature, salinity and σ_t over both tidal cycles comply with the results from the CTD survey conducted between the mooring sites. Comparison of the temperature and salinity results from the bed and surface RCMs reveals little or no barotropic component in the temperature field (the conductivity cell on the near surface RCM at IS1 failed to operate properly).

6.2.2 IS3 CTD Survey Time Series Results.

The second CTD survey conducted during cruise CH102 was at site IS3 in St. George's Channel where 21 temperature, salinity and SPM concentration profiles were completed. The water is deeper (90m) and the currents weaker than at IS1_2. The temperature, salinity and σ_t plots obtained are shown in figure 6.04.

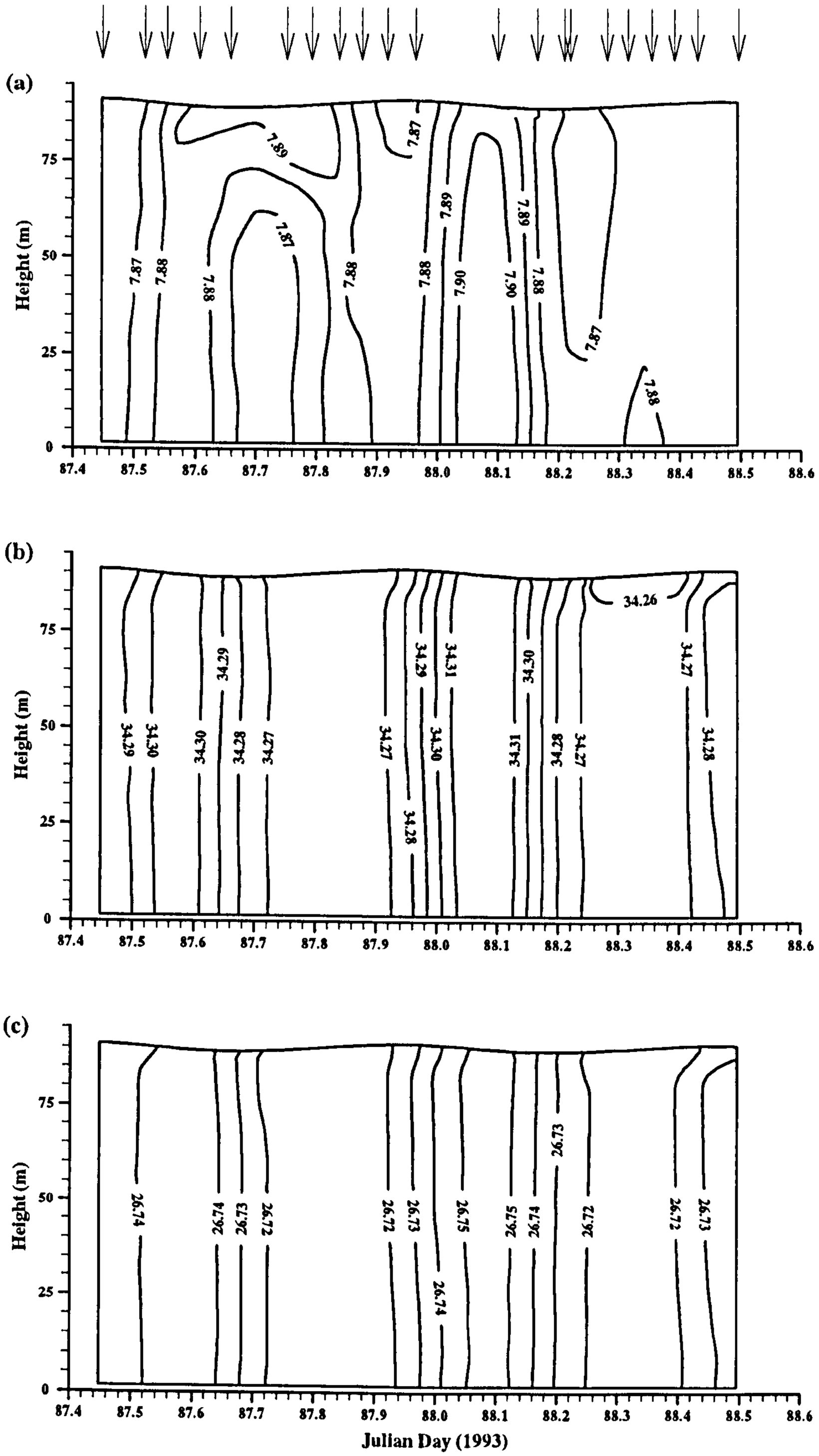

Figure 6.04 : IS3 CTD survey results : (a) temperature, (b) salinity and (c) σ_t.

As can be seen from figure 6.04, the water column remains mixed for the duration of the experiment, to an even greater extent than at IS1_2 since the incident radiation and diurnal heating is reduced. The temperature field can be given by 7.88°C ± 0.02°C. The variation of 0.02°C over the tidal cycle is found largely in the advected (horizontal) component. As before, the tidal excursion is of the order of several kilometres and so this change represents a very weak gradient.

Both the salinity and density fields are vertically uniform with S = 34.28psu ± 0.02psu and $\sigma_t = 26.73 kgm^{-3} \pm 0.02 kgm^{-3}$ so that the water column can be considered vertically homogeneous with weak horizontal gradients.

6.2.3 ISS CTD Survey Time Series Results.

In July 1993, during cruise PM93, 24 CTD profiles were completed during the survey at the thermally stratified site ISS. This data has been processed as before and contour plots of the temperature, salinity and σ_t fields are given in figure 6.05.

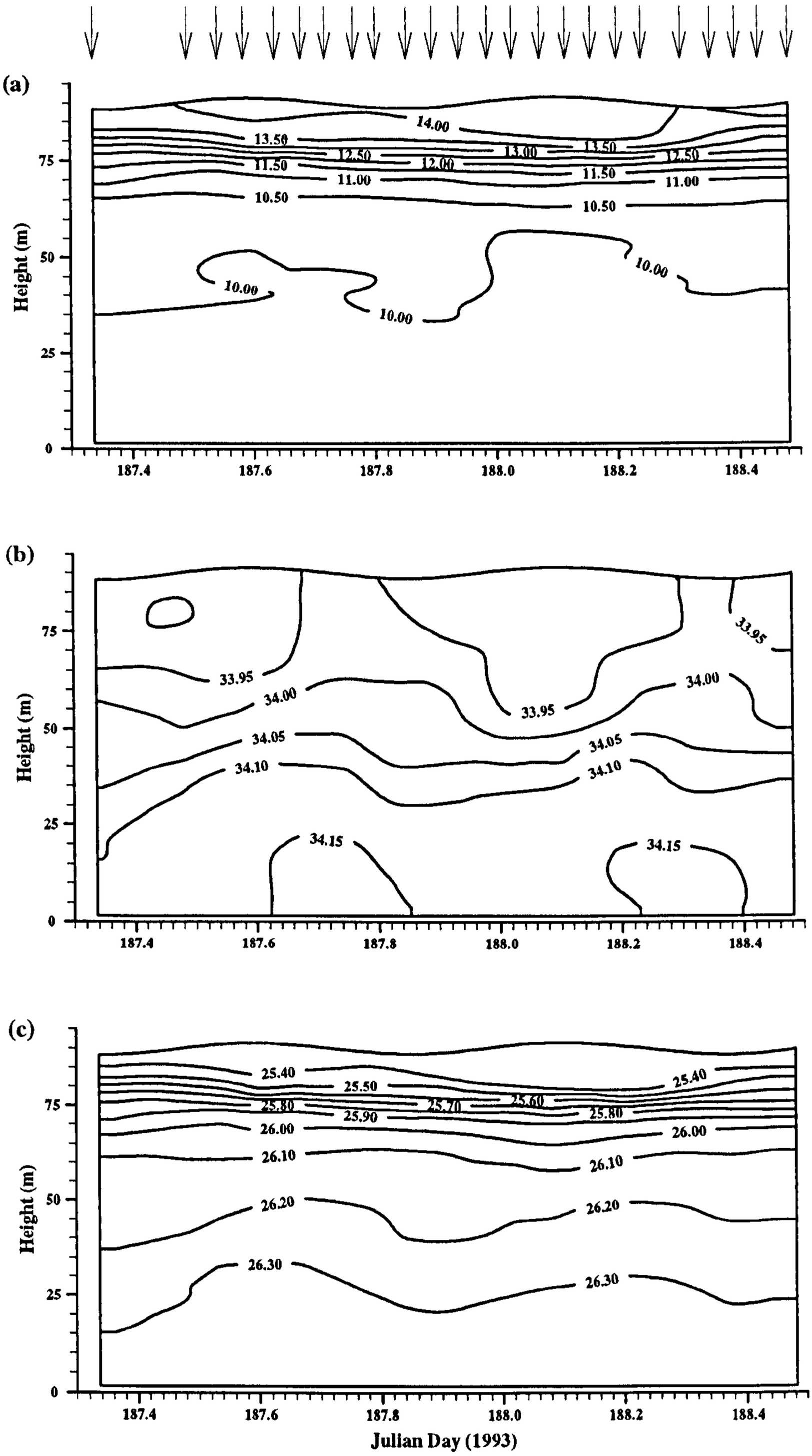

Figure 6.05 : ISS CTD survey results : (a) temperature, (b) salinity and (c) σ_t.

As expected, there is strong thermal stratification at this site. The bottom-surface temperature difference is of the order of 4-5°C, with bottom temperatures below 10°C and surface values usually over 14°C. The greatest vertical thermal gradient is to be found between 75 and 85m above the bed where the total temperature change is ~3°C. There is also some evidence in the surface layers of diurnal heating and cooling.

Figure 6.05(b) shows a largely uniform salinity field. Variations in the vertical are about 0.2psu with a very small horizontal variation, generally less than 0.05psu over the tidal cycle. Any haline stratification is dwarfed by the effects of the temperature field. This can be seen in the σ_t field where a strong pycnocline ($\Delta\sigma_t = 0.5 kgm^{-3}$) coincides with the observed thermocline. The total bottom-surface difference is approximately $1 kgm^{-3}$. Variations at any one height in the bottom waters are small ($\sim 0.05 kgm^{-3}$) but much larger in the surface waters ($\sim 0.6 kgm^{-3}$) where the vertical gradient is greater.

As before, the auxiliary (temperature and conductivity) sensors on the RCMs confirm the CTD results (see appendix A). RCM number 10666 was situated 80m above the bed and, as such is positioned in the middle of the thermocline where the vertical temperature gradient is greatest. This explains the nature of the large variations in temperature ($\Delta T \sim 3°C$, period~12hrs) recorded at this height which are due to the regular rise and fall of the sea surface. This temperature signature manifests itself in the density record as a change in density of $0.6 kgm^{-3}$ every 12 hours. Variations in salinity are small and fluctuate rapidly.

Temperature changes 12m above the bed (according to RCM 10665) are much smaller ($\Delta T \approx 0.2°C$) and salinity is approximately constant ($S = 35.2psu \pm 0.02psu$), as already shown by the CTD data. The overall result is a small variation in density with $\sigma_t = 27.17 kgm^{-3} \pm 0.02 kgm^{-3}$.

The data presented in this section shows that, during cruise CH102 the water column

remained vertically uniform for the duration of the experiments at both sites. In July thermal stratification has developed in the Western Irish Sea, providing an ideal site for study of the relationship between turbulent dissipation rate and SPM concentration in a stratified water column, one of the principal aims of the thesis. However, the next step is to discuss the mean flow conditions at each of the sites and this is the subject of the next section.

6.3 Mean Flow Results.

6.3.1 IS1, IS2 and IS1_2 Mean Flow Results.

The mean flow data presented here is from the Aanderaa current meters, two of which were deployed on each of IS1 and IS2. The data from the ship-mounted ADCP has not been presented but is in accord with the RCM measurements.

Figures 6.06 and 6.07 show time series of current velocity from the two RCMs on IS1 and IS2 respectively.

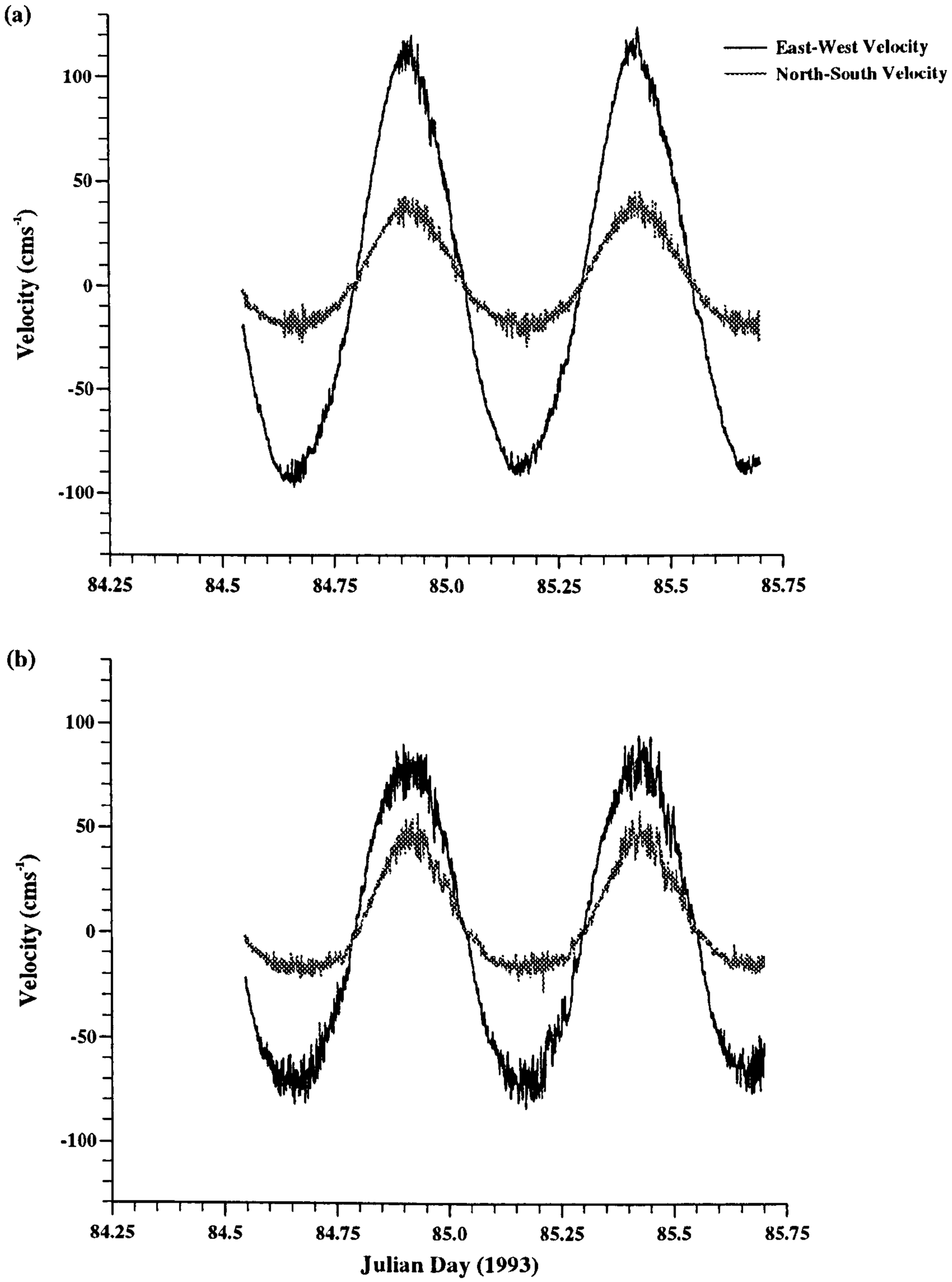

Figure 6.06 : IS1 u- and v-velocity components.

a) RCM 9580, 41m above the bed.

b) RCM 3321, 5m above the bed.

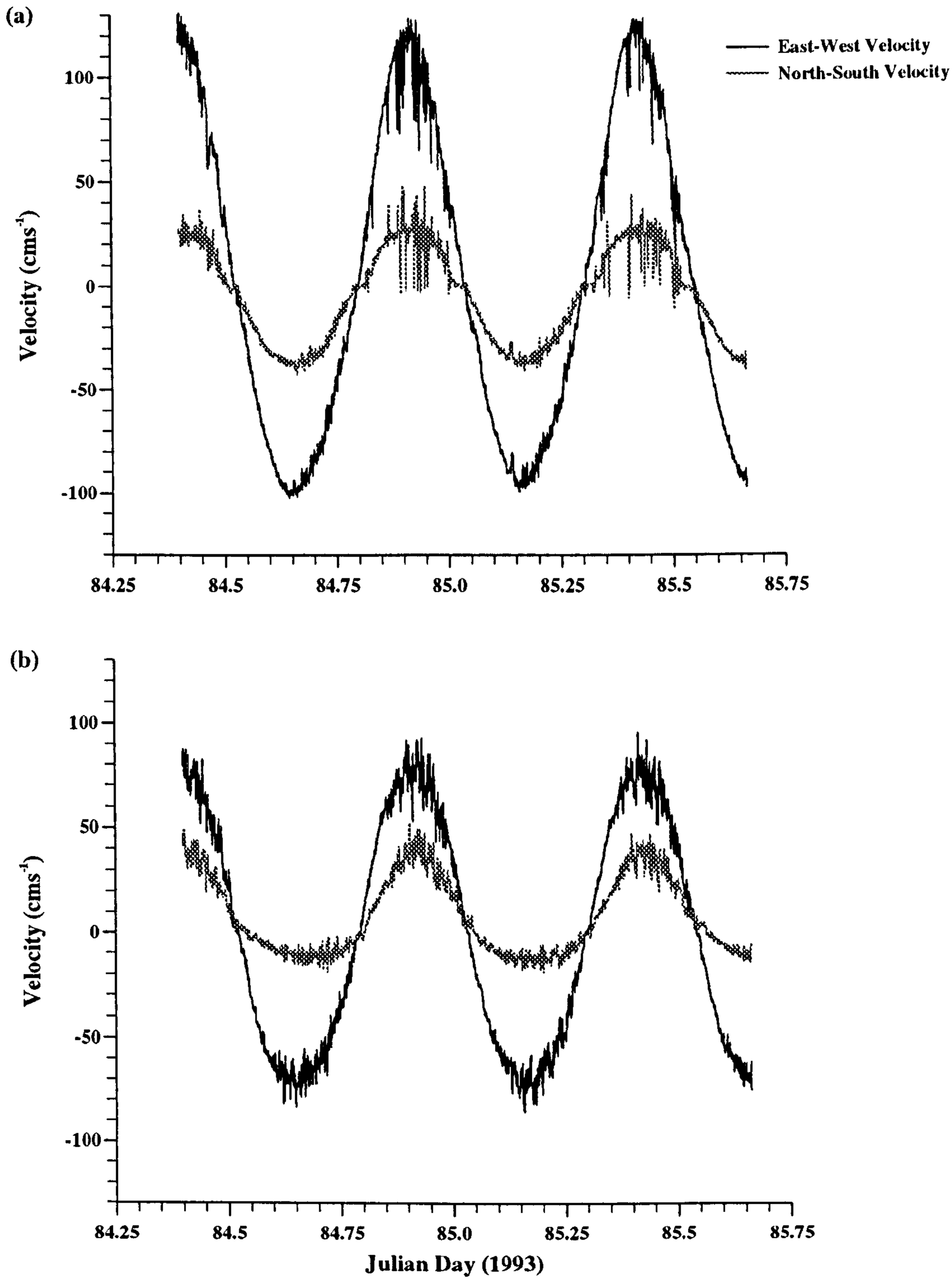

Figure 6.07 : IS2 u- and v-velocity components.

a) RCM 9415, 44m above the bed.

b) RCM 8248, 9m above the bed.

For both IS1 and IS2, the strongest currents are found on the flood phase of the tide with currents reaching a maximum of around 1.2ms^{-1} at IS1 and 1.3ms^{-1} at IS2. Near bed values are, as expected, lower at about 0.9ms^{-1}. Currents on the weaker, ebb phase reach 0.9ms^{-1} at IS1 and 1.0ms^{-1} at IS2 with near bed values of approximately 0.75ms^{-1}. The east-west velocity (from now on known as the u-velocity) is much stronger, by a factor of 2 to 3, than the north-south (v-) velocity.

The observed currents are dominated by the regular tidal currents which are known to exist in the Irish Sea. As shown earlier, horizontal gradients are weak and vertical density gradients almost non-existent due to lack of buoyancy input and the high levels of tidal stirring. Wind driven currents are unlikely to be a factor since winds were no more than 10 ms^{-1} for the 24 hour period before the deployment and were even lower and more variable for the duration of the deployment itself. Given that the maximum wind driven current at the surface will be of the order of 2% of the total wind speed, the currents resulting from the observed wind speeds will be negligible compared with the total flow speed.

In order to visualise both the direction and directionality of the observed flow it is instructive to plot the v-velocity component against its u counterpart. Such scatter plots reveal the nature of the tidal ellipse. Any significant residual flow will also become apparent. By using the same scale on both axes the direction of the current can be easily visualised since a straight, vertical line will represent north-south flow and a horizontal line east-west flow. Scatter plots of v versus u-velocity are shown in figure 6.08 for the IS1 instruments and figure 6.09 for IS2.

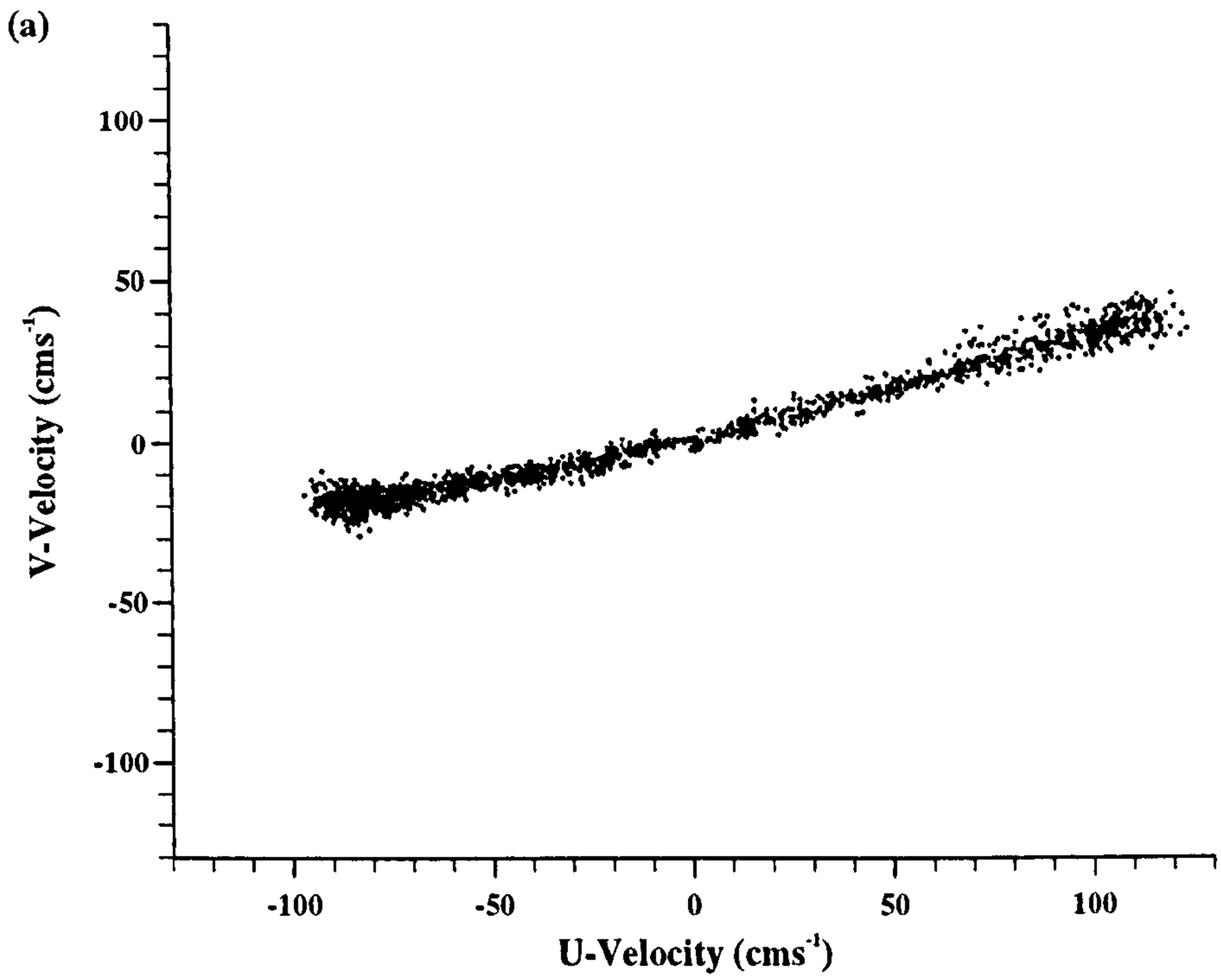

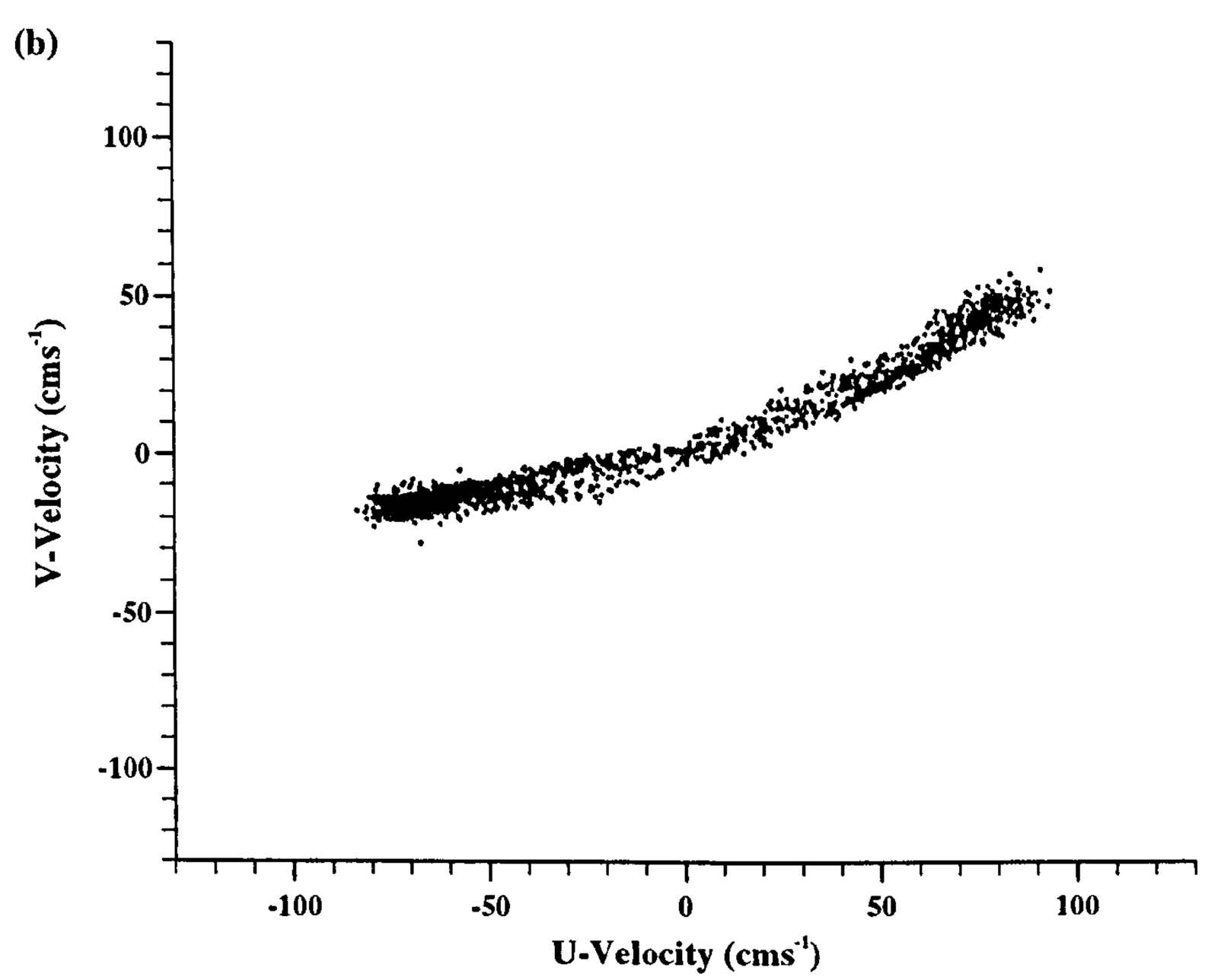

Figure 6.08 : IS1 velocity scatter plots.

a) RCM 9580, 41m above the bed.

b) RCM 3321, 5m above the bed.

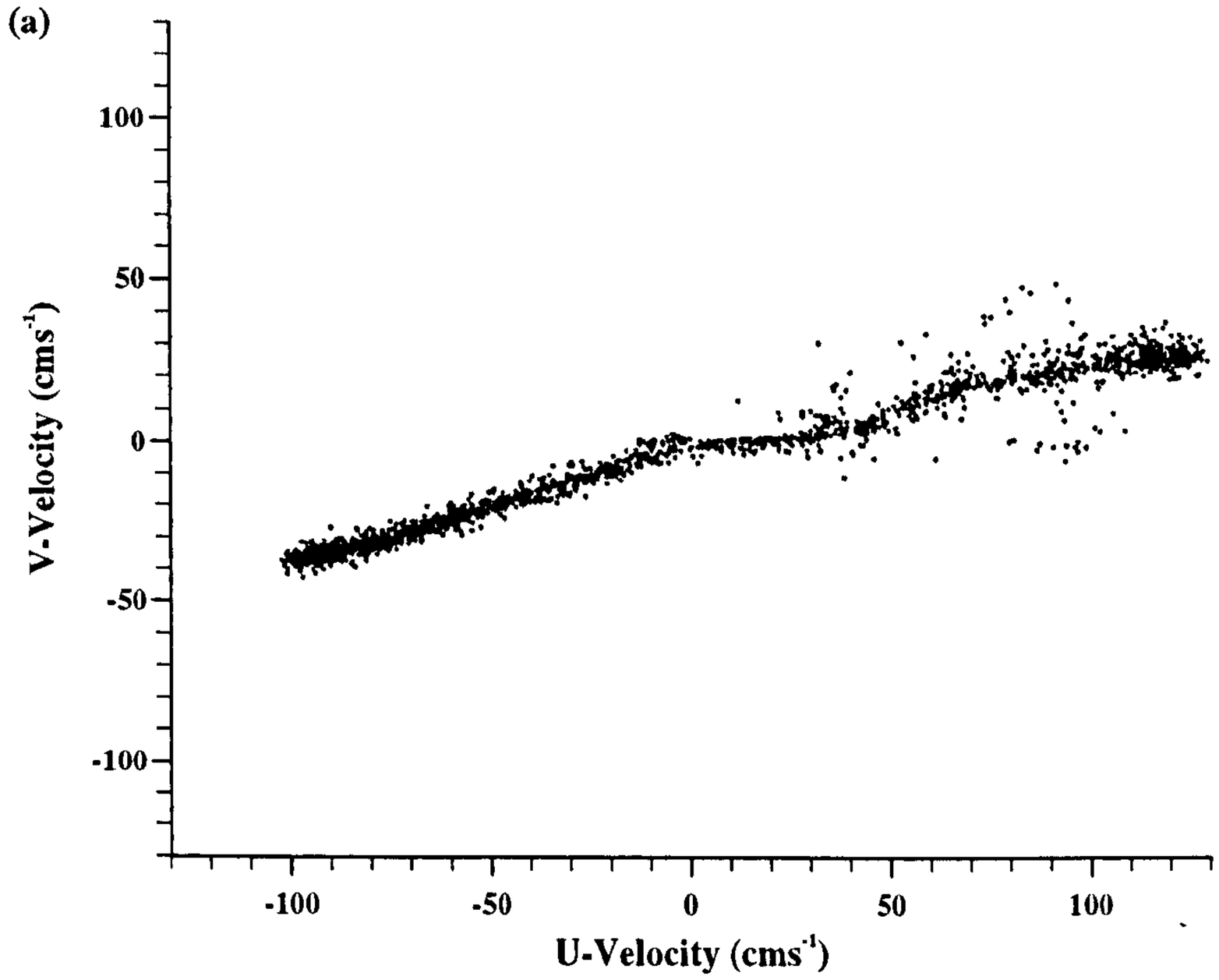

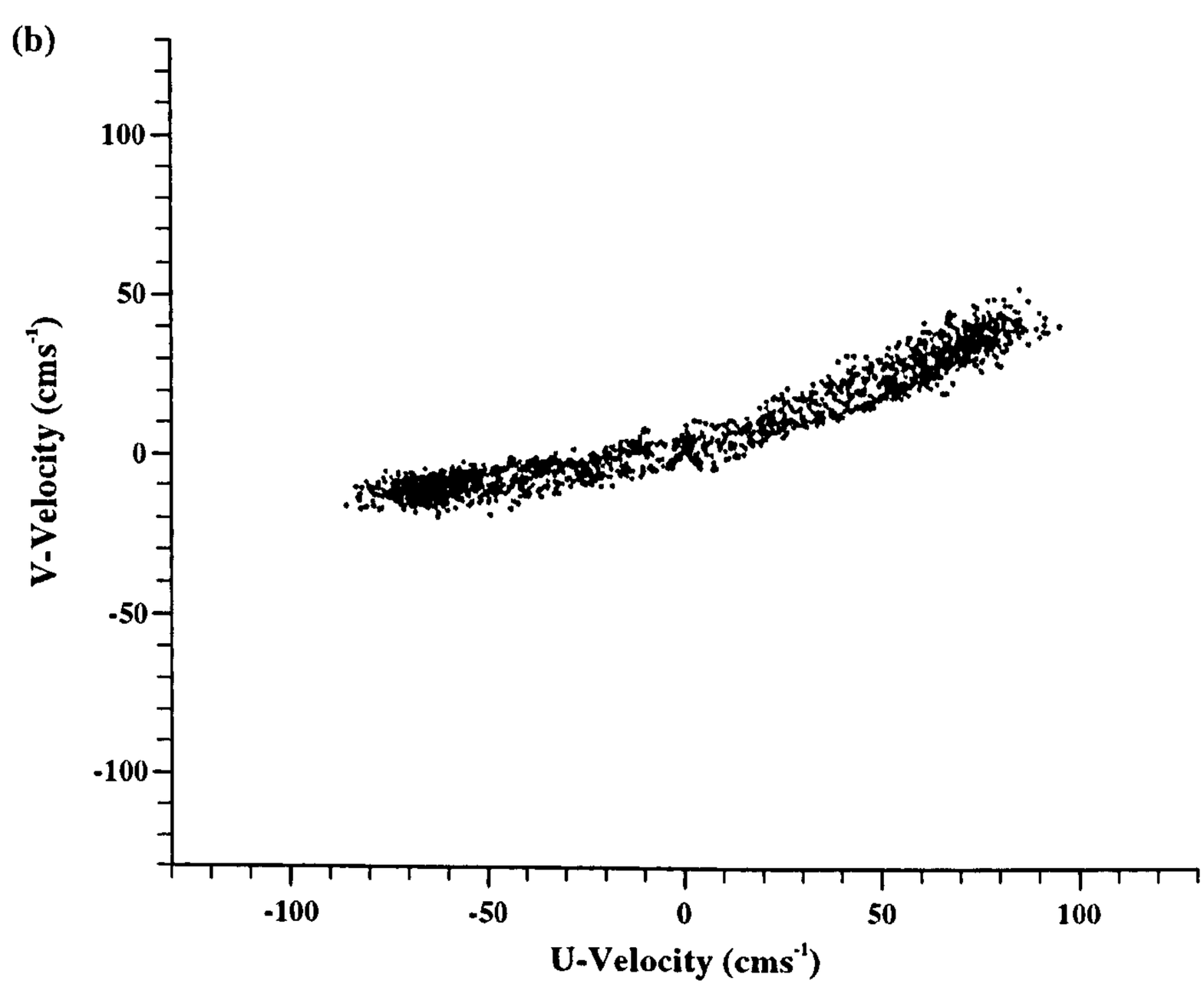

Figure 6.09 : IS2 velocity scatter plots.

a) RCM 9415, 44m above the bed.

b) RCM 8248, 9m above the bed.

It can be seen from figures 6.08 and 6.09 that the currents at both sites are largely rectilinear, flowing in an ENE (flood phase)-WSW (ebb phase) direction, the same direction along which the line joining the two moorings lies in. On the flood tide, the surface meter on mooring IS2 (figure 6.09(a)) deviates from the almost pure rectilinear flow suggested by the ebb tide data. Such a discontinuity on a scatter plot is unlikely to be genuine and is more likely to be due to instrument failure such as compass error. The scatter plots for the near bed instruments show a greater curvature than those for the surface instruments and the data is displaced further from the origin of the plot, especially for RCM 8248, 9m above the bed on mooring IS2. This suggests a residual flow over the tidal cycle which is more easily seen on a progressive vector plot.

The asymmetry between the tidal phases demonstrated will result in a net transport of water over the tidal cycle. Figures 6.10 and 6.11 show progressive vector plots for the current meters on IS1 and IS2 respectively. The net flow of water tends to be in a north-westerly direction, consistent with the fact that the highest degree of asymmetry is found in the v-velocity component, the larger velocities being found on the flood (positive) phase of the tide. The only exception is the current record from the surface instrument on IS2 where the negative v-velocity is larger than the positive component resulting in an apparent net southerly transport at the surface of IS2. This could be due to the compass error indicated in the scatter plot (figure 6.09(a)) and discussed above. For the other three current meters, net transports are of the order of 2 to 3km in a north-westerly direction per tidal cycle.

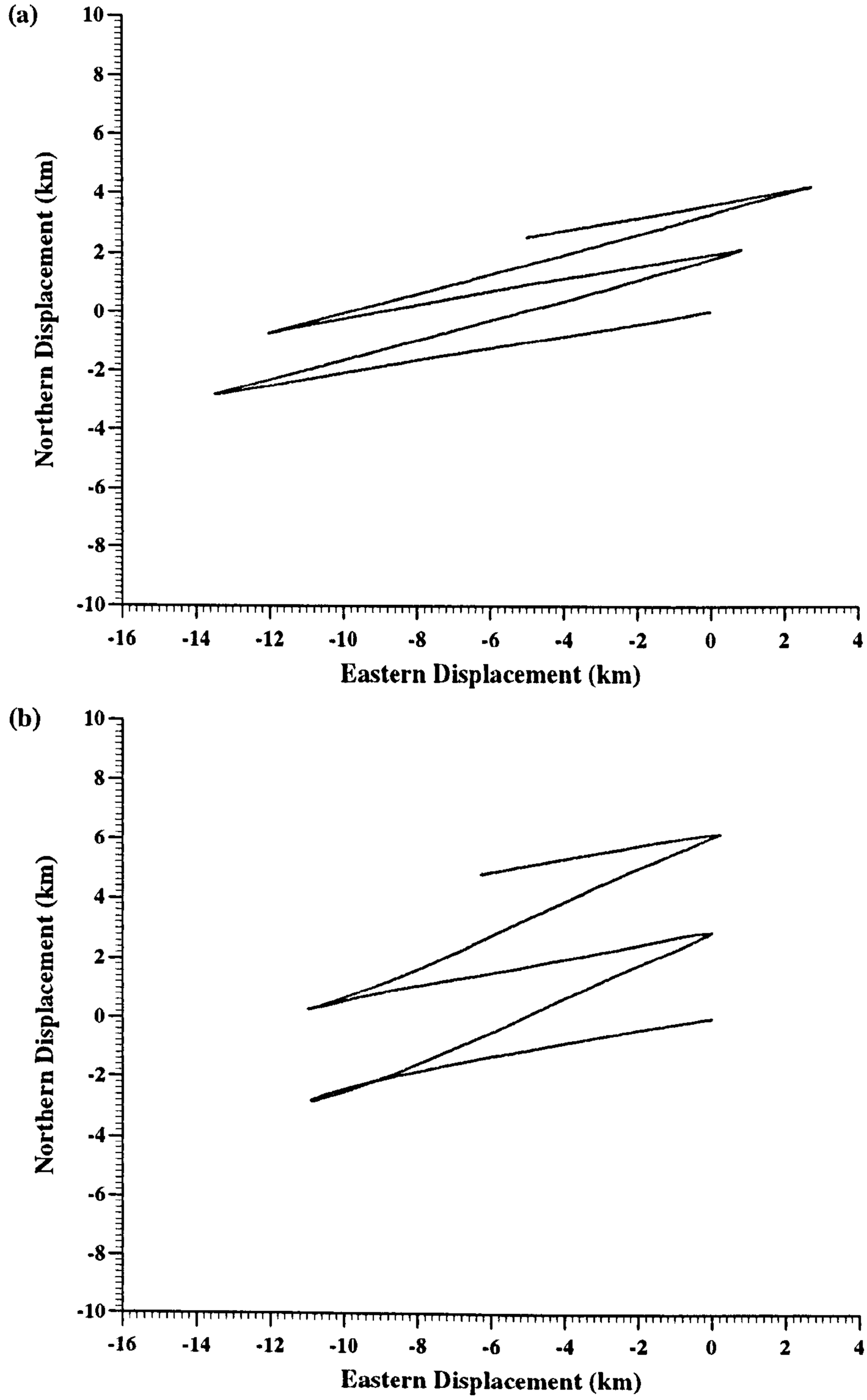

Figure 6.10 : IS1 progressive vector plots.

a) RCM 9580, 41m above the bed.

b) RCM 3321, 5m above the bed.

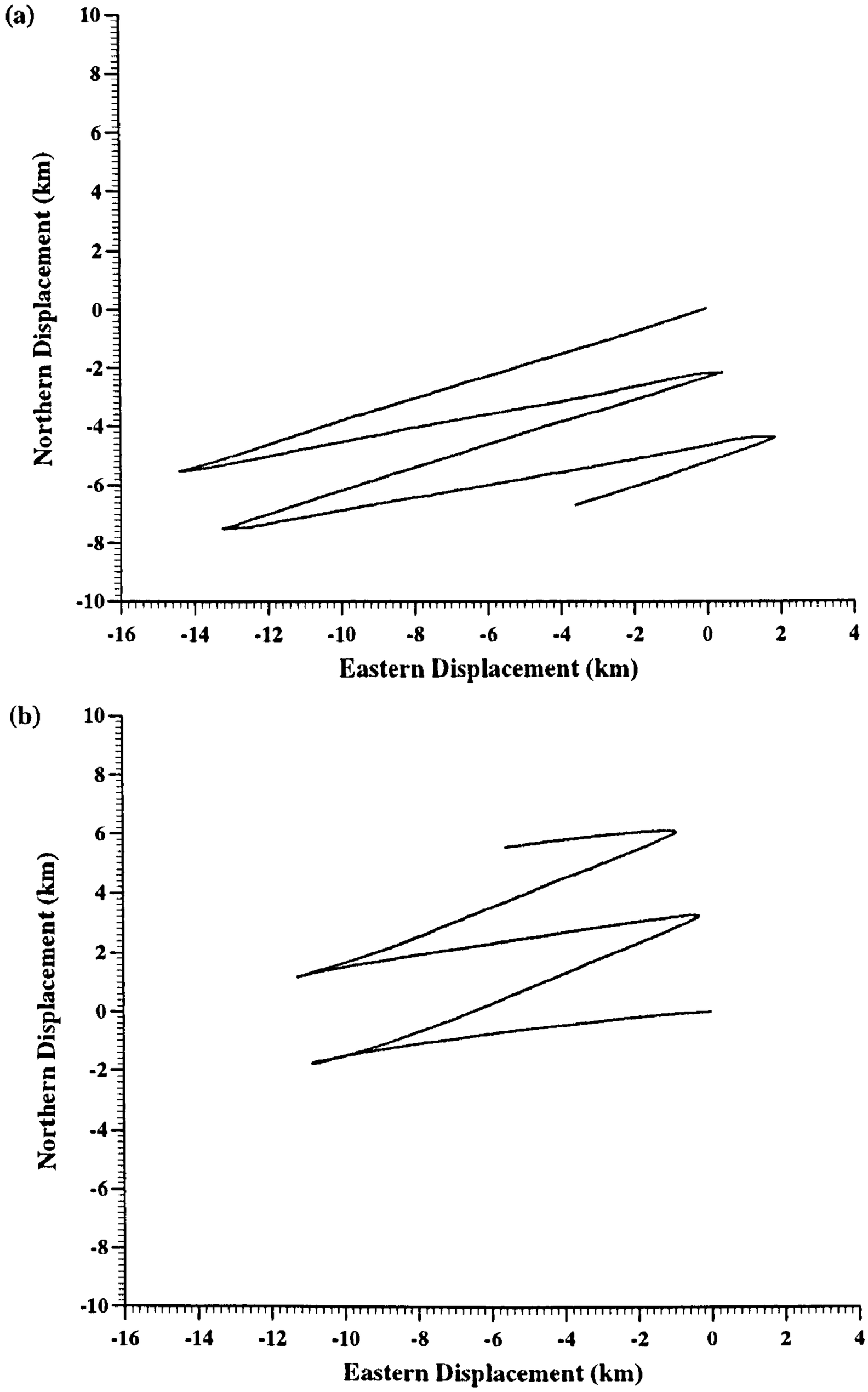

Figure 6.11 : IS2 progressive vector plots.

a) RCM 9415, 44m above the bed.

b) RCM 8248, 9m above the bed.

The results from the ship-mounted ADCP for IS1_2 are consistent with those from the RCMs, as would be expected.

6.3.2 IS3 Mean Flow Results.

For site IS3 at which there was no mooring provision, the ADCP results are the only current measurements available and are shown in figure 6.12.

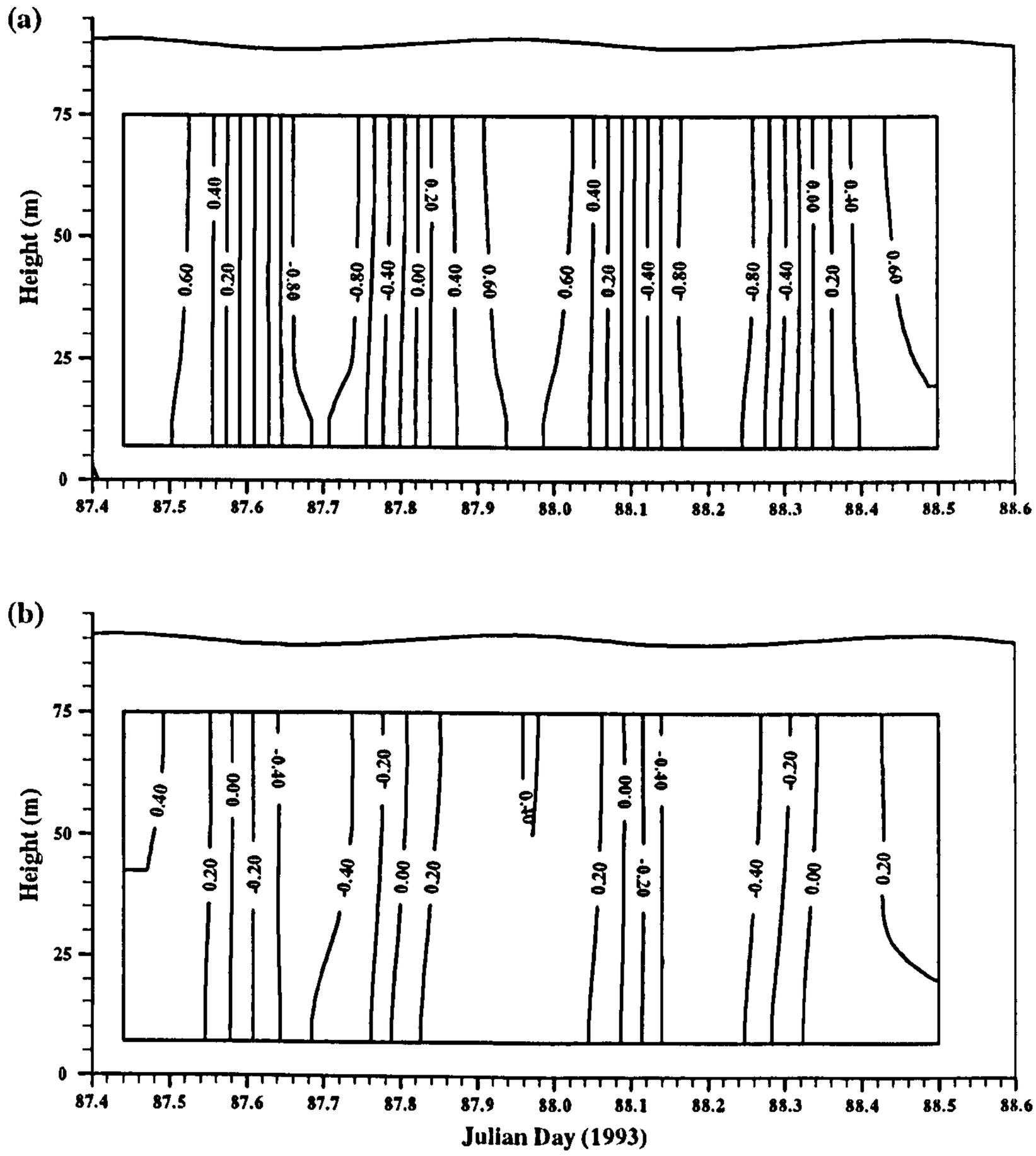

Figure 6.12 : IS3 velocity field as measured by R.R.S. Challenger's 150 kHz ADCP:

a) u-component (ms^{-1}).

b) v-component (ms^{-1}).

The water is deeper at this site (90m) and the currents are weaker. Maximum u-velocities are about 90cms^{-1} whereas the maximum v-velocity is about half this. Positive u-currents coincide with positive v-currents indicating flow in a roughly NE-SW direction. The CTD results presented earlier show no significant change in temperature or salinity structure over the tidal cycle. Thus, horizontal gradients are weak so that any density driven current will be small and, although winds were stronger during the survey at 10-15ms^{-1} and more coherent in direction, the tidal flow is sufficiently strong to render any wind driven flow insignificant.

6.3.3 ISS Mean Flow Results.

The mooring deployed at ISS was similar in design to those used on cruise CH102. The mean flow was monitored by the two Aanderaa current meters. Figures 6.13, 6.14 and 6.15 show u and v-velocity components, scatter and progressive vector plots respectively for both RCMs.

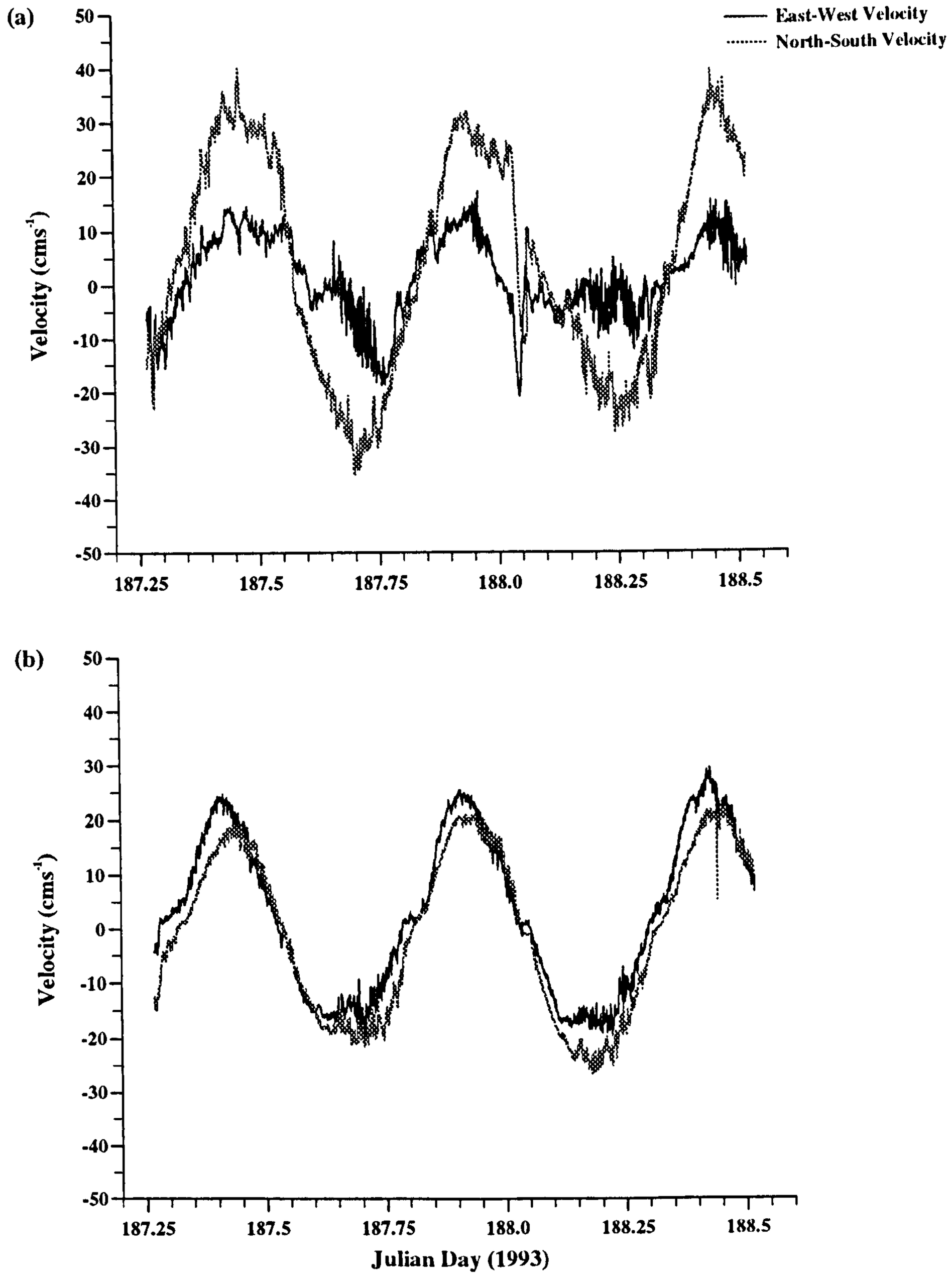

Figure 6.13 : ISS u- and v-velocity components.

a) RCM 10666, 80m above the bed.

b) RCM 10665, 12m above the bed.

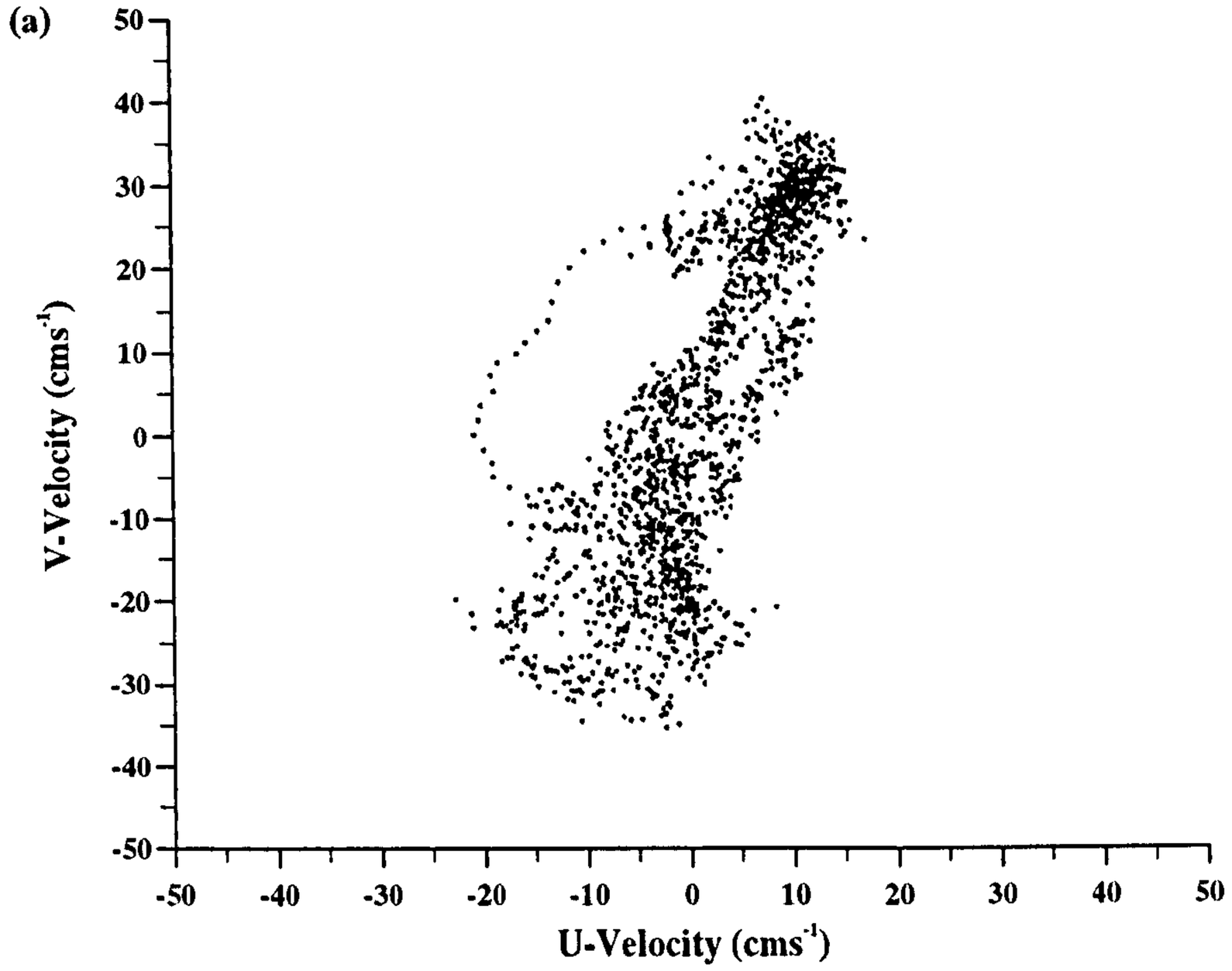

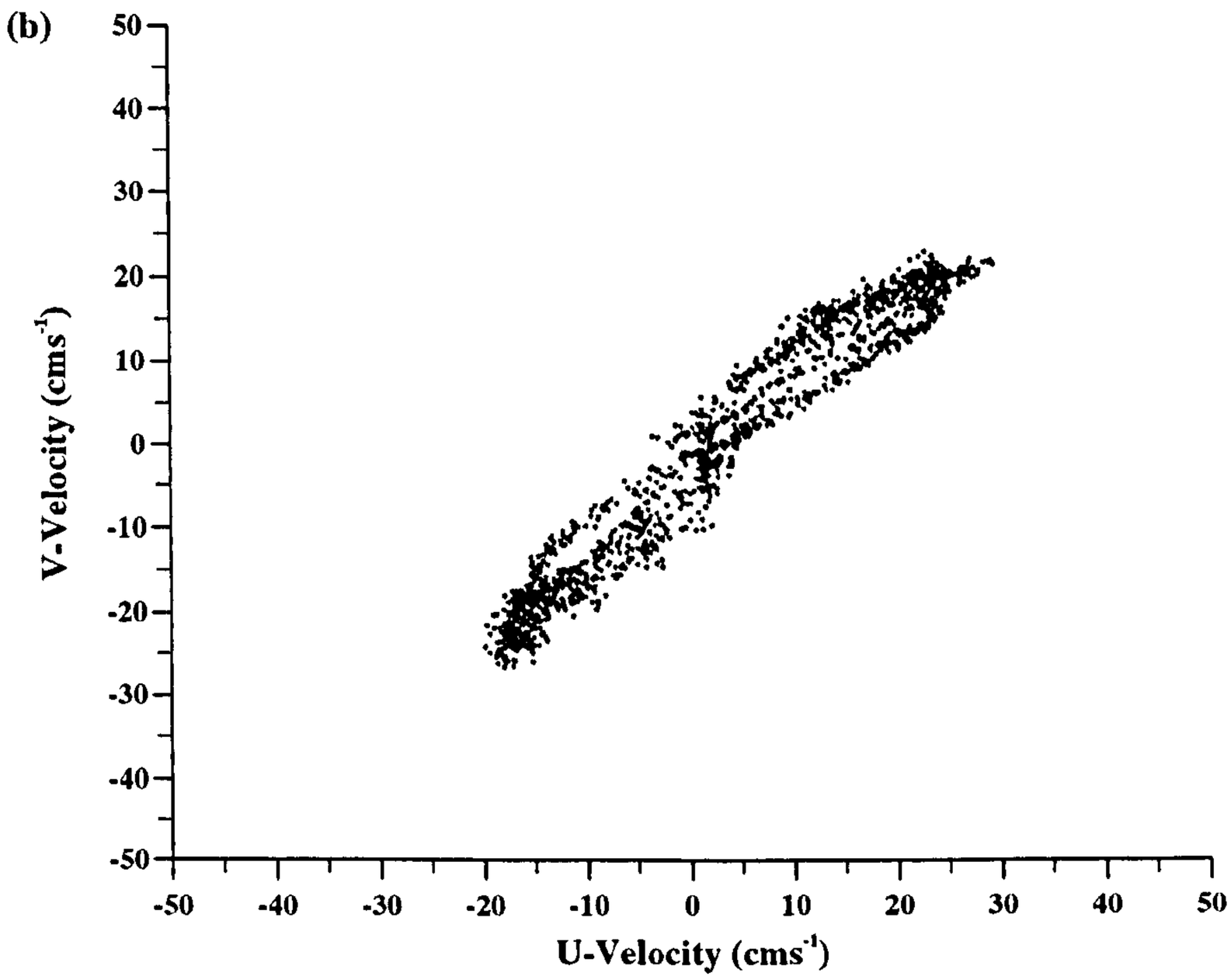

Figure 6.14 : ISS velocity scatter plots.

a) RCM 10666, 80m above the bed.

b) RCM 10665, 12m above the bed.

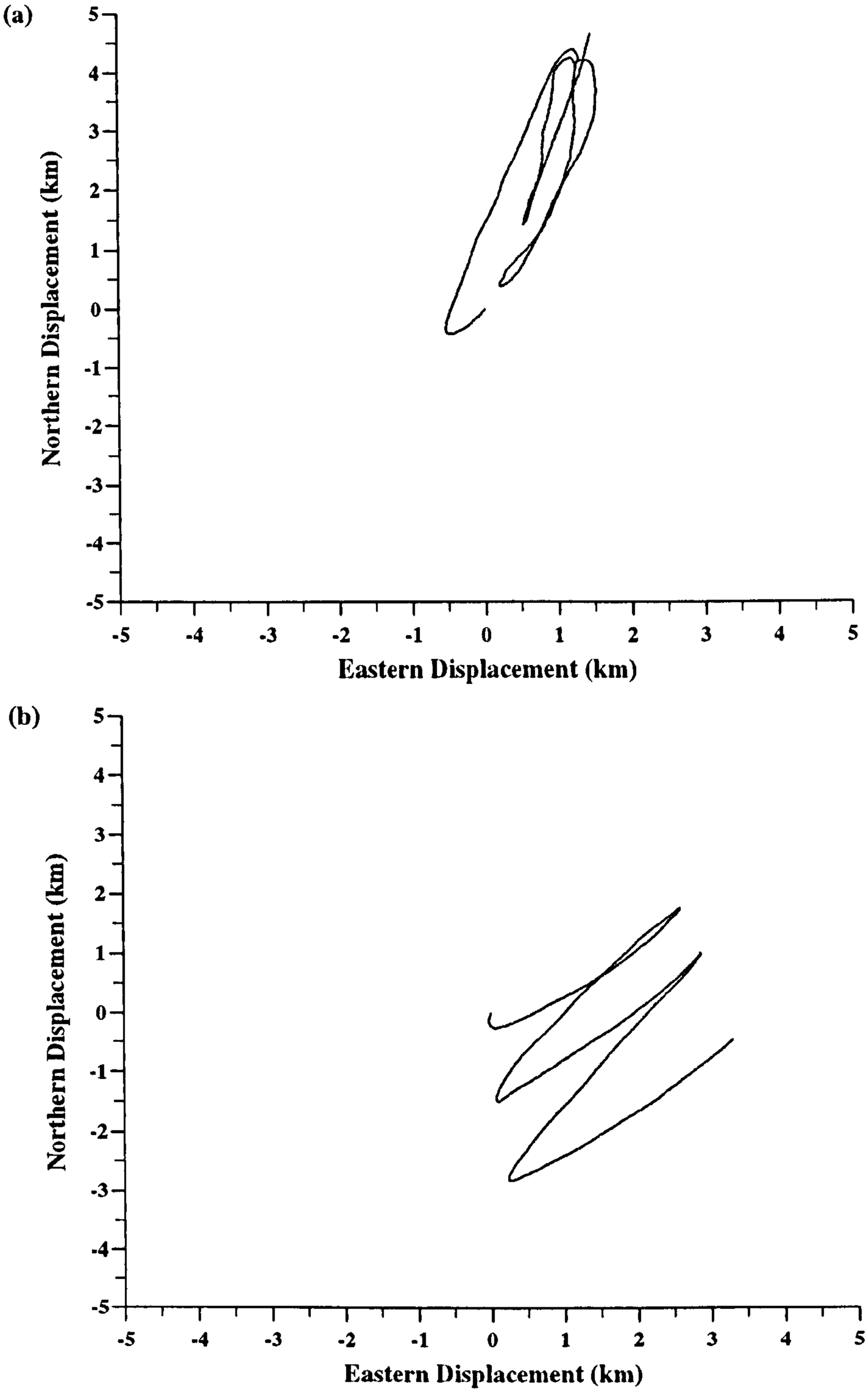

Figure 6.15 : ISS progressive vector plots.

a) RCM 10666, 80m above the bed.

b) RCM 10665, 12m above the bed.

Consider first the flow regime in the bottom waters, as measured by RCM 10665, positioned 12m above the bed. Both u- and v-components are very similar, peaking at between 20-25cms^{-1} on the flood phase and 15-20cms^{-1} on the ebb. The flow is strongly rectilinear as indicated by figure 6.14(b) with flow along a SW-NE axis. The asymmetry between the u- and v-currents in that u is stronger on the flood and v on the ebb and that maximum north-south flow occurs after maximum east-west flow results in a net displacement of water to the south-east of approximately 1-2km per tidal cycle as shown in figure 6.15(b).

Flow in the surface waters is more complicated. RCM 10666 was positioned 80m above the bed in the area of greatest vertical density gradient. Winds were light so that there is unlikely to be any wind driven flow. Again, horizontal density gradients were weak ruling out the possibility of any significant density driven flow. Although the velocity data is noisy in places several features are obvious. The v-velocity component (maximum value≈35cms^{-1}) is more than twice as strong as the u-component which is actually weaker (maximum value≈15cms^{-1}) than that measured 12m off the bed. Examination of the scatter plot from RCM 10666 (figure 6.14(a)) reveals that the flow is broadly in a NNE-SSW direction although there is significant scatter, with a net transport of water to the NNE because of the stronger flood phase currents.

6.4 SPM Concentration Results.

In this section the results of the SPM concentration studies at all three sites are presented. The SPM concentration data available for analysis has already been described and is summarised in table 6.03 along with a brief description of the important site characteristics.

Table 6.03 : SPM concentration data for IS1_2, IS3 and ISS and site information.

Site (depth)	Typical $(u^2+v^2)^{1/2}$	Bed Material	SPM Measurements
IS1_2 (60m)	1.25 ms^{-1}	sandy gravel	CTD survey 2 moored transmissometers 1 settling velocity tube
IS3 (90m)	0.9 ms^{-1}	sandy gravel	CTD survey 3 settling velocity tubes
ISS (90m)	0.35 ms^{-1}	mud	CTD survey 2 moored transmissometers

6.4.1 SPM Observations at IS1_2.

Consider first the results from the moored transmissometers. Both instruments, deployed on mooring IS2 operated well, providing beam transmission records every 60 seconds for 29 hours. These have been averaged to give a result every 5 minutes and then converted to SPM concentrations using the calibration technique described in §5.5.2. It was necessary to apply a correction to the near-bed instrument results in order to bring them into agreement with those from the CTD (Sea-Tech) transmissometer. This correction took the form of a constant which was subtracted from the moored transmissometer data. As the transmissometers were inter-calibrated in surface waters it is assumed that pressure effects on the instrument result in the observed offset. The results from the IS2 transmissometers are shown in figure 6.16.

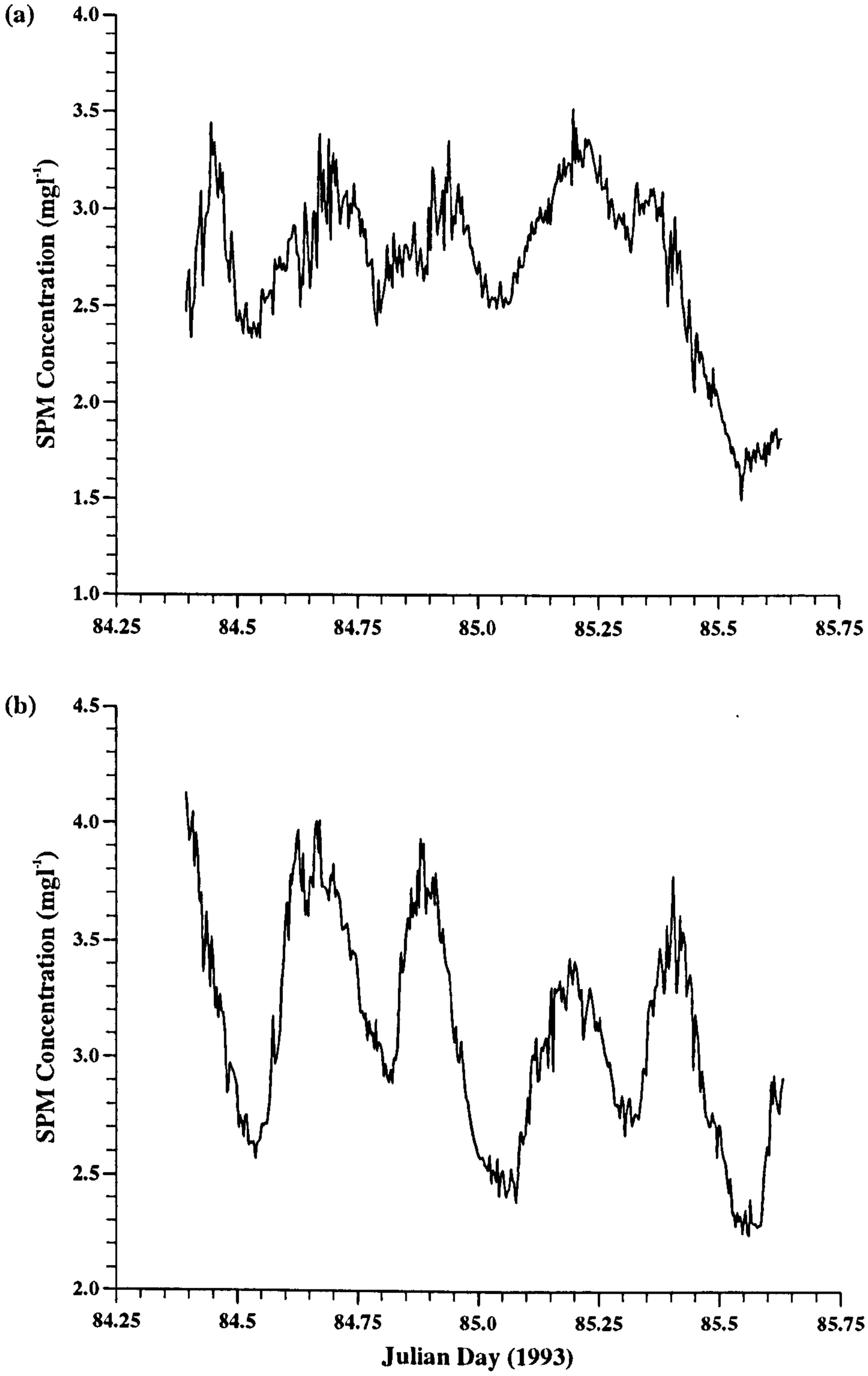

Figure 6.16 : SPM concentration data from the transmissometers deployed at site IS2.

(a) 47m above the bed.

(b) 4m above the bed.

The average value of SPM concentration 4m above the bed over the deployment period was 3.1mgl^{-1}. Superimposed upon an overall reduction in SPM concentration are clear variations at both semi- and quarter-diurnal frequencies associated with advection and resuspension/settling processes respectively. This dataset is a good example of the 'twin-peaks' sediment signature introduced earlier (§ 3.6).

According to figure 4.06 the bed material at this site is sandy gravel. In order to account for the large quarter-diurnal resuspension/settling signal in the data there probably exists an additional fine-grained sediment fraction. This is resuspendable by the strong tidal currents found at this site and is also sufficiently coarse in order to settle out during slack water. The average peak-trough difference, representative of this resuspended component is approximately 1mgl^{-1}.

The semi-diurnal variation is due to advection of a horizontal concentration gradient past the mooring site and the reduction in concentration over the entire deployment is due to a net transport of this gradient over the tidal cycle. The net transport of water has already been demonstrated from the current meter results (§ 6.3.1) and is of the order of a few kilometers per tidal cycle.

The slight flattening of the SPM concentration peaks observed at around Julian days 84.7 and 85.2 suggests that the amount of resuspendable material at this site is limited. In this situation the SPM concentration at this height is referred to as source-limited as the bed is effectively exhausted of sediment that can be added to the total suspended load either because none exists or the flow no longer possesses sufficient energy to induce resuspension.

As might be expected, SPM concentrations in the surface waters are lower than those in the near bed region. The average value of SPM concentration 47m above the bed over the deployment is 2.7mgl^{-1}. This is because with increasing height above the bed, the less coarse sediment is found.

The quarter-diurnal resuspension/settling variation is again evident with an average peak-trough difference of approximately 0.7 mgl^{-1}. The semi-diurnal signal is less prominent indicating that the horizontal concentration gradient is weaker than closer to the bed. However, the effects of advection can be seen towards the end of the deployment. From Julian day 85.3 until the end of the record there is a reduction in SPM concentration of about 1.5 mgl^{-1}. This is a result of less turbid water being advected past the instrument. The net transport of water over the tidal cycle means that any spatial variation in the sediment source/sink characteristics or the sediment itself will manifest itself in the concentration record when advected past the mooring.

Peaks in SPM concentration corresponding to maximum flow events generally occur about an hour after those measured at the bed. This is because the sediment requires a non-zero time to penetrate up the water column via turbulent diffusion. Minima in the surface record usually occur before the minimum concentrations are measured near the bed. This is due to the effects of settling as the resuspended component settles down through the water column at slack water.

As well as the usual pressure, conductivity and temperature sensors, the Neil Brown CTD profiler was equipped with a Sea-Tech transmissometer to measure vertical profiles of SPM concentration. The SPM concentration profiles from the 22 casts made at IS1_2 have been interpolated and plotted using the UNIMAP graphics package and are shown in figure 6.17.

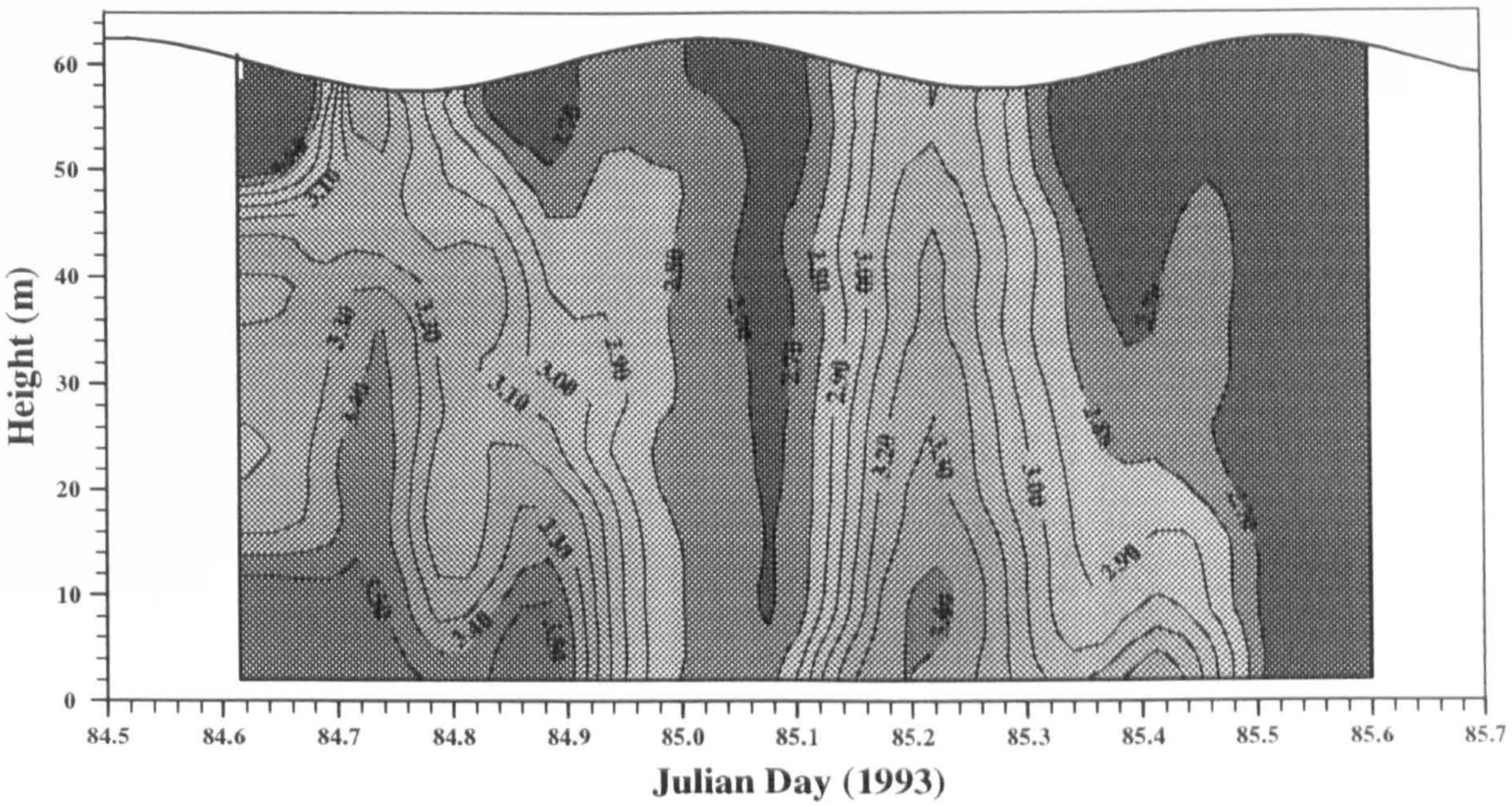

Figure 6.17 : Observed SPM concentration (mgl^{-1}) at IS1_2.

The principal features identified from the moored transmissometer records are reproduced in the CTD data. However, with a reading every 10cm there is the added advantage of much greater vertical resolution. The quarter-diurnal signal due to resuspension and settling of the bed material is clearly seen in the bottom 20m of the water column. Further up, the semi-diurnal variation due to advection of the horizontal concentration gradient becomes the important signal as the resuspended signal becomes weaker. The importance of this horizontal gradient is outlined by the fact that higher SPM concentrations are measured on the weaker (ebb) phase of the tide. Without the semi-diurnal, largely depth uniform variation, the greatest concentrations would be measured on the flood tide. The overall decrease in SPM concentrations because of the non-zero tidal excursion is also evident.

At the beginning of the IS1_2 survey, during the first peak flow event at around Julian day 84.7, a settling velocity tube was deployed in mid-water (approximately 30m above the bed). The results are shown in figure 6.18 in the form of a histogram with settling velocity class on the abscissa and concentration on the ordinate.

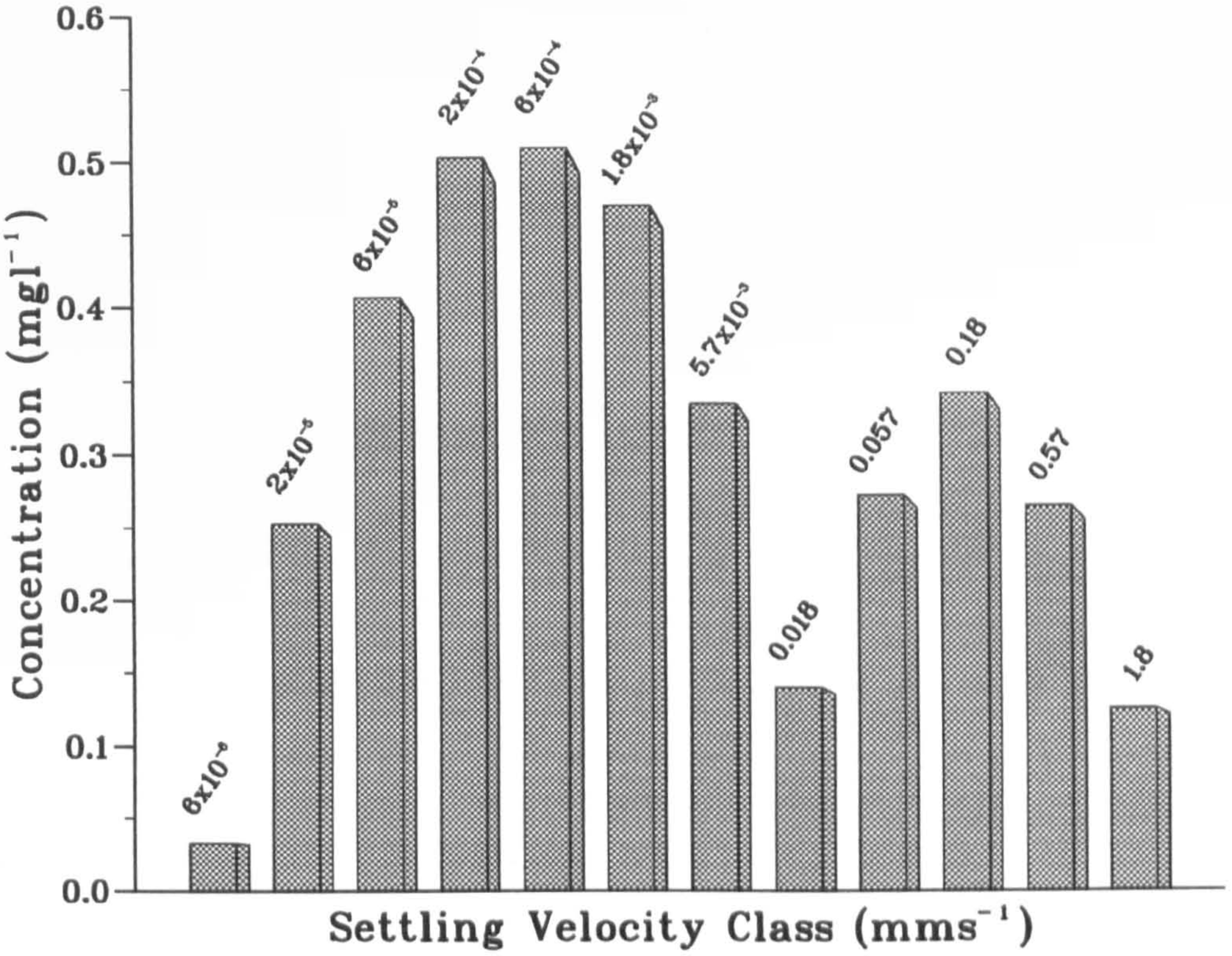

Figure 6.18 : Settling velocity tube data from 30m above the bed at IS1_2.

Two distinct sediment fractions can be seen, centred on $6x10^{-4}$ mms^{-1} and 0.18 mms^{-1}. The finer of these fractions is not actually observed since it settles so slowly. Rather, it arises from the assumption of a log-normal tail-end distribution for the SPM population (Jones and Jago (1996)). This population settles very slowly and so is representative of the background component, permanently in suspension. The coarser fraction, which settles through 65cm in an hour forms part of the resuspended population. Because the settling tube was deployed 30m above the bed the great majority of the resuspended component is not represented. Given the CTD transmissometer results in figure 6.17 there exist coarser fractions that contribute to the total resuspended signal. Harmonic analysis of these results to be presented in the next chapter, will help to clarify the nature of the sediment population.

6.4.2 SPM Observations at IS3.

The only SPM concentration measurements made at IS3 are those from the CTD

transmissometer. A number of settling velocity tubes were deployed and the particle settling velocity spectra obtained are also discussed. The 21 SPM concentration profiles completed at IS3 have been interpolated as before and the resulting contour plot is shown in figure 6.19.

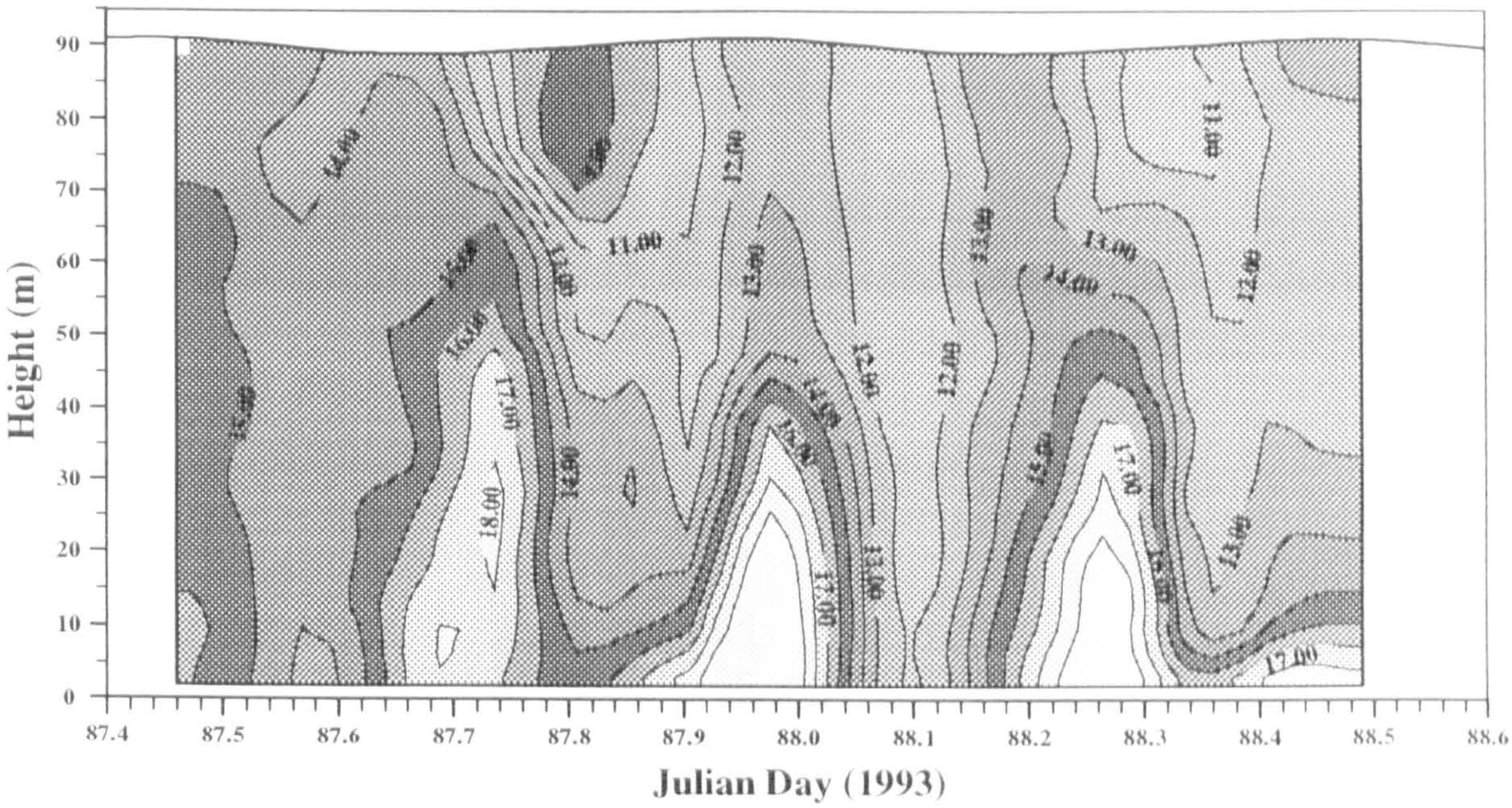

Figure 6.19 : Observed SPM concentration (mgl^{-1}) at IS3.

As with the previous survey at IS1_2, there is a strong quarter-diurnal variation in SPM concentration. However, at this site this signal extends further up into the interior of the water column. Overall SPM concentrations are much higher here, reaching a maximum of approximately 20 mgl^{-1} around peak flow with minimum values of 10 mgl^{-1} at slack water.

Three settling velocity tubes were deployed during the survey, at 20m below the surface (70m above the bed). Because of this they are unlikely to contribute significantly to knowledge of the resuspended sediment population. They will however, reflect the nature of the background component. The first tube was deployed on Julian day 87.53 (about 1.5 hours before flow reversal), the second on Julian day 87.62 (1.5 hours after flow reversal) and the third just after peak flow on Julian day 87.72. The resulting spectra are shown in figure 6.20.

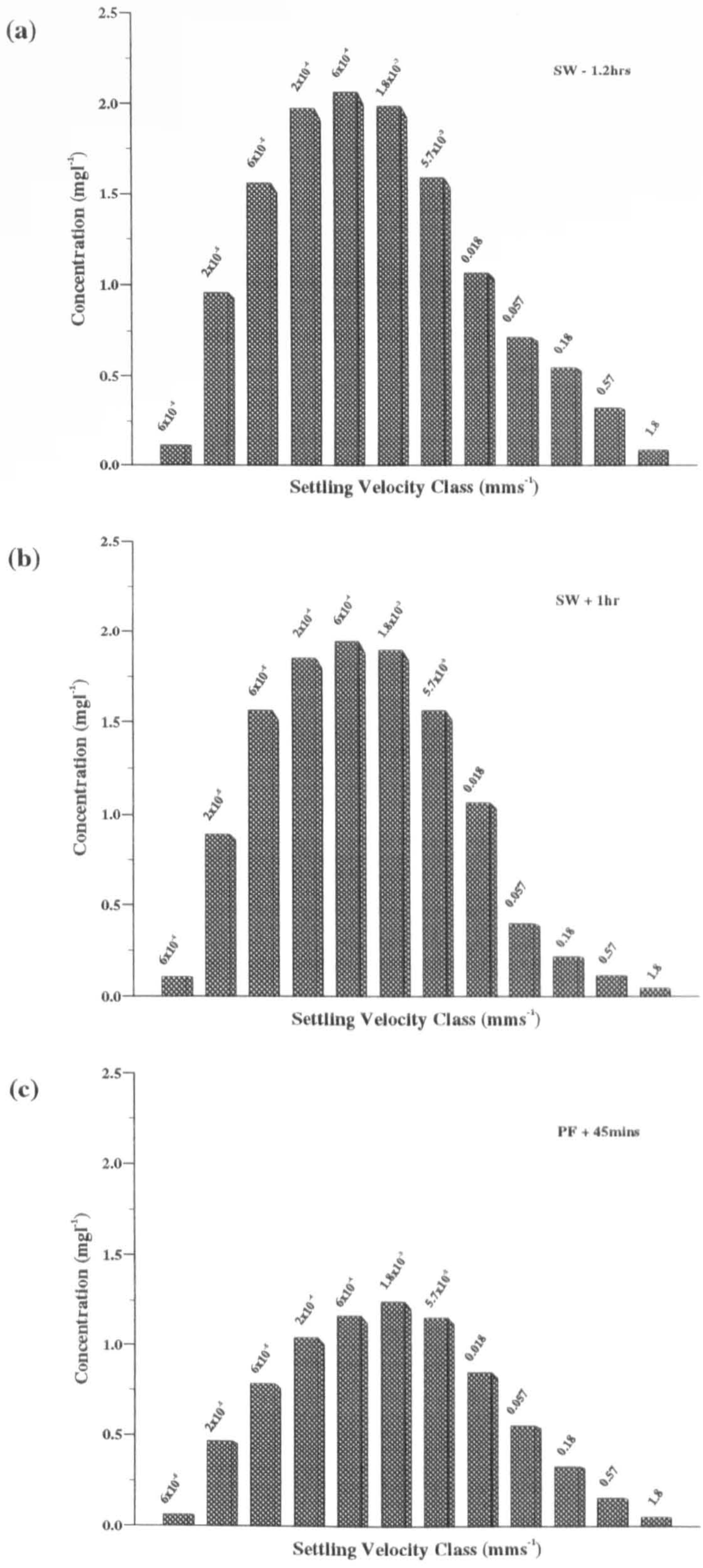

Figure 6.20 : SVT data for IS3 : (a) tube 1, (b) tube 2 and (c) tube 3.

In contrast to the settling velocity tube data from IS1_2, at this site there is only a single peak in the spectrum which is centred around a settling velocity of approximately $6x10^{-4}$ mms^{-1}. This is a very slowly settling sediment fraction (less than 2.5mm in an hour) and is likely to represent the advected background component already described. There are faster settling fractions, perhaps representative of the resuspended component but since the tubes were deployed 70m above the bed the resuspended component will not be strongly represented.

The sediment distributions from tubes 1 and 2 are similar except that 1 hour after slack water concentrations are slightly lower, especially among the more rapidly settling populations ($0.057mms^{-1} \rightarrow 1.8mms^{-1}$). This is because minimum concentrations are generally found at around this period of the cycle due to settling. Considering the results from tube 3, it is seen that SPM concentrations have fallen by an appreciable amount (of the order of $1mgl^{-1}$). Because this is evident for all size fractions it is likely to be due to advection and not settling/resuspension which would favour certain particle sizes. This hypothesis is reinforced by figure 6.19 which shows the contour plot for the CTD SPM study at this site. At 70m above the bed the quarter-diurnal resuspension/settling signal is weaker than that at greater depths and the semi-diurnal, advected signal becomes more prominent. This advection results in less turbid water passing the site as indicated on the graph, coinciding with the deployment of the third settling velocity tube.

6.4.3 SPM Observations at ISS.

The transmissometers on mooring ISS were positioned in the near bed region and in the warmer surface layer. The SPM concentration records obtained are shown in figure 6.21.

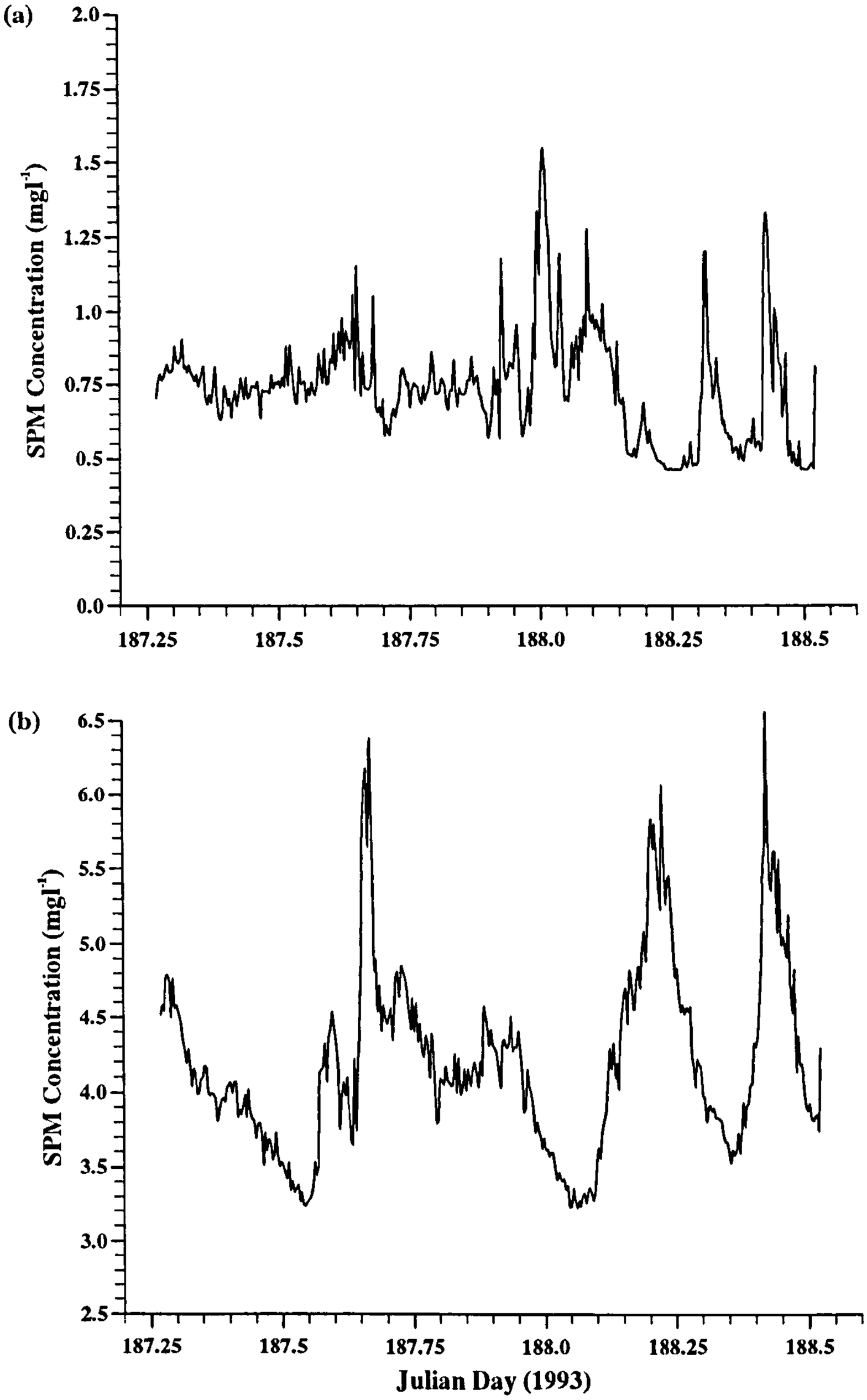

Figure 6.21 : SPM concentration data from the transmissometers deployed at site ISS.

(a) 83m above the bed.

(b) 6m above the bed.

Once again, a constant offset value had to be applied to the SPM concentration record from the near-bed instrument so that the results comply with those from the Sea-Tech instrument. The offset was larger than that for the previous experiment (which also used a different instrument, positioned 56m below the sea surface) lending support to the assumptions that this is a pressure effect since this instrument is situated some 84m below the sea surface.

Average concentrations from the near bed transmissometer are approximately 4.2mgl^{-1}, higher than at IS2. Although the currents are substantially weaker than at either of the mixed sites, a quarter-diurnal signal is evident, especially at the end of the record where the peak- trough difference is about 2mgl^{-1}, again greater than that observed at IS1_2.

The maxima in SPM concentration evident in figure 6.21 corresponding to peak flow events are very distinct with no rounding as seen in the bed record at IS2. This indicates that the supply of resuspendable material is not source-limited. The bed at this site is mud so that it is conceivable that much of the material in suspension is sufficiently fine that it does not experience significant settling and remains in suspension for longer than a single tidal period. This does not support the strong quarter-diurnal signal observed, especially towards the end of the record. The signal measured by the transmissometer could be due to the rise and fall of a vertical sediment concentration gradient with the sharp peaks corresponding to a particularly strong gradient. Unfortunately, no settling velocity tube data is available for this survey which would reveal further the nature of the sediment population.

A contributory factor resulting in the high SPM concentrations found in the bottom waters is likely to be the presence of the pycnocline. The density structure acts to confine any suspended sediment to the bottom layers. Another consequence of this would be low SPM concentrations in the surface waters. This is indeed what is observed by the surface transmissometer, positioned 83m above the bed.

SPM concentrations measured at this height are very low with an average value of ~0.75mgl^{-1}. No resuspension or advection signal is obvious. It appears that, as far as SPM concentrations are concerned, the surface layer is effectively decoupled from the bottom waters by the pycnocline. As a result, events at the bed do not affect SPM concentrations in the less dense surface waters.

24 CTD profiles were completed at ISS and the interpolated SPM concentration data is shown in figure 6.22.

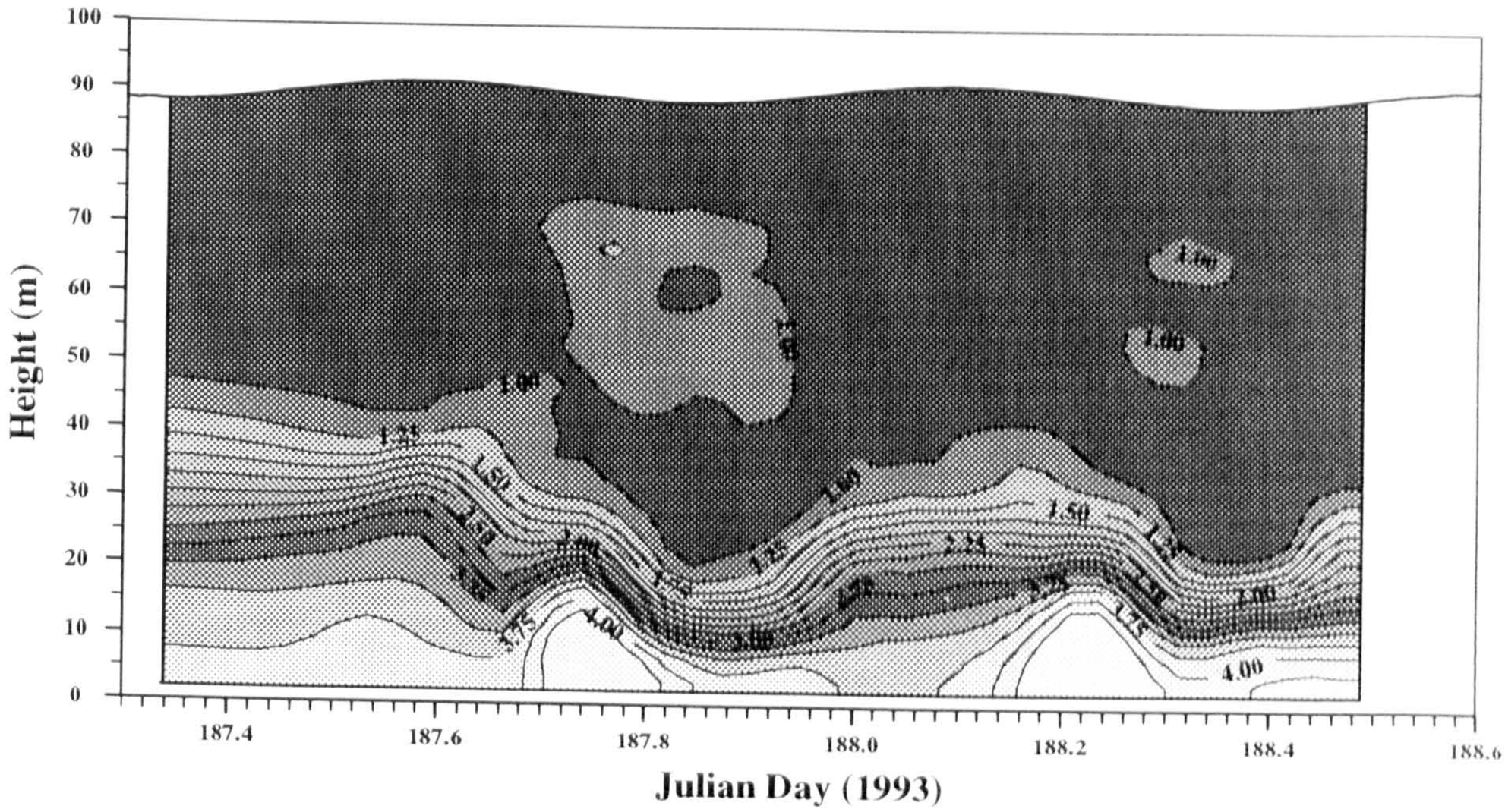

Figure 6.22 : Observed SPM concentration (mgl^{-1}) at ISS.

These results show the effectiveness of the pycnocline in suppressing vertical transport of sediment above 30m. This results in the high concentrations in the bottom waters as recorded by the near bed transmissometer. The maximum height to which the sediment diffuses is also observed to change with the phase of the tide. This variation occurs at a roughly semi-diurnal frequency, biasing the near bed SPM concentration signal towards this frequency and away from the expected quarter-diurnal variation. This also results in strong vertical gradients in sediment concentration.

6.5 Turbulent Flow Results.

The measurements of vertical shear in the horizontal velocity field from which turbulent dissipation (ϵ) can be calculated were made with the FLY profiler, which is described fully in chapter five.

Prior to the deployment of moorings IS1 and IS2, 6 hours of testing allowed the profiler to be correctly configured ensuring that it was operating efficiently for the start of the IS1_2 survey. Tests were also conducted before the IS3 and ISS surveys. Profiling was carried out continuously for 24.5 hours at IS1_2 and 23.5 hours at each of IS3 and ISS. The fall speed of the profiler was adjusted to approximately 80cms^{-1} allowing about 10 profiles to be completed between the hourly CTD dips at IS1_2 and 6 at IS3 and ISS. The hourly interruptions proved useful for carrying out essential maintenance on the FLY profiler such as replacing the batteries and cleaning the sensors. In total, 224 profiles were completed at IS1_2, 122 at IS3 and 132 at the thermally stratified site ISS.

Upon completion of the cruises, the data was processed at the Institute of Ocean Sciences in British Columbia, Canada as outlined in chapter five. Each individual ϵ profile was then interpolated using the cubic spline method, giving a dissipation rate every 15cm through the water column from 15cm above the bed (the probe guard prevents measurement of velocity shear down to the water-sediment interface) to within 10m of the surface. The data from the top 10m of the water column is ignored because the profiler may not yet have reached terminal velocity and more importantly, the wake generated by the ship will corrupt the shear measurements. The ship remains on station by steaming ahead into the current at between 0.5 and 1knot and the instrument is dropped from the stern of the ship.

The interpolated data is then averaged to give hourly profiles of $\mathrm{Log}_{10}(\epsilon)$. The Log_{10} function is necessary because of the wide dynamic range of ϵ. Without a logarithmic representation, the majority of observed variation in ϵ is confined to the bottom

meters of the water column. To demonstrate this, figure 6.23 shows ϵ and $Log_{10}(\epsilon)$ data from a single profile during the IS1_2 survey.

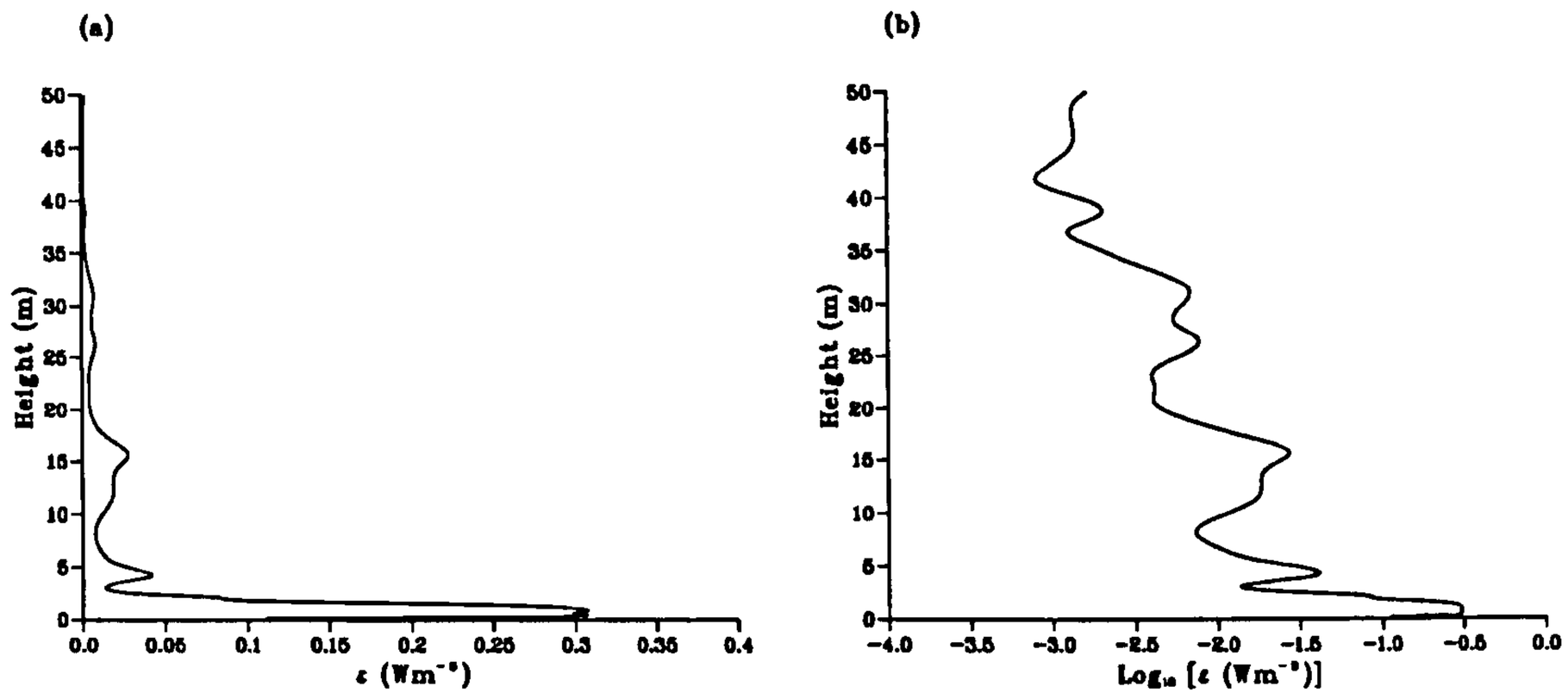

Figure 6.23 : FLY dissipation rate data from a profile during the IS1_2 survey.

a) ϵ.

b) $Log_{10}(\epsilon)$.

Figure 6.23(b) shows that, by using the logarithmic representation described above, examination of the relationship between ϵ and height above the bed is easier. Further interpolation is then performed so that the data can be presented in the form of a contour plot. As with the CTD data, this is achieved using the UNIMAP graphics package. The following sections will describe the FLY measurements made at IS1_2, IS3 and ISS respectively.

6.5.1 Turbulent Dissipation Observations at IS1_2.

The contour plot of $Log_{10}(\epsilon)$ obtained from the FLY survey at IS1_2 is shown in figure 6.24.

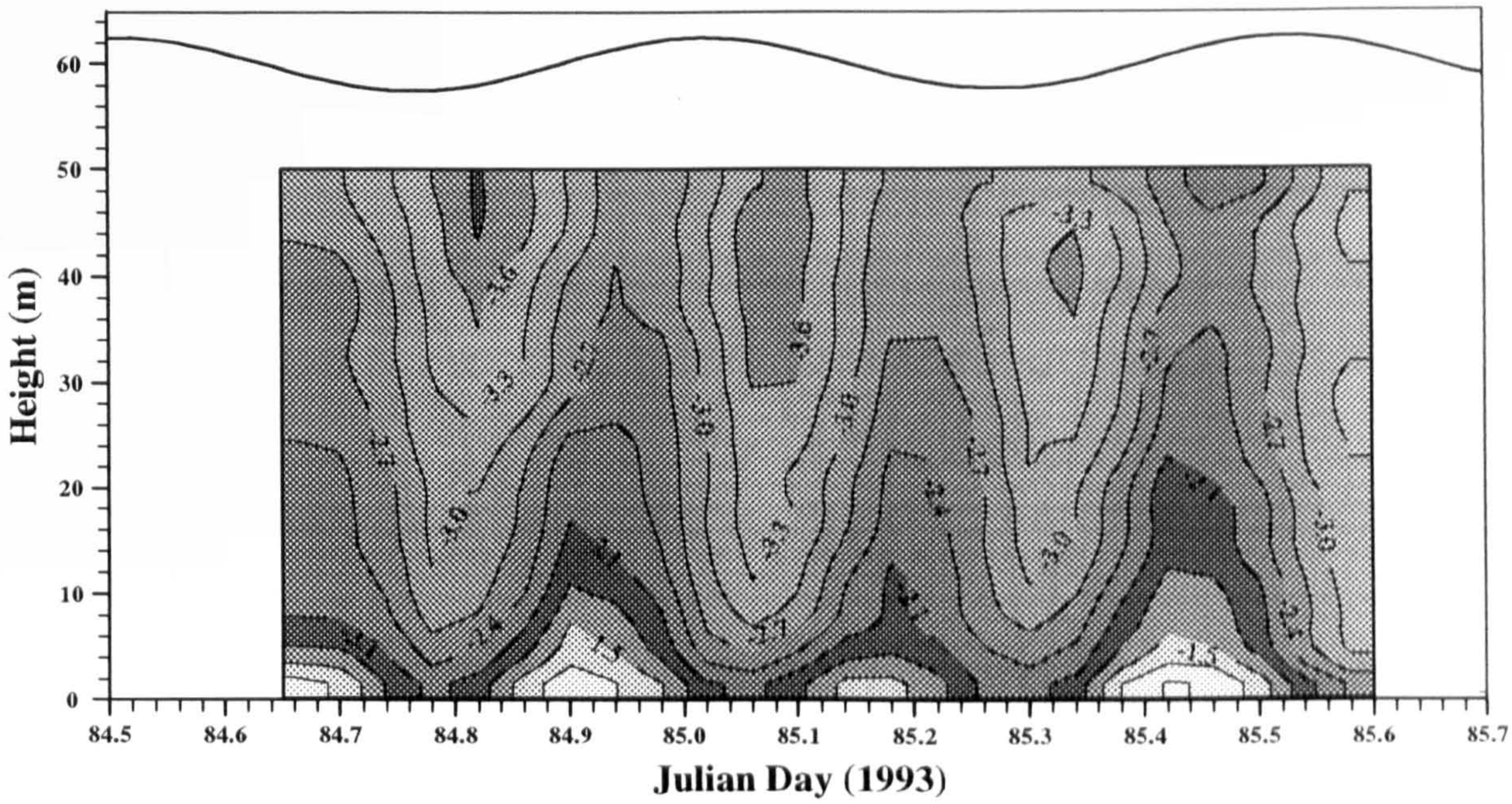

Figure 6.24 : Observed Log_{10} [ϵ (Wm^{-3})] at IS1_2.

The most prominent features of the data shown in figure 6.24 are the large difference between the observed dissipation rates in the near bed region and further up the water column and the strong quarter-diurnal signal which is evident at all heights. Maximum dissipation rate is found near the bed on the flood tide where values are as high as 0.6 Wm^{-3}. Values on the ebb reach about 0.3 Wm^{-3}, about half of the flood values. 45m above the bed dissipation rates are approximately two orders of magnitude lower than those adjacent to the bed. At this height the variation over the tidal cycle is significant. Minimum values of approximately $4x10^{-5}$ Wm^{-3} are found around times of slack water whereas at peak flow values up to $3x10^{-3}$ Wm^{-3} are common.

The close relationship between the dissiation rate and current magnitude is illustrated in figure 6.25 which shows the dissipation rate measurements and RCM current magnitude results from 5m and 41m above the bed. The RCMs were on mooring IS1, situated about 3 miles from the survey site.

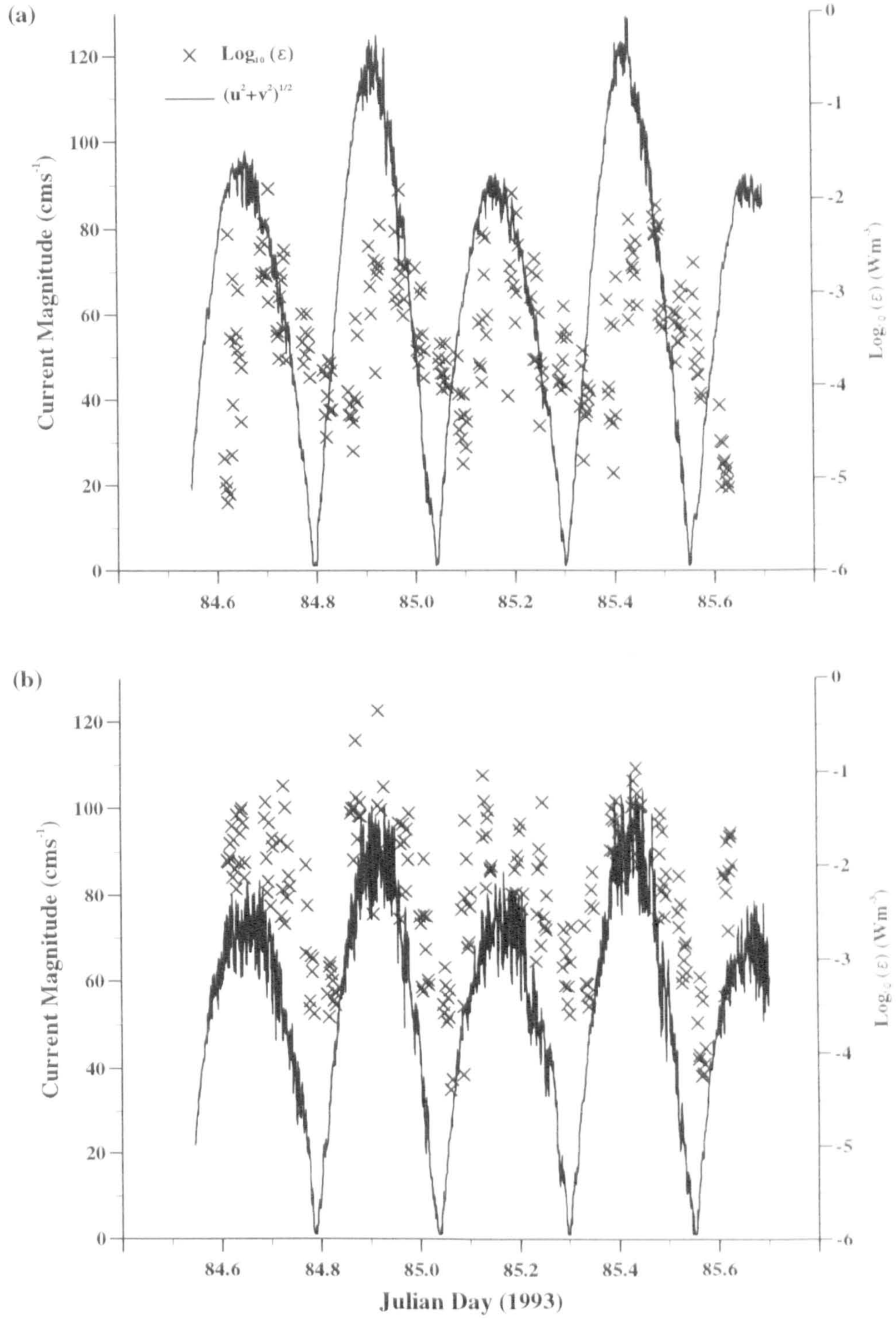

Figure 6.25 : IS1 current magnitude (—) and IS1_2 dissipation rate (x).

(a) 41m above the bed.

(b) 5m above the bed.

Figure 6.25 shows the highly significant relationship that exists between current magnitude and turbulent dissipation rate at all depths, even to the extent that the different dissipation rates observed from one phase of the tide to the next correlate well with the current magnitude data. As shown earlier, the flood phase is stronger than the ebb and this is reflected in the higher dissipation rates observed on the flood at all levels in the water column. This is to be expected since it is the current and the requirement of continuity (such that the velocity at the bed must drop to zero) that generates, via vertical velocity shear the turbulence and subsequent dissipation observed.

Examination of figure 6.24 reveals that the $Log_{10}(\epsilon)$ contours are inclined increasingly to the right with height above the bed. This indicates that the dissipation rate signal is increasingly lagged behind the bed variation with height. This is clearly the case in figure 6.25(a). Since the phase of the current magnitude can be considered to display little depth variation, the increased phase lag of the dissipation rate 41m above the bed is seen. This phase relationship will be examined in further detail in chapter seven as we seek to investigate the relationship between the generation and dissipation mechanisms for turbulent kinetic energy. In the meantime we consider the dissipation rate observations at the second mixed site IS3, situated in St. George's Channel.

6.5.2. Turbulent Dissipation Observations at IS3.

Figure 6.26 shows the contour plot of $Log_{10}(\epsilon)$ from the IS3 survey.

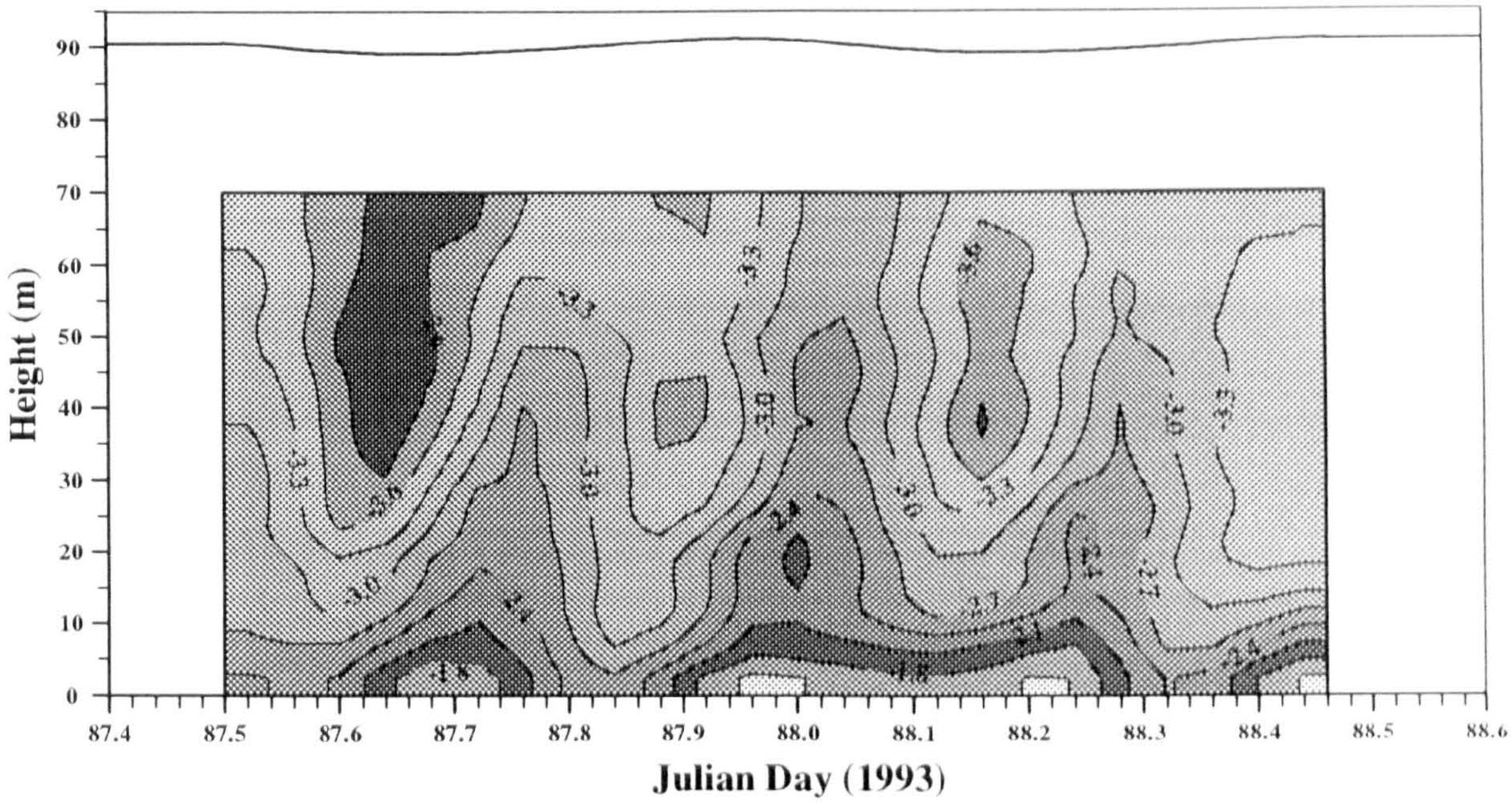

Figure 6.26 : Observed Log_{10} [ϵ (Wm^{-3})] at IS3.

As with the IS1_2 results, the vast majority of energy is dissipated in the near bed region. Also, there is once again a strong quarter-diurnal variation in dissipation rate, well correlated to the magnitude of the tidal current. However, currents at IS3 are weaker than at IS1_2 and consequently, the dissipation rates are lower.

Maximum dissipation rates 15cm above the bed are of the order of $0.3Wm^{-3}$ with values 70m above the bed typically 3 orders of magnitude lower. The increasing phase lag of the dissipation rate signal with height is also evident.

6.5.3. Turbulent Dissipation Observations at ISS.

The 22 averaged dissipation rate profiles obtained during the survey at the stratified site ISS during cruise PM93 have been interpolated to produce the contour plot shown in figure 6.27

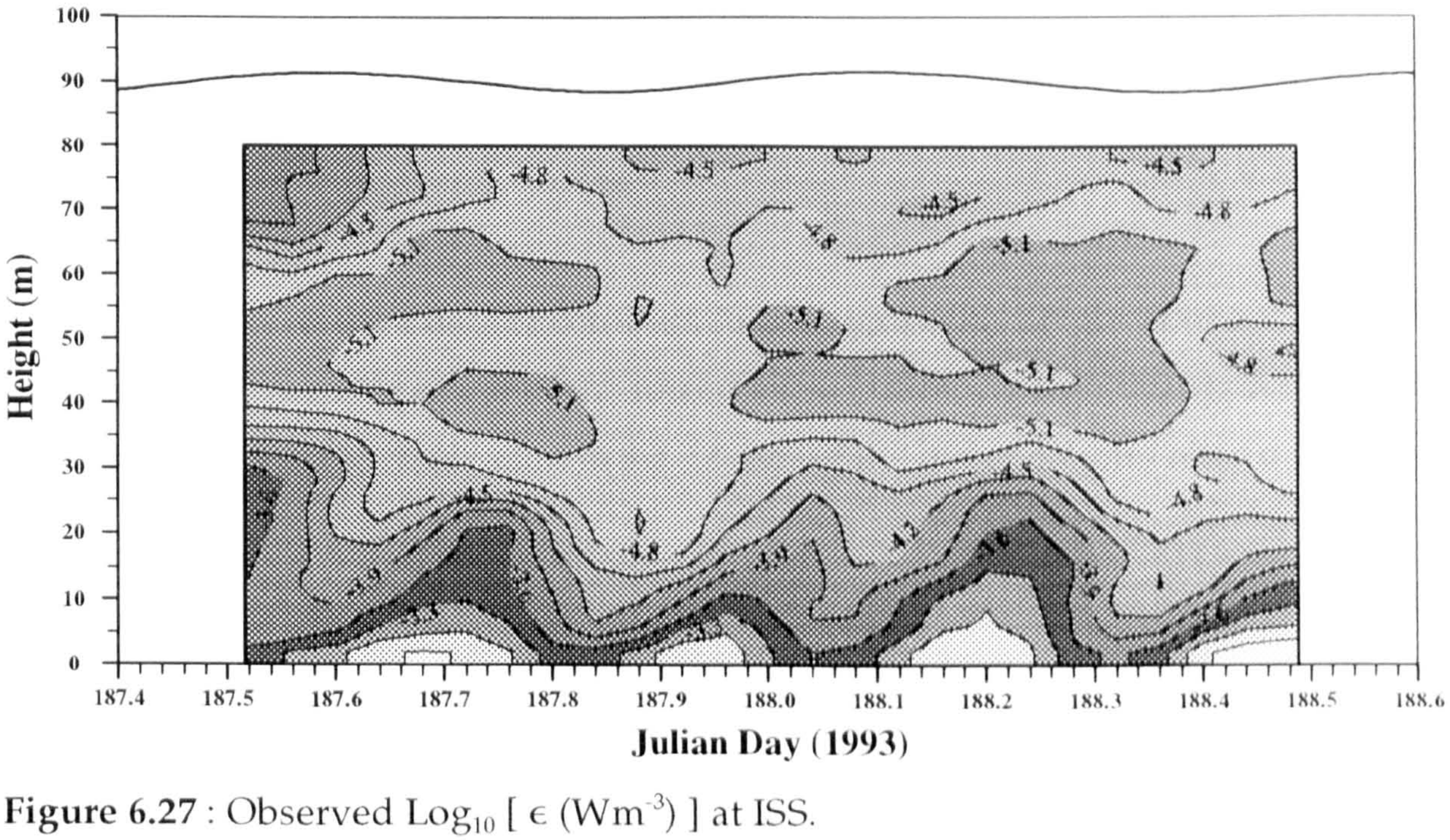

Figure 6.27 : Observed Log_{10} [ϵ (Wm^{-3})] at ISS.

These results show the same essential features as those obtained at the two mixed sites, namely a strong quarter-diurnal variation, especially near the bed and a rapid decrease in dissipation rate with height. However, as shown earlier in § 6.3.3, of the three surveys carried out, the currents were are weakest at ISS, reflecting the lower levels of tidal stirring necessary for thermal stratification to develop. This is the reason for the lower observed dissipation rates. The average dissipation rate 15cm above the bed is 4.2×10^{-3} Wm^{-3} with maximum values at peak flow of $0.013 Wm^{-3}$ and minimum values of approximately $5 \times 10^{-5} Wm^{-3}$ at slack water, an order of magnitude lower than at either of the mixed sites.

40m above the bed average dissipation rates have fallen by a factor of approximately 200 from the near bed value (to a value of $O(10^{-5}$ $Wm^{-3})$). Dissipation rates remain low between 40 and 60m above the bed before rising slightly so that there is a distinct

dissipation rate minima in midwater. This is in contrast to what was found at the mixed sites earlier in the year where there was a marked reduction in dissipation through almost the entire water column. Dissipation rates are reduced to their lowest values only 40m above the bed because this height corresponds with an increase in the vertical density gradient. Although the strongest density gradients are to be found in the surface layers, this demonstrates that only a small density gradient is required to cause significant reduction in levels of turbulent kinetic energy as it has to work against the buoyancy forces.

The inclination of the $Log_{10}(\epsilon)$ contours to the right with height above the bed is much stronger than for either of the mixed sites, indicating significant phase lag in the onset of maximum dissipation in the interior of the water column after that at the bed.

6.6 Summary.

The results of the CTD surveys, mean flow current measurements, SPM concentration and turbulent dissipation rate measurements for all 3 sites have been presented.

The CTD surveys at IS1_2 and IS3 show some evidence of diurnal heating and cooling. Apart from this input of buoyancy, the water column remained vertically homogeneous. Additionally, horizontal density gradients were observed to be weak. The survey at the thermally stratified site ISS revealed a strong pycnocline with a bottom surface density difference of the order of $1kgm^{-3}$. The strongest vertical density gradients were to be found 75-80m above the bed. Once again, horizontal gradients were weak.

The mean flow at IS1_2 was monitored using Aanderaa current meters and the ship-mounted ADCP. The currents were observed to be rectilinear, flowing in an ENE-WSW direction and relatively strong. Maximum currents found at the surface on the

flood are of the order of 1.2ms^{-1}. Ebb currents are weaker, resulting in a net transport over the tidal cycle of the order of 2-3km. At IS3 the ADCP measurements showed weaker currents with the east-west component twice as strong as the north-south flow. At both sites wind and density-driven flows are unlikely to contribute significantly to the observed flow field.

At ISS, a pair of Aanderaa current meters positioned near the bed and in the surface layer measured the much weaker currents at this site. Flood values peaked at around 30cms^{-1} with 20cms^{-1} measured on the ebb. The flow is broadly in a NNE-SSW direction although there is significant scatter. The light winds and weak horizontal gradients rule out the possibility of significant density or wind-driven flow.

The SPM concentration and settling velocity tube datasets presented show that there is a significant resuspension/settling (quarter-diurnal) signal near the bed at all 3 sites visited. Superimposed upon this is advection of a horizontal gradient at the semi-diurnal frequency resulting in a familiar 'twin-peaks' signature. At both mixed sites this was found throughout the majority of the water column. However, at the stratified site the pycnocline is very effective in confining suspended sediment to the bottom waters, thereby producing low concentrations of fine grained sediment in the surface layers.

The settling velocity tube data from the mixed sites reveal the nature of the population in the middle and surface of the water column. At IS1_2 the supply of material appears to be limited. At slack water, the resuspendable sediment forms a thin layer on top of the gravel/sand known to exist at IS1_2/IS3. The stratified site has a muddy bed, indicative of the weaker currents. The high concentrations observed below the pycnocline indicate the presence of a permanent layer of fine suspended sediment that is modified by resuspension and settling processes.

The FLY results at IS1_2 show that there is large variation in dissipation rate between the bed and the upper water column and also through the tidal cycle. 45m above the

bed the dissipation rate is typically 2 orders of magnitude lower than that 15cm above the bed. The maximum dissipation rates found at the bed for the flood and ebb tides are $0.6Wm^{-3}$ and $0.3Wm^{-3}$ respectively. The correlation between dissipation rate and current magnitude is strong so that there is an evident variation in ϵ at the M_4 frequency. The phase lag of the quarter-diurnal signal increases with height above the bed and will be investigated further in the next chapter. The dissipation rate results from the second mixed site, IS3 are similar in form to those from IS1_2. However the weaker currents at this site result in lower dissipation rates.

The weakest currents and consequently the lowest dissipation rates are to be found at the stratified site. Once again, there is significant variation at the quarter-diurnal frequency, below the pycnocline. A weak vertical density gradient is effective in suppressing turbulent activity and there is a distinct ϵ minimum in mid-water. The phase lag in the M_4 signal with height is more evident at this site.

CHAPTER SEVEN

Quarter-Diurnal Analysis and Data Synthesis

7.1 Introduction.

In chapter six the mean flow, dissipation rate and SPM concentration measurements made at the thermally stratified and both mixed sites were presented. It was noted that SPM concentrations and dissipation rates are closely related to the magnitude of the mean flow. The tidal regime at all three sites is dominated by the semi-diurnal constituent so that the primary variation in both SPM concentration and turbulent dissipation rate is at the quarter-diurnal frequency.

It is the aim of this study to increase our understanding of how the three observed variables affect and interact with each other. To this end, a harmonic analysis technique is used to isolate and quantify the amplitude and phase of the quarter-diurnal signal in each of the datasets. Conclusions can then be drawn regarding the importance of this signal in determining overall levels of SPM or dissipation rate.

In §7.3, the results of the quarter-diurnal analyses performed on the FLY and CTD datasets allow us to study the relationship between SPM concentration and turbulent dissipation rate throughout the water column. §7.4 expands the comparison to include the moored instruments so that the mean flow field can be included and variations between the flood and ebb tides can be examined.

7.2 Quarter-Diurnal Analysis.

A least squares method has been used to fit the dissipation rate, transmissometer and current magnitude datasets to a function of the form

$$z = a_0 + a_1 \sin(\omega t - \phi) \qquad (7.01)$$

where a_o is the mean amplitude of the signal over the observational period. a_1 and ϕ are the amplitude and phase (relative to t=0 *i.e.* the start of 1993) of the periodic variation of angular frequency ω.

A quarter-diurnal (M_4) analysis ($\omega=2\pi/6.21hr^{-1}$) has been performed on each of the dissipation rate and SPM concentration datasets from IS1_2, IS3 and ISS. There are dissipation rate time series every 15cm from a height of 15cm above the bed to within ~10m of the surface at all 3 sites and SPM concentration time series every 10cm at the mixed sites and every 20cm at ISS from near bed to surface. Typically, there are 20-25 datapoints at each height, depending on how many CTD or hourly averaged dissipation rate profiles are available. Also analysed were the current magnitude datasets from the current meters on moorings IS1, IS2 and ISS.

The purpose of this analysis is to calculate the amplitude and phase of the M_4 variation that best parameterises a particular time series. However, this may not be the only signal present in the data and a measure of the suitability of an M_4 variation in describing the data can be gained by calculation of the explained variance (R^2) when the data is compared with the predicted signal ($=a_o+a_1(\omega t+\phi)$). It is also possible to calculate a minimum value of R^2 above which the analysis can be considered to be statistically significant. In statistical terms, there are few samples in each dataset and an R^2 value above 20% is usually required for the regression to be considered significant. This limit is displayed on each graph, since it varies slightly from one dataset to the next.

7.3 M_4 Analysis Results.

7.3.1 Profiling Instruments (CTD,FLY).

7.3.1.1 The Vertically Homogeneous Sites (IS1_2,IS3).

Consider the M_4 analysis results for the dissipation rate and SPM concentration data obtained during the survey at IS1_2, shown in figures 7.01 and 7.02 respectively.

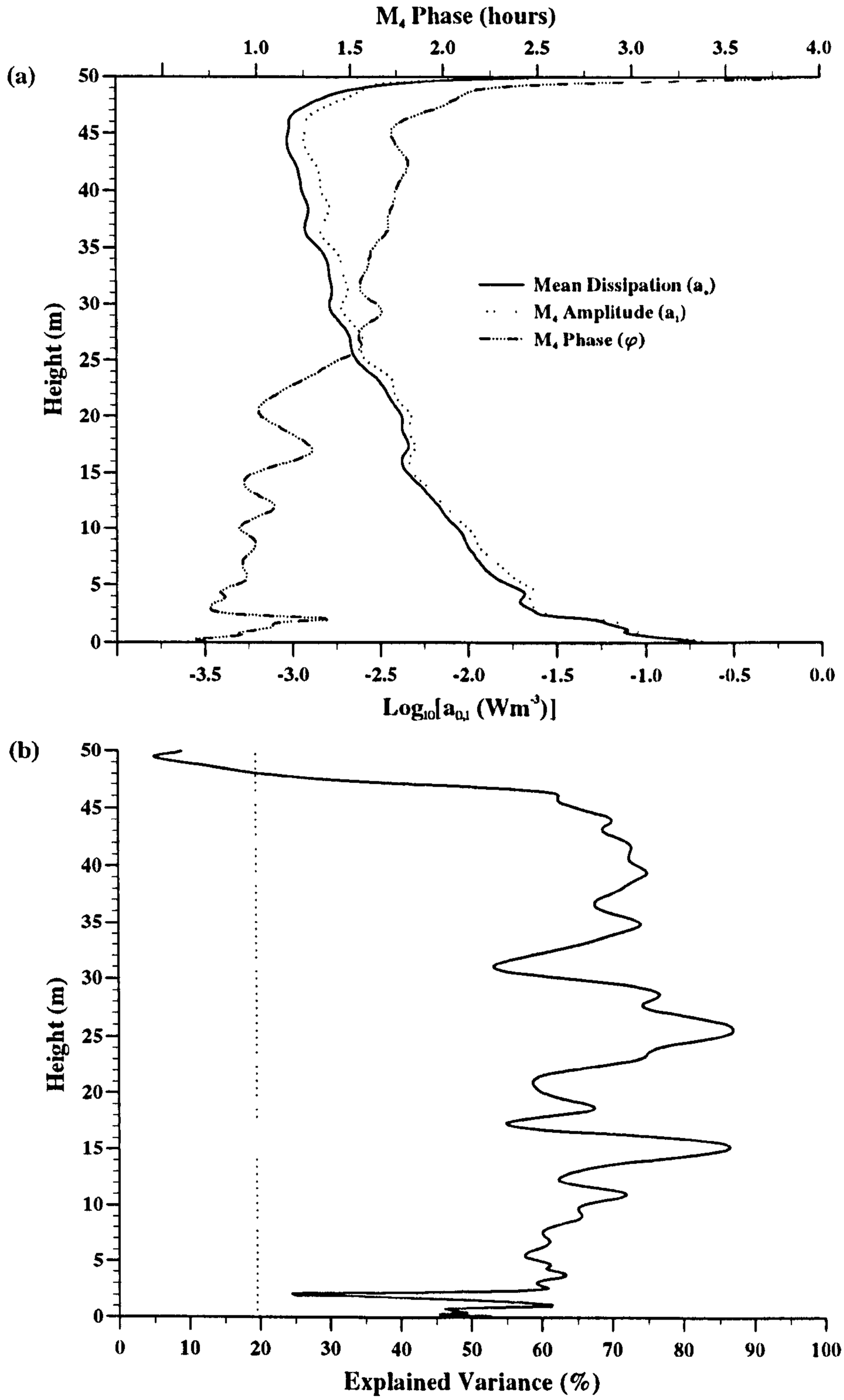

Figure 7.01 : M_4 analysis of observed turbulent dissipation rate at IS1_2.

(a) Mean dissipation, M_4 amplitude and phase.

(b) Explained variance.

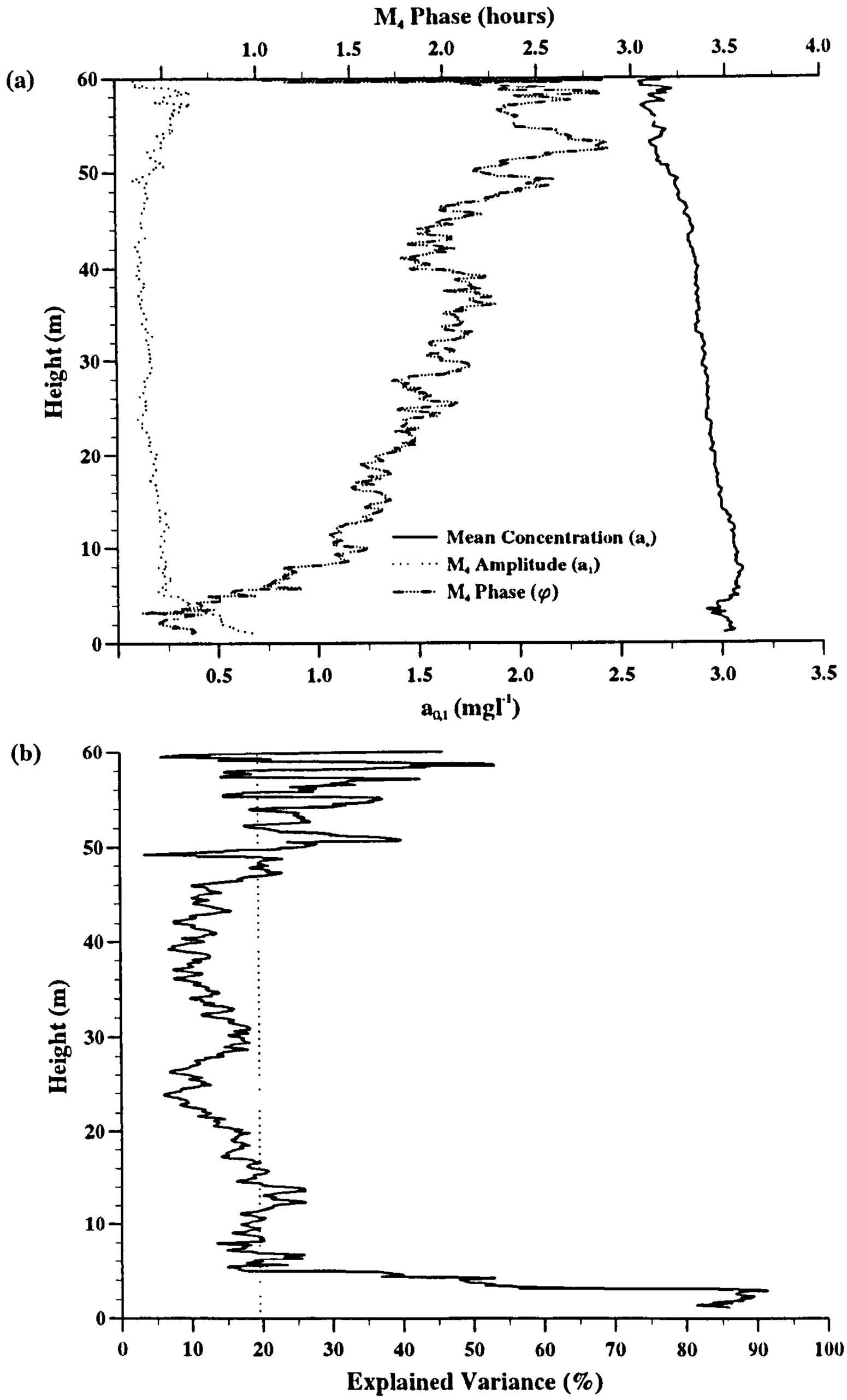

Figure 7.02 : M_4 analysis of observed SPM concentration at IS1_2.

(a) Mean concentration, M_4 amplitude and phase.

(b) Explained variance.

This analysis has isolated and quantified the M_4 signal in the turbulent dissipation rate and SPM concentration datasets. Interpretation of these results must be made with consideration of the explained variance calculation. The dotted vertical line in figures 7.01 (b) and 7.02 (b) indicates the level below which the results of the analysis cannot be considered statistically significant at the 95% confidence limit.

Figure 7.01 (a) shows that the total dissipation rate signal is dominated by the M_4 variation. This is indicated by the similarity of the mean dissipation (a_o) and M_4 amplitude (a_1) and the consistently high R^2 values. a_o and a_1 are almost identical up to a height of 50m, above which the dissipation data is considered unreliable and is excluded. Because both amplitudes are practically the same, the dissipation rate varies from approximately zero at around slack water to a_o+a_1 at peak flow *i.e.* there is virtually no residual or background dissipation rate component. This implies that the dissipation rate time series at every level throughout the water column at IS1_2 depends entirely on the state of the tide and distance from the bed.

The M_4 amplitude and phase profiles reveal much about the temporal and spatial nature of the turbulent dissipation rate signal. The strong decrease in the amplitude of the dissipation rate with height is evident. At a height of 5m, dissipation rates have already been reduced by an order of magnitude on those measured 15cm above the bed where the greatest levels of vertical shear and turbulent kinetic energy are to be found. They fall by a further order of magnitude over the next 40m.

The phase lag of the M_4 signal increases with height so that at 45m the signal is lagged 60° (~1hr) behind that at the bed. Aside from variations over a few meters, this rate of increase of the phase can be considered constant with height. Confidence in this result is high because of the high R^2 values found up to a height of 45m.

Turning to the SPM results, it is obvious that the M_4 harmonic analysis approach is less applicable for the SPM concentration dataset. R^2 values are lower, except for near the bed, indicating the presence of additional signals in the data. The analysis

isolates the sediment resuspension and settling signal from these other variations but the low R^2 values mean that the results must be interpreted with caution.

The low explained variance values found throughout most of the water column at this site are due partly to the presence of a semi-diurnal (M_2) signal in the dataset. This is the advected background component in the SPM concentration field, introduced in chapter 3 and identified in the data in §6.4. A harmonic analysis at this frequency ($\omega=2\pi/12.42hr^{-1}$) reveals a depth-uniform M_2 amplitude of ~$0.3mgl^{-1}$, larger than the M_4 amplitude. Removal of this signal from the data and re-calculation of the quarter-diurnal analysis increases R^2 values by 15-20% throughout the water column, raising them above the 95% confidence limit so that they become statistically significant.

The difference between the mean concentration and M_4 amplitude results reveals the contribution to the total SPM signal of the resuspension/settling cycle. Adjacent to the bed, where the resuspension signal is strongest, the M_4 amplitude is highest. However, it rapidly diminishes to an approximately constant level (10% of the mean concentration) above 8m. The mean concentration results are in accord with the moored transmissometer measurements.

Although the M_4 signal is weak throughout much of the water column, the increase in phase with height is evident. The SPM concentration and turbulent dissipation rate M_4 phase profiles are compared in figure 7.03.

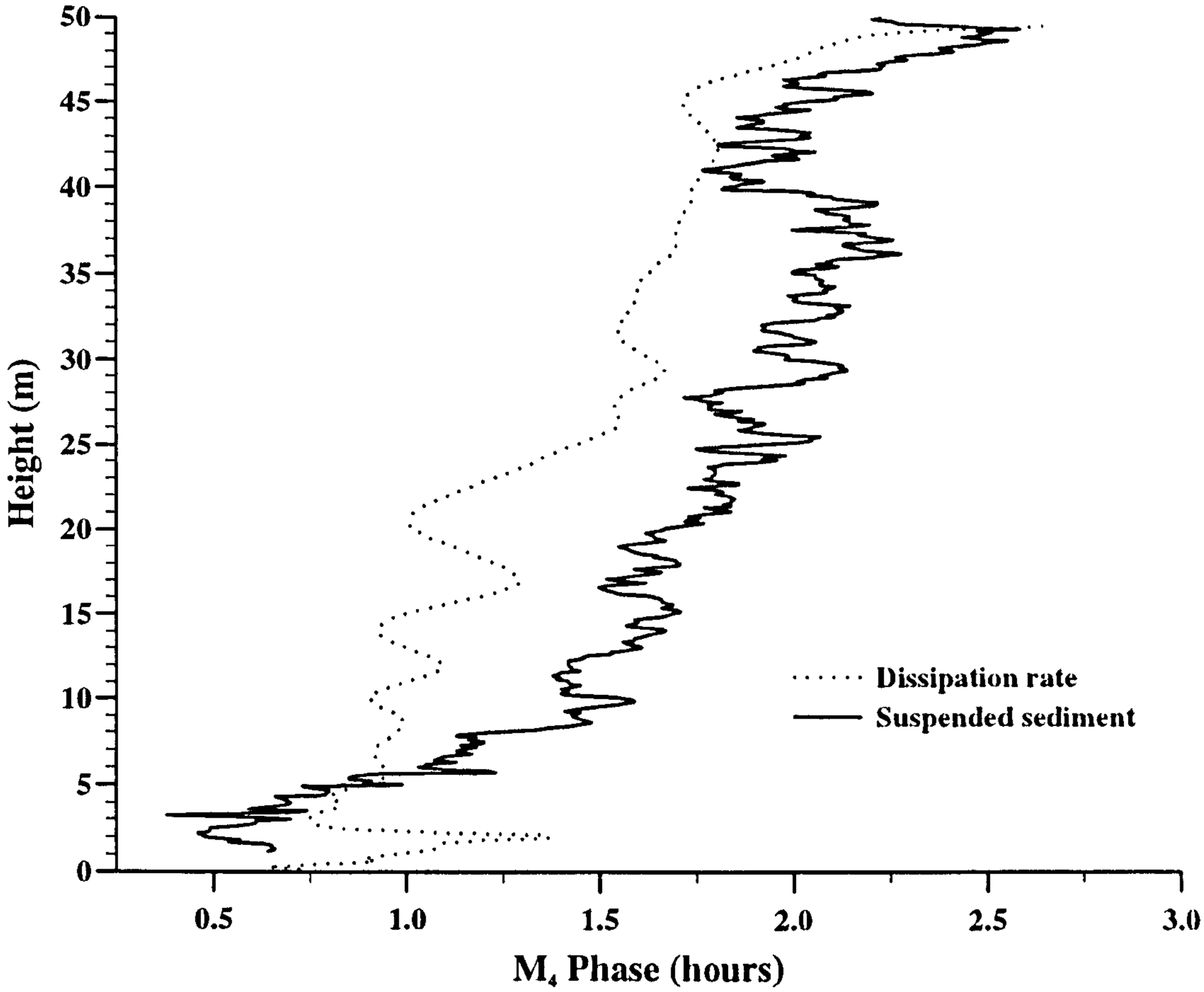

Figure 7.03 : M_4 phase for SPM concentration and turbulent dissipation rate measurements at IS1_2.

Figure 7.03 shows a clear lead of the resuspended SPM signal below 4m *i.e.* maximum resuspended sediment concentration below 4m occurs before maximum dissipation rate. This is consistent with the evidence from the bed transmissometer on IS2 (figure 6.16 (b)) which suggests a degree of source-limitation at this site.

The rate of increase of the M_4 phase for the turbulent dissipation rate is approximately constant. A straight line fitted to the data has a gradient of $0.027 hrm^{-1}$ (an increase of ~15min every 10m). This is not the case for the SPM results where the rate of increase is greater in the bottom 10m, before reducing to a level similar to that of the dissipation rate. Between 10m and 40m the SPM concentration M_4 signal lags behind the turbulent dissipation rate M_4 signal by ~0.5hr. The IS3 results are shown in figures 7.04 and 7.05.

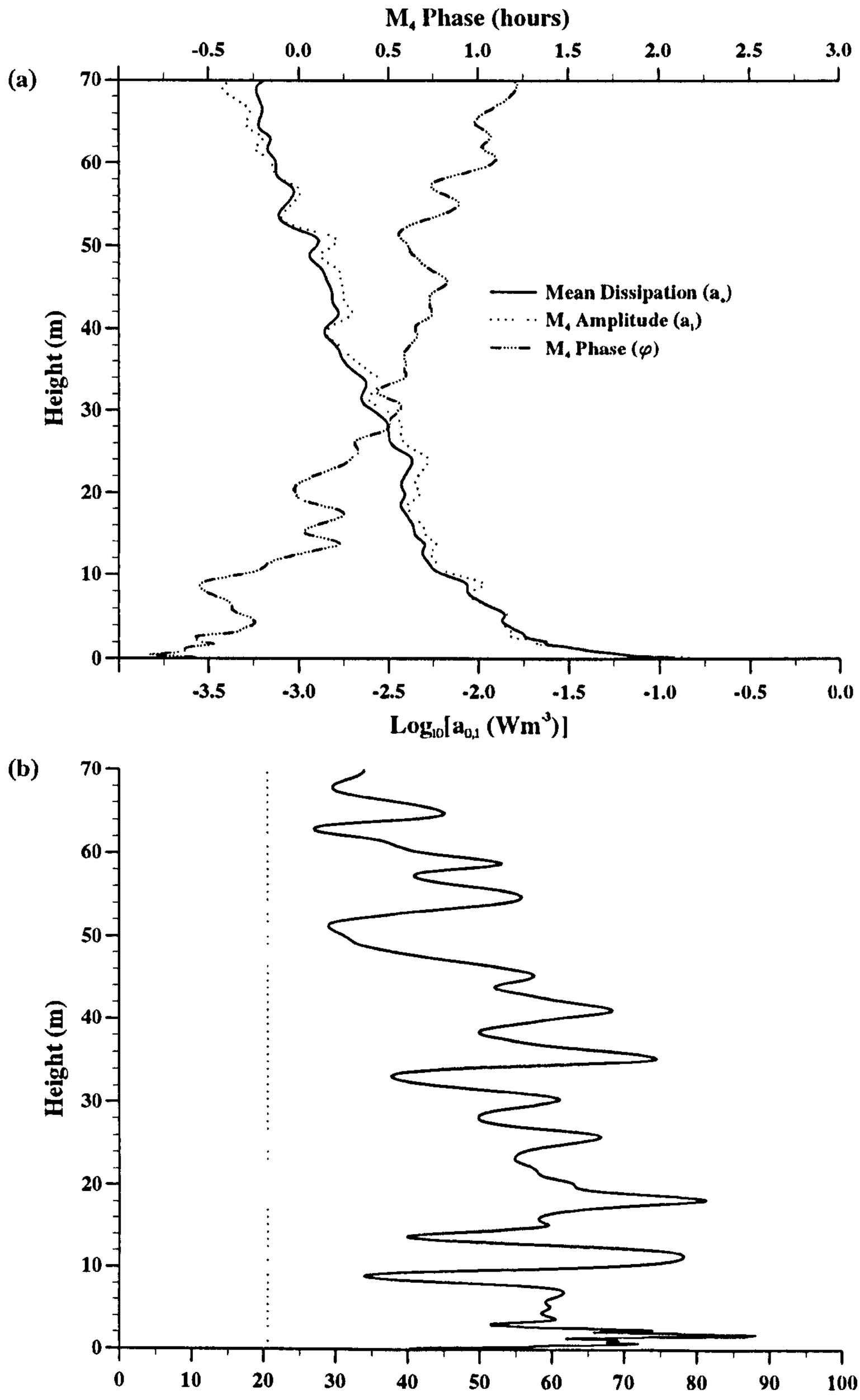

Figure 7.04 : M_4 analysis of observed turbulent dissipation rate at IS3.

(a) Mean dissipation, M_4 amplitude and phase.

(b) Explained variance.

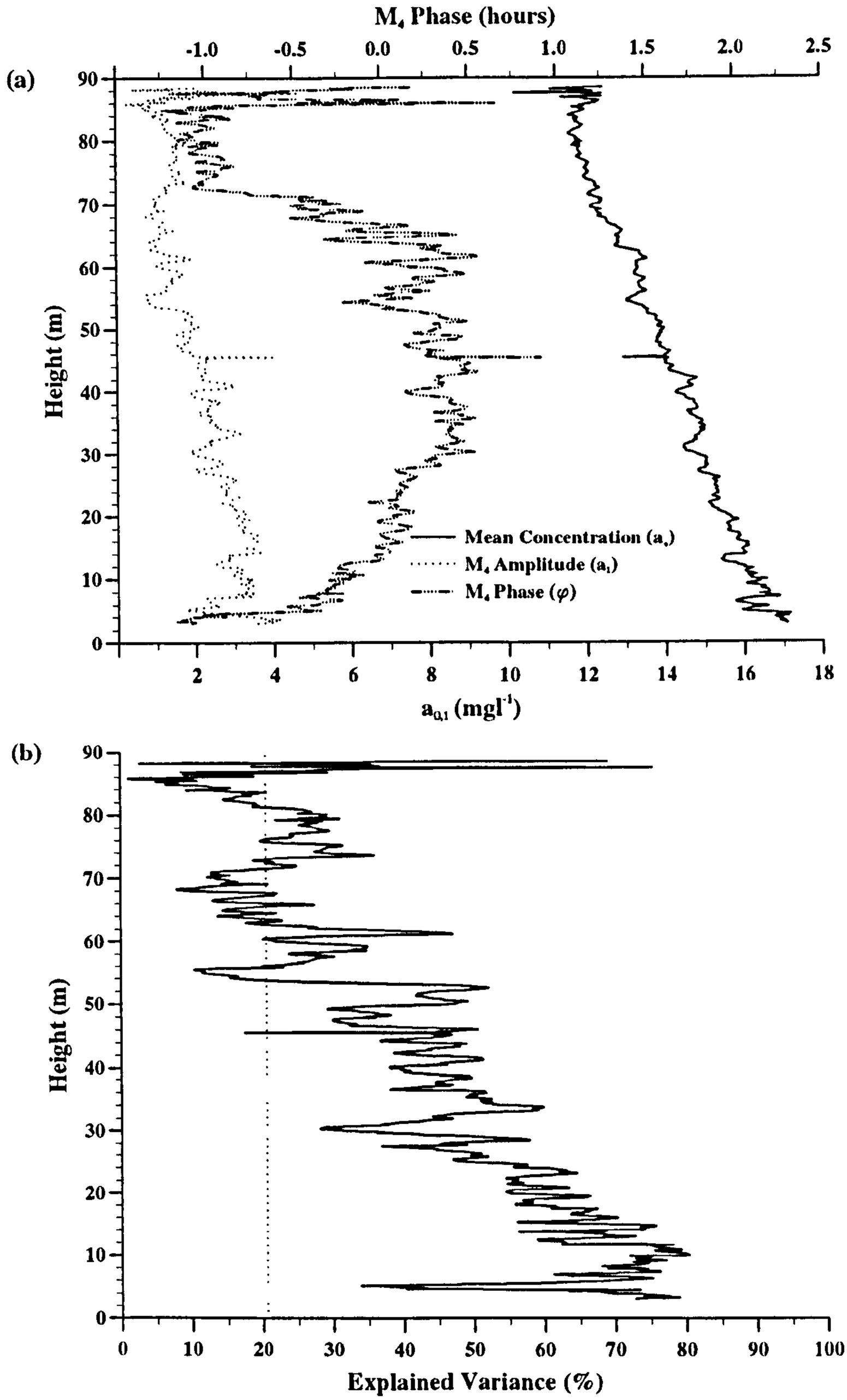

Figure 7.05 : M_4 analysis of observed SPM concentration at IS3.

(a) Mean concentration, M_4 amplitude and phase.

(b) Explained variance.

As at IS1_2, the dissipation rate analysis results can be considered significant throughout the water column. However, R^2 values for the SPM concentration results are higher than before so that the total variation in concentration at a single height above the bed can be more readily understood in terms of an M_4 signal than at IS1_2. This is consistent with the observations presented in the previous chapter which showed that there was a significant semi-diurnal signal at IS1_2 throughout the water column, due to advection of a horizontal concentration gradient. This is less in evidence at IS3 where the dominant signal appears to be the M_4 variation.

a_0 and a_1 are smaller than at IS1_2 *i.e.* dissipation rates are lower. This is commensurate with the weaker tidal currents known to exist at this site. The mean dissipation and M_4 amplitude reduce significantly with height above the bed and are very similar throughout the water column so that, as before, the tidal currents can be considered to be the only major source of turbulent kinetic energy, with little background component.

The phase of the dissipation rate signal generally increases with height. The rate of increase is approximately constant and is similar to that found at IS1_2 so that at a height of 70m the dissipation rate signal is lagged ~2 hr behind that at the bed.

In contrast to the dissipation results but consistent with observations at IS1_2, there is a distinct difference between the mean concentration and SPM concentration M_4 amplitude, due primarily to a fine background population which is not subject to significant modulation. The mean concentration at this site decreases uniformly from ~17mgl^{-1} at the bed to ~12mgl^{-1} near the surface. The M_4 amplitude also displays a uniform reduction from ~4mgl^{-1} at the bed to ~1mgl^{-1} near the surface.

The phase of the SPM quarter-diurnal signal increases with height up to about 45m above the bed (mid-water) at which point the M_4 signal is lagged ~1.5hr behind that at the bed. Above this height the phase reduces to the point that the signals at the bed and 90m above the bed appear to be in phase.

The phase profiles for the turbulent dissipation rate and SPM concentration M_4 signals are compared in figure 7.06.

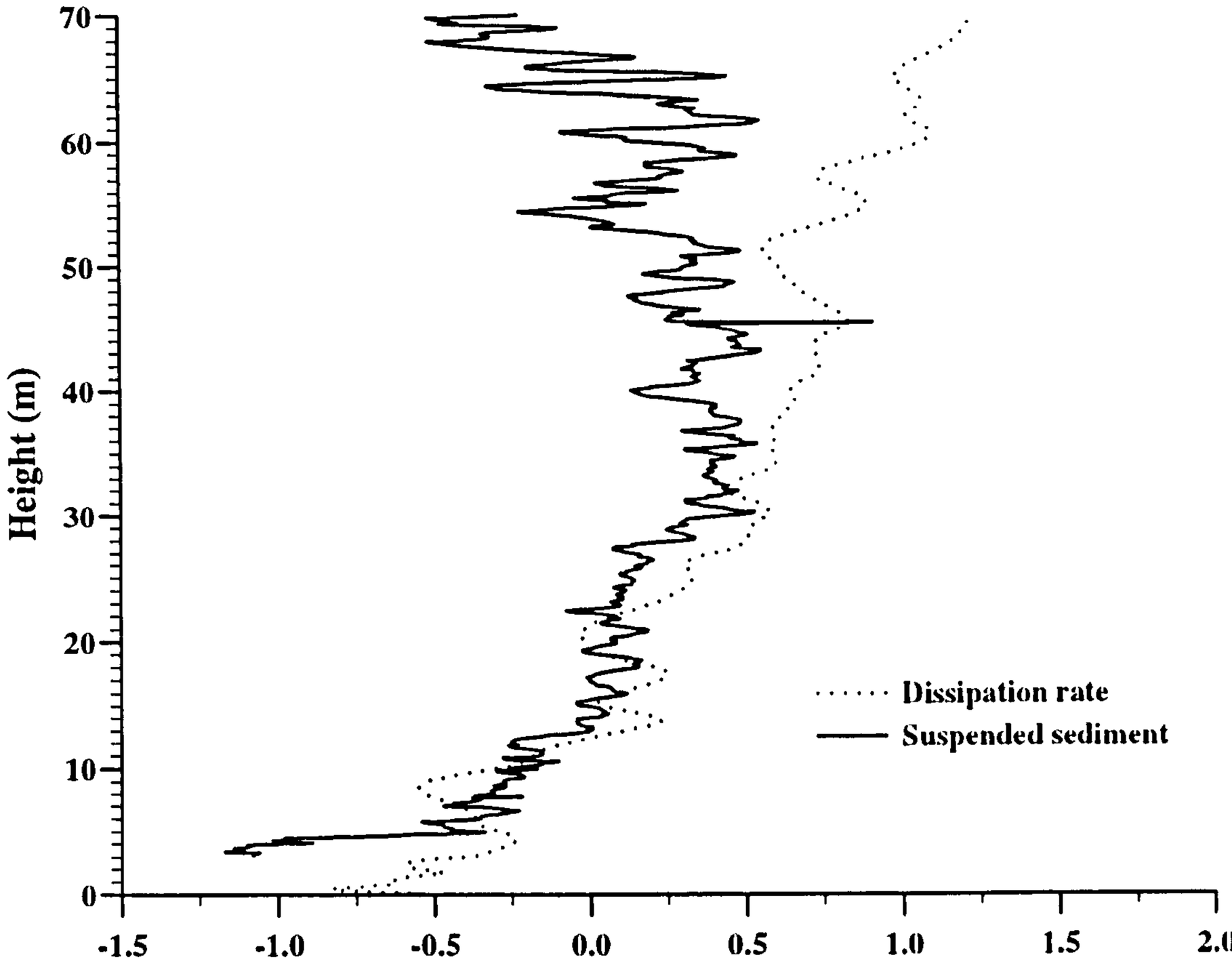

Figure 7.06 : M_4 phase for SPM concentration and turbulent dissipation rate measurements at IS3.

The rate of change of phase with height for the dissipation rate M_4 signal can again be considered constant. A straight line fit gives this rate of increase as $0.025 hrm^{-1}$, similar to that found at IS1_2 ($0.027 hrm^{-1}$).

The behaviour of the SPM M_4 phase profile is more complex. Near to the bed the resuspended sediment signal leads the turbulent dissipation rate, again possibly due to the effects of source-limitation. The phase increases rapidly up to a height of 6m after which the rate is reduced to a level similar to that seen in the turbulent dissipation rate until a height of 35m. Furthermore, the absolute phase of the two

signals is approximately equal between 6m and 35m above which the SPM M_4 phase reduces. This was not the case at IS1_2 where, although the phases increased at the same rate above 10m, there was a distinct lag between the two signals.

7.3.1.2 The Stratified Site (ISS).

We now consider the results of the M_4 analysis for the stratified site datasets. Figure 7.07 shows the turbulent dissipation rate M_4 analysis data and 7.08 reveals the nature of the resuspension/settling SPM signal at this site.

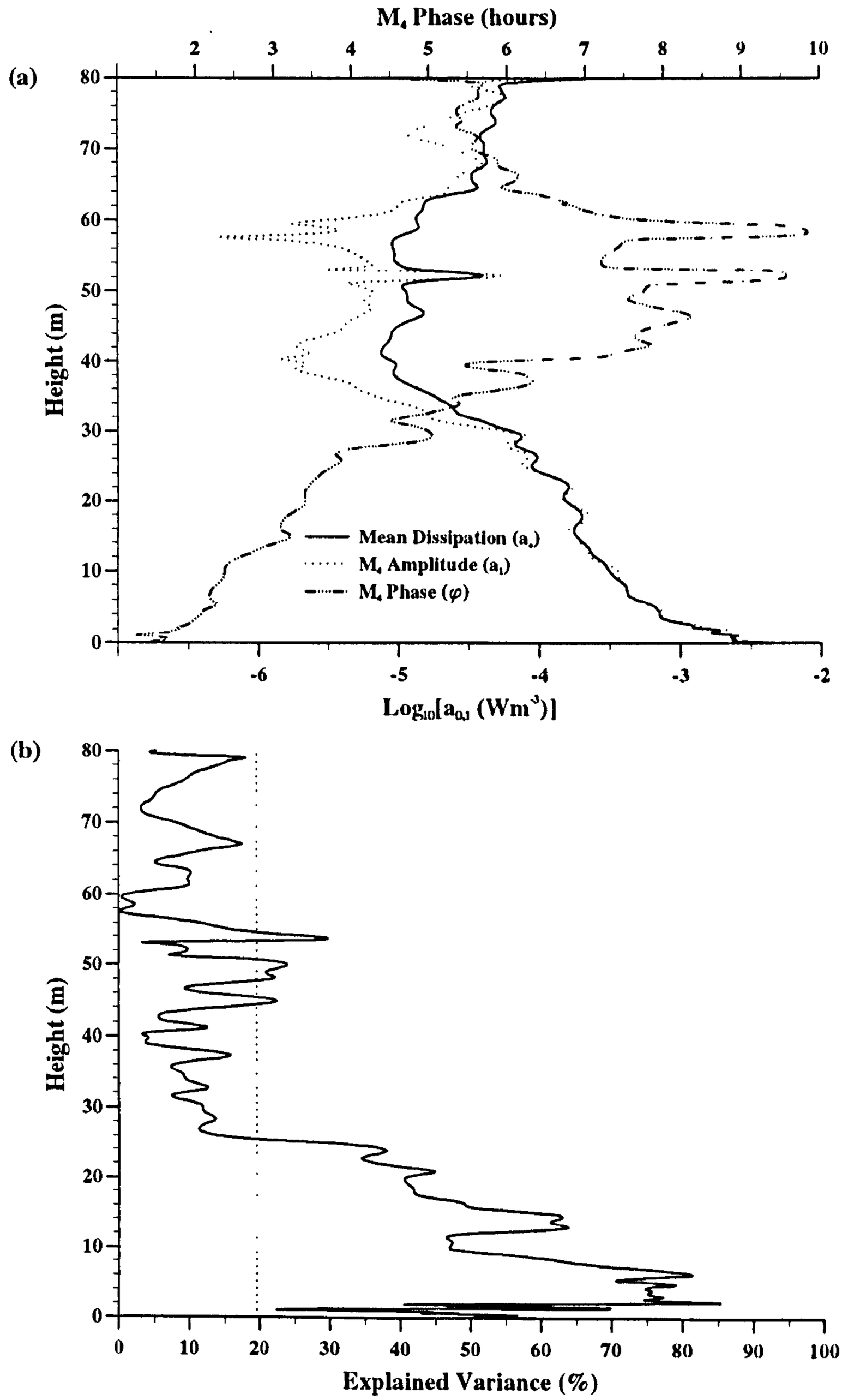

Figure 7.07 : M_4 analysis of observed turbulent dissipation rate at ISS.

(a) Mean dissipation, M_4 amplitude and phase.

(b) Explained variance.

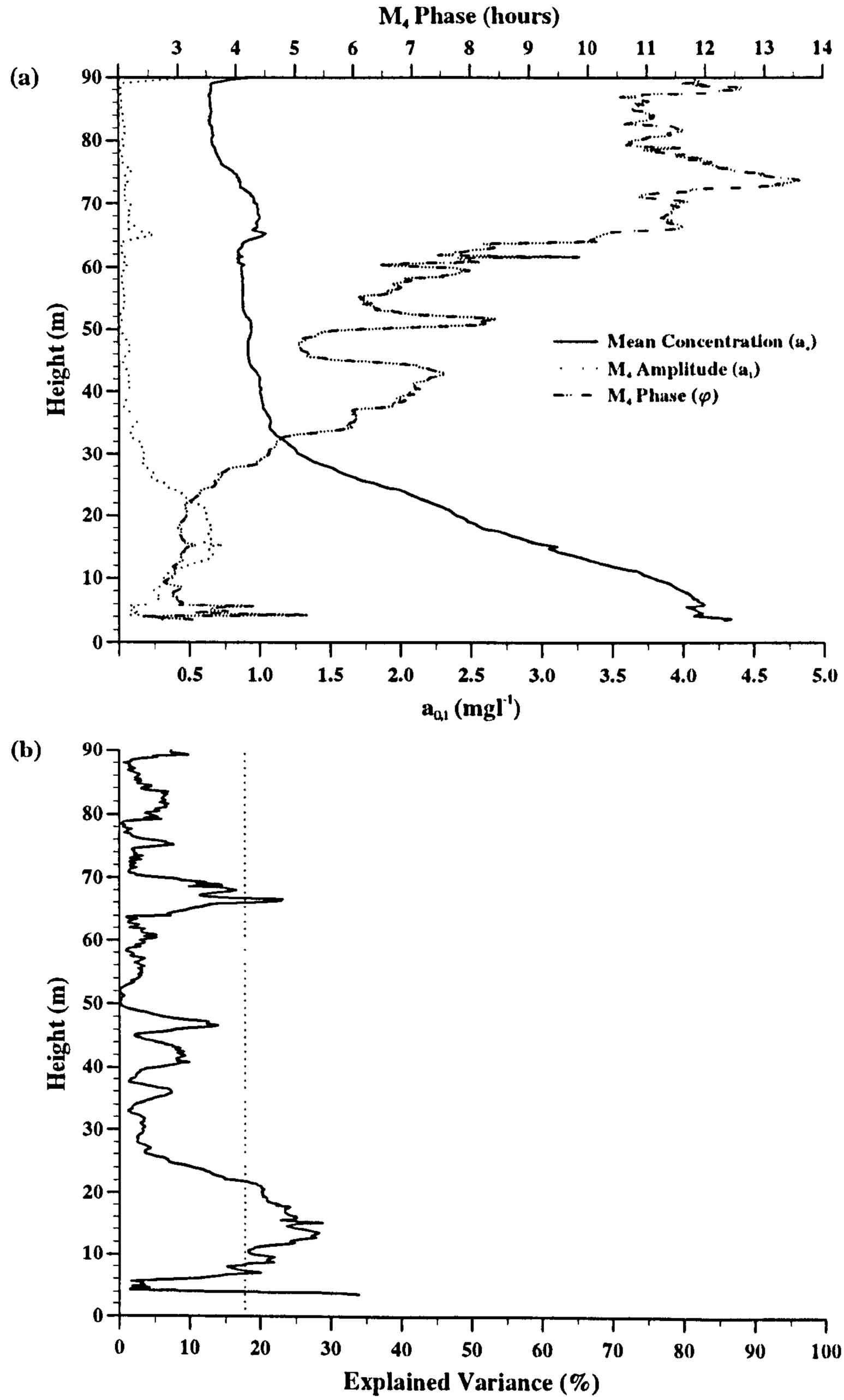

Figure 7.08 : M_4 analysis of observed SPM concentration at ISS.

(a) Mean concentration, M_4 amplitude and phase.

(b) Explained variance.

These results demonstrate the dramatic effect of the seasonal pycnocline on the distribution of both turbulent dissipation rate and SPM concentration. Confidence in the analysis above 25m is very low for both datasets, indicating the lack of importance of the quarter-diurnal variation in and above the pycnocline. The explained variance increases to over 50% near the bed for the dissipation rate analysis but remains low (20-30%) for the equivalent SPM results. Indeed, very close to the bed there is very little M_4 variation in SPM concentration at all.

The dissipation rate M_4 analysis results in the bottom third of the water column *i.e.* below the pycnocline are qualitatively the same as before, with decreasing mean dissipation rate and M_4 amplitude and increasing phase with height. The relatively weak tidal currents that permit stratification to develop mean that dissipation levels at ISS are much lower than at either of the mixed sites. Again, a_0 and a_1 are almost identical but phase lags here are much greater. For example, the bed dissipation rate signal leads that 30m above it by some 4 hours.

The lowest dissipation rates are to be found in the middle third of the water column. In this area, the mean dissipation rate is greater than the M_4 amplitude indicating that not all of the turbulent dissipation observed is explained by a quarter-diurnal variation. This is evidence for another source of turbulent kinetic energy which is not modulated at the quarter-diurnal frequency.

Figure 7.08 (a) indicates that at this site there is no SPM M_4 signal above 25m. Also, the mean concentration drops to a constant value of ~1.0mgl^{-1}, similar to levels measured by the surface transmissometer. However, below this height the mean concentration increases steadily towards the bed. This is not seen in the M_4 amplitude which increases to ~0.7mgl^{-1} and then reduces to zero below 15m. As with the dissipation rate results, phase lags are large. To study the temporal relationship between SPM and turbulent dissipation, we compare the two phase profiles in figure 7.09.

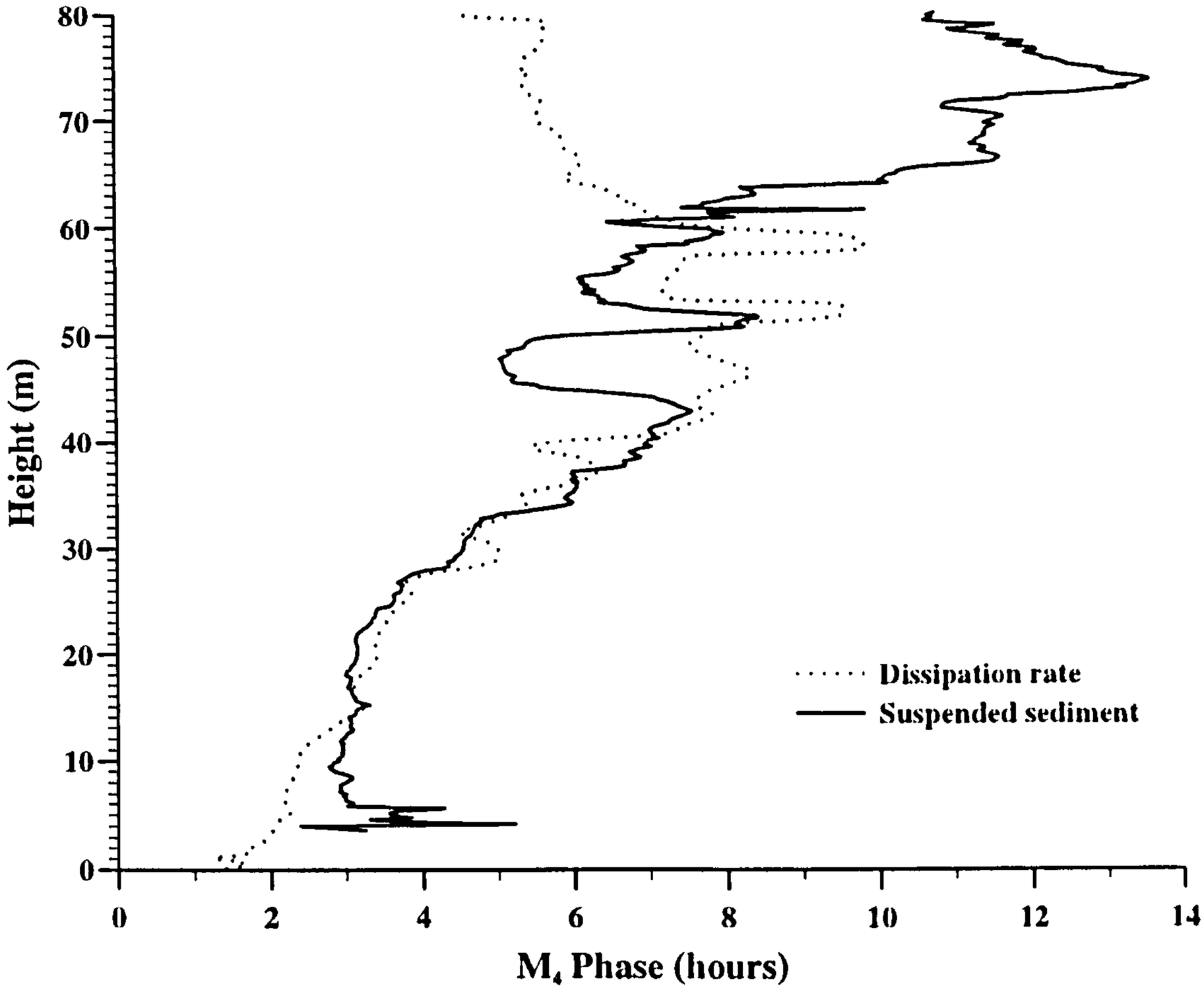

Figure 7.09 : M_4 phase for SPM concentration and turbulent dissipation rate measurements at ISS.

In the previous section it was shown that, in the absence of stratification, the rate of increase of the dissipation rate M_4 phase profile with height was approximately constant. Indeed, the rate of increase was found to be the same at both mixed sites. However, at this site where there is significant vertical density structure, the rate of increase of phase displays a height dependence. Above a height of 25m (which corresponds to the bottom of the pycnocline) the rate appears to reduce although confidence in the results is reduced.

Between 20m and 40m the phase profiles coincide so that the dissipation rate and SPM M_4 signals are in step. Below 20m this is not the case and the SPM M_4 phase remains constant. Figure 7.08 (a) demonstrates that the quarter-diurnal amplitude falls to zero in this bottom layer. Recalling the SPM concentration contour plot

(figure 6.22), the dominant variation in SPM concentration near the bed appears to be at the semi- rather than the quarter-diurnal frequency. A repeat of the analysis but this time at the semi-diurnal frequency shows that the M_2 signal is larger and more determined than the M_4 variation with R^2 values between 40% and 60% below the pycnocline. This implies that the dominant process determining the nature of the SPM concentration signal in the near bed region is one which displays a distinct M_2 variation.

Asymmetry in the magnitude of the tidal current will result in different amounts of resuspension on each phase of the tide, contributing to an M_2 variation in SPM concentration near the bed. However, the current meter data presented in §6.3.3 which shows that the flood and ebb currents are similar, so this is unlikely.

Advection of a horizontal gradient in SPM concentration by the mean flow field will also result in an enhanced M_2 signal. The tidal excursion calculated from the moored current meters shows a net displacement of the bottom waters of approximately 4km over the deployment period. Given the strong horizontal gradient that would be required to produced the observed M_2 signal, this would result in an overall change in SPM concentration, as observed at IS1_2. However, there is no indication of this in the moored or profiling transmissometer records.

Vertical migration of the pycnocline occurs at the semi-diurnal frequency due to the rise and fall of the sea surface and also advection as the density structure varies with water column depth and the magnitude of the tidal currents. The vertical density gradient has been calculated from the CTD survey data (figure 6.05 (c)) and is compared with the SPM concentration data in figure 7.10.

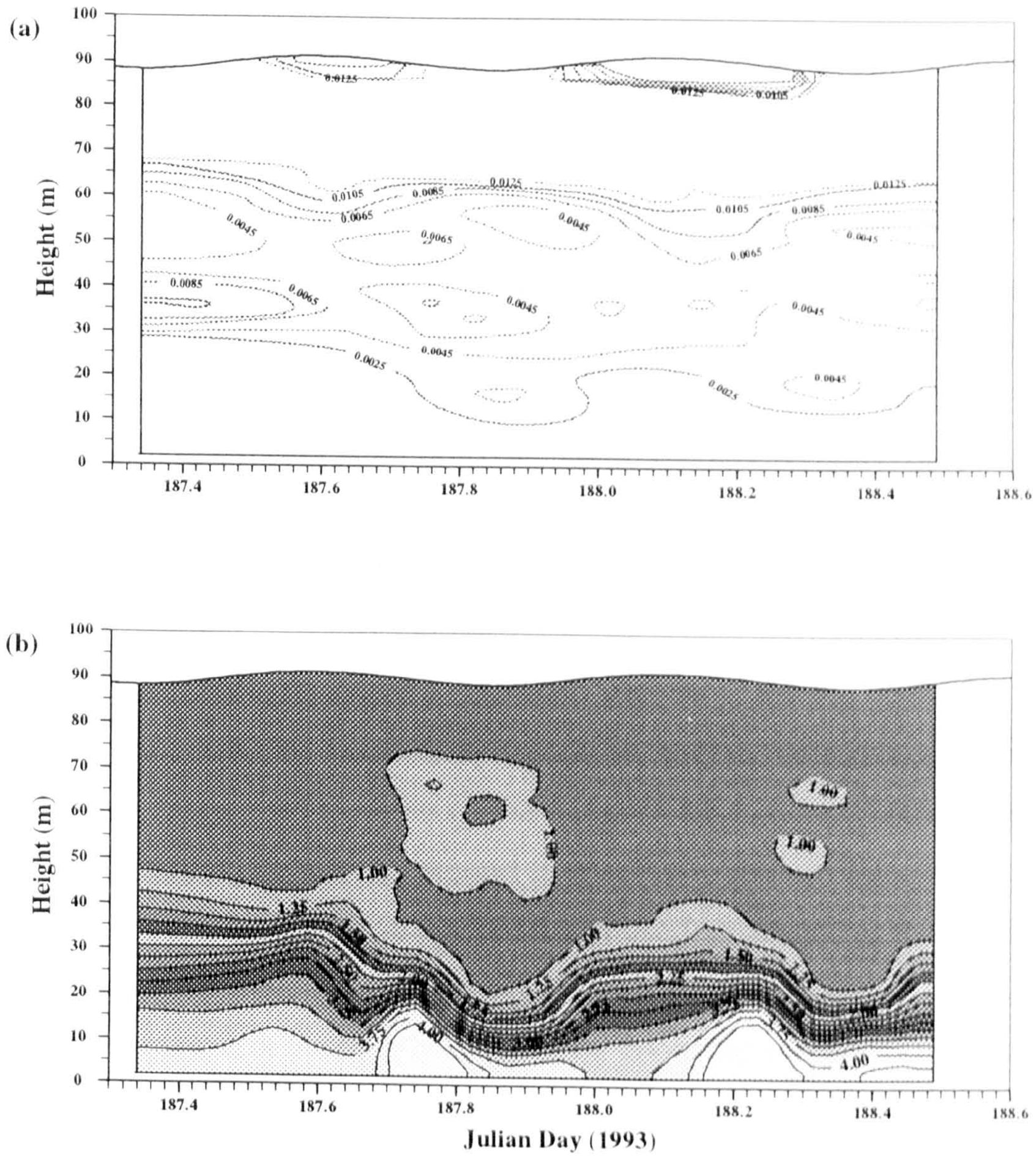

Figure 7.10 : ISS contour maps.

(a) Vertical density gradient (kgm^{-3}/m).

(b) SPM concentration (mgl^{-1}).

Figure 7.10 shows that the maximum height to which the SPM can penetrate coincides with the $2.5x10^{-3}kgm^{-3}/m$ contour *i.e.* the bottom of the pycnocline. When the pycnocline is furthest from the bed, the suspended sediment can reach heights of 45m. At other times it is confined below 20m and vertical gradients in SPM increase, as indicated by the closely packed contours around Julian days 187.8 and 188.3. This vertical movement of the pycnocline has a semi-diurnal period, so

enhancing the SPM concentration M_2 variation in this bottom layer.

The SPM concentration contour plot from this site (figure 6.22) and the M_4 analysis results presented in the previous section indicate that in the bottom 10m variations in SPM concentration both vertically and temporally are much weaker than higher up, where the vertical density gradient increases. The sea bed at this site is known to be muddy so that it consists principally of very fine silt and clay particles. It is possible that much of the suspended sediment population that is confined below the pycnocline exists as a turbid layer of permanently suspended material that diffuses up as far as the density structure permits, reducing concentration variations close to the bed.

So far in this chapter the results of a harmonic analysis approach have been used to isolate and quantify the important signals in the dissipation rate and SPM concentration datasets at all three sites. This has permitted an insight into how levels of suspended particulate matter respond to changes in the turbulent flow field. In the next section, the moored instrument data is used to study this relationship at a single height above the bed. This approach has the advantage of revealing any change in the response of the signals between the flood and ebb tides and also allows comparisons to be made regarding the response of both turbulent dissipation rate and SPM concentrations to the mean flow field, from which the energy for redistribution of TKE and sediments is derived.

7.3.2 Moored Instruments.

The current meters and transmissometers deployed on moorings IS2 and ISS were positioned in pairs : one near the bed and the other in the surface waters. This was to facilitate the comparison of the suspended sediment and mean flow fields. Plotted in figures 7.11 and 7.12 are the transmissometer and RCM current magnitude measurements from IS2 and ISS respectively. Also shown are the turning points and vertical lines indicating peak flow and slack water events. The SPM turning points were determined from the smooth curve, fitted by the UNIGRAPH graphics package. The large variations in current magnitude (up to 20cms^{-1}) around peak flow made curve fitting inappropriate for determining the time of maximum current. Instead, a Fast Fourier Transform was performed and the signal reconstructed using the mean amplitude and the first harmonic. This eliminated the high frequency contributions and the turning point was easily identified. The minima are much sharper and so were easily identified directly from the data.

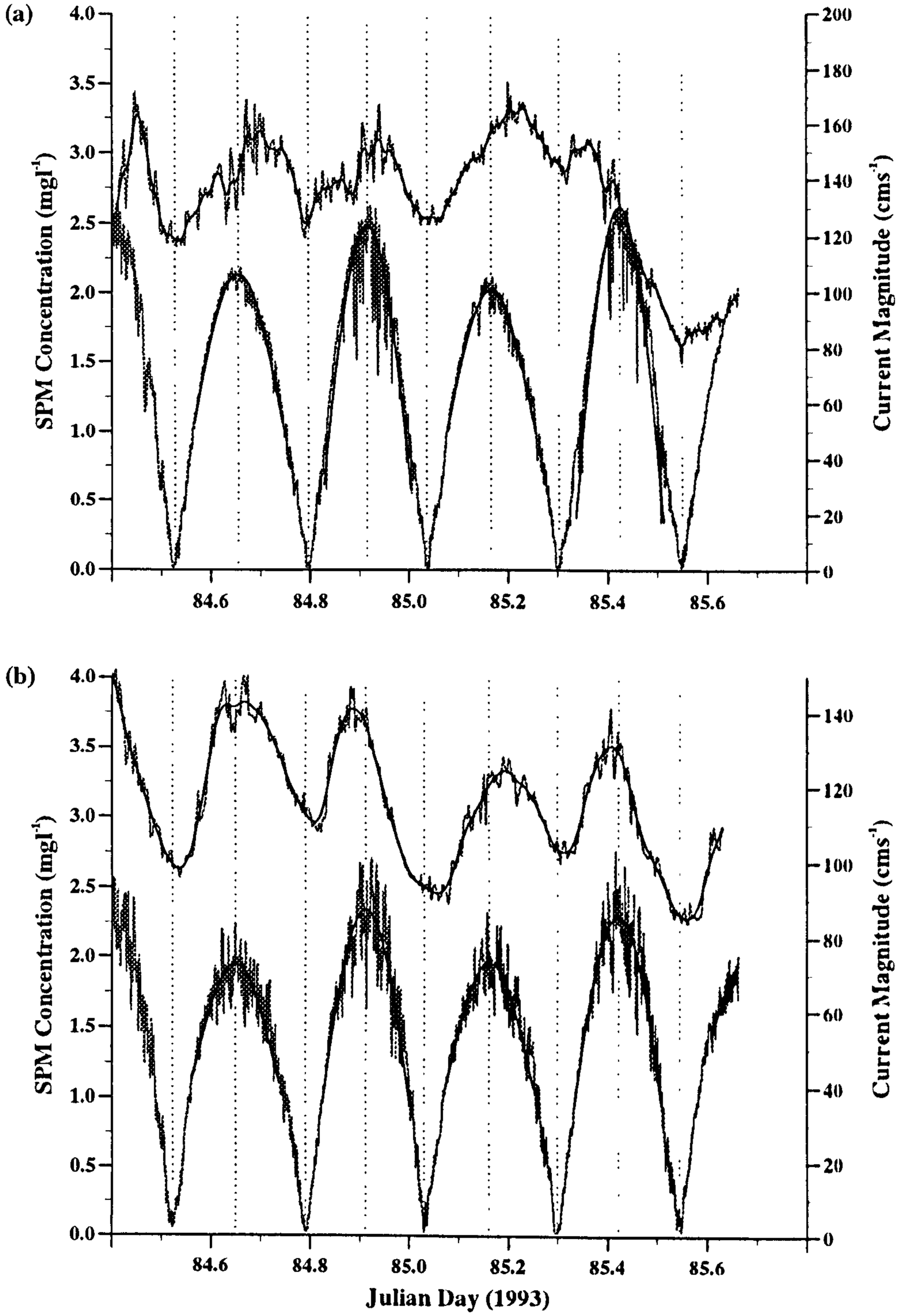

Figure 7.11 : SPM concentration and current magnitude at IS2.

(a) Surface instruments.

(b) Bed instruments.

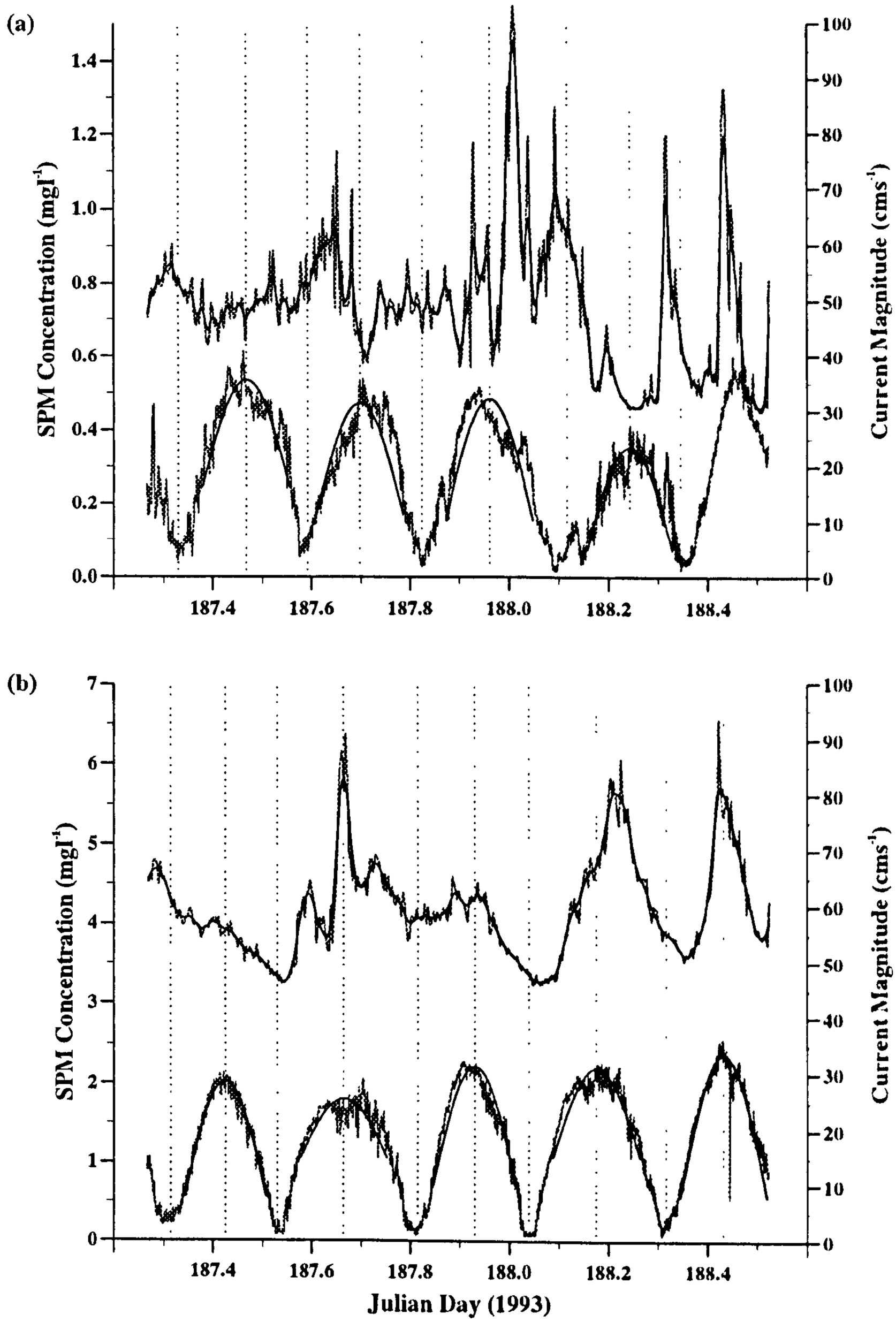

Figure 7.12 : SPM concentration and current magnitude at ISS.

(a) Surface instruments.

(b) Bed instruments.

The strong dependence of SPM concentration on current magnitude is most evident near the bed at IS2. The two signals are well correlated with resuspension of the bed material by the flood and ebb currents and settling at slack water. This relationship can also be seen in the surface instrument pair at this site and near the bed at the stratified site ISS. The presence of the pycnocline means that there is little correlation between the signals in the surface waters at ISS.

During the deployment of mooring IS2 there were 5 slack water events and a corresponding 5 recorded SPM concentration minima. For the bed pair of instruments, SPM concentration minima occured after the current had passed through its minimum value. This also true for 3 of the 5 minima recorded by the surface instruments at this site and can also be seen towards the end of the near bed deployment at the stratified site. The reason for this delay is the time required for the settling of sediment. When the vertical velocity shear falls to zero around slack water, the generation mechanism for the turbulent kinetic energy that is responsible for the vertical transport of the sediment is removed and the sediment starts to settle out under the influence of gravity. The time required for the sediment to fall below the transmissometer accounts for the observed delay, so that the effect of settling increases towards the bed. The average delay as recorded by the bed instruments at IS2 was 25 minutes while that measured in the surface waters was 10 minutes. Delays at ISS are greater because the sediment is finer at this site and it takes longer to settle.

In addition to delays at slack water, there are phase differences between peak flow events and SPM concentration maxima. At IS2, the SPM maxima 4m above the bed occurs before maximum current magnitude by, on average 29 minutes on the stronger (flood) phase of the tide. This suggests that the supply of material is source-limited. In contrast to this is the situation at ISS where peaks in SPM concentration are much sharper, indicative of a continuous supply of resuspendable material.

Further examination of the mixed site results reveals that, on the flood phase, SPM

concentrations have started to fall before peak flow and that on the ebb phase concentration maxima occur after peak flow. This is unlikely to be due simply to the effects of source-limitation and suggests that advection of a horizontal concentration gradient is taking place. This is consistent with earlier remarks and with the overall decrease in SPM concentration over the deployment since the net displacement over a tidal period is significant (2-3km to the NW per tidal cycle).

The IS2 surface instrumentation indicates that, in the majority of cases, the SPM concentration maxima this far from the bed occur after both the maximum current and also the corresponding SPM maxima near the bed. This is due to the time that the sediment requires to diffuse up and away from the bed, into the interior of the water column. After the sediment has been resuspended *i.e.* when the vertical turbulent velocities possess sufficient energy to overcome the effects of gravity and cohesion then the sediment is lifted off, and transported away from, the bed, along the SPM concentration gradient. This process is usually referred to as turbulent diffusion and the resulting delay in the onset of maximum SPM concentration will increase with height above the bed and will be dependent on the turbulent flow conditions and the size of the particles.

We have already seen that the turbulent dissipation rate signal can be approximated by a quarter-diurnal variation and that the phase of this signal increases with height above the bed. The RCM data from moorings IS1 and IS2 which were both situated about 3 miles from the survey site IS1_2 has also been analysed and the phase of the current amplitude is compared with that of the turbulent dissipation rate signal in figure 7.13.

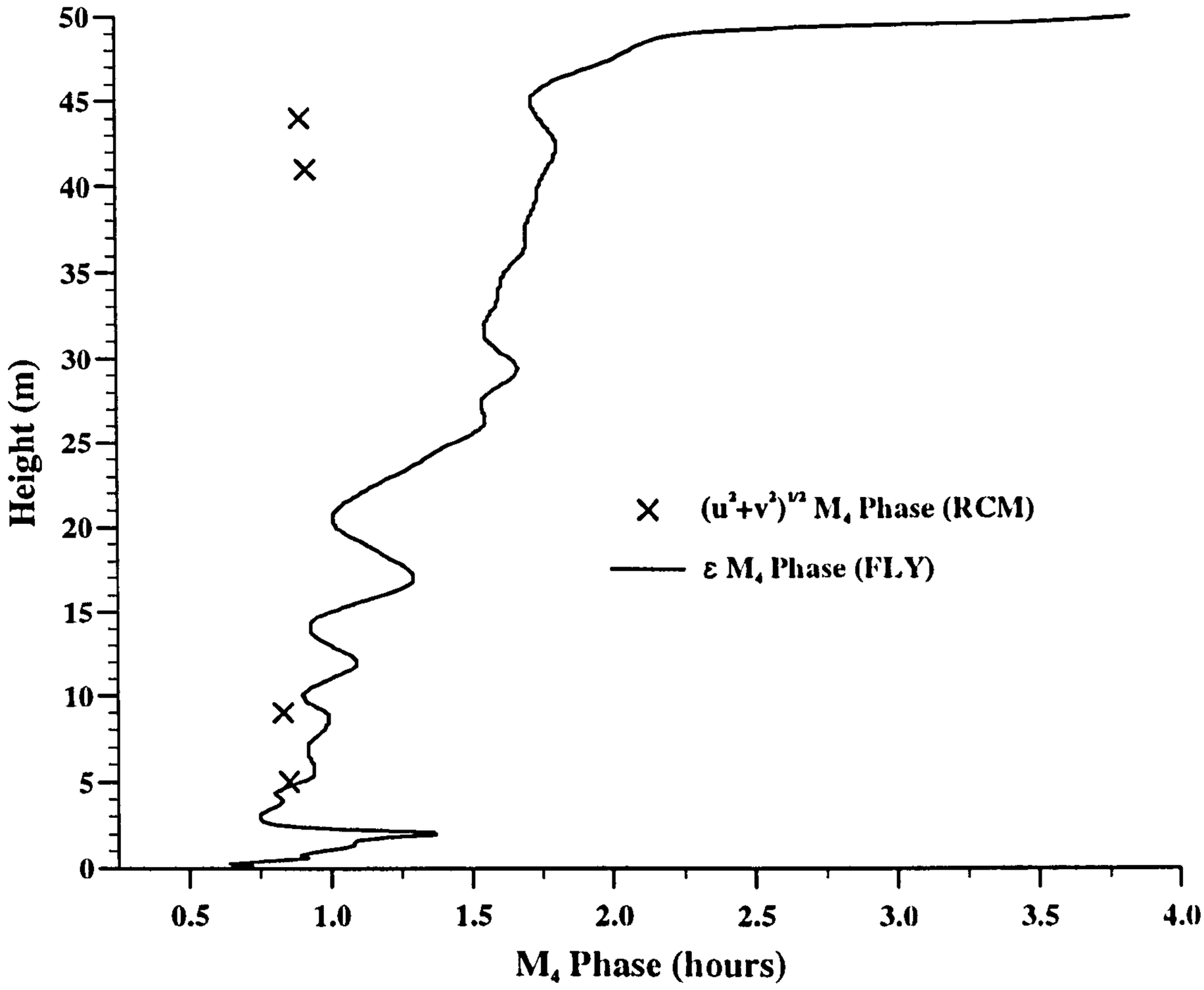

Figure 7.13 : IS1_2 turbulent dissipation rate and RCM current magnitude M_4 phases.

Figure 7.13 shows that the turbulent dissipation rate signal is increasingly lagged behind the current magnitude with height. There are two processes responsible for the increasing phase lag of the dissipation rate signal. The first and most important of these is the lag in production of the turbulent kinetic energy (TKE) by local vertical velocity shear. The time of maximum/minimum velocity shear is phase lagged behind the peak flow/slack water events, a delay which increases with height. The second process is that of diffusion of TKE. The vast majority of TKE is generated in the bottom few centimeters of the water column. This leads to strong vertical TKE gradients, especially around peak flow and so diffusion of TKE along the steep gradients might be expected.

As with the M_4 analysis presented earlier, the phase result is an average for the whole observation period. Analysis of the moored transmissometer and current meter

datasets revealed an assymetry between the tidal phases. Repeating this for the RCM data and the turbulent dissipation rate measurements allows calculation of the phase difference at peak flow and slack water. Denoting the average slack water/peak flow phase difference by $\Phi_{min/max}$ the results for all six current meter/dissipation rate datasets are summarised in table 7.01. The turbulent dissipation rate turning points were determined by fitting a polynomial to the hourly averaged FLY measurements at the height of the RCM.

Table 7.01 : Phase lag of turbulent dissipation rate at a given height above the bed.

Mooring	Height (m)	ϕ_{min} (min)-slack water	ϕ_{max} (min)-peak flow
IS1	5	22	0
	41	70	44
IS2	9	34	0
	44	78	53
ISS	12	90	51
	80	-	-

There is no result for the surface current meter on ISS as there is no correlation between current magnitude and dissipation rate (cross correlation analysis found a maximum explained variance of 2%).

These results show that the phase lag of the dissipation rate at peak flow increases with height above the bed. At IS1_2 the lag at peak flow near the bed is approximately zero. This is because of the proximity to the major source of TKE *i.e.* the seabed. Further up the water column this lag increases to 40-50 minutes due to the lag in production and possibly diffusion effects. At slack water, when the TKE generation mechanism has been removed, the dissipation rate continues to decrease. The phase lag here is consistently 20-30 minutes larger than for the peak flow events. This could be due to larger phase lags of the shear signal around slack water or perhaps the lifetime that TKE possesses before it is all dissipated. Diffusion will also

be in operation although at a much reduced level because of the weaker gradients. Phase lags at the stratified site where currents are less than half of those at IS1_2 are much larger, consistent with the results presented earlier in this chapter.

7.4 Summary.

The results of an M_4 analysis on the SPM concentration and turbulent dissipation rate datasets have been presented. TKE is generated almost solely by the shear in the tidal flow and dissipation rates rapidly decrease with distance from the bed. The phase of the M_4 dissipation rate signal increases uniformly with height and the rate of increase is the same for both mixed sites.

The M_4 harmonic analysis approach is less applicable for the SPM datasets because of the presence of additional signals such as advection of a background concentration gradient. This is especially evident at IS1_2. Comparing the M_4 phase profiles for SPM concentration and dissipation rate reveals a lead of the resuspended sediment signal near the bed. This occurs at both sites and is probably due to the effects of source-limitation. In the near bed region the rate of increase of M_4 phase with height for the SPM signal is more rapid than that for dissipation rate. However, the SPM rate of increase reduces until they are both the same and this is maintained until confidence in the result is low. Although the rate of increase is the same for both parameters at both mixed sites, the absolute values are different at IS1_2 where the dissipation rate leads the SPM signal by ~0.5hr. This is not seen at IS3 where there is no phase difference between the signals.

The ISS results demonstrate the dramatic effect of the pycnocline, which results in no M_4 variation in either SPM or dissipation rate above 30m. The M_4 results suggest that there exists an additional process, besides local tidal shear, for the generation of TKE in the middle third of the water column.

Quarter-diurnal phase lags at this site are much larger than at the mixed sites. Both profiles exhibit a reducing rate of phase increase with height. Explained variance values in the SPM M_4 calculation are very low. Instead, SPM concentrations vary more strongly at the semi-diurnal frequency, as the height to which the sediment diffuses is controlled by the pycnocline. The suspended sediment may exist as a turbid layer of fine sediment that does not settle appreciably extending up to the bottom of the pycnocline.

Examination of the moored instrument data shows the effects of settling, turbulent diffusion and advection which manifest themselves as phase differences between the SPM concentration and current magnitude at peak flow and slack water. The vertical and temporal variability in the delay in the onset of minimum/maximum dissipation rate after slack water/peak flow is due to the effects of delayed local shear (production), diffusion and the finite lifetime of TKE.

Following the results presented in this and the previous chapter, we now present the results from a 1-d numerical model which is used to hindcast the dissipation rate and SPM concentration datasets at each of the sites. This permits further insight into the observations and tests the predictive capabilities of the model scheme.

CHAPTER EIGHT

Turbulence Closure Modelling

8.1 Introduction.

In this chapter we consider the simulation of turbulent dissipation rate and SPM distributions using a relatively simple 1-d hydrodynamic/turbulent energy model, utilising a Mellor-Yamada turbulence closure scheme. The hydrodynamic model which is capable of reproducing the mean flow and density fields has been in use for some time (Sharples (1992), Simpson and Sharples (1991)). A version including a suspended sediment dynamics module has been developed to simulate sediment resuspension and settling processes at three contrasting sites in the North Sea (Jago and Jones (1993), Jones *et al.* (1996a)) and for the Rhine outflow region (Jones *et al.* (1996b)).

In contrast to earlier, analytical models which require the velocity, density and eddy viscosity profiles to be prescribed, turbulence closure models calculate new velocity, density and turbulent mixing parameter profiles every timestep. Such models are based on the schemes of Mellor and Yamada (1974). They allow levels of turbulent exchange to adjust to local levels of stability via a Richardson number calculation. Since we are primarily interested in vertical processes we use a simple 1-d, level 2 turbulence closure scheme. Such a scheme contains all of the essential physics and assumes a local equilibrium of TKE. An explicit calculation is used to integrate the equations of motion and continuity at several discrete levels throughout the water column.

In the next section the turbulence closure model is described in more detail. The results from all three sites are then discussed independently before they are compared in the final section.

8.2 Model Description and Formulation.

8.2.1 The Hydrodynamic/Advection-Diffusion Scheme.

The forcing for the mean currents is via two components of tidal pressure gradient calculated from surface slopes and, where necessary two additional components to account for non-tidal flows. The 2-d vertically integrated model of Proctor and Smith (1991) is used to obtain 6 tidal constituents (M_2, S_2, N_2, MS_4, O_1 and K_1) for each site.

To calculate the current profiles, the model uses two equations.

$$\frac{\partial u}{\partial t} = -\sum_{i-1}^{6} A_{x_i} \sin(\omega_i t - \phi_{x_i}) + g\frac{\partial \bar{\eta}}{\partial x} + fv + \frac{\partial}{\partial z}\left(N_z \frac{\partial u}{\partial z} \right) \qquad (8.01)$$

$$\frac{\partial v}{\partial t} = -\sum_{i-1}^{6} A_{y_i} \sin(\omega_i t - \phi_{y_i}) + g\frac{\partial \bar{\eta}}{\partial y} - fu + \frac{\partial}{\partial z}\left(N_z \frac{\partial v}{\partial z} \right) \qquad (8.02)$$

where

z is the vertical coordinate, equal to zero at the sea bed and to h at the surface,

N_z (z) is the turbulent eddy viscosity profile,

f is the Coriolis parameter,

A_{xi} , A_{yi} are the surface slope amplitudes,

ϕ_{xi} , ϕ_{yi} are the surface slope phases and

$\bar{\eta}$ represents the surface slope for non-tidal flow.

Vertical turbulent diffusion and horizontal advection of scalar quantities such as heat (T) and salt (S) are incorporated into the model scheme via the advection-diffusion equation, given below.

$$\frac{\partial T,S}{\partial t} = -u\frac{\partial T,S}{\partial x} - v\frac{\partial T,S}{\partial y} + \frac{\partial}{\partial z}\left(K_z \frac{\partial T,S}{\partial z} \right) \qquad (8.03)$$

Turbulent diffusion is assumed to be the dominant vertical transport process so that the value of the eddy diffusivity is the same for both heat and salt.

8.2.2 Boundary Conditions.

There is no flux of salt through either of the surface or bottom boundaries and no flux of heat through the sea bed. Surface heating is parameterised using an algorithm based on Edinger *et al.* (1968), with the appropriate meterological dataset.

For the momentum boundary condition surface stress is related to the observed wind speed via an aerodynamic drag coefficient. Wind speed (W) and direction measurements are used to derive wind speed components ($W_{x,y}$) which are then used to calculate the surface stresses ($S_{x,y}$) via

$$S_{x,y} = \rho_a C_D W_{x,y} (W_{x,y}^2 + W_{y,x}^2)^{\frac{1}{2}} \qquad (8.04)$$

where

ρ_a is the density of air (=1.2 kgm^{-3}) and

$C_D = (0.8+0.065W)/1000.0$

At the bed the boundary condition is a quadratic friction law where the components of bed shear stress are related to the near bed flow velocity.

$$\tau_{b_{x,y}} = -k\rho (u_1^2 + v_1^2)^{1/2} u_1, v_1 \qquad (8.05)$$

where k is a quadratic friction coefficient and u_1 and v_1 are the near bed velocity components.

8.2.3 The Turbulence Closure Scheme.

The turbulence closure scheme parameterises fluxes of momentum and heat and salt by relating turbulent fluxes to vertical concentration gradients *i.e.*

$$(\overline{u'w'}, \overline{v'w'}) = -N_z\left[\frac{\partial U}{\partial z}, \frac{\partial V}{\partial z}\right] \tag{8.06}$$

$$(\overline{t'w'}, \overline{s'w'}) = -K_z\left[\frac{\partial T}{\partial z}, \frac{\partial S}{\partial z}\right] \tag{8.07}$$

with the turbulent mixing parameters related to local stability levels via

$$N_z = S_M l q \qquad K_z = S_H l q \tag{8.08}$$

l is the turbulent lengthscale and can be thought of as a description of the physical dimensions of the largest turbulent eddy motion and q is the turbulent velocity scale. S_M and S_H are stability functions for momentum and scalar quantities, dependent on the local gradient Richardson number (R_i) via a flux Richardson number (R_f) where

$$S_M = B_1^{-1/3}\frac{(1 - R_{fc}^{-1}R_f)(1 - R_{f1}^{-1}R_f)}{(1 - R_f)(1 - R_{f2}^{-1}R_f)} \qquad S_H = \frac{B_1^{-1/3}}{P_r^{N}}\frac{(1 - R_{fc}^{-1}R_f)}{(1 - R_f)} \tag{8.09}$$

$$R_f = \frac{1}{2}\left[R_{f1} + R_i R_{f1} R_{f2}^{-1} - \left(\left(R_{f1} + R_i R_{f1} R_{f2}^{-1}\right)^2 - 4 R_{f1} R_i\right)^{1/2}\right] \tag{8.10}$$

$$Ri = \frac{-\frac{g}{\rho}\frac{\partial \rho}{\partial z}}{\left(\frac{\partial u}{\partial z}\right)^2 + \left(\frac{\partial v}{\partial z}\right)^2} \tag{8.11}$$

P_r^{N} is known as the Prandtl number and is the ratio N_z/K_z under neutral stability conditions. For the formulation used here the constants in equations (8.09) and (8.10) are taken as

$$R_{fc} = \frac{1}{6}; \quad R_{f1} = \frac{1}{4}; \quad R_{f2} = \frac{1}{5}; \quad P_r^N = 1.0; \quad B_1 = 15.0 \qquad (8.12)$$

A property of the level 2 turbulence closure scheme presented by Mellor and Yamada (1974) is that turbulence is nearly suppressed at a local gradient Richardson number of 0.21. The constants given in equation (8.12) result from more recent experiments and imply a critical Richardson number of 0.33. For R_i greater than this the stability functions are equal to zero thus inhibiting turbulent transport of momentum or scalar quantities. However, setting N_z and K_z to zero is physically unrealistic and so a background level is set ($1x10^{-4}m^2s^{-1}$), below which they are not allowed to fall.

In the level 2 scheme q is calculated from a local equilibrium condition which specifies that turbulent kinetic energy (TKE) is dissipated where it is produced without any lag *i.e.* advection or diffusion of TKE is ignored.

$$lqS_M\left[\left(\frac{\partial U}{\partial z}\right)^2 + \left(\frac{\partial V}{\partial z}\right)^2\right] + lqS_H\left(\frac{g}{\rho}\frac{\partial \rho}{\partial z}\right) = \frac{q^3}{B_1 l} \qquad (8.13)$$

If TKE is allowed to diffuse, a differential equation for TKE is utilised in the level 2.2 formulation.

$$\frac{\partial E}{\partial t} = \frac{\partial}{\partial z}\left(K_E \frac{\partial E}{\partial z}\right) + N_z\left[\left(\frac{\partial U}{\partial z}\right)^2 + \left(\frac{\partial V}{\partial z}\right)^2\right](1 - R_f) - \frac{(2E)^{1.5}}{B_1 l} \qquad (8.14)$$

where E represents the TKE and K_E is the diffusivity for TKE, set equal to N_z. The turbulent intensity q is then found from $q=(2E)^{1/2}$.

The turbulent lengthscale profile is assumed to take a simple parabolic-like form, given by

$$l(z) = \kappa z (1 - z/h)^{1/2} \qquad (8.15)$$

h is the water depth, z is the height above the bed and κ is von Karman's constant (0.41). The resulting profile is not symmetric with a maximum value biased towards the surface, decreasing to approximately zero at both boundaries.

8.2.4 The Sediments Module.

The total concentration of suspended particulate matter at any point in the water column at any time is assumed to consist of two sub-populations : a fine background component and a coarser, locally resuspended component. Throughout the model operation, both populations are considered separately and are summed at the output stage to calculate the total predicted SPM concentration.

The settling velocities for both sediment populations are prescribed at the beginning of the run. The settling velocity of the background population is usually sufficiently low that this fraction of the SPM population can be considered to remain in suspension indefinitely. The principal changes in the background population concentration are due to horizontal advection of a gradient by the modelled currents. The background horizontal gradients in the x and y directions need to be prescribed and are inferred from the current meter and transmissometer datasets.

The coarser SPM fraction is also subject to horizontal advection but gradients are assumed to be zero and the bed uniform in the region of the experiment. Rather, variation in concentrations of this second size fraction are assumed to be due to vertical processes such as resuspension and settling. Diffusion also plays a part in the upward flux.

The advection-diffusion equation used is similar to that for heat and salt except for an additional term to account for settling.

$$\frac{\partial C}{\partial t} = -u\frac{\partial C}{\partial x} - v\frac{\partial C}{\partial y} + \frac{\partial}{\partial z}\left(K_z\frac{\partial C}{\partial z}\right) + w_s\frac{\partial C}{\partial z} \qquad (8.16)$$

There is no flux of sediment across the sea surface. At the bed the following

condition is imposed:

$$-w_s C - K_z \frac{\partial C}{\partial z} = E - w_d C \tag{8.17}$$

where w_d and w_s are deposition and settling velocities respectively. Deposition is assumed to occur principally due to gravity so that deposition via diffusion is ignored and $w_d = w_s$. E is the entrainment rate and is given by

$$E = f_i \alpha |\tau_o|^n \tag{8.18}$$

where τ_o is calculated from the velocity at 1m using

$$\tau_{o_{x,y}} = N_z \rho \frac{\partial u,v}{\partial z}\Big|_{z \cdot z_o} = -C_{D_{100}} \rho \left(u_{100}^2 + v_{100}^2\right)^{\frac{1}{2}} u_{100}, v_{100} \tag{8.19}$$

u_{100} and v_{100} are interpolated from the bottom model depth bins and C_{D100} is set equal to the bottom friction coefficient introduced earlier. α and n are adjustable parameters and f_i represents the available fraction of entrainable material of the i^{th} sediment population. Although two separate values of E are calculated (one for each size fraction), the same values of α and n were used for both populations. The amount of each size fraction resuspended is controlled by f_i. When the supply of erodible material is unlimited f_i remains constant. It is also possible to limit the amount of material available for resuspension by altering f_i in accordance with the total amount of material remaining on the bed.

The model does not include aggregation and flocculation. Neither does it account for consolidation of the bed material and there is no simulation to account for any benthic biological activity such as bioturbation.

8.2.5 Model Execution.

The vertical grid used by the model subdivides the water column into 2m bins so that

30 layers are used at IS1_2 and 45 at each of IS3 and ISS. The timestep for the numerical integration was chosen with consideration of the stability condition given by

$$\Delta t < \frac{1}{2}\frac{(\Delta z)^2}{N_z} \tag{8.20}$$

For a Δz value of 2m and a typical maximum N_z of $0.4 m^2 s^{-1}$ the maximum timestep that complies with equation (8.20) is 5s and so a value of 0.0012hrs (4.3s) was used at each site.

After initialisation, the model is given 4 days to spin up before the parameters of interest are output every 20 minutes. A flow diagram of the model operation is shown in figure 8.01.

1 Model spin-up, initialisation of T, S & SPM profiles.

2 Read in met data at start of each hour and calculate surface wind stresses.

3 Calculate water depth and length scale array.

4 Calculate x and y current profiles.

5 Interpolate currents to calculate U_{100}.

6 Heat surface and distribute heat down through the water column.

7 Vertical diffusion and horizontal advection of heat and salt.

8 Vertical diffusion and horizontal advection of sediment.
i) Calculate erosion rates for both populations.
ii) Calculate quantity of material available for resuspension.
iii) Apply advection-diffusion equation to each population.
iv) Sum contributions from both size fractions for total signal.

9 New density profile from T & S profiles using international equation of state.

10 TC section using u,v and ρ profiles to calculate R_i , R_f and N_z,K_z via stability functions and length scale.

11 Output data and increase timestep.

12 Go to step no.2 or end

Figure 8.01 : Turbulence closure model schematic.

8.3 Modelling of the IS1_2 Observations.

Before attempting to model the turbulent flow field and SPM dynamics it is important that the mean flow and density simulations are successful. Six components of tidal pressure gradient and an additional term to account for non-tidal flow are used at this site to simulate the velocity field. Meterological forcing is achieved using the data presented in figure 6.01 and the density field is satisfactorily reproduced. These results (and those for the IS3 and ISS simulations) are presented and discussed in greater detail in the parallel study by Cheok (1996).

The modelled turbulent dissipation rate and SPM concentration time series have been harmonically analysed at the M_4 frequency for direct comparison with the observations. This is both a convenient and comprehensive test of the capability of the model. The dissipation rate results are shown in figure 8.02.

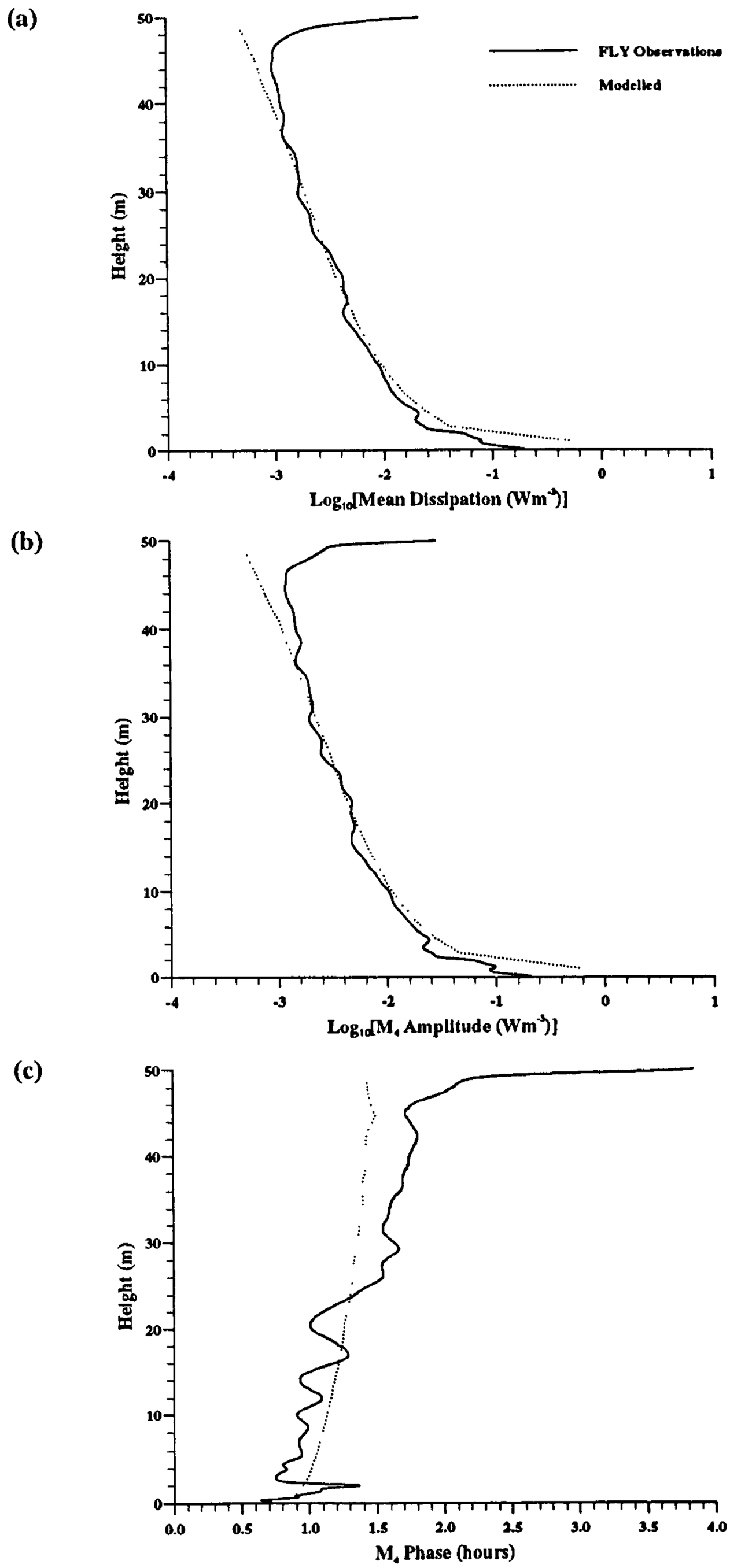

Figure 8.02 : IS1_2 M_4 analysis results for simulated and observed dissipation rate. (a) Mean dissipation, (b) M_4 amplitude and (c) M_4 phase.

Figure 8.02 shows generally good agreement between the modelled and observed dissipation rate signals at IS1_2. The predicted mean and M_4 amplitude of dissipation rate are very similar and comply with the observations, with excellent agreement between 5 and 40m. Below 5m there is an overestimation whereas above 40m the model fails to predict the observed sharp increase in dissipation rate. As this is unlikely to be due to local shear in the tidal velocity field and since winds were light, it is unsurprising that the model fails to predict this feature of the data.

Aside from observed variations on the scale of a few meters the model phase prediction is reasonable with a uniform increase in the M_4 phase from bed to surface.

Since the mean flow and density structures are reproduced by the model, the encouraging dissipation rate results suggest that the turbulence closure scheme seems capable of relating turbulent flow parameters to prevailing levels of vertical velocity shear and stratification, although buoyancy effects are weak at this site.

Having modelled the interaction between the mean and turbulent flow parameters, the various sediment erosion, deposition and background gradient parameters were adjusted to give the best fit of the SPM concentration M_4 predictions to the observations.

The sea bed was considered to be both horizontally uniform in the vicinity of the site and also a source-limited supply of resuspendable material, as suggested by the data presented earlier in the thesis. This was implemented by setting the quantity of material available for resuspension to zero at an appropriate time before the start of the run. The background sediment fraction was considered to remain permanently in suspension, with horizontal gradients inferred from transmissometer and current meter data. The remaining settling velocity and erosion rate parameters were then adjusted to give the best fit to the data. The sediment parameters are summarised in appendix B and the M_4 analysis results for both simulated and observed SPM concentration signals at IS1_2 are compared in figure 8.03.

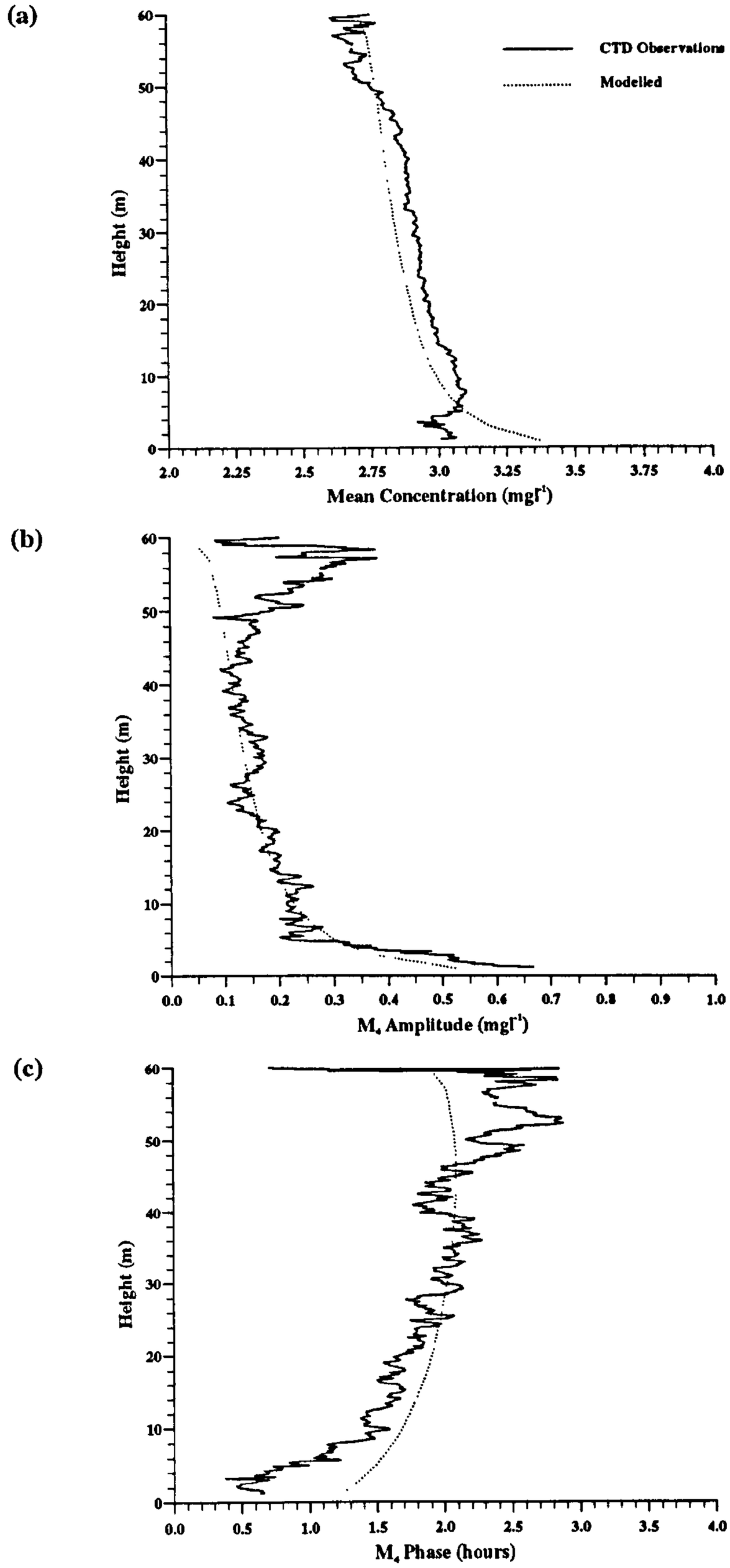

Figure 8.03 : IS1_2 M_4 analysis results for simulated and observed SPM concentrations. (a) Mean concentration, (b) M_4 amplitude and (c) M_4 phase.

As with the turbulent dissipation rate results, discrepancies between the observed and the modelled profiles are confined largely to the boundaries. From a height of 8m up to the surface, mean SPM concentrations are reasonably predicted. However, approaching the bed, the model predicts a sharp increase in concentration, a feature not seen in the observations. The M_4 amplitude prediction near the bed is more successful as the threefold increase in M_4 amplitude in the bottom few meters is reproduced. The model prediction remains in line with observations up to a height of ~45m above which the two profiles deviate, with the modelled M_4 amplitude continuing to steadily decrease whereas the observed signal increases. At the surface the difference between the two is ~0.2mgl^{-1}. Interestingly, a similar increase was also a feature of the turbulent dissipation rate results.

The M_4 phase prediction between 10 and 50m is good. The general increase with height is reproduced and differences between the model and the observations are usually less than 10 minutes. However, in the surface waters and in the near bed region there are significant differences. Although the model predicts a reduction in the rate of increase of phase with height, vertical gradients are too weak and the predicted phase at the bed is 30 minutes greater than that observed.

The response of the suspended sediment population to changes in the mean and turbulent flow fields is of particular interest here. For a more direct comparison, figure 8.04 compares the observed and modelled M_4 phases for both parameters.

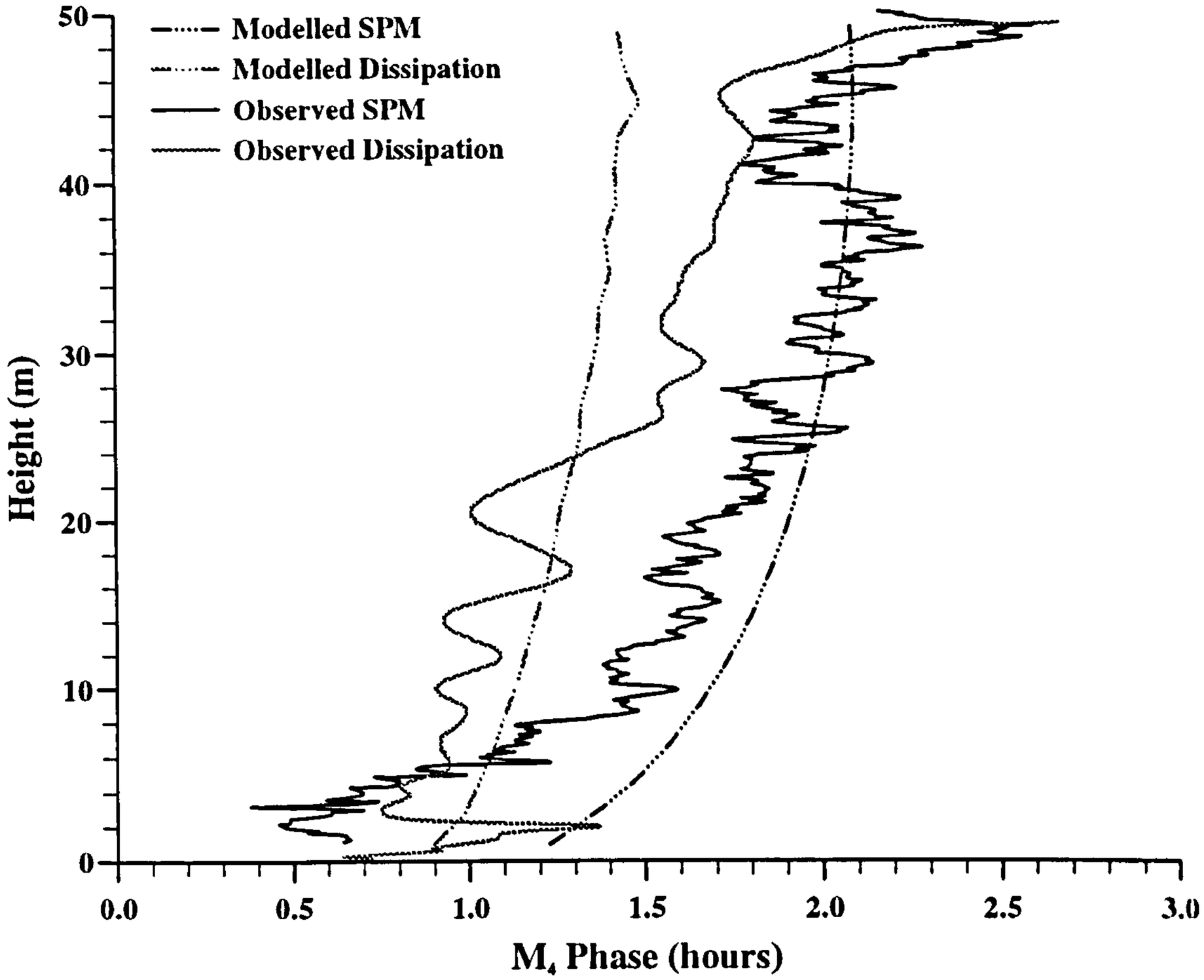

Figure 8.04 : Observed and simulated SPM concentration and turbulent dissipation rate M_4 phases at IS1_2.

In the last chapter the M_4 analysis showed that above a height of 10m, the dissipation rate M_4 signal leads that of the SPM concentration by ~0.5hr. This can be seen in the model output. However, below 10m, the model fails to predict the observed phase lead of the sediment resuspension signal.

The moored transmissometer measurements and simulations are shown in figure 8.05. Also shown is a predicted signal based on the 'twin-peaks' model which assumes that the signal can be represented by an equation of the form

$$\text{SPM Conc} = C_1 + C_2 \int u\,dx + C_3 \int v\,dy + C_4 \sqrt{(u^2+v^2)}^n \qquad (8.21)$$

C_1 represents a mean background component. C_2 and C_3 introduce advection of a

background concentration gradient, u and v being the velocities as supplied by the moored RCMs. The final term represents resuspension of the bed material.

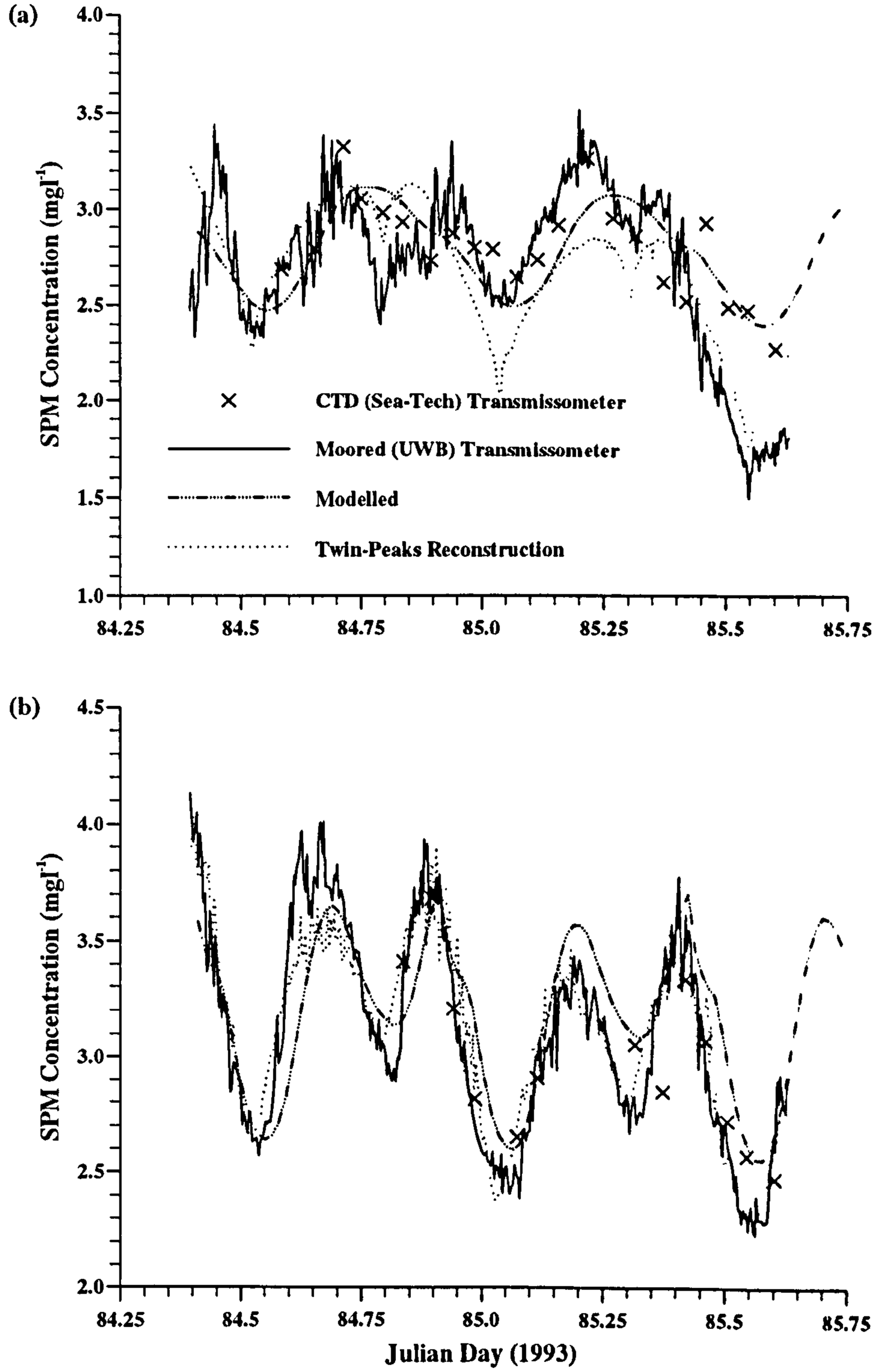

Figure 8.05 : Observed and simulated SPM concentrations at IS2.

(a) 47m above the bed.

(b) 4m above the bed.

The 'twin-peaks' approach, parameterising SPM concentrations in terms of fluctuations at tidal frequencies is seen to be particularly applicable near the bed. In the surface waters there are additional signals present and so this method is less successful. However, this model does not account for the physical processes that result in the vertical exchange of sediment. The turbulence closure model results are based upon a more physically defensible approach and thus permit more definite conclusions to be drawn.

The principal discrepany between the TC model results and the observations near the bed is due to the fact that the model was configured to best reproduce the M_4 analysis results and not the moored transmissometer measurements. However, the predicted SPM time series near the bed is good. The gradients of the rising and falling slopes are reproduced and the timing of the turning points is better than for the 'twin-peaks' reconstruction.

In the surface waters where the resuspended signal is less in evidence, the TC model prediction is poorer. The general trend of the signal is largely in line with the observation but the simulated signal is dominated by the semi-diurnal variation and the resuspension signal is too weak, indicating that vertical exchanges of sediment are not properly simulated. The assumption of a constant background population gradient is restrictive, especially near the end of the deployment since the advection of a non-uniform horizontal gradient is thought to be responsible for the observed sharp reduction in SPM concentration.

8.4 Modelling of the IS3 Observations.

As before, tidal slopes derived from the 2-d model of Proctor and Smith (1991) and observed meterological parameters were used to simulate the mean flow and density fields before the sediment parameters were adjusted to give the best fit of the simulation results to the observations. It was assumed the bed is a source-limited supply of resuspendable material and that background concentration gradients are zero. This is suggested by the CTD transmissometer results which show a regular M_4 variation dominating the SPM field. Since there is significant transport over a tidal cycle at this site, a background gradient in SPM concentration would result in a net increase or decrease in concentration over the deployment. There is no evidence to suggest that this has occurred and so the gradients are taken as zero.

The turbulent dissipation rate and SPM concentration results are shown in figures 8.06 and 8.07 respectively.

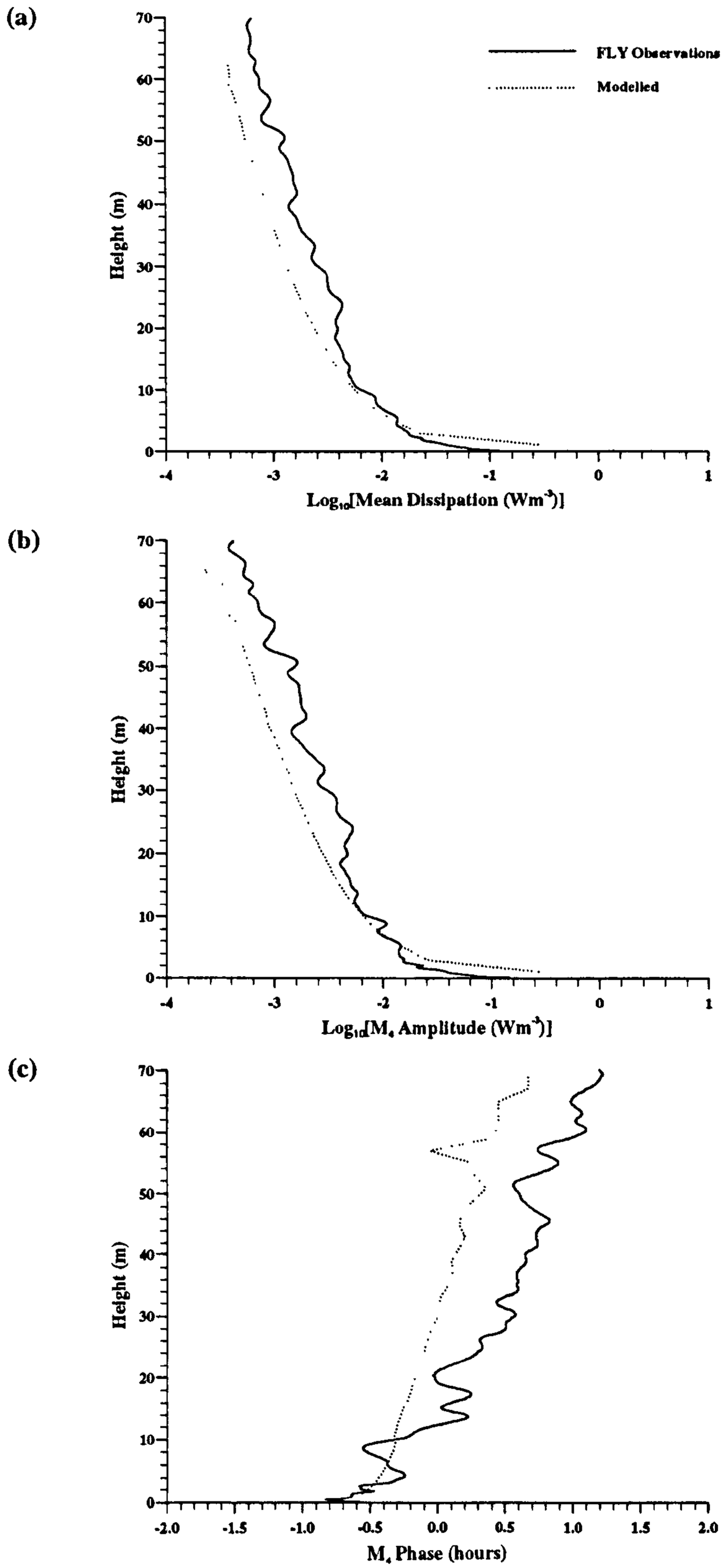

Figure 8.06 : IS3 M_4 analysis results for simulated and observed dissipation rate. (a) Mean dissipation, (b) M_4 amplitude and (c) M_4 phase.

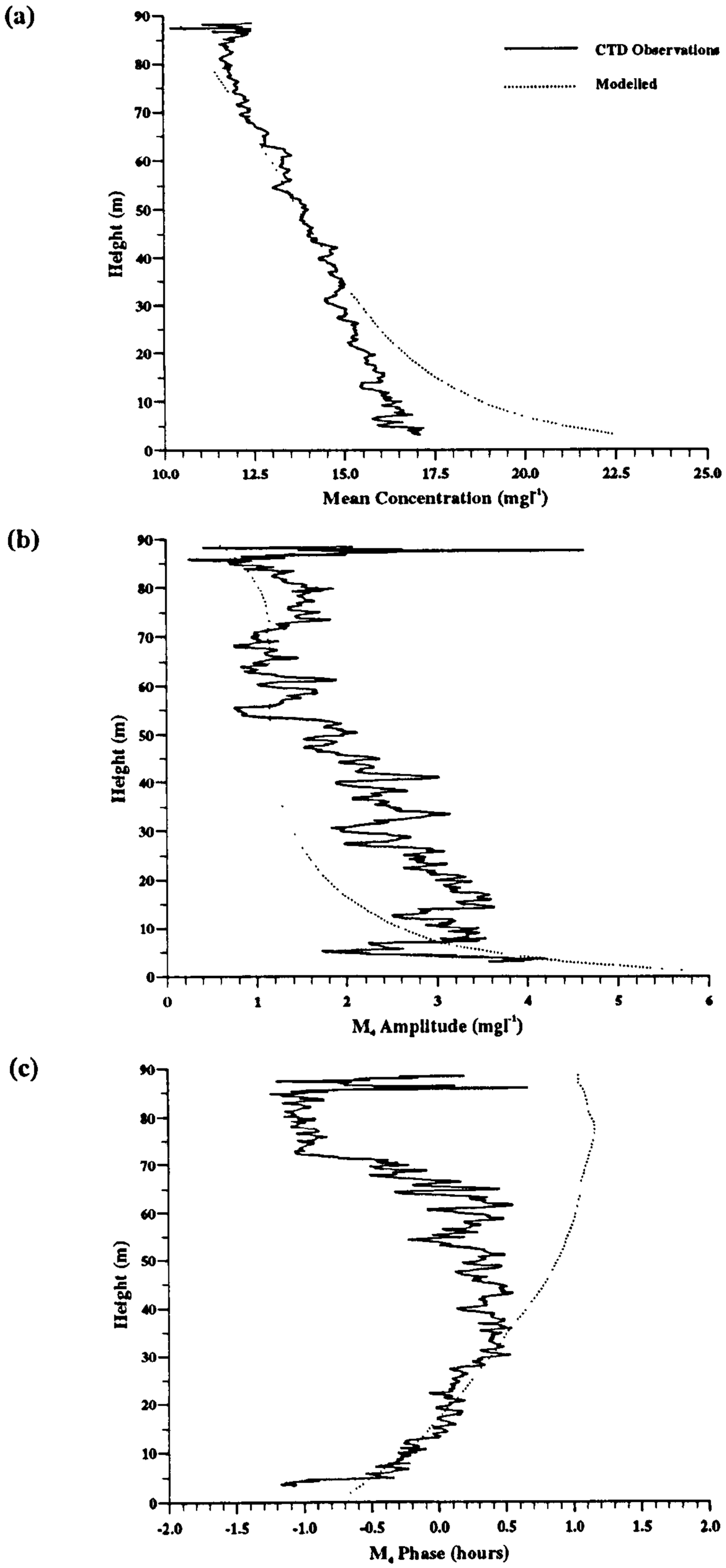

Figure 8.07 : IS3 M_4 analysis results for simulated and observed SPM concentrations. (a) Mean concentration, (b) M_4 amplitude and (c) M_4 phase.

As at IS1_2, the dissipation rate mean and M_4 amplitudes are satisfactorily simulated. The phase results are less successful but are broadly in line with observations, once again indicating a steadily increasing phase with height.

For both the mean and M_4 amplitudes of SPM concentration, which were observed to increase steadily towards the bed, the model predicts a sharp increase in the bottom 10m. This is a consistent feature of the model simulations indicating a more fundamental inadequacy of the scheme rather than inappropriate selection of the erosion, settling and advection parameters.

The SPM M_4 phase results are encouraging between 5 and 45m with excellent agreement between simulated and observed values. Above 45m the model predicts an increasing phase (for all simulations) whereas the observed phase remains constant before reducing towards the surface, although confidence in the results of the M_4 analysis is reduced this far from the bed.

8.5 Modelling of the ISS Observations.

As at the previous sites, once the hydrodymanic scheme was in place, the sediment parameters were adjusted to give the best fit of the model M_4 analysis results to the observations. No source-limitation was imposed as previous evidence suggests that this is not a feature. Because the water column at this site is stratified, instead of the depth-uniform profile of background SPM used for initialisation in mixed waters, a two stage profile with lower background SPM concentration above the pycnocline was used.

We now consider the results of the optimum model simulation at this site. Figures 8.08 and 8.09 compare the M_4 analysis results for the modelled and observed turbulent dissipation rate and SPM concentration datasets respectively.

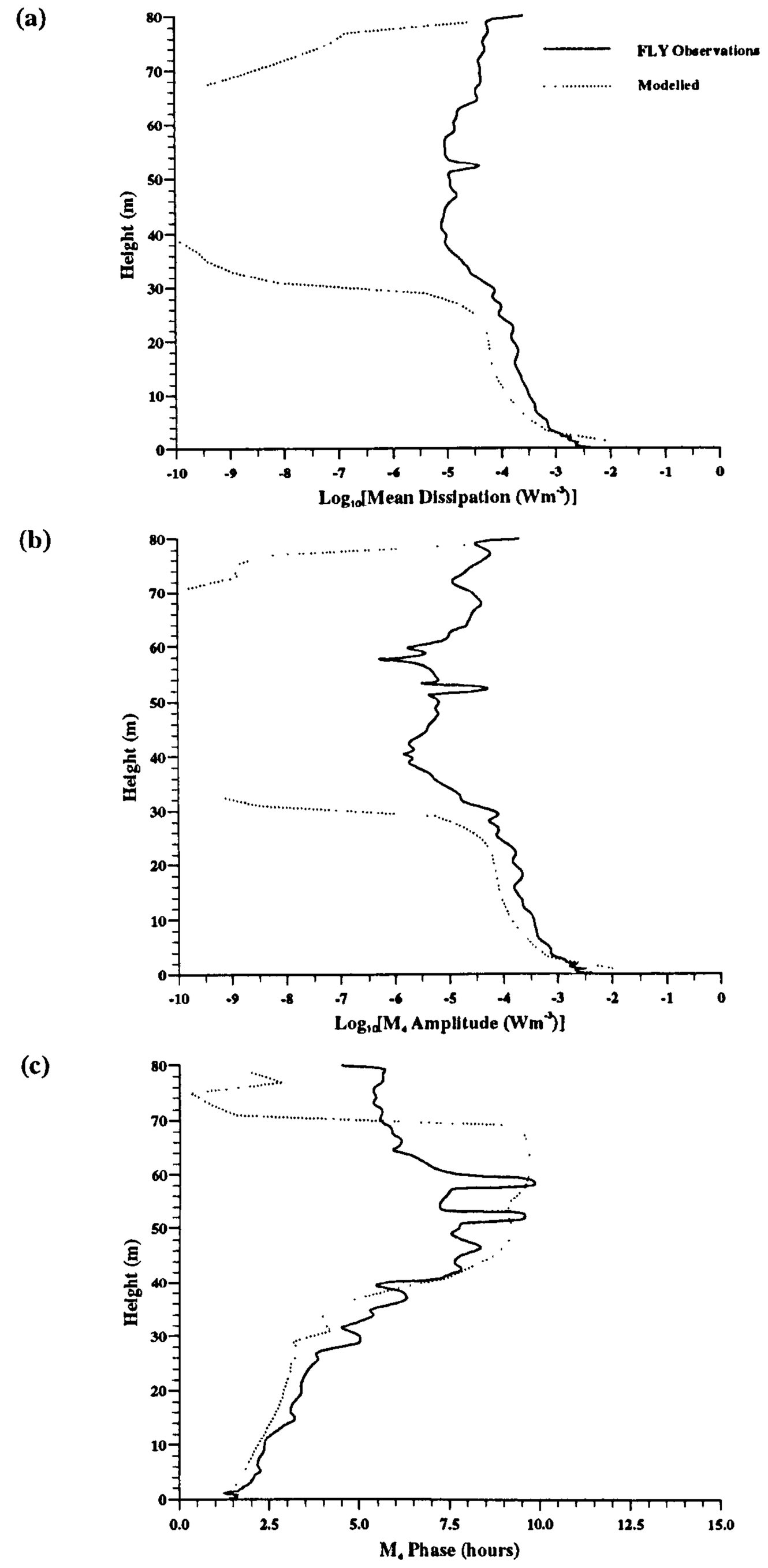

Figure 8.08 : ISS M_4 analysis results for simulated and observed dissipation rate. (a) Mean dissipation, (b) M_4 amplitude and (c) M_4 phase.

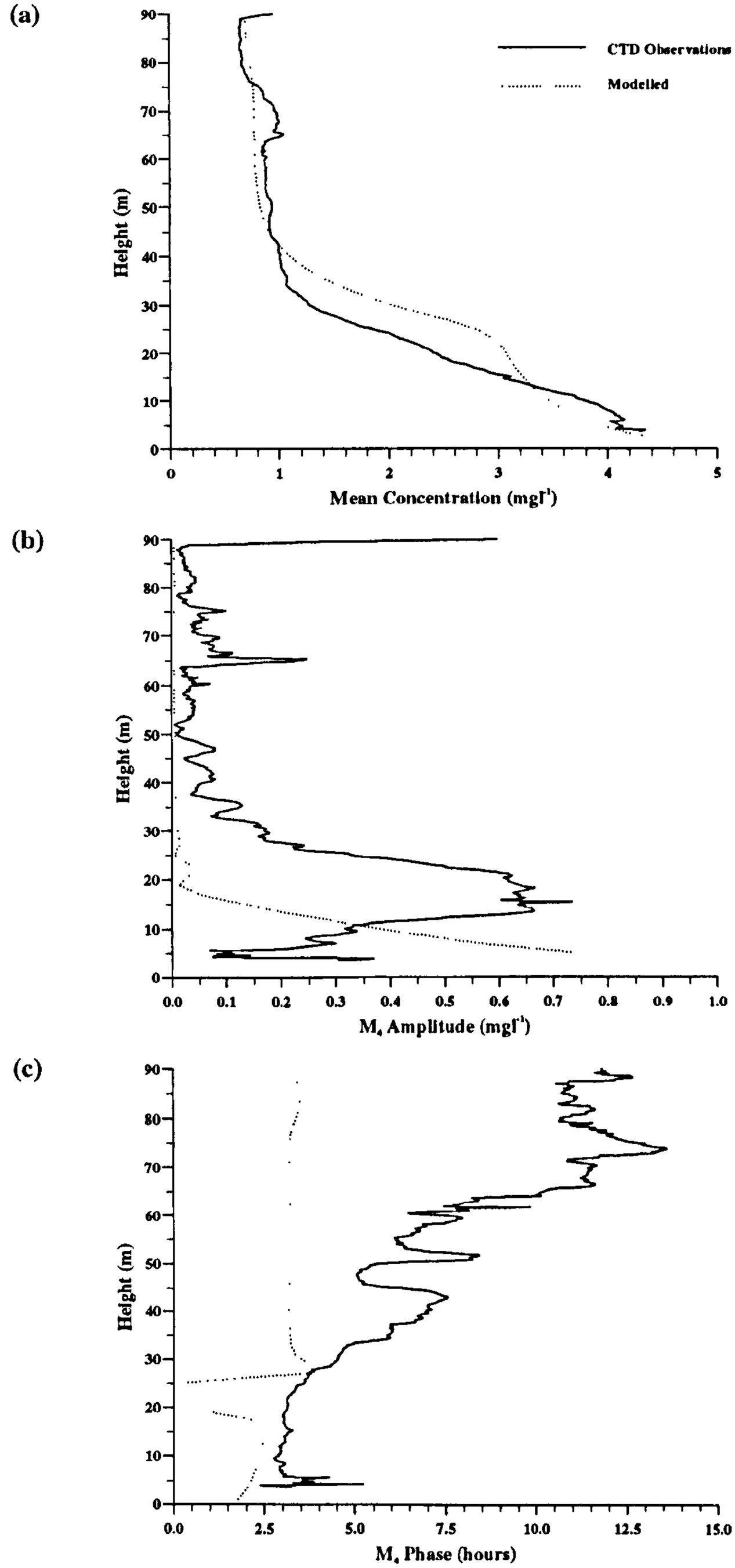

Figure 8.09 : ISS M_4 analysis results for simulated and observed SPM concentrations. (a) Mean concentration, (b) M_4 amplitude and (c) M_4 phase.

Figure 8.08 shows that, below 30m the model is relatively successful in its simulation of the mean and M_4 amplitudes of dissipation rate. However, in the interior of the water column *i.e.* between 40 and 70m where dissipation rates are very low (O(10^{-5} Wm^{-3})), the model badly underestimates both signals. This is likely to be due to limitations in the modelling of the vertical density gradient and parameterisation of the vertical exchange coefficients by the turbulence closure scheme. Alternatively, the model fails to predict the existence of another source of TKE besides vertical velocity shear in the mean flow, which is suggested by the inconsistency between the observed mean and M_4 amplitude.

Increasing the background eddy viscosity will raise the predicted dissipation rate in midwater. However, the increased mixing associated with this means that it is impossible to model the density field accurately. Rather, improvements in the predictive capability for dissipation rate at this stratified site are obtained via implementation of higher order turbulence closure schemes, such as those that incorporate the diffusion of TKE or include lengthscale calculations within the turbulence closure routine (J.Cheok - pers. comm.). The phase results are good up to a height of 40m above which the quarter-diurnal variation is small and poorly defined.

Turning to the SPM results, the mean concentration result is satisfactory although the steady reduction in concentration is not predicted. Instead, a sharp increase in concentration approaching the bed (which was also predicted at the mixed sites) is predicted. The simulated M_4 amplitude is of the correct form but reduces to zero at 20m instead of 40m. In addition, the diminishing M_4 amplitude near the bed is not reproduced.

The comparison of the model with the moored transmissometer and 'twin-peaks' analysis data is shown in figure 8.10.

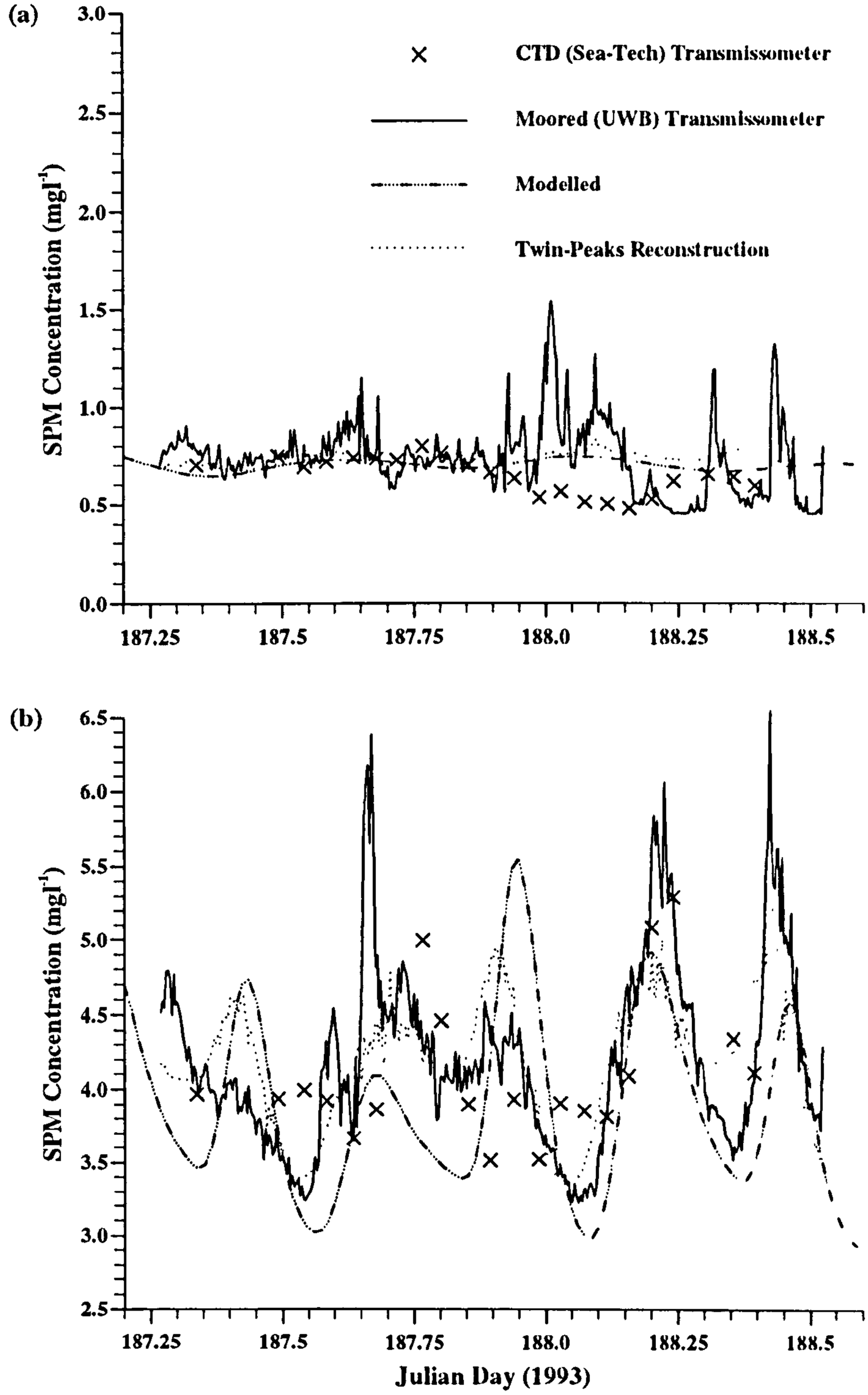

Figure 8.10 : Observed and simulated SPM concentrations at ISS.

(a) 83m above the bed.

(b) 6m above the bed.

In the surface waters, concentrations are low and resuspension events weak so that the 'twin-peaks' analysis finds a weak correlation between current magnitude and SPM concentration. Given the effectiveness of the modelled density structure in the suppression of sediment resuspension above a height of 20m as indicated by the very low M_4 amplitude above this height, the turbulence closure model signal is due entirely to advective processes.

Although resuspension events are seen in the first half of the deployment at the bed their timing and magnitude do not conform to the 'twin-peaks' variation, reflected in the poorer 'twin-peaks' fit. However, for the turbulence closure simulation the timing of the turning points, the slopes of the rising and falling edges and the SPM concentrations are well predicted for the second half of the deployment and the majority of the predicted turning points agree broadly with those observed for the first half of the experiment.

8.6 Site Comparison.

A 1-d, level 2 turbulence closure numerical model has been described and used to hindcast the water column structure, the mean and turbulent flow fields and SPM concentrations at each of the three experimental sites. Tidal and meterological forcing was used in conjunction with the TC routine to simulate the density, mean and turbulent flow structures. Sediment erosion, settling and background concentration gradients were then adjusted, using experimental observations as a guide, to best reproduce the observed SPM concentration data available from both moored and profiling instrumentation.

The dissipation rate results from the mixed sites are satisfactory. At the stratified site the results are generally good except that the model fails to indicate the presence of an additional source of TKE in the middle of the water column.

Many model runs were completed at each site to obtain the best simulation of suspended sediment concentrations. The sediment population consists of a fine, permanently suspended fraction subject to horizontal advection and a coarser resuspended fraction. Different values for the erosion, settling and background gradients were used at each site. They are summarised below in table 8.01.

Table 8.01 : Sediment erosion, deposition and background gradient parameters.

	IS1_2 mixed	IS3 mixed	ISS stratified
SPM Class 1: w_s (mms^{-1})	0.0	0.0	0.0
x,y concentration gradients (mg/l/km)	0.037,0.015	0.0,0.0	0.21,0.07
SPM Class 2: w_s (mms^{-1})	7.0 (fine sand)	4.0 (very fine sand)	3.0 (coarse silt)
x,y concentration gradients (mg/l/km)	0.0,0.0	0.0,0.0	0.0,0.0
Erosion Rate			
Supply limit	Yes	Yes	No
n	1.5	1.0	3.0
α ($x10^{-7}$ $kg/m^2/s$)	1.0	100.0	30.0

The background gradients used were inferred from the moored transmissometer and current meter datasets. They were then adjusted to give the best fit to the data. When available, settling velocities were taken from the settling velocity tube results. However, accurate simulation of the observations using these values was not possible, probably due to the fact that the tubes were deployed in either the surface waters or the middle of the water column, away from the near bed region where the resuspended sediment population is largely confined.

The settling velocities used at the three sites are broadly in line with the dynamical conditions with the coarsest fraction being used at the most energetic site and the finest at the deep, stratified site. The settling velocity used at IS1_2 corresponds to fine sand and that at IS3 to very fine sand. Figure 4.06 indicates that the bed at ISS is muddy and the settling velocity used here (corresponding to coarse silt) indicates that perhaps flocculation is an important process.

The erosion parameters used for each site were also different. The exponent (n) used at the mixed sites (1.0,1.5) was much lower than that at ISS (3.0). This is consistent with the findings of Jones *et al.* (1996a) who used the same model to hindcast data from three corresponding sites in the North Sea. The multiplying factors also varied widely. The value used at IS3 was 100 times greater than that at IS1_2, indicating that sediment at this site is more easily entrained, consistent with the settling velocities used.

These simulations have revealed much about the ability of this model scheme to accurately predict SPM concentrations at three contrasting sites. The results from the stratified site show that accurate simulation of the density field is is necessary prerequisite if vertical sediment processes are to be modelled. The performance and limitations of the model are discussed further in the next, and last chapter.

CHAPTER NINE

Discussion

9.1 Introduction.

In recent years, the increasingly important role of SPM in the determination of water quality and the fate of pollutants has been recognised (Tett *et al.* (1993), Eisma and Irion (1988)) and has been a prime motivation for scientists seeking to understand the processes responsible for the spatial and temporal distribution of SPM in the shelf seas. Observations have revealed that SPM concentrations often display variability from seasonal down to quarter-diurnal time scales (Weeks and Simpson (1991), Boudjelas (1994), Jones *et al.* (1994)). Whereas the longer term variations are the result of a number of effects including stratification, biological activity and enhanced resuspension by winter waves, the higher frequency modulations can be attributed to the tidal flow. Studies have investigated the relationship between the mean flow field and SPM concentrations, notably that of Weeks (1989) who explained much of the observed variation (up to 70%) in SPM concentration in terms of semi-diurnal (advection) and quarter-diurnal (resuspension) tidal signals for a site in the Irish Sea.

It is widely recognised that turbulence, derived from energy in the mean flow field, is responsible for the resuspension and redistribution of SPM throughout the water column so that SPM studies such as those described above are limited in scope. Furthermore, the few documentated investigations into the relationship between the turbulent flow field and SPM concentrations tend to be confined to the bottom boundary layer and concerned with coarse (sand) fractions (*e.g.* Soulsby *et al.* (1984)). Thus, the principal aim of this study was to directly investigate the relationship between levels of SPM and the turbulent flow field throughout the water column and hence, to gain an insight into the processes responsible for the vertical distribution and temporal variation of these two paramaters. Recent advances in instrumentation have facilitated this approach and an extensive suite of observations of water column structure, mean flow, SPM concentration and turbulent dissipation rate have been

made at three contrasting sites, including both well mixed and thermally stratified conditions. The process interpretation emerging from the observations was further investigated by a modelling study.

We now proceed to discuss the principal results of the observational and modelling studies and their significance, and conclude the chapter with a section on future developments that are needed to advance our understanding in this area.

9.2 The Observational Study.

9.2.1 The Vertically Homogeneous Sites.

The mean flow at both sites is dominated by the semi-diurnal tidal component and so turbulent dissipation rates display a strong M_4 variability with the highest dissipation rates found where velocity shear is greatest *i.e.* adjacent to the bed at peak flow. The vast majority of TKE is dissipated where it is produced so that dissipation rates diminish rapidly with height.

A harmonic analysis has revealed the dominance of the tidal flow field in the generation of TKE and has shown that the phase of the turbulent dissipation rate increases uniformly with height above the bed. The reason for this is that the phase of the shear signal (the production mechanism for TKE) also increases with height (Wolf (1980)) . Diffusive processes may also affect the phase although our modelling study has shown that it is the delay in the production of TKE that is the dominant factor (Cheok (1996), Simpson *et al.* (1996)).

The SPM observations show that the total SPM population at both mixed sites can be considered to consist of two sub-populations : a fine, permanently suspended fraction subject to modulation via advective (semi-diurnal) processes and a coarser fraction which is resuspended by the tidal currents and so fluctuates at the quarter-diurnal signal, in accord with the semi-empirical 'twin-peaks' model of Weeks (1989).

To investigate the response of the SPM population to changes in the turbulent flow field, an M_4 harmonic analysis has also been applied to the SPM data. The results show that at both mixed sites, the magnitude of the resuspension/settling signal decreases with height above the bed. This is because less resuspendable material is to be found with increasing distance from the bed. As with the turbulent dissipation rate, the phase of this signal increases with height with the sediment responding to changes in the turbulent flow field. The sediment is mixed upwards by turbulent diffusion during energetic periods and settles under gravity around slack water. A striking result is that the rate of increase of phase is closely similar to that displayed by the dissipation rate. Where this is not the case, such as near the bed and in the surface waters, processes other than resuspension and settling are in operation.

The moored transmissometer results indicate that IS1_2 is a source-limited site. This feature is apparently not uncommon (*e.g.* Jago *et al.* (1993), Jones *et al.* (1996a)) and results in a phase lead of the resuspended sediment signal at the bed. This interpretation in terms of a limited supply of resuspendable material is consistent with the M_4 phase results at this site (figure (7.03)) and also at IS3, although the effect is not as pronounced (figure (7.06)).

Comparing the responses of the SPM populations to the turbulent flow field at each of IS1_2 and IS3 indicates the contrasting nature of the SPM populations at the two sites. Near the bed at IS1_2, the M_4 variation is the dominant signal. However, above 10m this is not the case and the resuspension signal is small leading to the conclusion that the resuspended SPM population consists of two fractions : a coarse fraction confined below 10m and a finer fraction more evenly distributed throughout the water column. In contrast to this are the IS3 results which indicate a more even distribution of the resuspended sediment fraction throughout the water column. The sediment at IS3 must be coarser than that at IS1_2 in order to account for the higher M_4 amplitudes observed at this less energetic site. The presence of coarser sediment at IS3 also results in smaller phase lags, as it settles more rapidly, and is consistent with the observation that the phase lag of the SPM signal at IS3 is less than at IS1_2.

Neither SPM concentration, nor dissipation rate display a purely sinusoidal M_4 variation and so, while the results of the M_4 analysis are useful, the presence of additional signals within the datasets must be recognised. This is particularly true of the SPM datasets which contain an M_2 variation in addition to higher frequency signals, also seen in the dissipation rate results. M_2 harmonic analyses have also been conducted and the results taken into consideration. It should also be recognised that such harmonic analysis results are averages over the experimental period and so do not report any inconsistencies between the tidal phases.

The extensive observational program described early in this thesis has produced a unique dataset regarding the temporal and spatial evolution of both the dissipation rate and SPM concentration fields. Prior to this study it was suspected that a strong relationship exists between these two quantities. This has now been investigated, principally via the use of a harmonic analysis technique, and a significant relationship between levels of SPM and the turbulent flow conditions has been demonstrated. Employing a simple, steady state energy argument an assuming a constant settling velocity it can be postulated that the turbulent dissipation rate should be directly proportional to the SPM concentration at any height above the bed. Using the near bed results from the first mixed site, a regression analysis reveals that there is indeed a significant relationship between the two variables with almost 50% of the observed variance explained. Moreover, the regression results confirm what was already believed in that only a fraction of one percent of the available power is expended in maintaining sediment in suspension.

9.2.2 The Stratified Site.

Tidal currents and hence dissipation rates are lower at this site. As before, the highest dissipation rates are found in the near bed region, decreasing rapidly with height. However, at this site the presence of the pycnocline results in a midwater minimum in dissipation rate. The M_4 analysis results reveal a component of dissipation within the pycnocline, not modulated at the quarter-diurnal frequency, the source of which is uncertain (Simpson *et al.* (1996)). The harmonic analysis also

reveals well defined phase shift with height, much larger than at either of the mixed sites because of the larger delay in the local shear signal.

The distribution of, and variation in, SPM at this site is dominated by the presence of the pycnocline. Only a weak density gradient is apparently required to confine suspended sediment to the bottom waters as turbulent transport of particulates is suppressed by the density gradient. Resuspension and settling of the fine-grained particulates that exist at this site is occuring, the suspended fractions forming an almost uniform turbid layer between the bottom of the pycnocline and the bed.

The behaviour of the phase with height above the bed is summarised schematically for all three sites in figure 9.01. A brief description of the processes thought to be responsible for the observed features is also given.

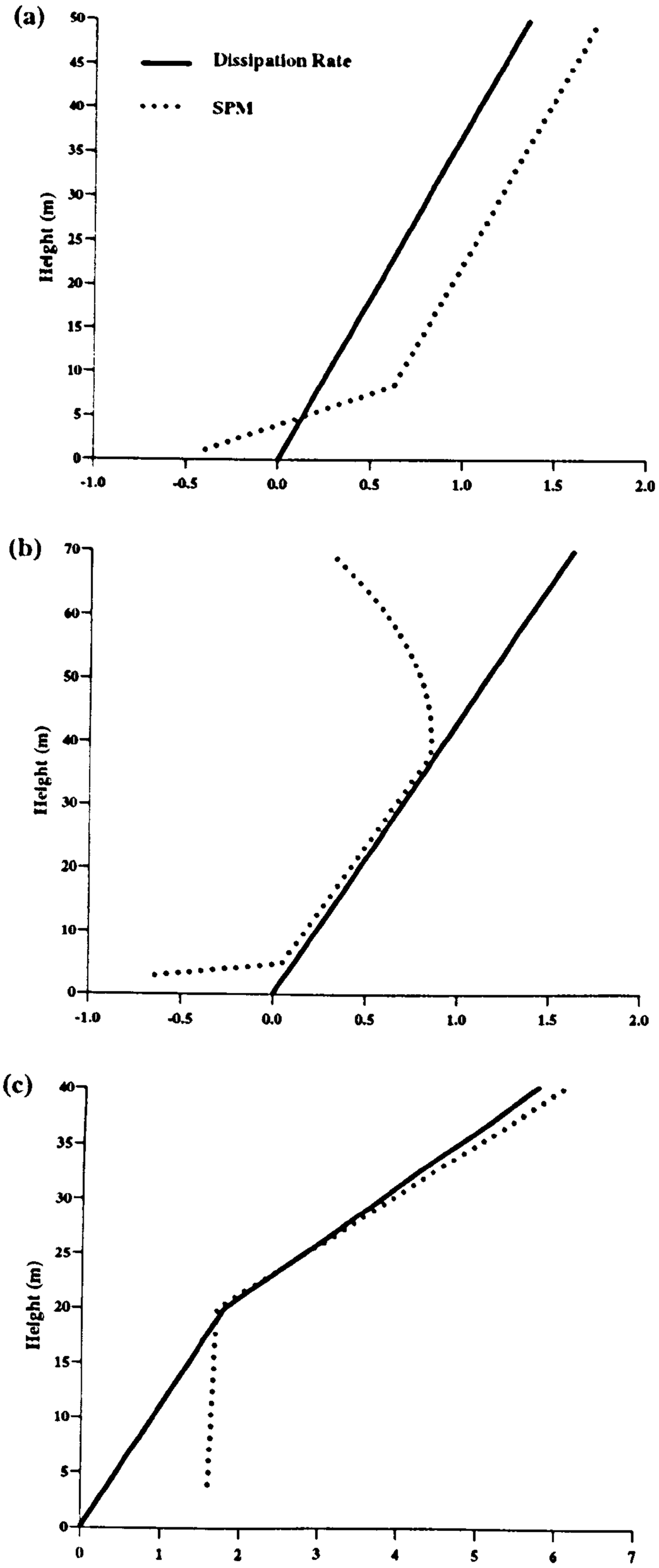

ϵ : phase increases with height due to delay in TKE production, also diffusion of TKE (small).

SPM : Source-limited coarse fraction confined below 10m. From 10-60m a fine fraction contributes to a small M_4 signal. R^2 low.

ϵ : as at IS1_2, TKE diffusion less important as currents are weaker.

SPM : source-limited below 5m? From 5-40m a distribution of sizes, coarser than at IS1_2 results in a larger M_4 signal with reduced phase lag. Advection above 40m?

ϵ : delay in TKE production increased and modified by $\Delta\rho/\Delta z$.

SPM : Up to 20m very fine sediment exists as a turbid layer. From 20-40m, top of turbid layer corresponds to lower extremity of pycnocline.

Figure 9.01 : Turbulent dissipation rate and SPM concentration M_4 phase profiles. (a) IS1_2, (b) IS3 and (c) ISS.

9.3 Turbulence Closure/SPM Modelling.

An existing level 2 turbulence closure model has been used to hindcast the observations. In general, the dissipation rate simulations at the mixed sites give a satisfactory account of the observations. The model also reproduces the dissipation rate observations in the bottom 30m at ISS where the water is well mixed. However, the model fails in mid-water, severely underestimating dissipation rates.

Whereas in modelling dissipation rate the model parameters are either set by the Mellor-Yamada scheme or constrained by observations, for the SPM simulations, there are a number of parameters (6) which are not constrained *a priori* and need to be selected. With an optimal choice of these parameters and several simplifying assumptions concerning the nature of the bed and the SPM population, the results are generally, though not always, satisfactory.

The IS1_2 SPM simulation is largely in agreement with the observations although the assumption of a constant, depth uniform background gradient is limiting. The IS3 results are less successful, most probably due to over simplification of the SPM population in terms of the number of size fractions and background gradients.

For the stratified site, inconsistencies between the model and observations of SPM are due primarily to differences between the observed and simulated density structures, unsurprising since this feature of the observed density field is due to advective effects. The settling velocity of the resuspended fraction used to reproduce the observed SPM signals is representative of a coarse silt, inconsistent with the muddy bed thought to exist at this site. This suggests that flocculation may be an important process at this site although concentrations are rather low.

The simulated dissipation rate phase at all three sites is in generally good agreement with the observations. The rate of increase of phase is reproduced as are the much larger phase shifts with height at the stratified site. The SPM phase results are

satisfactory throughout the majority of the water column both in terms of the rate of change of phase and the relationship with the dissipation rate results. The model is less successful in the near-bed region at IS1_2 and ISS. This is because the observed features are due to a complex sediment population and advective processes at IS1_2 and ISS respectively, neither of which are accounted for in the model scheme.

9.4 Future Work.

Many of the important properties of turbulent flow such as its role in facilitating the vertical exchange of heat, salt and particulates are recognised but not fully understood. This study has shown that there exists a strong relationship between the turbulent flow field and the vertical distribution of SPM. Although valuable insight has been gained into the nature of the relationship between these two parameters, many questions remain. Improved understanding of the evolution and decay of the turbulent layer is required in order to investigate its effect on the SPM population. This is best achieved via improved observational techniques coupled with modelling studies, turbulence closure methods being the most likely candidate in the absence of the computing power for formulation of a full Reynolds stress approach.

The ability to accurately measure turbulent intensity over the time and space scales required for a study such as this one would be a very real step forward, although the immediate future for turbulence observations probably lies with instruments such as the FLY probe. A major disadvantage of this approach is the extensive technical support required, although with continuing advancements in electronics, material science and computational techniques, the ability to make accurate measurements of dissipation rate will be facilitated. A more long term strategy is the development of an instrument based on acoustic measurements to measure turbulent properties.

Transmissometers have been in use for some 15 years and the limitations are recognised. A lack of information regarding the nature of the sediment population

and its associated settling velocity distribution is the principal drawback of this approach. However, instruments capable of monitoring particle size, settling velocity and composition are currently being developed for both *in situ* and laboratory use.

The ultimate aim of studies of the sort presented in this thesis is the development of a fully predictive hydrodynamic/turbulent SPM model for the shelf seas. The most popular approach is based on turbulence closure techniques. This allows examination of the individual terms in the TKE equation so that the contribution of each of the processes such as local shear production and diffusion affecting TKE levels can be examined. Combined with improved turbulence and mean flow measurements from a variety of conditions, the predictive capability of these schemes will improve.

There exist many obstacles in particle dynamics modelling. Parameterisation of the erosion of bed material for cohesive sediments is a major problem. Such is the diversity of sediments and dynamical conditions in the ocean this is likely to remain a problem with an empirical approach most common. With more extensive SPM and current measurements, especially close to the bed over a range of conditions an improved parameterisation may be possible. However, relatively simple modifications can be made to the existing model given improved measurements of particle settling velocity and horizontal concentration gradients, allowing inclusion of more size fractions and advection effects. Particle processes such as flocculation along with biological and chemical interactions which affect the nature of the sediment population are also currently under development.

REFERENCES

Aanderaa (1992) RCM 7 & 8 Operating Manual, technical description no. 159. Aanderaa, Bergen, Norway.

Bartz R.J., R.V.Zaneveld and H.Pak (1978) A transmissometer for profiling and moored observations in water. *SPIE Ocean Optics V*, **160**, 102-108.

Batchelor G.K. (1953) *The theory of homogeneous turbulence*. Cambridge University Press, London.

Belderson R.H. (1964) Holocene sedimentation in the western half of the Irish Sea. *Mar. Geol.*, **2**, 147-163.

Boudjelas S. (1994) *Temporal and spatial variations of suspended sediments in the Irish Sea determined from AVHRR visible band and in-situ data*. Ph.D. Thesis, University of Wales, Bangor, UK.

Bowden K.F. and L.A.Fairbairn (1956) Measurement of turbulent fluctuations and Reynolds stresses in a tidal current. *Proc. Roy. Soc. Lond. A*, **237**, 422-438.

Bradshaw P. (1971) *An introduction to turbulence and its measurement*. Pergamon Press.

Bridge J.S. and D.F.Dominic (1984) Bed load grain velocities and sediment transport rates. *Water Resour. Res.*, **20**(4), 476-490.

Cheok J.V.S. (1996) *Modelling of turbulent dissipation*. Ph.D. Thesis (in prep.), University of Wales, Bangor, UK.

Corey A.J. (1949) *Influence of shape on the fall velocity of sand grains*. MS Thesis, Colo. A&M College, Fort Collins, Colo.

Crawford W.R. (1992) Turbulence observations in the upper ocean during the surface wave processes program in the northeast Pacific, February to March 1990. Canadian Data Report of Hydrography and Ocean Sciences No. 106.

Crawford W.R. and R.K.Dewey (1988) Turbulence and mixing : sources of nutrients on the Vancouver Island continental shelf. *Atmosphere-Ocean*, **27**(2), 428-442.

Davies A.G. (1986) A model of oscillatory rough turbulent boundary layer flow. *Estuarine, Coast. Shelf Sci.*, **23**, 353-374.

Davies A.G. (1990) A model of the vertical structure of the wave and current bottom boundary layer. In *Modelling Marine Systems*, A.M.Davies Ed.,263-297, CRC Press Inc..

Davies A.M. and J.E.Jones (1992) A three dimensional model of the M_2, S_2, N_2, K_1 and O_1 tides in the Celtic and Irish Seas. *Prog. Oceanog.*, **29**, 197-234.

Dewey R.K., W.R.Crawford, A.E.Gargett and N.S.Oakey (1987) A microstructure instrument for profiling oceanic turbulence in coastal bottom boundary layers. *J. Atmos. Ocean. Technol.*, **4**(2), 288-297.

Dewey R.K. and W.R.Crawford (1988) Bottom stress estimates from vertical dissipation rate profiles on the continental shelf. *J. Phys. Oceanogr.*, **18**(8), 1167-1177.

Drake D.E. and D.A.Cacchione (1986) Field observations of bed shear stress and sediment resuspension on continental shelves, Alaska and California. *Cont. Shelf Res.*, **6**(3), 415-429.

Durazo-Arvizu R. (1993) *Horizontal circulation and diffusion at tidal fronts*. Ph.D Thesis, University of Wales, Bangor, UK.

Dyer K.R. (1986) *Coastal and estuarine sediment dynamics*. Wiley-Interscience.

Eisma D. and G.Irion (1988) Suspended matter and sediment transport. In *Pollution of the North Sea an Assessment*. W.Salomons, B.L.Bayne, E.K.Duursma and U.Förstner Eds., Springer-Verlag.

Edinger J.F., D.W.Duttweiler and J.C.Geyer (1968) The response of water temperatures to meteorological conditions. *Water Resour. Res. ,4*(5), *1137-1143.*

Francis J.R.D.(1973) Experiments on the motions of solitary grains along the bed of a water stream. *Proc. Roy. Soc. Lond. A*, **332**, 443-471.

Gargett A.E., T.R.Osborn and P.W.Nasmyth (1984) Local isotropy and the decay of turbulence in a stratified fluid. *J. Fluid Mech.*, **144**, 231-280.

Grant H.L., R.W.Stewart and A.Moilliet (1961) Turbulence spectra from a tidal channel. *J. Fluid Mech.*, **13**, 237-263.

Guildline Instruments (1985) Operating manual for model 8400a AUTOSAL. Pub:Guildline Instruments, Ontario, Canada. 52pp.

Jago C.F. and S.E.Jones (1993) Dynamics of suspended matter in the Southern North Sea I. Tidally mixed waters. Submitted to *Cont. Shelf Res.*

Jago C.F., A.J.Bale, M.O.Green, M.J.Howarth, S.E.Jones, I.N.McCave, G.E.Millward, A.W.Morris, A.A.Rowden and J.J.Williams (1993) Resuspension processes and seston dynamics, southern North Sea. *Phil. Trans. R. Soc. Lond. A*, **343**, 475-491.

Janke N.C. (1966) Effects of shape upon the settling velocity of regular convex geometric particles. *J. Sed. Petrol.*, **36**, 370-376.

Jerlov N.G. (1976) *Marine optics*. Elsevier Oceanography Series No.14, Elsevier Scientific Publishing Co., Amsterdam-Oxford-New York, 231pp.

Jones S.E., C.F.Jago, D.Prandle and D.Flatt (1994) Suspended sediment dynamics:measurement and modelling in the Dover Strait. In *Mixing and Transport in the Environment*. K.J.Beven, P.C.Chatwin and J.H.Millbank Eds., John Wiley & Sons Ltd.

Jones S.E. and C.F.Jago (1996) Determination of settling velocity in the Elbe estaury using QUISSET tubes. Submitted to *J. Sea Res.*

Jones S.E., C.F.Jago and J.H.Simpson (1996a) Modelling suspended sediment dynamics in tidally stirred and periodically stratified waters : progress and pitfalls. In *Mixing Processes in Estuaries and Coastal Seas*. C.B.Pattiarachi (Ed.), Coastal and Estuarine Studies Vol.41, American Geophysical Union pp315-338.

Jones S.E., A.R.Campbell, C.F.Jago and A.J.Souza (1996b) Suspended sediment dynamics in the region of freshwater influence of the Rhine. (In prep.).

Joyce T.M. (1989) On *in-situ* 'calibration' of shipboard ADCP's. *J. Atoms. Ocean. Technol.*, **6**, 169-172.

Jumars P.A. and A.R.M.Nowell (1984) Effects of benthos on sediment transport : difficulties with functional grouping. *Cont. Shelf Res.*, **3**, 115-130.

Kenyon N.H. and A.H.Stride (1970) The tide-swept continental shelf sediments between the Shetland Isles and France. *Sedimentology*, **14**, 159-173.

Kineke G.C. and R.W.Sternberg (1989) The effect of particle settling velocity on computed suspended sediment concentration profiles. *Mar. Geol.*, **90**, 159-174.

Kolmogoroff A.N. (1941) The local structure of turbulence in incompressible viscous fluid for very large Reynolds numbers. *Compt. rend. acad. sci. U.R.S.S.*, **30**, 301.

Kundu P.K. (1990) *Fluid Mechanics*. Academic Press, Inc.

Lavelle J.W. and H.O.Mofjeld (1987) Do critical stresses for incipient motion and erosion really exist? *J. Hydraul. Eng.*, **113**(3), 370-393.

Lavelle J.W., H.O.Mofjeld and E.T.Baker (1984) An *in-situ* erosion rate for a fine-grained marine sediment. *J. Geophys. Res.*, **89**, 6543-6552.

Lwiza K.M.M. (1990) *A study of tidal front dynamics using ADCP*. Ph.D. Thesis, University of Wales, Bangor, UK.

Lwiza K.M.M., D.G.Bowers and J.H.Simpson (1991) Residual and tidal flow at a tidal mixing front in the North Sea. *Cont. Shelf Res.*, **11**, 1379-1395.

Matthews D.J. (1913) The salinity and temperature of the Irish Channel and the waters south of Ireland. *Scient. Invest. Brch. Ire.*, **4**, 1-26.

McCave I.N. (1984) Erosion, transport and deposition of fine-grained marine sediments. In: *Fine-Grained Sediment:Deep Water Processes and Facies*. Stow and Piper Eds., *Geol. Soc. Lond. Special Publication*, **15**, 35-69.

Mehta A.J. (1991) Characterization of cohesive soil bed surface erosion, with special reference to the relationship between erosion shear strength and bed density. Coastal and Oceanographic Engineering Department, University of Florida.

Mellor G.L. and T.Yamada (1974) A hierarchy of turbulence closure models for planetary boundary layers. *J. Atmos. Sci.*, **31**, 1791-1806.

Miyake Y. and M.Koizumi (1988) The measurement of the viscosity coefficient of seawater. *J. Mar. Res.*, **7**, 63-66.

Miller M.C., I.N.McCave and P.D.Komar (1977) Threshold of sediment motion under unidirectional currents. *Sedimentology*, **24**, 507-527.

Monin A.S. and A.M.Yaglom (1975) *Statistical Fluid Mechanics:Mechanics of Turbulence*, **2**, The MIT Press, 874pp.

Nasmyth P.W. (1970) *Oceanic turbulence*. Ph.D. Thesis, Institute of Oceanography, University of British Columbia, Canada.

Ninnis R. (1984) *The spatial transfer function of the airfoil turbulence probe*. Ph.D. Thesis, Institute of Oceanography, University of British Columbia, Canada.

Osborn T.R. (1974) Vertical profiling of velocity microstructure. *J. Phys. Oceanogr.*, **12**, 171-185.

Osborn T.R., and W.R.Crawford (1980) An airfoil probe for measuring turbulent velocity fluctuations in water. In *Air-Sea Interactions: Instruments and Methods*. F.Dobson, L.Hasse and R.Davies, Eds. Plenum, 801pp.

Pollard R. and J. Read (1989) A method for calibrating ship-mounted acoustic doppler profilers and the limitations of gyro compasses. *J. Atmos. Ocean. Tech.*, **6**, 859-856.

Prangsma G.J. and J.N.Roozekrans (1989) Using NOAA AVHRR imagery in assesing water quality parameters. *Int. J. Remote Sensing*, **10**, 811-818.

Proctor R. and J.A.Smith (1991) The depth averaged residual circulation on the North West European Shelf. Proudman Oceanographic Laboratory, Report 20.

Rouse H. (1937) Modern conception of the mechanics of fluid turbulence. *Trans. Am. Soc. Civ. Engrs.*, **102**, 463-543.

Sharples J. (1992) *Time dependent stratification in regions of large horizontal gradient.* Ph.D. Thesis, University of Wales, Bangor, UK.

Shi N.C., L.H.Larsen and J.P.Downing (1985) Predicting suspended sediment concentration on continental shelves. *Mar. Geol.*, **62**, 255-275.

Shields A. (1936) Application of similarity principles and turbulence research to bed-load movement. Mitteilungen der Preussischen Versuchsanstalt für Wasser bau und Schiffbau, Berlin. In:Ott and Uchelen (translators), California Institute of Technology, W.M. Keck Laboratory of Hydraulics and Water Resources, Report No. 167.

Simpson J.H. (1971) Density stratification and microstructure in the western Irish Sea. *Deep-Sea Res.*, **18**, 309-319.

Simpson J.H. (1972) A free fall probe for the measurement of velocity microstructure. *Deep-Sea Res.*, **19**, 331-336.

Simpson J.H. and J.R. Hunter (1974) Fronts in the Irish Sea. *Nature*, **250**, 404-406.

Simpson J.H. and J.Sharples (1991) Dynamically active models in the prediction of estuarine stratification. In *Dynamics and Exchanges in Estuaries and the Coastal Zone, Coastal Estuarine Stud. Ser.* D.Prandle Ed., **40**, 101-113.

Simpson J.H., W.R.Crawford, T.P.Rippeth, A.R.Campbell and J.V.S.Cheok (1996) The vertical structure of turbulent dissipation in shelf seas. Submitted to *J. Phys. Oceanogr.*

Smith J.D. (1977) Modelling of sediment transport on continental shelves. In *The Sea*, **6**. E.D.Goldberg, I.N.McCave, J.J.O'Brien and J.H.Steele Eds., 539-577.

Soulsby R.L., A.P.Salkield and G.P.Le Good (1984) Measurements of the turbulence characteristics of sand suspended by a tidal current. *Cont. Shelf Res.*, **3**(4), 439-454.

Souza A.J. (1994) *Controls on stratification in the Rhine ROFI system.* Ph.D. Thesis, University of Wales, Bangor, UK.

Spitzer D., R.Laane and J.N.Roozekrans (1990) Pollution monitoring of the North Sea using NOAA/AVHRR imagery. *Int. J. Remote Sensing*, **11**, 967-977.

Sternberg R.W. (1971) Measurements of incipient motion of sediment particles in the marine environment. *Mar. Geol.*, **10**, 113-119.

Stumpf R.P. (1988) Sediment transport in Chesapeake Bay during floods : Analysis using satellite and surface observations. *J. Coast. Res.*, **4**, 1-15.

Teisson C. (1991) Cohesive suspended sediment transport:feasability and limitations of numerical modelling. *J. Hydraul. Res.*, **29**(6), 755-769.

Tennekes H. and J.L.Lumley (1972) *A first course in turbulence.* MIT Press, Cambridge, Massachusetts.

Tett P.B., I.R.Joint, D.A.Purdie, M.Baars, S,Oosterhuis, G.Daberi, F.Hannah, D.K.Mills, D.Plummer, A.J.Pomroy, A.W.Walne and H.J.Witte (1993) Biological consequences of tidal stirring gradients in the North Sea. Phil. *Trans. Roy. Soc. Series A*, **343** (1669), 493-508.

Thorne P.D., C.E.Vincent, P.J.Hardcastle, S.Reham and N.Pearson (1991) Measuring suspended sediment concentrations using acoustic backscatter devices. *Mar. Geol.*, 98, 7-16.

Topliss B.J. (1986) Spectral variations in upwelling radiant intensity in turbid coastal waters. *Estuarine, Coast. Shelf Sci.*, **22**, 395-414.

Topliss B.J., C.L.Almos and P.R.Hill (1990) Algorithms for remote sensing of high concentration, inorganic suspended sediment. *Int. J. Remote Sensing*, **11**, 947-966.

Tritton D.J. (1977) *Physical Fluid Dynamics*. Van Nostrand Reinhold (UK).

UNESCO (1981). UNESCO technical paper in marine science no. 36.

Weeks A.R. (1989) *Spatial and time-dependent variations in suspended particulate material concentrations in the shelf seas*. Ph.D. Thesis, University College of North Wales, Bangor, Wales, UK.

Weeks A. and J.H.Simpson (1991) The measurement of suspended particulate concentrations from remotely-sensed data. *Int. J. Remote Sensing*, **12**(4), 725-737.

Wolf J. (1980) Estimation of shearing stresses in a tidal current with application to the Irish Sea. In *Marine Turbulence*, J.C.J. Nihoul (Ed.), 319-343.

APPENDIX A

RCM TEMPERATURE AND SALINITY DATA

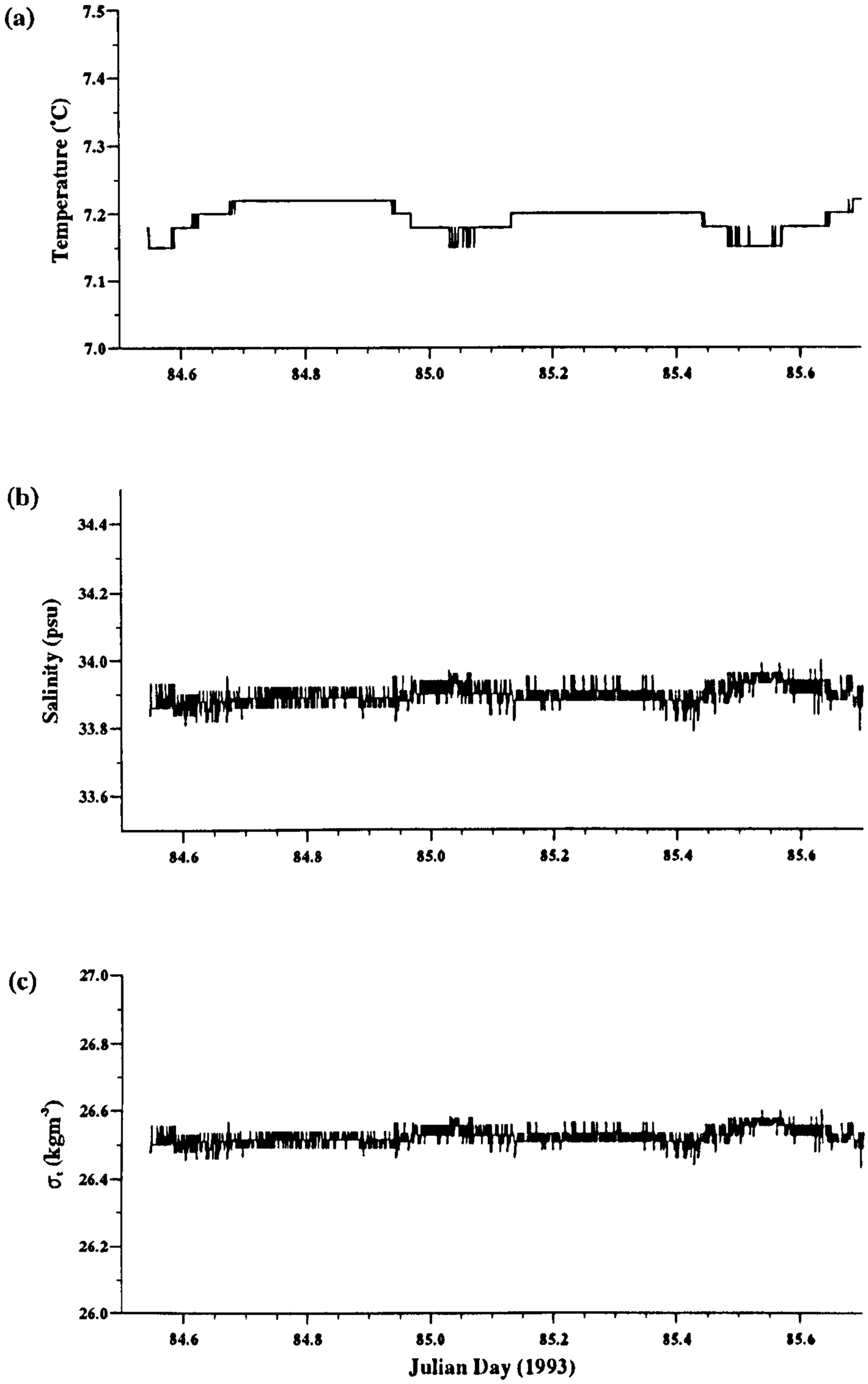

Figure A.01 : Temperature, salinity and σ_t data from RCM 3321.

(a) Temperature.

(b) Salinity.

(c) σ_t.

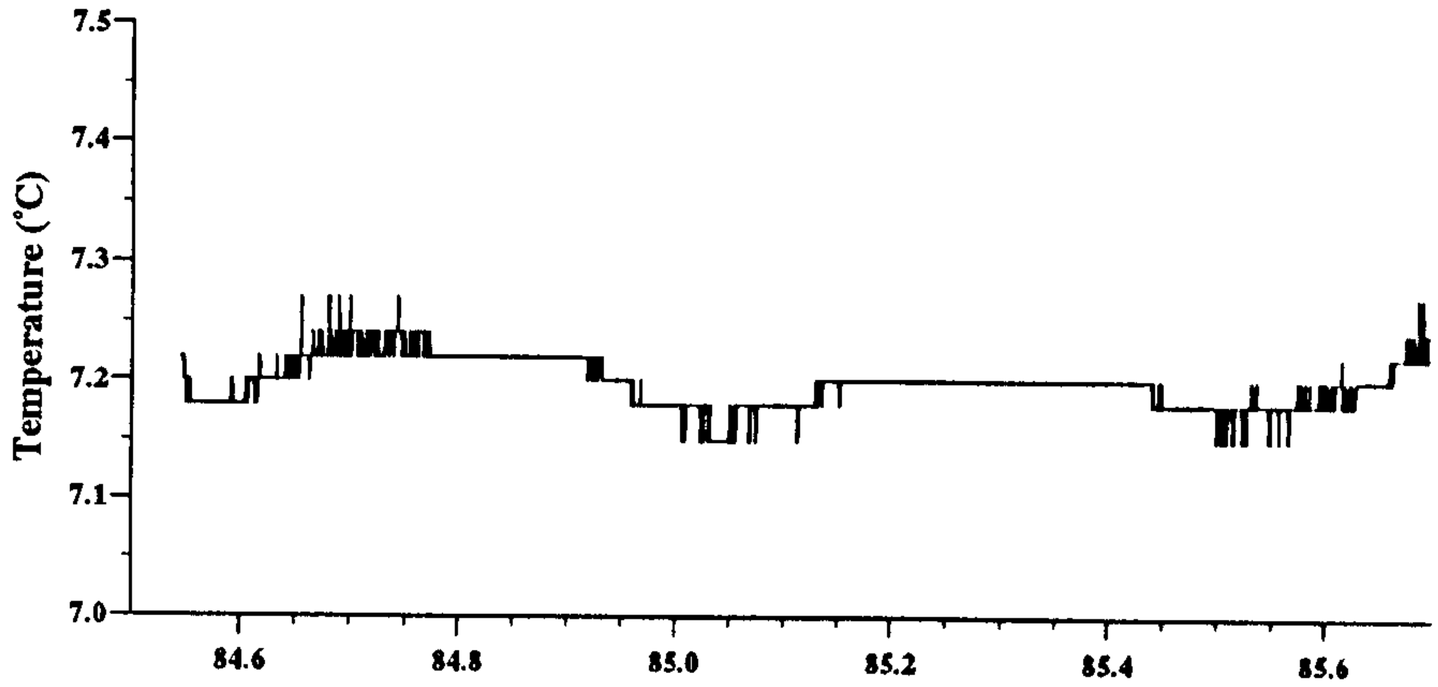

Figure A.02 : Temperature data from RCM 9580.

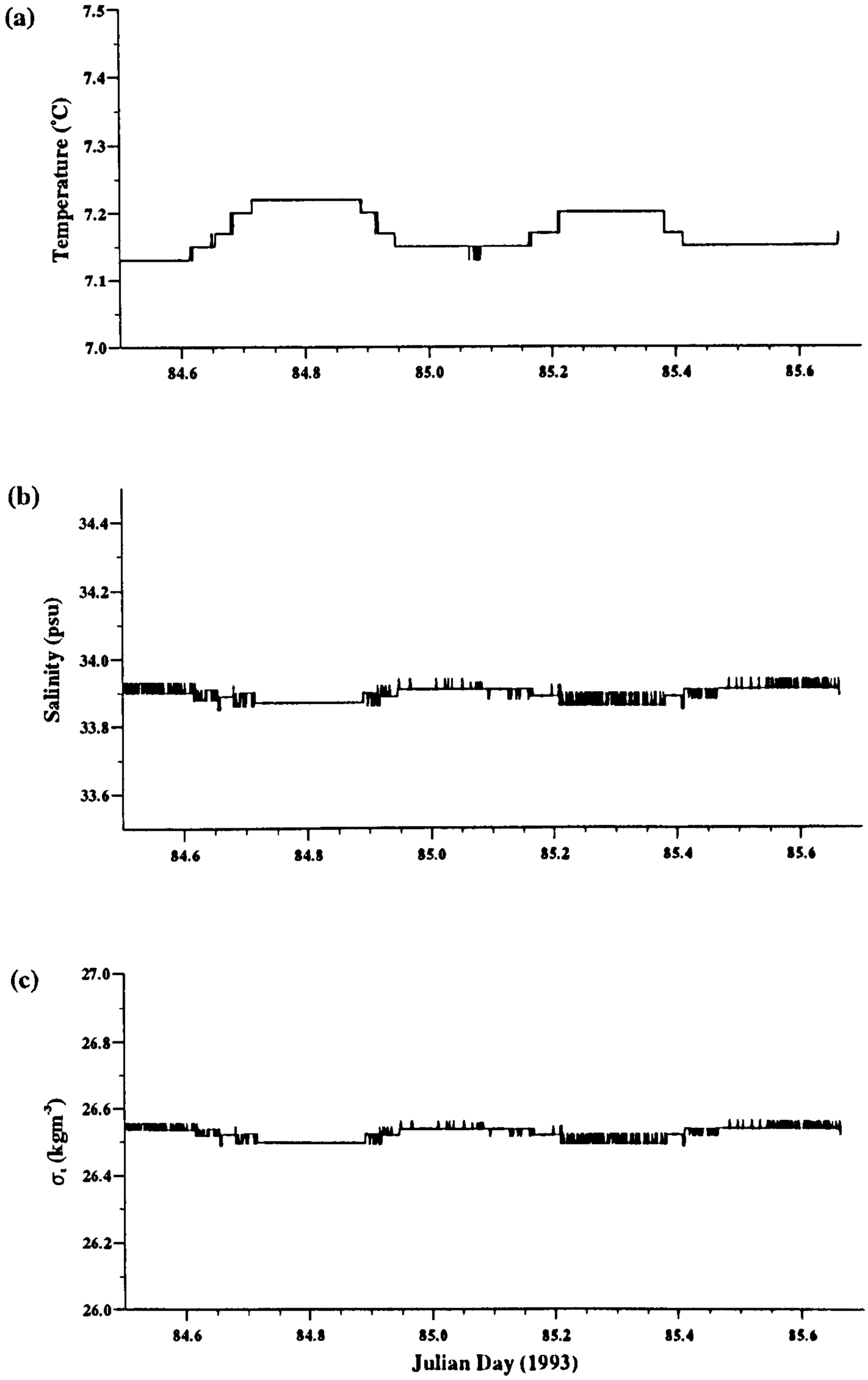

Figure A.03 : Temperature, salinity and σ_t data from RCM 8248.

(a) Temperature.

(b) Salinity.

(c) σ_t.

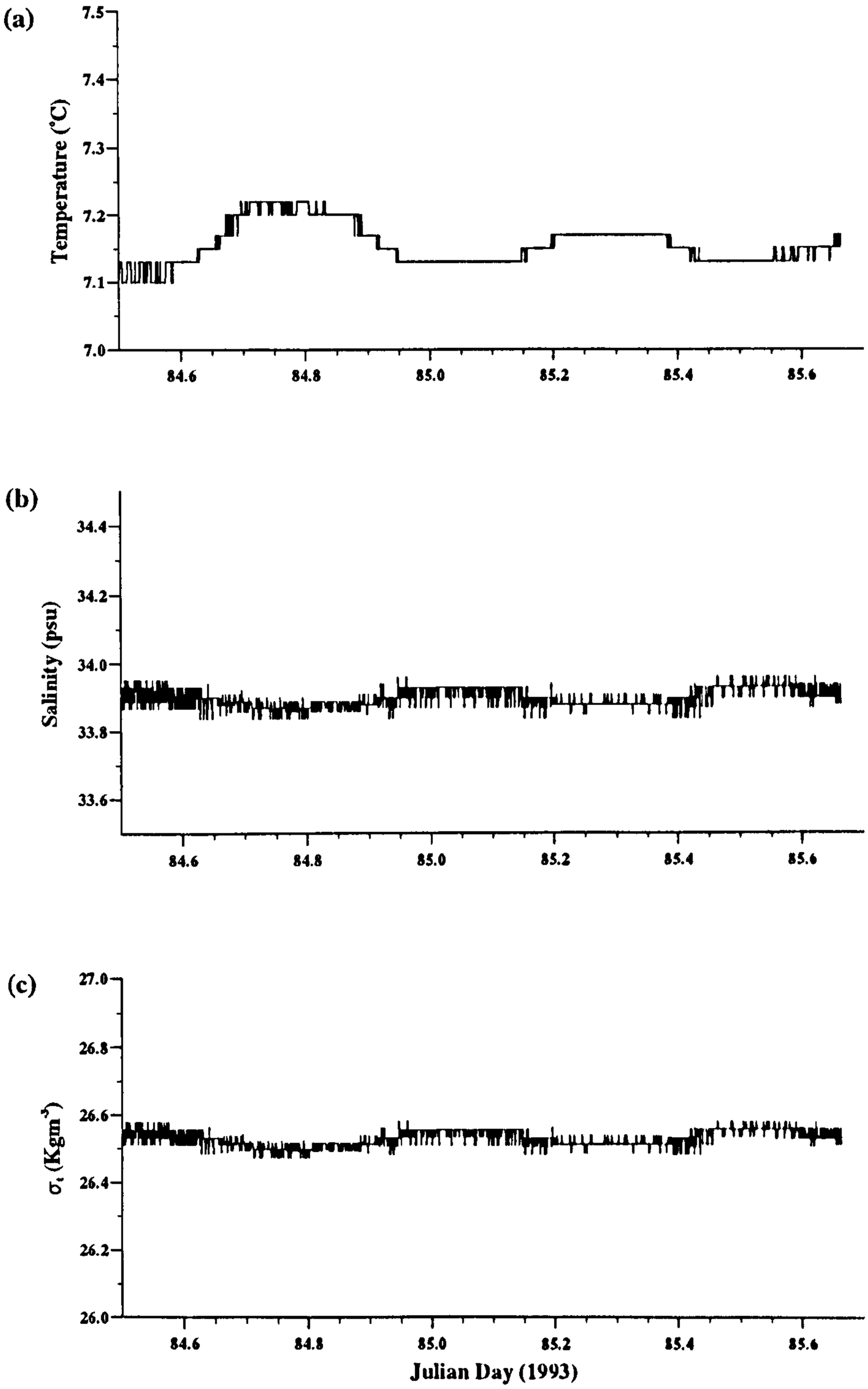

Figure A.04 : Temperature, salinity and σ_t data from RCM 9415.

(a) Temperature.

(b) Salinity.

(c) σ_t.

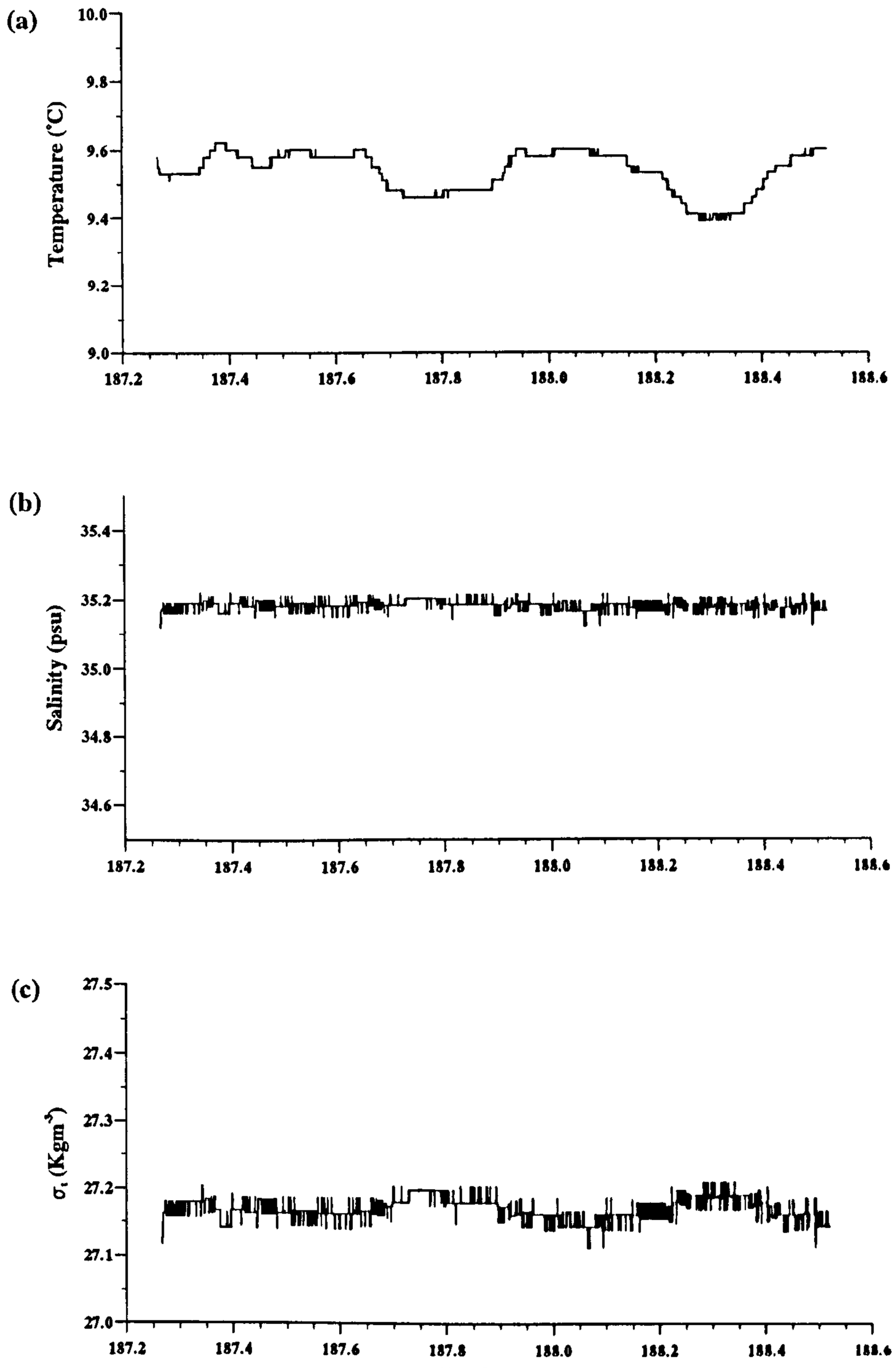

Figure A.05 : Temperature, salinity and σ_t data from RCM 10665.

(a) Temperature.

(b) Salinity.

(c) σ_t.

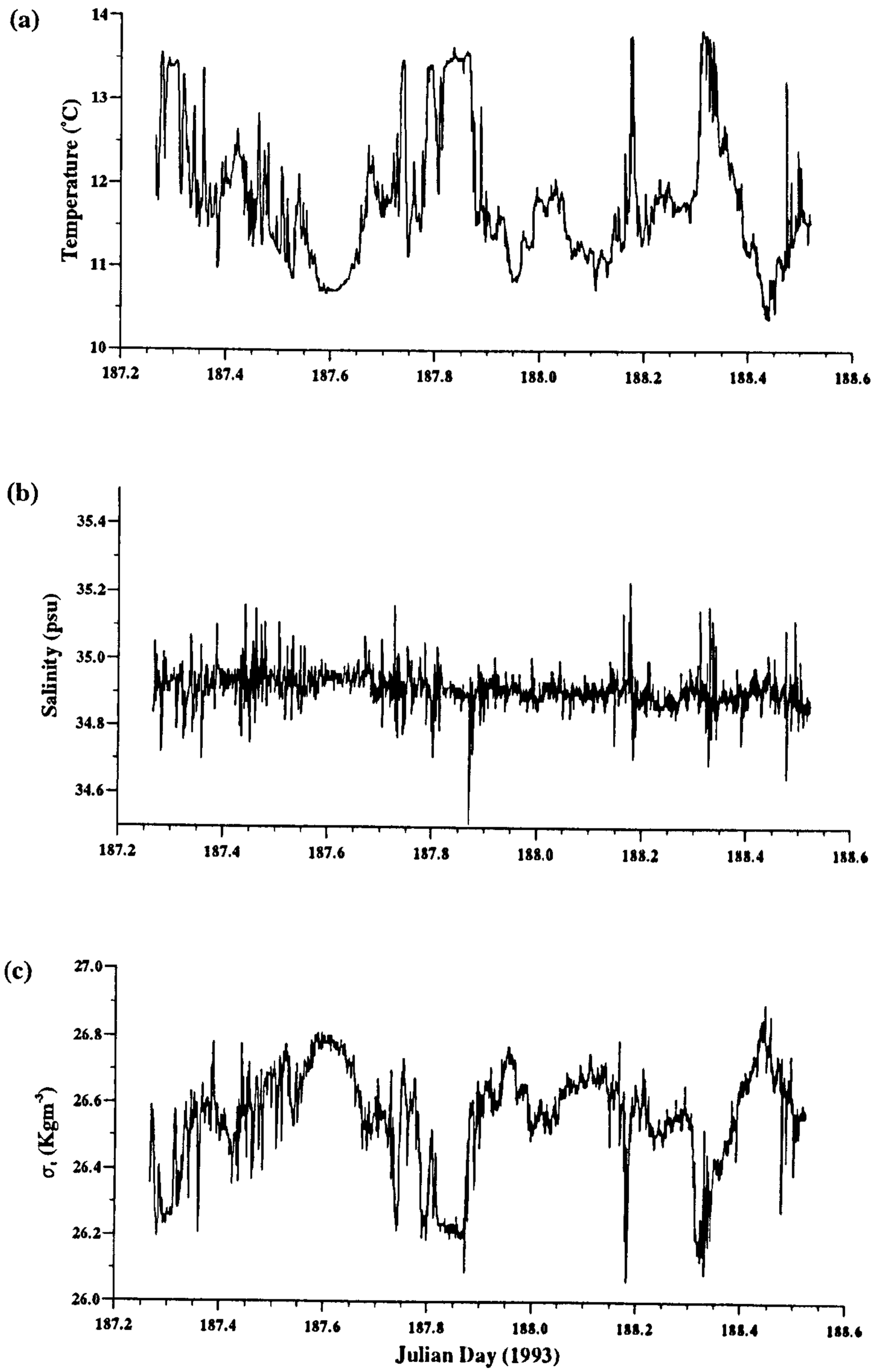

Figure A.06 : Temperature, salinity and σ_t data from RCM 10666.

(a) Temperature.

(b) Salinity.

(c) σ_t.

APPENDIX B

TURBULENCE CLOSURE MODEL INITIALISATION PARAMETERS

Site	IS1_2
Depth	60m
No. of Layers	30
Timestep	0.0012hrs
First initialisation (t,s,spm)	79.0
Second initialisation (impose source-limitation)	84.4
Latitude	53.863
Background N_z,K_z	$1x10^{-4}m^2s^{-1}$
Bottom drag coefficient	$4x10^{-3}$
Local settling velocity	$7.0mms^{-1}$
Background settling velocity	$0.0mms^{-1}$
Local x concentration gradient	0.0mg/l/km
Local y concentration gradient	0.0mg/l/km
Background x concentration gradient	0.037mg/l/km
Background y concentration gradient	0.015mg/l/km
n	1.5
α	$1.0x10^{-7}$ kg/m^2/s
Source-limitation	Yes

Site	IS3
Depth	90m
No. of Layers	45
Timestep	0.0012hrs
First initialisation (t,s,spm)	79.0
Second initialisation (impose source-limitation)	87.4
Latitude	52.443
Background N_z,K_z	$1x10^{-4}m^2s^{-1}$
Bottom drag coefficient	$4x10^{-3}$
Local settling velocity	$4.0mms^{-1}$
Background settling velocity	$0.0mms^{-1}$
Local x concentration gradient	0.0mg/l/km
Local y concentration gradient	0.0mg/l/km
Background x concentration gradient	0.0mg/l/km
Background y concentration gradient	0.0mg/l/km
n	1.0
α	$1.0x10^{-5}$ kg/m^2/s
Source-limitation	Yes

Site	ISS
Depth	90m
No. of Layers	45
Timestep	0.0012hrs
First initialisation (t,s,spm)	179.0
Second initialisation (impose source-limitation)	N/A
Latitude	53.817
Background N_z,K_z	$1x10^{-4}m^2s^{-1}$
Bottom drag coefficient	$4x10^{-3}$
Local settling velocity	$3.0mms^{-1}$
Background settling velocity	$0.0mms^{-1}$
Local x concentration gradient	0.0mg/l/km
Local y concentration gradient	0.0mg/l/km
Background x concentration gradient	0.21mg/l/km
Background y concentration gradient	0.07mg/l/km
n	3.0
α	$3.0x10^{-6}$ kg/m^2/s
Source-limitation	No